REMOVAL OF AMMONIA, ARSENIC AND DYESTUFFS FROM WATER BY OZONE MICROBUBBLES

Thesis

Submitted in partial fulfillment of the requirements

for the degree of

DOCTOR OF PHILOSOPHY

by

Snigdha Khuntia

Department of Chemical Engineering

Indian Institute of Technology Guwahati

Guwahati-781039, India

REMOVAL OF AMMONIA, ARSENIC AND DYESTUFFS FROM WATER BY OZONE MICROBUBBLES

Snigdha Khuntia

Removal of Ammonia, Arsenic and Dyestuffs from Water by Ozone Microbubbles

Thesis

Submitted in partial fulfillment of the requirements

for the degree of

DOCTOR OF PHILOSOPHY

By

Snigdha Khuntia

Roll No: 11610706

Department of Chemical Engineering

Indian Institute of Technology Guwahati

Guwahati-781039, India

DEDICATION

To my Family

And

Lord Jagannath

Department of Chemical Engineering

Indian Institute of Technology Guwahati

Guwahati-781039, India

CERTIFICATE

It is certified that the work contained in the thesis entitled "**Removal of Ammonia, Arsenic and Dyestuffs from Water by Ozone Microbubbles**", by **SnigdhaKhuntia**, has been carried out under our guidance and supervision. The work documented in this thesis has not been submitted to any other University or Institute for the award of any degree or diploma.

Dr. PallabGhosh
Professor
Department of Chemical Engineering
Indian Institute of Technology Guwahati
Guwahati-781039, India

Dr. Subrata Kumar Majumder
Associate Professor
Department of Chemical Engineering
Indian Institute of Technology Guwahati
Guwahati-781039, India

Signature **Signature**

Date **Date**

ACKNOWLEDGEMENTS

This doctoral thesis and the related study were completed under the devoted guidance and supervision of **Prof. Pallab Ghosh** and **Dr. Subrata Kumar Majumder**. First of all, I would like to express my cordial gratitude to **Prof. Ghosh** and **Dr. Majumder** for giving me the opportunity to work on this intriguing project.

I am grateful to **Prof. Pallab Ghosh** for his immense support, encouragement, and endurance, which helped me to finish this work within time. I always admire his advises, energy and hard work for all his students. I am very thankful to him for his enormous efforts on correcting all my mistakes and making my work and research publications more valuable. I am also very grateful to my Co-supervisor **Dr. Subrata Kumar Majumder** for his helping nature and sharing his valuable experiences with me to complete this work. His great efforts and valuable suggestions always helped me in my work. Besides this, I feel very fortunate that I got a chance to work with two such experienced and enthusiastic supervisors, whom I will have a high regard throughout my career.

I would like to thank my doctoral committee members, **Dr. Mihir Kumar Purkait** (Department of Chemical Engineering), **Dr. Chandan Das** (Department of Chemical Engineering), and **Prof. Saswati Chakraborty** (Department of Civil Engineering) for their valuable suggestions and constructive criticism during the project evolutions, which helped me to make necessary improvements in various stages of my research work.

I thank the **Department of Science and Technology** (Water Technology Initiative), Government of India, for the financial support of this work, through the grant number: DST/TM/WTI/2k10/266/(G), dated September 5, 2011.

I am also very thankful to **Dr. Animes Kumar Golder** for guiding me during my M.Tech at IIT Guwahati. The knowledge I have gained from him in my M.Tech, helped me a lot during the Ph.D work.

Acknowledgements

I must thank to all the technical staffs of my department specially, **Mr. Lukumoni Borah**, **Mr. Balen Chandra Mahanta**, **Mr. Prasun Bhattacharjee**, **Mr. Kaustavmoni Deka**, **Mr. Debajit Borah**, **Mr. Dipak Kumar Barman,** and the Scientific Officers, **Mrs. Ritumoni Kalita and Mr. Harsaraj Biswanath.** The experimental works presented in this thesis would never have been possible without the help of these proficient technicians. I am also very thankful to **Mr. Bijoy Kumar Choudhury** (Senior Technician, Department of Mechanical Engineering), who helped me in installing my experimental setup.

I am fortunate enough to have my friend around me, **Mr. Manish Kumar Sinha,** whose presence and cooperation comforted me in many ways. I could never have achieved my goal without his moral support. He always helped and encouraged me to be strong enough to surpass all my difficulties, frustrations and worries. His assistance, suggestions and care made my stay cheerful at IITG.

I am thankful to all my departmental friends, seniors and juniors for their supports and good wishes. I thank to my friends from Subansiri Hostel, **Mahsina Rehman**, **Pranti Dutta**, **Ebria Khakhlari**, and **Mudhulika Kumari** for sharing some wonderful moments with me.

Last but not the least, I would like to thank my father **Mr. Hrushikes Khuntia**, My mother, **Mrs. Bishnupriya Khuntia**, my elder brother, **Mr. Himanshu Khuntia**, and my younger sister, **Miss. Smita Khuntia**, for supporting me to do Ph.D. Their love, affection, blessings and sacrifices made me stronger to overcome my huddles and achieve my target.

Finally, I thank **Lord Jagannath**, **Maa Kamakhya**, and Guru **Shri Shri Thakur Abhiram Paramahansa Dev**, for giving me the blessings and courage to face the difficulties of life and complete this project successfully.

Snigdha Khuntia

ABSTRACT

Microbubble-based methods, in recent times, have been widely used for purification of water and wastewater. Microbubbles have several physicochemical properties, which make them eminently suitable for wastewater treatment. These properties have been discussed from the perspective of application. Various types of microbubble generators and their operation principles have been discussed. Many practical applications of ozone, oxygen and air microbubbles, some of which are currently at various stages of commercialization, have been presented. In addition, directions for future research of microbubble technology and their potential applications have been identified.

Ammonia is a major source of water pollution. One of the most common methods for removal of ammonia from water is oxidation. In this work, ozonation of ammonia using microbubbles was studied in a pilot plant. The microbubbles were effective in dissolving ozone in water. The experimental results indicate that ozone microbubbles were quite effective in oxidizing ammonia. Oxidation of ammonia was effective at high pH and high ozone generation rates. Ozonation was found to occur by direct reaction of ozone with ammonia at the higher pH. However, the hydroxyl radicals were also involved at the lower pH. Bromide ions acted as a catalyst in the ozonation process, and a faster rate of oxidation of ammonia and lower yield of nitrate was observed. The volumetric mass transfer coefficient of ozone in water was determined. It increased with the increasing rate of ozone generation and the pH of the medium.

Arsenic is one of the most toxic elements found in water. As(III) and As(V) are the major sources of arsenic poisoning. It is known that As(V) can be more easily removed from water by adsorptive methods than As(III). In this work, oxidation of more toxic As(III) to less toxic As(V) was studied by using ozone microbubbles. The oxidation was fast over a wide range of pH (e.g. 4−9). The role of hydroxyl radical in the oxidation of As(III) under acidic

conditions was investigated by using 2-propanol as the hydroxyl radical scavenger. Under acidic conditions, the addition of 2-propanol slowed down the oxidation, which proves that hydroxyl radicals were involved in the oxidation process. The effect of carbonate ions on the rate of oxidation was investigated. It was found that the generation of carbonate ion radical from the carbonate ion accelerated the oxidation of As(III). The kinetics of oxidation of As(III) by ozone was studied. Adsorption of As(V) on zirconium impregnated activated carbon (Zr–AC) and amorphous zirconium oxide (Am-Zr) has been studied in this work. The adsorption of As(V) on both of these adsorbents was fast and effective. The As(V) adsorption capacity of Am-Zr was larger than that of Zr–AC. Characterization of these adsorbents was performed by various methods (viz. SEM, EDX, XRD and FTIR). The electric charge on the surface of these adsorbents in aqueous media was measured at different pH. The adsorption of As(V) followed a pseudo second-order kinetics. However, from the intra-particle-diffusion model, it was found that film-diffusion and intra-particle-diffusion took place simultaneously during adsorption. Langmuir, Freundlich and Redlich–Peterson adsorption isotherms were fitted to the experimental data. The adsorption of As(V) on these adsorbents was found to be spontaneous and endothermic in nature. The thermodynamic parameters (viz. changes in Gibbs free energy, enthalpy and entropy) were calculated at different temperatures.

Oxidation of Brilliant Green dye was performed using ozone microbubbles. Decolorization was very effective at both acidic and alkaline pH. The color of the aqueous solution was below detectable limit after 30 min at 1.7 mg s^{-1} ozone generation rate. The reaction between the dye and ozone was first-order in nature with respect to both ozone and the dye. The enhancement factor increased with increasing dye concentration. The samples were analyzed by the UV–Visible spectrophotometry, GC–MS and FTIR spectroscopy. From the GC–MS analysis, 13 intermediates were detected as oxidation products of this dye at various stages of oxidation. The changes in the FTIR spectra showed the destruction of the

dye and the formation of new compounds. The oxidation mechanism was divided into two reaction pathways. The mineralization of the dye was up to 80% in 60 min, as determined by total organic carbon analysis.

Concentration of hydroxyl radicals generated from ozone microbubbles was determined by using an indirect method over a wide range of pH (i.e. pH 3−10). *p*-Chlorobenzoic acid (PCBA) was used as the probe compound to calculate the concentration of hydroxyl radicals. A constant, R_{ct}, was defined as the ratio of ·OH and O_3 exposures, which was employed to estimate the concentration of hydroxyl radicals. The effects of pH and carbonate ions on the generation of hydroxyl radicals were studied. It was observed that the O_3 exposure and the depletion of PCBA were higher at acidic pH than at the alkaline pH. At acidic pH, CO_3^{2-} acted as the ·OH scavenger only, whereas at alkaline pH, it inhibited ozone decomposition. This changed the values of ·OH exposure, O_3 exposure, and hence, R_{ct}. The degradation of phenol was performed at pH 3−10 by using ozone microbubbles. The contributions of ·OH and O_3 on the oxidation of phenol were calculated. A mechanism of the generation of ·OH from the ozone microbubbles under acidic and alkaline conditions was developed.

RESEARCH PUBLICATIONS

Published Online

- Khuntia, S., Majumder, S.K., Ghosh, P., 2012. Microbubble-aided water and wastewater purification: a review. Rev. Chem. Eng. 28, 191−221.
- Khuntia, S., Majumder, S.K., Ghosh, P., 2013. Removal of ammonia from water by ozone microbubbles. Ind. Eng. Chem. Res. 52, 318−326.
- Khuntia, S., Majumder, S.K., Ghosh, P. 2014. Oxidation of As(III) to As(V) using ozone microbubbles. Chemosphere 97, 120−124.
- Khuntia, S., Majumder, S.K., Ghosh, P., 2015. A pilot plant study of the degradation of Brilliant Green dye using ozone microbubbles: mechanism and kinetics of reaction. Environ. Technol. 36, 336–347.
- Khuntia, S., Majumder, S.K., Ghosh, P., 2014. Adsorption of As(V) on zirconium based adsorbents. Desalin. Water Treat. DOI. 10.1080/19443994.2014.978389.
- Khuntia, S., Majumder, S.K., Ghosh, P., 2015. Quantitative prediction of generation of hydroxyl radicals from ozone microbubbles. Chem. Eng. Res. Des. 98, 231–239.

Conference/Presentations

- Khuntia, S., Majumder, S.K., Ghosh, P., 2013. Enhanced oxidation of ammonia using ozone microbubbles. International Conference on Frontiers in Chemical Engineering (ICFCE-2013), NIT Rourkela, Odisha, India, pp 351−356, ISBN 978-93-80813-24-0, 09−11 December.

CONTENTS

Contents

Contents

Contents

LIST OF FIGURES

LIST OF TABLES

Contents

CHAPTER 1

INTRODUCTION

CHAPTER 1

INTRODUCTION

This chapter presents a summary of the properties of the microbubbles from the perspective of applications. Various types of microbubble generators and their operation principles have been discussed. The transport of gas into the aqueous phase has been explained, and the correlations to predict the volumetric mass transfer coefficient have been presented. Many practical applications using ozone, oxygen and air microbubbles, some of which are currently at various stages of commercialization, have been presented. Other important uses of microbubbles for wastewater treatment, namely, removal of fine solid particulate matter and oil, have also been discussed. In addition, directions for future research of microbubble technology and their potential applications have been identified.

1.1 OVERVIEW

Water pollution occurs when there is any chemical, physical or biological change in the quality of water, which can adversely affect good living organism. With the increase in population, the necessity and scarcity of drinking water has become a big issue for the scientists. The disposal of toxic and organic chemicals from industries, farm lands and household areas to the river and the sea is the main reason of water pollution. It is not possible to eliminate all such chemicals due to a number of reasons, e.g. essentiality of the final product during whose development these chemical are generated, and an economic rate of production. Therefore, in recent years, scientists are more inclined toward environment-friendly technologies in which such chemicals are minimized, which would lead to a safer future and save Earth.

Small bubbles are extensively used in many environmental processes (Agarwal et al., 2011). In recent years, microbubbles have received a good attention among the water

purification technologies (Matsuo et al., 2006). Air, oxygen and ozone microbubbles are extensively used in various water treatment applications. Microbubbles are tiny spherical bubbles having diameter 10−100 µm. They are different from the common bubbles (also known as *macrobubbles or millibubbles*) not only in terms of size, but also in terms of the physical properties.

Apart from water treatment, microbubbles are used in various other fields. In the medicine therapeutic applications, microbubbles are used for scanning body organs, and also as a drug or gene carrier (Kurup and Naik, 2010). Microbubbles have been tested for antibacterial activities under aerobic and anaerobic conditions (Jauregi and Varley, 1998). Microbubbles, stabilized by various surfactants, are used for adsorption of protein from aqueous solution (Kukizaki and Baba, 2008). Petroleum-based surfactants as well as biosurfactants have been used for stabilizing microbubbles (Xu et al., 2011). Microbubbles have been functionalized by surfactants, nanoparticles, pharmaceuticals and bioactive molecules. Due to their small size, microbubbles are highly effective in industrial separation processes such as, removal of volatile contaminants and particulate matters present in the aqueous phase (Terasaka and Shinpo, 2007). Nowadays, microbubbles are used in the treatment of dyestuff wastewater (Chu et al., 2007a), textile wastewater (Chu et al., 2008a), sludge solubilization (Chu et al., 2008b), phenol degradation (Li et al., 2009) and many other applications.

1.2 PROPERTIES OF MICROBUBBLES

Microbubbles are endowed with several special physico-chemical properties, which have made them particularly useful in various water and wastewater treatment processes (Ohnari et al., 2002; Takahashi, 2010; Tsuge et al., 2009). These features are: low rising velocity, surface with a high curvature, large gas–liquid interfacial area, and electrically charged

surface. Many of the useful features of microbubbles for wastewater treatment are associated with these properties.

1.2.1 Size and Shape

Microbubbles are spherical in shape. For a three dimensional object, the area is minimal when the object has a spherical shape. Therefore, the gas–liquid interfacial energy is minimal when the bubble is spherical. *Macrobubbles*, which are commonly used in fermentors, gas–liquid reactors and ore flotation equipment, have diameter in the range of 2−5 mm. Bubbles, which have diameter < 200 nm, are known as *nanobubbles* (Agarwal et al., 2011). Bubbles, whose diameters lie between 200 nm and 10 µm, are called *micro-nanobubbles* (Tsuge, 2010). As of now, there is hardly any universally-accepted classification of the various types of bubbles in terms of their size.

A photomicrograph of microbubbles is shown in Figure 1.1 (a) (Sumikura et al., 2007). The photograph was taken 20 s after the generation of the microbubbles. In water, the microbubbles form a milky dispersion, as shown in Figure 1.1 (b). According to Sebba (1988), a surfactant-stabilized microbubble is composed of two concentric gas spheres, inside which a layer of water is sandwiched. This structure is shown in Figure 1.1 (c). The diameter of the inner gas core is about 50−60 µm, and the thickness of the internal water film is ~1 µm (Bredwell and Worden, 1998).

The surfactant molecules impart a stabilizing influence to the bubble against coalescence by various repulsive interfacial forces (e.g. electrostatic double layer, steric and hydration forces). Microbubbles, formed ultrasonically or by special generators, have a wide size distribution. The size distribution can be unimodal or bimodal. The generation technique has a significant effect on the size of the microbubbles (Li, 2006).

Tsuge et al. (2009) have studied single pore nozzle and rotating flow microbubble generators, and compared the size of the bubbles formed by them. With the rotating flow microbubble generator, the bubbles are sheared and crushed by the rotating flow, which results in smaller microbubbles. Besides this, bubbles of smaller size are produced (with both the generators) when the outlet pressure of the pump is large, because the change in pressure at the time of bubble formation is greater, which results in smaller bubbles.

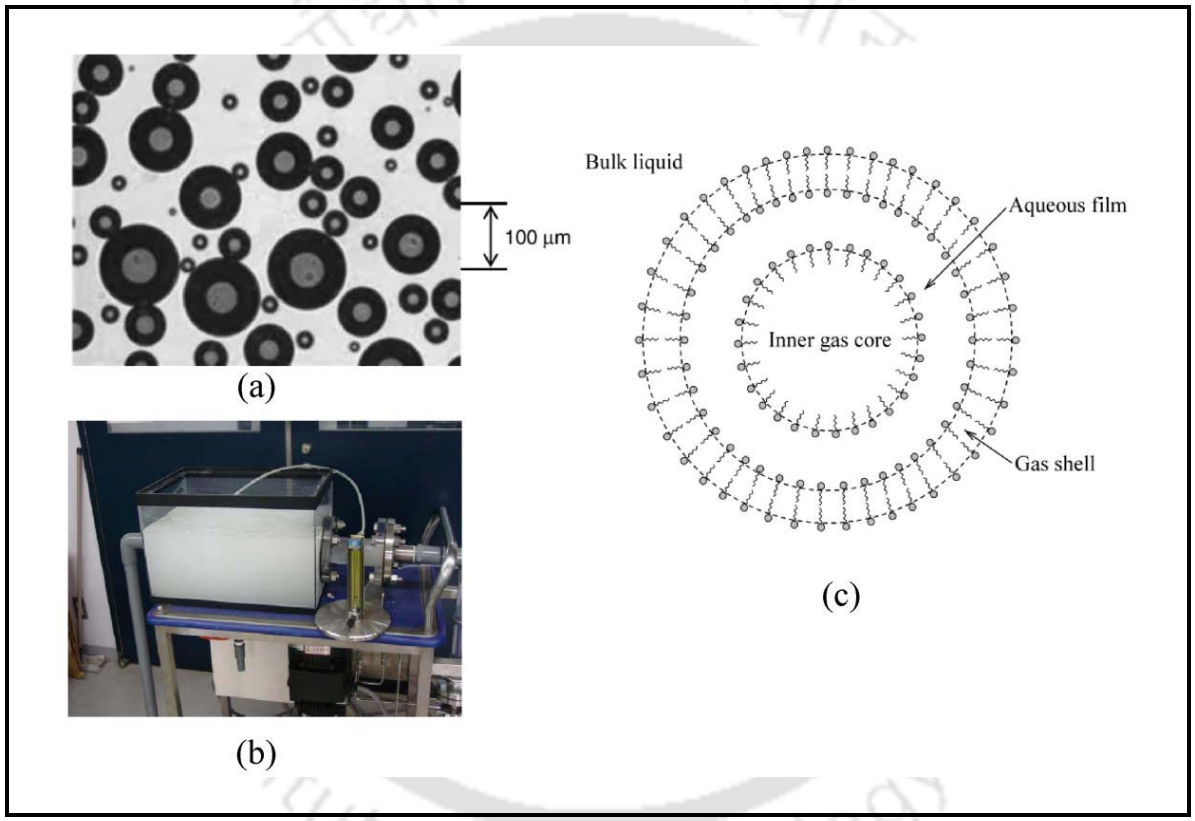

Figure 1.1 (a) Photomicrograph of microbubbles (Sumikura et al., 2007), (b) milky dispersion of microbubbles, and (c) surfactant-stabilized microbubbles (Sebba, 1988).

Walker et al. (2001) have reported that the size of microbubbles decreased with increasing NaCl concentration up to 1 mol dm^{-3}. Hofmeier et al. (1995) suggested that the surface elasticity plays an important role in the formation of smaller bubbles in presence of NaCl. Pure liquids, which have small surface elasticity, give rise to large bubbles through

coalescence. In aqueous solutions, where the surface elasticity is larger, bubble size is reduced through the inhibition of coalescence.

1.2.2 Measurement of Size of Microbubbles

Several methods are available for measuring the diameter of microbubbles. In the simple visualization approach, the microbubbles are photographed with a microscope and camera (Kawahara et al., 2009). The image is digitally processed to measure the diameter. Bubble diameter down to ~1 μm can be measured by this technique. In the more sophisticated laser light scattering technique, the dispersion containing the microbubbles is irradiated by a laser, and the scattered light is detected by a photomultiplier tube. The relationship between the intensity of the scattered light and the bubble diameter varies with the size of the bubbles.

Dynamic light scattering is a sophisticated technique which measures Brownian motion and correlates this to the size of the bubbles (Berne and Pecora, 2000). The Brownian motion becomes slower with the increase in the size of the bubble. The diameter of a bubble is calculated by using the Stokes–Einstein equation (Ghosh, 2009).

$$d = \frac{RT}{3\pi\mu N_A D_b} \tag{1.1}$$

Other available technologies for measuring the size of the microbubbles are given in Table 1.1. As the bubbles generally have a broad size distribution, the average diameter of the microbubbles is often expressed in terms of the Sauter mean diameter (d_{32}), which is defined as (Liu et al., 2010)

$$d_{32} = \frac{\sum n_i d_i^3}{\sum n_i d_i^2} \tag{1.2}$$

Table 1.1 Methods for the measurement of size of microbubbles.

Method	Apparatus used	Microbubble diameter	Reference
Photograph	Video camera and microscope	≤ 1 μm	Sadatomi et al. (2005)
Laser light scattering	Single particle optical sizing	0.2−2000 μm	Pelssers et al. (1990)
Acoustic induced deflation	Microscope and fast camera	≤ 1 μm	Guidi et al. (2010)
Phase Doppler Anemometry	Transmitter, receiver and processor	0−150 μm	Hosokawa et al. (2009)
X-ray particle tracking velocimetry	X-ray holography and particle tracking system	10−60 μm	Lee and Kim (2005)

1.2.3 Kinetic Properties

The motion of microbubbles in water under gravity is similar to that of a hard colloid particle. The rising velocity of a microbubble through a liquid is determined by the balance of the buoyancy and drag forces acting on it. In water, if the Reynolds number of the microbubbles is well below unity, the terminal rising velocity (u_b) can be expressed by the Stokes law as (Ghosh, 2009)

$$u_b = \frac{gd^2\rho_l}{18\mu} \tag{1.3}$$

Experimental data reported in the literature closely obey the Stokes law (Takahashi, 2005a). The average bubble rising velocity, $\bar{u}_b$, in a bubble column can be expressed in terms of the fractional gas hold-up, ε_g, and the superficial gas velocity, u_{sg}, as (Kawahara et al., 2009)

$$\bar{u}_b = u_{sg} / \varepsilon_g \tag{1.4}$$

$$\varepsilon_g = V_g / \left(V_g + V_l \right) \tag{1.5}$$

$$u_{sg} = Q_g / A_c \tag{1.6}$$

1.2.4 Thermodynamic Properties

One of the most important characteristics of the microbubbles dispersed in water is that they gradually decrease in size and ultimately collapse under water due to the dissolution of the gas present inside the bubble. But the macrobubbles rise rapidly toward the surface of water and burst. On the other hand, the nanobubbles are stable for a much longer time (sometimes for months) (Takahashi, 2005b). The general difference between macrobubbles, microbubbles and nanobubbles is depicted in Figure 1.2. The interior pressure varies inversely with the bubble diameter. The pressure–diameter relationship can be expressed by the Young–Laplace equation given by (Ghosh, 2009)

$$p_g - p_l = \Delta p = 4\gamma / d \tag{1.7}$$

Therefore, the excess pressure inside a 1-μm diameter microbubble in water at 298 K (γ = 72.5 mN m^{-1}) would be 290 kPa. The pressurized gas gets efficiently dissolved in the surrounding water obeying Henry's law: $\tilde{p} = Hc$. When the gas dissolves, pressure inside the bubble increases and the bubble shrinks further. The rate of shrinkage increases with time, which leads to the collapse of the microbubble (Takahashi, 2010). This implies that the gas substantially dissolves in water. The time required for collapse of microbubbles is of the

order of several minutes (Takahashi, 2010). On the other hand, some works have predicted very small lifetime of microbubbles in water (Katiyar and Sarkar, 2010). From Eq. (1.7), the nanobubbles are expected to have very high internal gas pressure. Consequently, the gas in the nanobubbles should rapidly dissolve in the ambient liquid. However, the nanobubbles have exceptional stability. It has been suggested that the formation of hydrate may impart stability to the nanobubbles for a prolonged time (viz. of the order of months) (Takahashi, 2009).

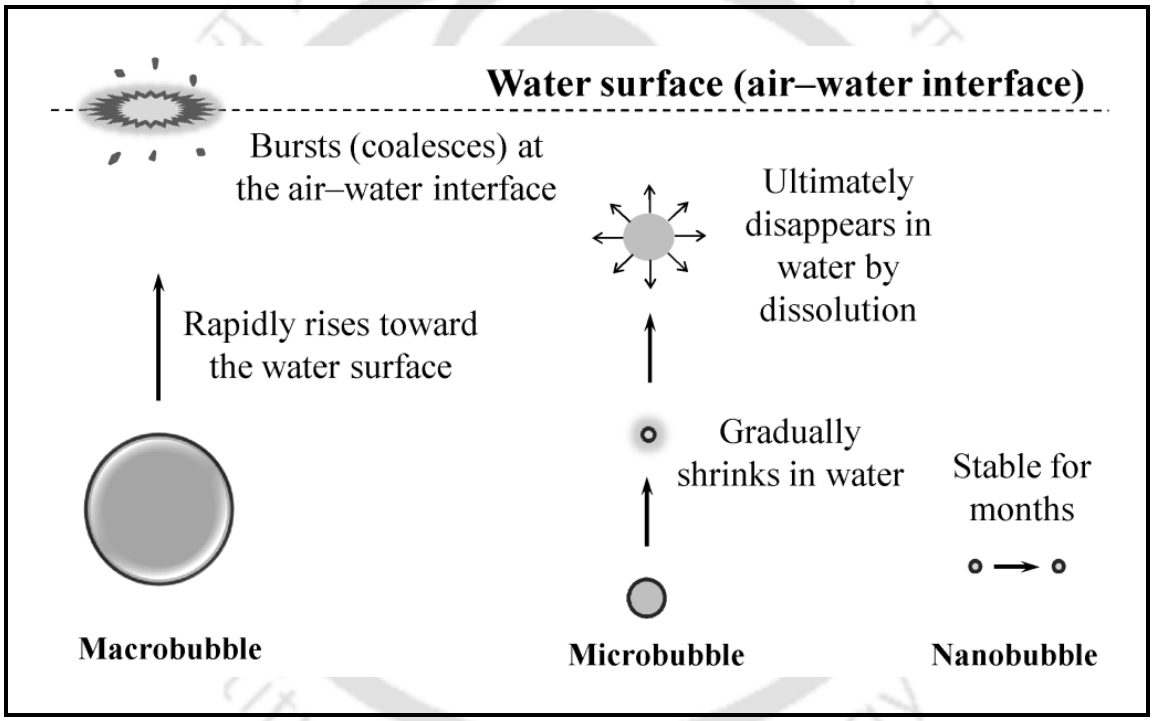

Figure 1.2 Difference between macrobubble, microbubble and nanobubble.

1.2.5 Electrical Properties

The surface of the microbubbles dispersed in water is charged. This surface charge can be measured in terms of zeta potential. Zeta potential is the potential at the surface of shear, which is located very close to the interface. This potential is determined by applying the Smoluchowski equation given by (Ghosh, 2009)

$$\zeta = \frac{\mu E}{\varepsilon \varepsilon_0} \tag{1.8}$$

The zeta potential of air microbubbles in distilled water is negative. The values reported by Takahashi (2005a) and Qu et al. (2009) are –35 mV and –57.9 ± 3.9 mV, respectively at pH 5.8. Hasegawa et al. (2009) have generated ozone microbubbles using two microbubble generators having $\pi/3$ and $\pi/6$ rad slit angles. The zeta potentials measured by them were −43 and −38 mV, respectively, for these two slit angles.

The zeta potential does not significantly vary with the bubble diameter (Takahashi, 2005a). However, when the microbubbles shrink in water, the transient value of zeta potential shows a significant variation with time, and hence, with bubble diameter (Takahashi, 2010). When the microbubbles collapse, an ionic field of very high ion concentration is created that helps the formation of free radicals, which are the main reactive species in the oxidative treatment of wastewater (Takahashi et al., 2007). The zeta potential strongly depends on the pH of the medium. Takahashi (2005a) has reported that the zeta potential of microbubbles in distilled water is negative above pH 4.5. In highly alkaline solutions (i.e. pH > 10), the zeta potential exceeds −100 mV. However, below pH 4.5, the zeta potential is positive.

The charge at the gas–water interface is developed due to the adsorption of OH^- and H^+ ions. The counter-ions are attracted toward the interface and form an electrostatic double layer. The presence of inorganic salts (e.g. NaCl and $MgCl_2$) makes the zeta potential less negative, depending on their concentration (Takahashi, 2005a). The zeta potential of a microbubble significantly depends on the presence of surface active compounds (e.g. surfactants and alcohols) in water. These compounds have a high concentration at the air–water interface even when they are present in small quantities. Therefore, they easily displace the OH^- and H^+ ions from the interface, because the surface activity of these ions is much smaller. The cationic surfactants present in water render the zeta potential positive

whereas, the anionic surfactants give rise to negative zeta potential (Yoon and Yordan, 1986). Wastewater contains various surface active compounds released from the animals, household, plants, and industrial effluents. Therefore, the electric charge of the microbubbles in the wastewater can vary widely.

1.2.6 Mass Transfer in Microbubble Systems

One of the most important aspects of the use of microbubbles in the water treatment is the transfer of gas from the microbubble into the aqueous phase. In oxidation applications (such as ozonation), the gas present in the microbubble must dissolve in the surrounding aqueous phase before reacting with the inorganic and organic contaminants. The overall mass transfer coefficients in the liquid and gas phases (viz. K_g and K_l) are given by (Cussler, 1997)

$$\frac{1}{K_l} = \frac{1}{K_g H} = \frac{1}{k_l} + \frac{1}{k_g H} \tag{1.9}$$

For microbubbles, the gas molecules have to diffuse through a small distance, and therefore, the gas-phase mass transfer resistance, viz. $1/(k_g H)$, is negligible (Motarjemi and Jameson, 1978). Also, for the sparingly soluble gases such as oxygen and ozone, the mass transfer resistance mainly lies in the liquid phase (Johnson and Davis, 1996). For a microbubble rising in water following the Stokes law, the mass transfer coefficient can be calculated from the following correlation (Clift et al., 1978).

$$k_l = \frac{D}{d}\left[1 + \left\{1 + \frac{du}{D}\right\}^{1/3}\right] \tag{1.10}$$

Equation (1.10) shows that the mass transfer coefficient increases with the decreasing size of the microbubbles. Wastewater often contains surface active impurities by which the mass transfer rate is reduced. Apart from the reduction in surface flow, surfactant molecules act as a physical barrier for the gas molecules to pass through the interface, which reduces mass

transfer rate (Koide et al., 1976). The Frössling equation is valid for "solid" microbubbles (i.e. microbubbles whose surface is immobile, and behave like solid particles) (Motarjemi and Jameson, 1978).

$$\frac{k_l d}{D} = 0.6\left(\frac{du\rho_l}{\mu}\right)^{1/2}\left(\frac{\mu}{\rho_l D}\right)^{1/3} \tag{1.11}$$

For the circulating microbubbles, the Higbie equation is applicable (Motarjemi and Jameson, 1978).

$$k_l = 2\left(\frac{D}{\pi t_d}\right)^{1/2} \tag{1.12}$$

The mass transfer coefficients predicted by Eqs. (1.11) and (1.12) differ considerably. Kawahara et al. (2009) have presented a comparison of k_l obtained by these two equations. The experimental data on oxygen transfer in tap water and saline water show an increase in mass transfer coefficient with increasing bubble diameter, which is opposite to that predicted by these equations. They attributed this to the bubble-induced turbulence, which is proportional to the bubble diameter (Sato et al., 1981). Kawahara et al. (2009) have presented modifications of Eqs. (1.11) and (1.12). They have reported that a unique relationship exists between k_l and the product of Sauter mean diameter (d_{32}) and bubble rising velocity (u_b), which is given by

$$\frac{k_l \mu}{\gamma} = 7.46\times10^{-10}\left(\frac{u_b d_{32}}{D}\right)^{0.756} \tag{1.13}$$

The following equation, given by Calderbank and Moo-Young (1961), is applicable to the bubbles, which have diameter less than 100 µm (Motarjemi and Jameson, 1978).

$$k_l = 0.31\left(\frac{\Delta\rho g}{\mu}\right)^{1/3} D^{2/3} \tag{1.14}$$

Another equation, similar to Eq. (1.14), has been proposed by Waslo and Gal-Or (1971) for industrial dispersions containing small bubbles.

$$k_l = 0.55\left(\frac{1-\varepsilon_g^{5/3}}{3+2\varepsilon_g^{5/3}}\right)^{1/3}\left(\frac{\Delta\rho g}{\mu}\right)^{1/3} D^{2/3} \tag{1.15}$$

Both Eqs. (1.14) and (1.15) are applicable for small microbubbles having rigid surface.

Bredwell and Worden (1998) have observed that the experimentally-determined values of k_l were similar in magnitude to those predicted by the correlations Eq. (1.15). The average value of the quantity, $0.55\left(\frac{1-\varepsilon_g^{5/3}}{3+2\varepsilon_g^{5/3}}\right)^{1/3}$, is about 0.31 over the gas hold-up range upto 0.8. Several correlations for the determination of ε_g have been reported by Kawahara et al. (2009). A comparison of the gas hold-up obtained by various methods has been given by Li and Tsuge (2006). Table 1.2 gives the values of volumetric mass transfer coefficient obtained by oxygen, ozone and CO_2 microbubbles in wastewater treatment. As the gas is dissolved in the aqueous phase, its concentration in the liquid phase increases. The rate of increase in concentration of the gas in the aqueous phase is given by (Waslo and Gal-Or, 1971)

$$\frac{dc}{dt} = k_l a\left(c^* - c\right) \tag{1.16}$$

The interfacial area per unit volume is related to the fractional gas hold-up $\left(\varepsilon_g\right)$ and Sauter mean diameter $\left(d_{32}\right)$ as (Kawahara et al., 2009)

$$a = 6\varepsilon_g / d_{32} \tag{1.17}$$

Table 1.2 Volumetric mass transfer coefficient using microbubbles.

Type of Microbubble generator	Gas Type	Microbubble diameter (μm)	$k_l a$ (s^{-1})	Other parameters	Reference
Sparger	O_2	20−100	0.05−0.057	Impeller speed (rpm): 100−600	Kaster et al. (1990)
Spinning disc	O_2	60*	0.06−0.5	–	Bredwell and Worden (1998)
Dissolution	CO_2	100*	0.002	–	Ago et al. (2005)
Rotating flow	O_2 O_3	40−120	0.00207−0.0068	Gas flow rate ($m^3 s^{-1}$): 4.17×10^{-7}– 1.66×10^{-5} Liquid flow rate ($m^3 s^{-1}$): $2.5 \times 10^{-4} - 3.25 \times 10^{-4}$	Li and Tsuge (2006b)
Microbubble diffuser	O_3	<58	0.1072−0.486	Air flow rate ($m^3 s^{-1}$): 3.33×10^{-7}– 2.5×10^{-5}	Li and Tsuge (2006b)
Microbubble generator and bubble contactor	O_3	58*	0.002383	Gas flow rate ($m^3 s^{-1}$): 8.33×10^{-6}	Chu et al. (2008a)

*Mean bubble diameter

The quantities, $k_l a$ and c^*, are also known as *clean water parameters*. If the initial concentration of the gas in water (i.e. at $t = 0$) is c_0, then integration of Eq. (1.16) gives the variation of concentration of the gas in the aqueous phase, which can be expressed as

$$\ln\left(\frac{c^* - c}{c^* - c_0}\right) = -k_l a t \tag{1.18}$$

The volumetric mass transfer coefficient, $k_l a$, can be determined from the slope of the plot of $\ln\left(\frac{c^* - c}{c^* - c_0}\right)$ versus time (Ago et al., 2005), or by a non-linear regression analysis, as described by ASCE (2007). Several correlations for the computation of $k_l a$ have been reported in the literature (Akita and Yoshida, 1973; Bredwell and Worden, 1998; Kawahara et al., 2009; Koide et al., 1983; Nedeltchev et al., 2006a, 2006b; Van'tRiet, 1979). However, only a few works have reported the applicability of these correlations for predicting the volumetric mass transfer coefficient in microbubble systems. The available experimental data indicate that these correlations are not accurate for the predictive purpose. The volumetric transfer rate (VGTR) of gas is defined as (Chu et al., 2008a)

$$\text{VGTR} = (k_l a) c^* \tag{1.19}$$

Experimental data reported in the literature on the microbubble systems indicate that high values of volumetric mass transfer coefficient can be obtained even in the (mechanically) unagitated systems. For example, Bredwell and Worden (1998) have reported $k_l a$ values for oxygen microbubbles (which had an average initial diameter of 60 μm) in the range of 0.06−0.5 s^{-1}. These values are considerably higher than those for mechanically agitated, commercial-scale fermentors. Similar results have been reported by Kaster et al. (1990). Ago et al. (2005) have measured $k_l a$ for carbon dioxide microbubbles. They observed an increase in the volumetric mass transfer coefficient by several times as compared

to the conventional bubbling technique. Chu et al. (2007b) have studied mass transfer of ozone in water by microbubbles. Compared to an ordinary bubble contactor, the mass transfer efficiency in the microbubble system was 1.6−2.7 times higher. Increase in the flow of gas led to the increase in the volumetric mass transfer coefficient and the gas transfer rate, as illustrated in Figure 1.3 (Chu et al., 2008a).

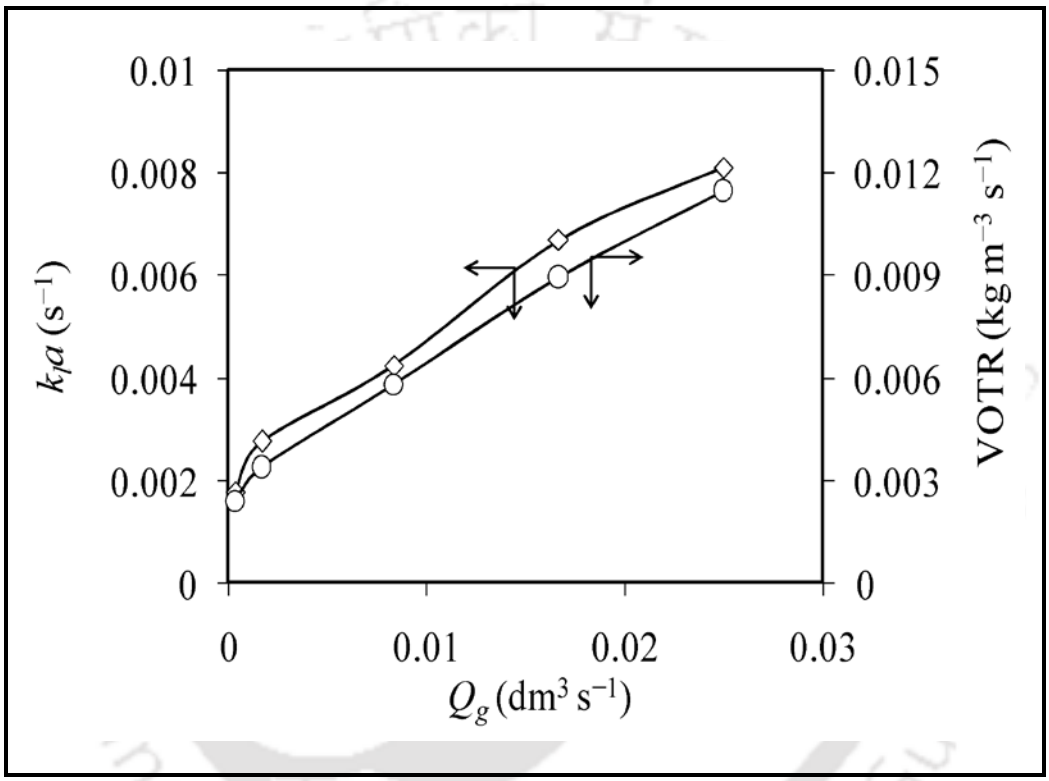

Figure 1.3 Variation of $k_l a$ and volumetric oxygen transfer rate (VOTR) with air flow rate.

Nakano et al. (2005) have compared the volumetric mass transfer coefficients of oxygen in water by the microbubble and air-stone dissolution methods. The microbubble generator produced a much higher $k_l a$ than the air-stone method. Li and Tsuge (2006b) have reported that the volumetric mass transfer coefficient for ozone in water increased with the increasing induced-gas and water flow rates. Yasuda et al. (2010) have studied mass transfer

of ozone in water in an airlift bubble column reactor with a draft tube. They observed that $k_l a$ increased with increasing diameter of the draft tube.

1.3 MICROBUBBLE GENERATORS

Microbubbles have been generated by a wide variety of methods (Ikeura et al., 2011; Takahashi, 2009; Terasaka et al., 2011). The method of generation has a significant effect on their properties, and consequently on the effectiveness of wastewater treatment. The microbubble generators are of two types, i.e. gas–water circulation and pressurization-followed-by-decompression. In the gas–water circulation type of microbubble generator, the gas is introduced into the water vortex, and the gas bubbles thus formed, are converted into microbubbles by breaking the vortex. In the pressurization–decompression type of microbubble generator, a sufficient amount of gas is dissolved in water under moderately high pressure to form a supersaturated solution. The solution is unstable and the gas escapes from water generating a large number of microbubbles. The spiral-liquid-flow microbubble generator (Ohnari et al., 1999) is shown in Figure 1.4 (a). The pumped water is tangentially introduced from a side hole into a cylinder. The spiral flow of liquid forms a maelstrom-like cavity in the cylinder (Terasaka et al., 2011). The gas is sucked from an orifice on the bottom and then spouts out with the liquid from a hole situated at the top of the cylinder. Microbubbles of 10−50 μm diameter are generated by the centrifugal force imparted by the high-speed rotating liquid.

In the venturi-type microbubble generator [Figure 1.4 (b)], a liquid stream containing macrobubbles flows from the inlet of a venturi tube. The two-phase flow is accelerated through the throat of the venturi tube. The pressure changes rapidly and the microbubbles are formed by reducing the macrobubbles and/or by cavitation.

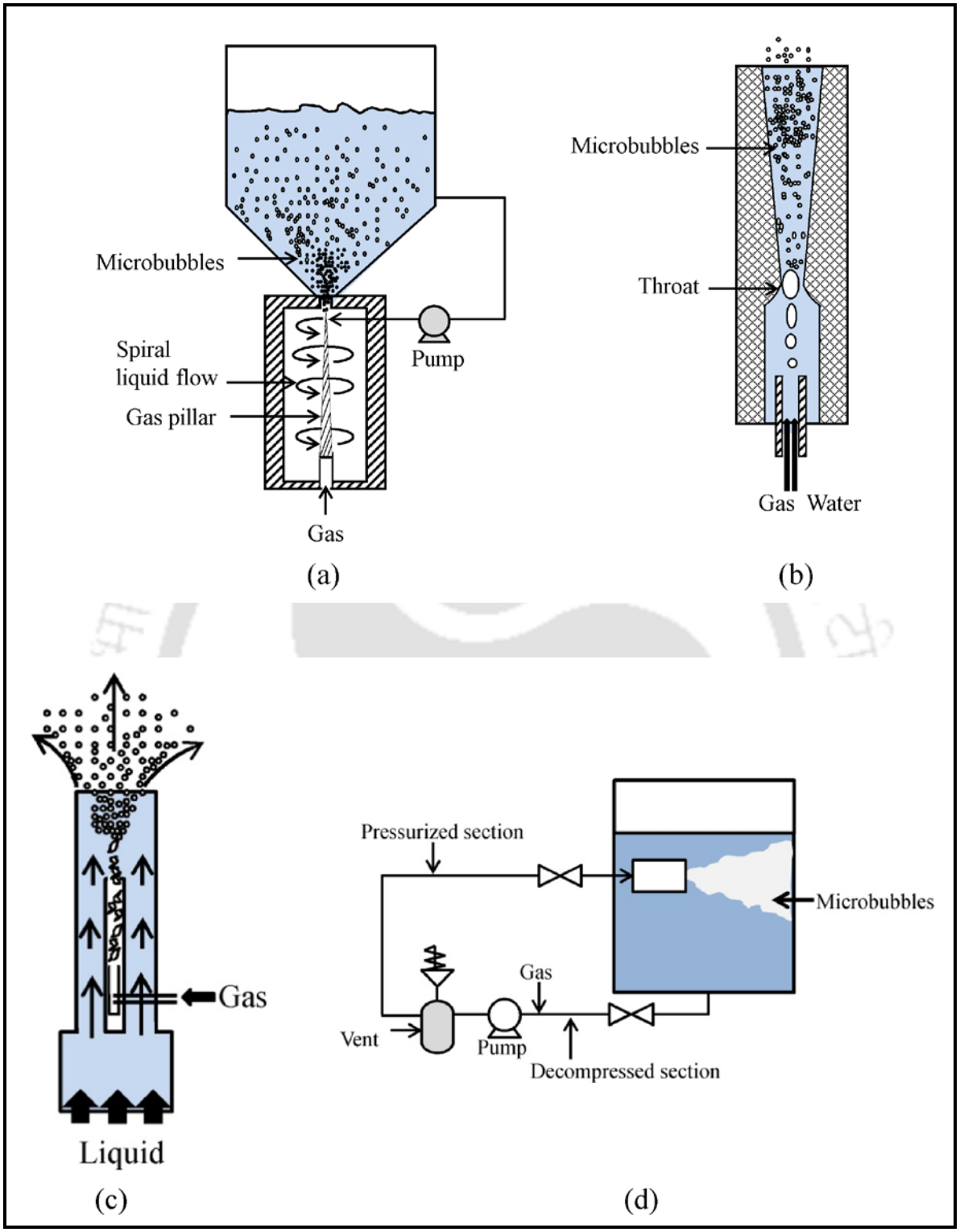

Figure 1.4 (a) Spiral-liquid-flow microbubble generator, (b) venturi-type microbubble generator, (c) ejector-type microbubble generator, and (d) pressurization–decompression type microbubble generator.

The ejector-type microbubble generator is shown in Figure 1.4 (c). The liquid flow-channels in the cylindrical generator are designed to shrink and stepwise enlarge. The gas is self-sucked from the most reduced pressure point, and reduced to a number of microbubbles by cavitation. The pressurization–decompression type of microbubble generator is shown in Figure 1.4 (d). The gas is dissolved in the liquid in a tank by pressurizing the gas–liquid mixture. When this supersaturated liquid is flashed using a reducing valve, the microbubbles are generated. The size and number of the microbubbles depend on the pressure and the decompression process. Terasaka et al. (2011) have reported that the spiral-liquid-flow and pressurization–decompression types of microbubble generators show high gas hold-up. However, the power requirement of the microbubble generators is high because of the power consumed by the pump, which is not required by the conventional gas distributors. Ikeura et al. (2011) have reported that the pressurization-decompression type of ozone microbubble generator produced smaller microbubbles, which were more effective for the decomposition of fenitrothion (a pesticide) due to better contact between ozone and the pesticide.

1.4 APPLICATIONS OF MICROBUBBLES

1.4.1 Applications of Ozone Microbubbles

Oxidation processes constitute a major step in the treatment of wastewater. The reaction of ozone with the pollutants in water is rather slow (Takić et al., 2008). The overall reaction rate can be affected by both the reaction kinetics and mass transfer (Zhou and Smith, 2000). Several advanced ozonation and catalytic ozonation processes have been attempted to render the use of ozone commercially attractive (Ikehata et al., 2008; Kasprzyk-Hordern et al., 2003). The mechanism of decomposition of ozone in water is presented in Table 1.3 (Beltrán, 2004; Kasprzyk-Hordern et al., 2003).

An important target in the ozonation process is to enhance the generation of hydroxyl radicals, which are very active oxidation species and more powerful than molecular ozone for oxidation. As mentioned in Section 1.2.5, it is believed that the significant increase in ion concentration around the shrinking gas–water interface helps generation of the free radicals (Takahashi et al., 2007). In recent times, a major application of microbubbles in wastewater treatment involves ozonation such as, decolorization (e.g. removal of dyestuff), degradation of pesticides and other harmful organic compounds, and removal of odor (e.g. residual ammonia). Some of the applications of ozone microbubble are given in Table 1.4.

Table 1.3 Mechanism of decomposition of ozone in pure water.

	Reaction	Rate constant
Initiation	$O_3 + OH^- \rightarrow HO_2\cdot + O_2^-\cdot$	70 $dm^3\ mol^{-1}\ s^{-1}$
Propagation	$HO_2\cdot \rightarrow O_2^-\cdot + H^+$	$7.9\times10^5\ s^{-1}$
	$O_2^-\cdot + H^+ \rightarrow HO_2\cdot$	$5\times10^{10}\ dm^3\ mol^{-1}\ s^{-1}$
	$O_3 + O_2^-\cdot \rightarrow O_3^-\cdot + O_2$	$1.6\times10^9\ dm^3\ mol^{-1}\ s^{-1}$
	$O_3^-\cdot + H^+ \rightarrow HO_3\cdot$	$5.2\times10^{10}\ dm^3\ mol^{-1}\ s^{-1}$
	$HO_3\cdot \rightarrow O_3^-\cdot + H^+$	$3.3\times10^2\ s^{-1}$
	$HO_3\cdot \rightarrow HO\cdot + O_2$	$1.1\times10^5\ s^{-1}$
	$O_3 + HO\cdot \rightarrow HO_4\cdot$	$2\times10^9\ dm^3\ mol^{-1}\ s^{-1}$
	$HO_4\cdot \rightarrow HO_2\cdot + O_2$	$2.8\times10^4\ s^{-1}$
Termination	$HO_4\cdot + HO_4\cdot \rightarrow H_2O_2 + 2O_3$	$5\times10^9\ dm^3\ mol^{-1}\ s^{-1}$
	$HO_4\cdot + HO_3\cdot \rightarrow H_2O_2 + O_2 + O_3$	$5\times10^9\ dm^3\ mol^{-1}\ s^{-1}$

Table 1.4 Use of ozone microbubbles in wastewater treatment.

Category of impurity	Type of impurity	Impurities for removal	Method of microbubble generation	Size of microbubble (μm)	% of removal	Time (min)	Reference
Soluble organics	Petroleum industrial wastewater	Benzene, toluene, ethylbenzene and xylenes	Electrostatic spraying	10−80	83	10	Walker et al. (2011)
Chlorinated organic compound	Underground water	Trichloroethylene	Air-shearing microbubble generator	10−30	100	125	Nakano et al. (2005)
Color	Textile wastewater	Reactive black 5 ($C_{26}H_{21}N_5O_{19}S_6.4Na$)	Spiral liquid flow microbubble generator	< 58	99	30	Chu et al. (2007b)
		Chemical Oxygen Demand	Spiral liquid flow microbubble generator	< 58	70	200	Chu et al. (2007a)
Decomposition of sludge	Sewage disposal plant	Phosphorus and nitrogen	Cascade type pressurization pump	50−70	50	60	Bando et al. (2008)
	Wastewater treatment plant	Sludge solubilization	Spiral liquid flow microbubble generator	< 58	80	20	Chu et al. (2008b)
Detergent/ photo resist stripping solvent	Semiconductor manufacturing industry	Dimethyl sulfoxide	Rotating flow microbubble generator	50*	70	10	Li et al. (2009)
Pesticide	Vegetables (Lettuce)	Residual fenitrothion	Decompression gas−water circulation	10* 40*	55 45	10 10	Ikeura et al. (2011)

*Mean bubble diameter

Microbubble-aided ozonation has been successfully attempted by several scientists. Ozone, by virtue of its strong oxidative power, is often used in disinfection (Khadre et al., 2009). Ozone is successful in inactivating bacteria, viruses and certain algae. The resistance of microorganisms follows the order: bacteria > viruses > cysts (Camel and Bermond, 1998). Table 1.5 gives the list of microorganisms, which have been successfully inactivated from wastewater.

Table 1.5 Disinfection of wastewater using microbubbles.

Microorganism sp.	Type of microbubble	Temperature (K)	Time (min)	Remarks	Reference
E. coli	O_3	297	–	Significant removal	Sumikura et al. (2007)
Bacillus subtilis	O_3	293	20	99% removal	Tsuge et al. (2009)
E. coli	O_2		60	No effect	
E. coli	CO_2	303	60	Significant removal	Kobayashi et al. (2009)
	N_2		60	No effect	
F. oxysporum f. sp. melonis	O_3	293	3	100% removal	Kobayashi et al. (2011)
P. carotovorum subsp. carotovorum	O_3	293	3	100% removal	Kobayashi et al. (2011)

1.4.2 Applications of Air and Oxygen Microbubbles

Increased transfer of oxygen to the liquid phase can enhance the biodegradation capabilities of microorganisms. Gas–liquid dispersions, such as foams, have been used to increase the

biodegradation of hydrocarbons (Ripley et al., 2002). Air microbubbles are often used to supply oxygen in aerobic biodegradation processes. Microbubbles can deliver oxygen to the rather inaccessible regions, and are more efficient than the conventional millibubbles (Kutty et al., 2010). Fresh microbubbles replace the oxygen-depleted bubbles, and the biodegradation continues effectively. Some works have been reported on the enhancement in the aerobic biodegradation of phenol (Michelsen et al., 1984), *p*-xylene (Jenkins et al., 1993), pentachlorophenol (Mulligan and Eftekhari, 2003), and trichloroethylene (Rothmel et al., 1998) using microbubbles. Michelsen et al. (1988) have developed a microbubble-based biodegradation system for treating hazardous wastes.

1.4.3 Removal of Fine Particles

The microbubble-based flotation method has been practiced in the processing of fine minerals (Yoon, 1993; Yoon et al., 1992). Li and Tsuge (2006b) have developed a separate induced air flotation system for the removal of fine kaolin dispersions in water. The microbubbles generated in their induced air flotation system had diameter in the range of 20−200 μm, and the average diameter was ~70 μm. The surface charge of the microbubbles and the particles played an important role in the separation.

Coagulants (e.g. alum) are added to reduce the electrostatic repulsion between the particles so that they can stick together and create flocs. Too much addition of alum decreases the zeta potential of the floc particles (Han and Dockko, 1998), which reduces the particle removal efficiency. Terasaka and Shinpo (2007) have developed a microbubble-based floatation system for removal of carbon particles (mean diameter = 1 μm) from wastewater. Various cationic, anionic and nonionic surfactants (viz. cetyltrimethylammonium bromide, sodium dodecyl sulphate and Tween 20) were added, depending on the charge requirements. Terasaka et al. (2008) have used microbubble flotation to recover iron oxide fine particles

(mean diameter = 4.5 μm) from a suspension containing small amounts of surfactants (viz. Tween 20 and sodium dodecyl sulphate).

1.4.4 Removal of Oil from Wastewater

Several methods such as gravity separation (with or without corrugated-plate interceptor), induced gas flotation, induced static flotation, and separation by hydrocyclone and centrifuge, are used for removing oil from wastewater. Rubio et al. (2002) have presented a review of the existing technologies for separating oil from wastewater. In the microbubble-based flotation of oil from wastewater, the oil droplets adhere to the surface of the bubbles, rise upward, and collect at the surface of water. On the surface, a frothy layer of oil and gas is formed, which is skimmed-off. Smaller microbubbles are more effective in separating the oil from water, which results in a drier froth and a very low skim volume. Flotation of the oil is promoted by decreasing the electrostatic repulsion between oil flocs and air bubbles (Gray et al., 1997). Thoma et al. (1999) have used the dissolved air flotation method to treat simulated produced waters that contained paraffins (e.g. octane and decane) and aromatic compounds. Al-Shamrani et al. (2002) have used the dissolution air floation method for separating oil from synthetic oily-wastewater, which was produced by emulsifying low concentrations of oil in water with a non-ionic surfactant (i.e. Span 20). Aluminum sulphate and four different cationic polyelectrolytes were used to destabilize the system.

Gotoh et al. (2006) have investigated the removal of oil from oil-polluted soil by air microbubbles. The separation of oil from high-concentration oil-in-water emulsion was significantly enhanced by the microbubble injection. About 70−80% of the oil droplets were successfully removed by flotation using the microbubbles. The oil-flotation was enhanced by the physical adsorption characteristics and a very low slip velocity of the microbubbles. Deng et al. (2011) have developed a T-tube dynamic state flotation device in which the

microbubbles were generated by using a porous polymeric membrane. The device had several bubble entry points situated at the lower part of the T-tube. This device could reduce the oil concentration from 38 to 12 g m^{-3}.

1.5 FUTURE PROSPECTS

During the past decade, several processes using the microbubbles have been commercialized for water treatment. Although rather new, this technology has a bright prospect. It is quite certain that the microbubbles will be at the center of various technologies to be used in the improvement of the aquatic environment. One major challenge in the microbubble technology is to reduce the power consumption, and use low-power methodologies without sacrificing the desired microbubble properties. The compression–decompression and the acoustic cavitation methods usually require high power consumption. New methods, such as fluidic oscillation, are promising in terms of lower power consumption.

Environmental hypoxia can be dramatically improved by air and oxygen microbubbles to the semi-closed water area. In addition, it is possible to use this technology for the protection against infectious diseases and sterilization of water used in bath. It can also be used in curbing infectious diseases where an antibiotic is not used. This can be a major step towards achieving a secure and safe society. A promising use of the microbubbles is in the treatment of wastewater released from the seafood processing plants. This wastewater contains blood, offal products, viscera, fins, fish heads, shells, skins and meat fines. Fats, oil, grease, and the microorganisms are among the most objectionable components from the seafood processing wastewater. Removal of these contaminants can significantly reduce the adverse impact of the seafood industries on adjacent water bodies such as rivers, lakes and oceans. Microbubbles can effectively remove these substances from wastewater.

Residual ammonia in the sewage from households is a major source of pungent odor. Ammonia can be removed from water by physical, biological and chemical methods. Chemical oxidation is effective when the amount of ammonia is low. Microbubble-aided ozonation can be a promising method for oxidation of ammonia by ozone. It has been reported by Kuo et al. (1997) that the reaction rate of ozone with ammonia increases as the pH is increased from 8 to 10. At pH 10, addition of hydrogen peroxide (i.e. peroxone oxidation) tremendously increases the rate constant. For wastewaters containing high amounts of ammonia, the peroxone process can be effective and economical.

The microbubbles may be effective in oxidizing the inorganic matters present in wastewater (e.g. by ozonation). One of the target applications is the removal of arsenic from water. Arsenic is found at low concentrations in natural water. The maximum permissible concentration of arsenic in drinking water has been set at 10 mg m^{-3} by the U. S. Environmental Protection Agency and the World Health Organization. Considerable amounts of arsenic are found in the water and soil of many countries (Mandal and Suzuki, 2002). In water, the most common valence states of arsenic are As(III) and As(V). In the pH range of 4 to 10, the predominant As(III) is neutral in charge, while As(V) is negatively charged. As(V) is generally more efficiently removed than As(III) in commonly practiced water treatment processes such as ion exchange, iron coagulation followed by microfiltration, and activated alumina adsorption. Hence, for drinking water supplies containing significant concentrations of As(III), preoxidation of As(III) to As(V) is mandatory for high arsenic removal. Chlorine, ferric chloride, potassium permanganate, ozone and hydrogen peroxide can perform this oxidation effectively. Therefore, oxidation using the ozone microbubbles can be an effective route for converting As(III) to As(V).

NOTATIONS

a	interfacial area per unit volume, m^{-1}
A_c	cross-sectional area of the column, m^2
c	concentration, mol m^{-3}
c^*	saturation concentration of the gas in water, mol m^{-3}
d	diameter of microbubble, m
d_{32}	Sauter mean diameter, m
D	diffusivity of gas in liquid, m^2 s^{-1}
D_b	translational diffusion coefficient of microbubble, m^2 s^{-1}
E	electrophoretic mobility, m^2 V^{-1} s^{-1}
g	acceleration due to gravity, m s^{-2}
H	Henry's law constant, Pa m^3 mol^{-1}
k_g	gas phase mass transfer coefficient, mol N^{-1} s^{-1}
K_g	overall gas-side mass transfer coefficient, mol N^{-1} s^{-1}
k_l	liquid phase mass transfer coefficient, m s^{-1}
K_l	overall liquid-side mass transfer coefficient, m s^{-1}
n	number of microbubbles
N_A	Avogadro's number, mol^{-1}
$\tilde{p}$	partial pressure of gas, Pa
p_g	gas pressure, Pa
p_l	liquid pressure, Pa
Q_g	volumetric gas flow rate, m^3 s^{-1}

R	gas constant, J mol^{-1} K^{-1}
t	time, s
T	temperature, K
u_b	rising velocity of microbubble, m s^{-1}
$\bar{u}_b$	average rising velocity of microbubbles, m s^{-1}
u_{sg}	superficial gas velocity, m s^{-1}
V_g	volume of the gas phase, m^3
V_l	volume of the liquid phase, m^3

Greek Letters

γ	surface tension of liquid, N m^{-1}
Δp	pressure difference between gas and liquid phases, Pa
$\Delta\rho$	density difference between the gas and liquid phases, kg m^{-3}
ε	dielectric constant of water
ε_0	permittivity of free space, C^2 J^{-1} m^{-1}
ε_g	fractional gas hold-up
μ	viscosity of liquid, Pa s
ρ_g	density of gas, kg m^{-3}
ρ_l	density of liquid, kg m^{-3}
ζ	zeta potential, V

Abbreviations

VGTR	volumetric transfer rate, kg m^{-3}
VOTR	volumetric oxygen transfer rate, kg m^{-3} s^{-1}

REFERENCES

Agarwal, A., Ng, W.J., Liu, Y., 2011. Principle and applications of microbubble and nanobubble technology for water treatment. Chemosphere 84, 1175−1180.

Ago, K., Nagasawa, K., Takita, J., Itano, R., Morii, N., Matsuda, K., Takahashi, K., 2005. Development of an aerobic cultivation system by using a microbubble aeration technology. J. Chem. Eng. Jpn. 38, 757−762.

Akita, K., Yoshida, F., 1973. Gas holdup and volumetric mass transfer coefficient in bubble columns. Ind. Eng. Chem. Process. Des. Dev. 12, 76−80.

Al-Shamrani, A.A., James, A., Xiao, H., 2002. Separation of oil from water by dissolved air flotation. Colloids Surf. A 209, 15−26.

ASCE, 2007. Measurement of Oxygen Transfer in Clean Water. ASCE/EWRI 2-06. ASCE, New York, USA.

Bando, Y., Yoshimatsu, T., Wang, Y., Yasuda, K., Sugie, T., Asai, T., 2008. Influence of micro-bubble on ozone-decomposition of excess sludge (in Japanese). Prog. Multiphase Flow Res. 3, 51−57.

Beltrán, F., 2004. Ozone Reaction Kinetics for Water and Wastewater Systems. CRC Press, Boca Raton, Florida, USA.

Berne, B.J., Pecora, R., 2000. Dynamic Light Scattering with Applications to Chemistry, Biology, and Physics. Dover Publications, New York, USA.

Bredwell, M.D., Worden, R.M., 1998. Mass-transfer properties of microbubbles. 1. experimental studies. Biotechnol. Prog. 14, 31−38.

Calderbank, H., Moo-young, M.B., 1961. The continuous phase heat and mass-transfer properties of dispersions. Chem. Eng. Sci. 16, 39−54.

Camel, V., Bermond, A., 1998. The use of ozone and associated oxidation processes in drinking water treatment. Water Res. 32, 3208−3222.

Chu, L.B., Xing, X., Yu, A., Zhou, Y., Sun, X., Jurcik, B., 2007a. Enhanced ozonation of simulated dyestuff wastewater by microbubbles. Chemosphere 68, 1854−1860.

Chu, L.B., Xing, X.H., Yu, A.F., Sun, X.L., Jurcik, B., 2007b. Enhanced ozonation of textile wastewater by microbubbles. In: Proceedings of the European Congress of Chemical Engineering (ECCE-6), 16−20 September, Copenhagen, Denmark, 1−7.

Chu, L.B., Xing, X.H., Yu, A.F., Sun, X.L., Jurcik, B., 2008a. Enhanced treatment of practical textile wastewater by microbubble ozonation. Process Saf. Environ. Prot. 86, 389−393.

Chu, L.B., Yan, S., Xing, X., Yu, A., Sun, X., Jurcik, B., 2008b. Enhanced sludge solubilization by microbubble ozonation. Chemosphere 72, 205−212.

Clift, R., Grace, J.R., Weber, M.E., 1978. Bubbles, Drops, and Particles. Academic Press, New York, USA.

Cussler, E.L., 1997. Diffusion Mass Transfer in Fluid Systems. Cambridge University Press, Cambridge, UK.

Deng, X., Xu, J., Wu, Y., Luo, D., 2011. Research on the technology of oil removal by dynamic state micro-bubbles flotation (in Chinese). Gongye Shuichuli 31, 89−102.

Ghosh, P., 2009. Colloid and Interface Science. PHI Learning, New Delhi, India.

Gotoh, Y., Serizawa, A., Eguchi, T., Tanaka, H., Izumi, M., 2006. Oil separation from oil polluted soil by microbubble injection and separation mechanisms (in Japanese). Jpn. J. Multiphase Flow 20, 39−49.

Gray, S.R., Harbour, P.J., Dixon, D.R., 1997. Effect of polyelectrolyte charge density and molecular weight on the flotation of oil in water emulsions. Colloids Surf. A 126, 85−95.

Guidi, F., Vos, H.J., Mori, R., DeJong, N., Tortoli, P., 2010. Microbubble characterization through acoustically induced deflation. IEEE Trans. Ultrason. Ferroelectr. Freq. Control 57, 193−202.

Han, B.M., Dockko, S., 1998. Zeta potential measurement of bubbles in DAF process. Water Supply 2, 461−466.

Hasegawa, H., Kataoka, H., Asano, K., 2009. Effect of electrical potential of microbubbles on ozone dissolution. J. Phys. Confer. Ser. 147, 12024−12032.

Hofmeier, U., Yaminsky, V.V., Christenson, H.K., 1995. Observations of solute effects on bubble formation. J. Colloid Interface Sci. 174, 199−201.

Hosokawa, S., Tanaka, K., Tomiyama, A., Maeda, Y., Yamaguchi, S., Ito, Y., 2009. Measurement of microbubbles generated by a pressurized dissolution method. J. Phys. Confer. Ser. 147, 012016−012026.

Ikehata, K., Gamal El-Din, M., Snyder, S.A., 2008. Ozonation and advanced oxidation treatment of emerging organic pollutants in water and wastewater. Ozone Sci. Eng. 30, 21−26.

Ikeura, H., Kobayashi, F., Tamaki, M., 2011. Removal of residual pesticide, fenitrothion, in vegetables by using ozone microbubbles generated by different methods. J. Food Eng. 103, 345−349.

Jauregi, P., Varley, J., 1998. Colloidal gas aphrons: a novel approach to protein recovery. Biotechnol. Bioeng. 59, 471−481.

Jenkins, K.B., Michelsen, D.L., Novak, J.T., 1993. Application of oxygen microbubbles for in situ biodegradation of *p*-xylene-contaminated groundwater in a soil column. Biotechnol. Prog. 9, 394−400.

Johnson, P.N., Davis, R.A., 1996. Diffusivity of ozone in water. J. Chem. Eng. Data 41, 1485−1487.

Kasprzyk-Hordern, B., Ziółek, M., Nawrocki, J., 2003. Catalytic ozonation and methods of enhancing molecular ozone reactions in water treatment. Appl. Catal. B 46, 639−669.

Kaster, J.A., Michelsen, D.L., Velander, W.H., 1990. Increased oxygen transfer in a yeast fermentation using a microbubble dispersion. Appl. Biochem. Biotechnol. 24−25, 469−484.

Katiyar, A., Sarkar, K., 2010. Stability analysis of an encapsulated microbubble against gas diffusion. J. Colloid Interface Sci. 343, 42−47.

Kawahara, A., Sadatomi, M., Matsuyama, F., Matsuura, H., Tominaga, M., Noguchi, M., 2009. Prediction of micro-bubble dissolution characteristics in water and seawater. Exp. Therm. Fluid Sci. 33, 883−894.

Khadre, M.A., Yousef, A.E., Kim, J.G., 2009. Microbial aspects of ozone applications in food: a review. J. Food Sci. 66, 1242−1252.

Kobayashi, F., Hayata, Y., Ikeura, H., Tamaki, M., Muto, N., Osajima, Y., 2009. Inactivation of *Escherichia coli* by CO_2 microbubbles at a lower pressure and near room temperature. Trans. ASABE 52, 1621−1626.

Kobayashi, F., Ikeura, H., Ohsato, S., Goto, T., Tamaki, M., 2011. Disinfection using ozone microbubbles to inactivate *Fusarium oxysporum f.* sp. melonis and *Pectobacterium carotovorum* subsp. *carotovorum*. Crop Prot. 30, 1514−1518.

Koide, K., Hayashi, T., Sumino, K., Iwamoto, S., 1976. Mass transfer from single bubbles in aqueous solutions of surfactants. Chem. Eng. Sci. 31, 963−967.

Koide, K., Sato, H., Iwamoto, S., 1983. Gas holdup and volumetric liquid-phase mass transfer coefficient in bubble column with draught tube and with gas dispersion into annulus. J. Chem. Eng. Jpn. 16, 407−413.

Kukizaki, M., Baba, Y., 2008. Effect of surfactant type on microbubble formation behavior using Shirasu porous glass (SPG) membranes. Colloids Surf. A 326, 129−137.

Kuo, C.H., Yuan, F., Hill, D.O., 1997. Kinetics of oxidation of ammonia in solutions containing ozone with or without hydrogen peroxide. Ind. Eng. Chem. Res. 36, 4108−4113.

Kurup, N., Naik, P., 2010. Microbubbles: a novel delivery system. J. Pharmacol. Res. Health Care 2, 228−234.

Kutty, S.R.M., Winarto, F.E.W., Gilani, S.I.U., Anizam, A.A., Karimah, W.W.Z., Isa, M.H., 2010. Degradation of organic matter using a submerged microbubble diffuser in a biological wastewater treatment system, in: Waste Management and the Environment V. WIT Press, Southampton, UK, pp. 415−423.

Lee, S.J., Kim, S., 2005. Simultaneous measurement of size and velocity of microbubbles moving in an opaque tube using an X-ray particle tracking velocimetry technique. Exp. Fluids 39, 490−495.

Li, P., 2006. Development of Advanced Water Treatment Technology Using Microbubbles. Ph.D Thesis, School of Science for Open and Environmental Systems, Keio University, Kanagawa, Japan.

Li, P., Takahashi, M., Chiba, K., 2009. Degradation of phenol by the collapse of microbubbles. Chemosphere 75, 1371−1375.

Li, P., Tsuge, H., 2006a. Water treatment by induced air flotation using microbubbles. J. Chem. Eng. Jpn. 39, 896−903.

Li, P., Tsuge, H., 2006b. Ozone transfer in a new gas-induced contactor with microbubbles. J. Chem. Eng. Jpn. 39, 1213−1220.

Liu, S., Wang, Q., Ma, H., Huang, P., Li, J., Takashige, K., 2010. Effect of micro-bubbles on coagulation flotation process of dyeing wastewater. Sep. Purif. Technol. 71, 337−346.

Mandal, B.K., Suzuki, K.T., 2002. Arsenic round the world: a review. Talanta 58, 201−235.

Matsuo, K., Maeda, K., Ohnari, H., Tsunami, Y., 2006. Water purification of a dam lake using microbubble technology (in Japanese). Prog. Multiphase Flow Res. 1, 279−286.

Michelsen, D.L., Smith, J.W., Suggs, J.A., 1988. Use of colloidal gas aphrons for in-situ biodegradation of contaminated water, in: Fourteenth Annual Research Symposium. Cincinnati, Ohio, USA, pp. 203−217.

Michelsen, D.L., Wallis, D.A., Sebba, F., 1984. In-situ biological oxidation of hazardous organics. Env. Prog. 3, 103−107.

Motarjemi, M., Jameson, G.J., 1978. Mass transfer from very samll bubbles−the optimum bubble size for aeration. Chem. Eng. Sci. 33, 1415−1423.

Mulligan, C.N., Eftekhari, F., 2003. Remediation with surfactant foam of PCP-contaminated soil. Eng. Geol. 70, 269−279.

Nakano, Y., Nishijima, W., Okata, M., Fukagawa, K., 2005. Microbubble-based groundwater treatment. Groundwater treatment technology with use of activated carbon-based solvent regeneration and ozone (in Japanese). Environ. Solution. Technol. 4, 11−16.

Nedeltchev, S., Jordan, U., Schumpe, A., 2006a. Correction of the penetration theory applied to the prediction of $k_L a$ in a bubble column with organic liquids. Chem. Eng. Technol. 29, 1113−1117.

Nedeltchev, S., Jordan, U., Schumpe, A., 2006b. A new correction factor for theoretical prediction of mass transfer coefficients in bubble columns. J. Chem. Eng. Jpn. 39, 1237−1242.

Ohnari, H., Saga, T., Watanabe, K., Maeda, K., Matsuo, K., 1999. High functional characteristics of microbubbles and water purification (in Japanese). Resour. Process 46, 238−244.

Ohnari, H., Takahashi, M., Himuro, S., Shakutsui, S., 2002. Roles of microbubble technique in multiphase flow (in Japanese). Jpn. J. Multiphase Flow 16, 130−137.

Pelssers, E.G.M., Stuart, M.A.C., Fleer, G.J., 1990. Single particle optical sizing (SPOS). I. Design of an improved SPOS instrument and application to stable dispersions. J. Colloid Interface Sci. 137, 350−361.

Qu, X., Wang, L., Karakashev, S.I., Nguyen, A.V., 2009. Anomalous thickness variation of the foam films stabilized by weak non-ionic surfactants. J. Colloid Interface Sci. 337, 538−547.

Ripley, M.B., Harrison, A.B., Betts, W.B., Dart, R.K., 2002. Mechanisms for enhanced biodegradation of petroleum hydrocarbons by a microbe-colonized gas−liquid foam. J. Appl. Microbiol. 92, 22−31.

Rothmel, R.K., Peters, R.W., Martin, E., Deflaun, M.F., 1998. Surfactant foam/bioaugmentation technology for in situ treatment of TCE-DNAPLs. Env. Sci Technol. 32, 1667−1675.

Rubio, J., Souza, M.L., Smith, R.W., 2002. Overview of flotation as a wastewater treatment technique. Miner. Eng. 15, 139−155.

Sadatomi, M., Kawahara, A., Kano, K., Ohtomo, A., 2005. Performance of a new micro-bubble generator with a spherical body in a flowing water tube. Exp. Therm. Fluid Sci. 29, 615−623.

Sato, Y., Sadatomi, M., Sekoguchi, K., 1981. Momentum and heat transfer in two-phase bubble flow–I. Int. J. Multiphase Flow 7, 167−177.

Sebba, F., 1988. Foams and Biliquid Foams (Aphrons). John Wiley and Sons, New York, USA.

Sumikura, M., Hidaka, M., Murakami, H., Nobutomo, Y., Murakami, T., 2007. Ozone micro-bubble disinfection method for wastewater reuse system. Water Sci. Technol. 56, 53−61.

Takahashi, M., 2005a. Zeta potential of microbubbles in aqueous solutions: electrical properties of the gas–water interface. J. Phys. Chem. B 109, 21858−21864.

Takahashi, M., 2005b. Water treatment technique based on microbubbles (in Japanese). Environ. Solution. Technol. 4, 6−10.

Takahashi, M., 2009. Base and technological application of micro-bubble and nano-bubble (in Japanese). Mater. Integr. 22, 2−19.

Takahashi, M., 2010. Water treatment based on microbubble technology (in Japanese). Bull. Soc. Sea Water Sci. Jpn. 64, 19−23.

Takahashi, M., Chiba, K., Li, P., 2007. Free-radical generation from collapsing microbubbles in the absence of a dynamic stimulus. J. Phys. Chem. B 111, 1343−1347.

Takić, L., Veljković, V., Pejanović, S., 2008. Ozone absorption in raw waters. Chem. Ind. Chem. Eng. Q 14, 35−38.

Terasaka, K., Aoki, S., Kobayashi, D., 2008. Removal of iron oxide fine particles from waste water using microbubble flotation (in Japanese). Prog. Multiphase Flow Res. 3, 43−50.

Terasaka, K., Hirabayashi, A., Nishino, T., Fujioka, S., Kobayashi, D., 2011. Development of microbubble aerator for waste water treatment using aerobic activated sludge. Chem. Eng. Sci. 66, 3172−3179.

Terasaka, K., Shinpo, Y., 2007. Separation of fine particles suspended in water using microbubble flotation (in Japanese). Jpn. J. Multiphase Flow 21, 77−83.

Thoma, J., Bowen, M.L., Hollensworth, D., 1999. Dissolved air precipitation/solvent sublation for oil-field produced water treatment. Sep. Purif. Technol. 16, 101−107.

Tsuge, H., 2010. Fundamentals of microbubbles and nanobubbles (in Japanese). Bull. Soc. Sea Water Sci. Jpn. 64, 4−10.

Tsuge, H., Li, P., Shimatani, N., Shimamura, Y., Nakata, H., Ohira, M., 2009. Fundamental study on disinfection effect of microbubbles (in Japanese). Kagaku Kogaku Ronbunshu 35, 548−552.

Van'tRiet, K., 1979. Review of measuring methods and results in nonviscous gas-liquid mass transfer in stirred vessels. Ind. Eng. Chem. Process. Des. Dev. 18, 357−363.

Walker, A.B., Tsouris, C., Depaoli, D., Klasson, K.T., 2001. Ozonation of soluble organics in aqueous solutions using microbubbles. Ozone Sci. Eng. 23, 77−87.

Walker, A.B., Tsouris, C., Depaoli, D.W., Klasson, K.T., 2011. Ozonation of soluble organics in aqueous solutions using microbubbles. Ozone Sci. Eng. 23, 77−87.

Waslo, S., Gal-Or, B., 1971. Boundary layer theory for mass and heat transfer in clouds of moving drops, bubbles or solid particles. Chem. Eng. Sci. 26, 829−838.

Xu, Q., Nakajima, M., Liu, Z., Shiina, T., 2011. Biosurfactants for microbubble preparation and application. Int. J. Mol. Sci. 12, 462−75.

Yasuda, K., Wang, Y., Haneda, K., Naito, T., Bando, Y., Takeyama, T., Kawase, Y., 2010. Development of airlift bubble column dispersed with micro-bubbles. Can. J. Chem. Eng. 88, 518−522.

Yoon, R.H., 1993. Microbubble flotation. Miner. Eng. 6, 619−630.

Yoon, R.H., Adel, G.T., Luttrell, G.H., 1992. Apparatus and process for the separation of hydrophobic and hydrophilic particles using microbubble column flotation together with a process and apparatus for generation of microbubbles. Patent No. US5397001A.

Yoon, R.H., Yordan, J.L., 1986. Zeta-potential measurements on microbubbles generated using various surfactants. J. Colloid Interface Sci. 113, 430−438.

Zhou, H.D., Smith, D.W., 2000. Ozone mass transfer in water and wastewater treatment: experimental observations using a 2D laser particle dynamics analyzer. Water Res. 34, 909−921.

CHAPTER 2

BACKGROUND AND OBJECTIVES OF RESEARCH

CHAPTER 2

BACKGROUND AND OBJECTIVES OF RESEARCH

With a brief review of the literature, this chapter presents the outcomes of various research works so as to identify some promising areas of research that will be addressed in this thesis. The state-of-the-art has been presented for the removal of ammonia, arsenic, and dyestuffs using ozone. The mechanism and method of detection of hydroxyl radicals generated from ozone has been discussed. The scope and objective of the present work are also highlighted in this chapter.

2.1 STATE-OF-THE-ART

2.1.1 Removal of Ammonia

2.1.1.1 Literature Survey

Ammonia is present in variable concentrations in surface and ground water. The presence of ammonia in water is undesirable due to several reasons. Ammonia is rapidly oxidized by bacteria to nitrite and nitrate, thereby consuming oxygen dissolved in water. Ammonia is a source of nitrogen, which is a nutrient for algae and other forms of plant life, and thus contributes to eutrophication (Huang et al., 2008). The total ammonia-content of water is the sum of that present as NH_4^+ (at low pH) and that as NH_3 (at high pH). Un-ionized ammonia (viz. NH_3) is the more toxic form, because it is a neutral molecule, and thus, it is able to diffuse across the epithelial membranes of aquatic organisms much more readily than the charged ammonium ion. Ammonia can block oxygen transfer in the gills of fish. Fish suffering from ammonia poisoning appears sluggish, and comes to the surface of water gasping for air. In marine environments, the safe level of ammonia is below 1 mg dm^{-3} (Udeh, 2004). The presence of ammonia reduces the efficiency of common water purification

methods, such as chlorination, because a part of chlorine is consumed by ammonia. In addition, ammonia is a major source of undesirable odor in sewage and wastewater.

The conventional methods of removal of ammonia from wastewater are biological denitrification, stripping, ion exchange, break-point chlorination and chemical precipitation (Adams, 1974; Delwiche, 1981). Some of the newer methods are based on photocatalytic and electrochemical oxidation (Kim et al., 2006; Wang et al., 1994; Zhu et al., 2005). Each of these methods is applicable under its own limitation. For example, the biological denitrification process includes a series of reactors such as nitrification tank, denitrification tank, BOD decomposition tank and solid–liquid separation tank (Ruiz et al., 2003). The bacteria used for this process are very sensitive and cannot withstand a wide range of pH, temperature, halogen compounds, cyanides and heavy metals present in the ammonia-containing water. The low nitrogen loading rate is also another limitation of this process (Tramper and Grootjen, 1986). The air-stripping method creates additional air pollution when ammonia is converted from liquid to gas (Obaid-ur-Rehman and Beg, 1990). Besides this, it is applicable for high ammonia concentrations (~1000 mg dm^{-3}), and lacks in efficiency for low ammonia concentrations. Although breakpoint chlorination is widely used for ammonia removal, large amounts of chlorine are required. Also, after the oxidation process, the unused chlorine remains in water, which requires further separation (Pressley et al., 1970).

Use of ozone is a well-known method for the oxidation of ammonia. The reaction of ammonium salts with ozone can be expressed as (Lin and Yen, 1996; Singer and Zilli, 1975)

$$NH_4^+ + 4O_3 \rightarrow NO_3^- + 4O_2 + H_2O + 2H^+ \qquad (2.1)$$

The lifetime of ozone in water is short (the half-life is ~15 minutes at 298 K at pH 7) (Rakness, 2005), and its rate of reaction with ammonia is slow (Haag, 1984). Several works have been reported on oxidation of ammonia by ozone millibubbles (Haag, 1984; Hoigné and Bader, 1978; Kuo et al., 1997; Lin and Wu, 1996; Lin and Yen, 1996, 1997; Singer and

Zilli, 1975; Tanaka and Matsumura, 2002, 2003; Yang et al., 1999, 2000). Ozone is unstable in water and undergoes self-decomposition reactions. The decay of ozone in natural water follows first-order kinetics. The mechanism and the kinetics of the ozone decomposition have been investigated in numerous studies (Beltrán, 2004; von Gunten, 2003). During the decomposition of ozone, the generation of hydroxyl radicals (·OH) is an advantage, as ·OH is a more powerful oxidant than ozone. The use of microbubbles significantly increases the efficiency of the ozonation process due to the larger gas−liquid interfacial area, slow rising velocity of the microbubbles, less ozone requirement, and generation of hydroxyl radicals (Chu et al., 2008; Takahashi et al., 2007).

2.1.1.2 Scope for Research

In recent years, ozone microbubbles have been extensively used for water treatment. The use of microbubbles significantly increases the efficiency of the ozonation process due to larger gas–liquid interfacial area, slow rising velocity, smaller amount of ozone requirement, and generation of hydroxyl radicals. So far, hardly any work has been reported in the literature on the removal of ammonia from water using the microbubble technology. The effects of ozone feed rate and pH of the aqueous medium on the rate of ammonia oxidation need to be tested by using a reactor connected to a microbubble generator. Oxygen is the most widely available material for oxidation. The capability of oxygen microbubbles on the oxidation of ammonia needs to be studied. The mechanism of oxidation of ammonia by microbubbles of these gases has to be investigated in details. The catalytic effect of bromide on ozonation efficiency needs to be studied. In addition, the rate of transfer of ozone to the aqueous phase needs to be determined.

2.1.2 Removal of Arsenic

2.1.2.1 Literature Survey

Arsenic is one of the most toxic elements found on the earth's crust. It dissolves or disperses in groundwater by various mechanisms. The average concentration of arsenic in igneous and sedimentary rocks is 2 mg kg^{-1} (Mandal and Suzuki, 2002). Arsenic exists in four oxidation states, i.e. −3 (Arsenide), 0 (elemental or metallic arsenic), +3 (arsenite) and +5 (arsenate). The arsenide and the elemental oxidation states of arsenic are rare in the environment. The most common forms of arsenic found in water and environment are arsenious acids (i.e. H_3AsO_3 and $H_3AsO_3^{2-}$), arsenic acids (i.e. H_3AsO_4, $H_3AsO_4^-$ and $H_3AsO_4^{2-}$), arsenites, arsenates, methylarsenic acid, dimethylarsenic acid, and arsine (Smedley et al., 2012). Pentavalent arsenic [viz. As(V) or arsenate] and trivalent arsenic [viz. As(III) or arsenite] are commonly found in surface and ground water as well as in soils and sediments. Different forms of inorganic and organic arsenic species enter into the human body mainly through food and water. Many acute and long-term effects of arsenic on human being have been studied (DeSesso et al., 1998; Jain and Ali, 2000; Juárez-Reyes et al., 2009; Naraharisetti et al., 2008; Petrick et al., 2000). It has been reported that the soluble inorganic arsenicals are more toxic than their organic counterparts, and As(III) is more toxic than As(V) (Mass et al., 2001). In cells, arsenate is reduced to arsenite, which may undergo a Fenton reaction to produce reactive oxygen species. Therefore, WHO has suggested a provisional upper limit of 0.01 mg dm^{-3} arsenic in drinking water (Mohan and Pittman Jr., 2007). However, the acceptable upper limit of arsenic in different countries varies from 0.01 to 0.05 mg dm^{-3} (e.g. 0.01 mg dm^{-3} in India and 0.05 mg dm^{-3} in Bangladesh) (Karim, 2000).

The occurrence of different forms of arsenite and arsenate depends on the redox conditions in the subsurface environment and pH (Mohan and Pittman Jr., 2007). The oxidation of different mineral species present in soil allows arsenic to become soluble and

enter into the surrounding environment through water (Robertson, 1989). The widely used removal technology of arsenic includes anion exchange, adsorption, reverse osmosis, modified coagulation/filtration, modified lime softening and oxidation/filtration. Oxidation of As(III) to As(V) followed by removal of As(V) is a suitable technology in which various chemical oxidants such as chlorine dioxide, sodium hypochlorite, monochloroamine, potassium permanganate (Ghurye and Clifford, 2001, 2004; Lee et al., 2011), manganese oxide (Driehaus et al., 1995; Nishimura and Umetsu, 2001), potassium ferrate (Fan et al., 2002), ozone (Kim and Nriagu, 2000), and hydrogen peroxide (Leupin and Hug, 2005) have been used. The reaction of these chemical oxidants with As(III) is given in Table 2.1. Some scientists have used photochemical oxidation using UV light along with chemical oxidant for generation of radicals which assist the oxidation of As(III) (Neppolian et al., 2008; Yoon et al., 2008).

The major advantage of pre-oxidation is that, As(V) thus produced has a higher adsorption efficiency than As(III). The dominant species of As(III) up to pH 8 is the nonionic H_3AsO_3, which is not adsorbed strongly to the mineral surface as compared to As(V). Therefore, removal of As(III) by adsorption is more difficult (Kinniburgh and Smedley, 2000). In recent times, adsorption has been widely used in the forms of biological materials, mineral oxides, activated carbons, polymeric resins, and many other low cost adsorbents, which are very effective in removing both As(III) and As(V) (Mohan and Pittman Jr., 2007). Many biological materials, mineral oxides, activated carbons, polymeric resins, and other low cost adsorbents have been developed, which are very effective in removing As(V) (Mandal and Suzuki, 2002; Mohan and Pittman Jr., 2007; Robertson, 1989). Several types of activated carbons have been prepared and studied for removal of arsenic from wastewater (Chuang et al., 2005; Gu et al., 2005; Huang and Fu, 1984). However, activated carbons impregnated with a metal (e.g. iron, zirconium, copper and silver) are more promising for arsenic removal

as compared to untreated activated carbon (Daus et al., 2004; Gu et al., 2005; Rajakovic, 1992).

Table 2.1 Reactions of As(III) with various chemical oxidants.

Reactions	References
Manganese(III) oxide: $H_3AsO_3 + 2MnOOH + 2H^+ \Leftrightarrow HAsO_4^{2-} + 2Mn^{2+} + 3H_2O$	Driehaus et al. (1995)
Sodium hypochlorite: $H_3AsO_3 + NaClO \rightarrow H_2AsO_4^- + Na^+ + Cl^- + H^+$	Ghurye and Clifford (2001)
Potassium permanganate: $3H_3AsO_3 + 2MnO_4^- \rightarrow 3H_2AsO_4^- + 2MnO_2 + H_2O + H^+$	Lee et al. (2011); Ghurye and Clifford (2001)
Chlorine dioxide: $H_3AsO_3 + 2ClO_2 + H_2O \rightarrow H_2AsO_4^- + 2ClO_2^- + 3H^+$ $5H_3AsO_3 + 2ClO_2 + H_2O \rightarrow 5H_2AsO_4^- + 2Cl^- + 7H^+$	Ghurye and Clifford (2001)
Monochloroamine: $H_3AsO_3 + NH_2Cl + H_2O \rightarrow HAsO_4^{2-} + NH_4^+ + Cl^- + 2H^+$	Ghurye and Clifford (2001)
Manganese(II) and ozone: $Mn^{2+} + O_3 + H_2O \rightarrow MnO_2 + O_2 + 2H^+$ $2MnO_2 + 3O_3 + H_2O \rightarrow 2MnO_4^- + 3O_2 + 2H^+$ $Mn^{3+} + H_3AsO_4 \rightarrow MnAsO_4 + 3H^+$	Nishimura and Umetsu (2001)
Manganese(IV) oxide: $H_3AsO_3 + MnO_2 + 2H^+ \Leftrightarrow H_3AsO_4 + Mn^{2+} + H_2O$	Manning et al. (2002)
Potassium ferrate: $3ClO^- + 2Fe(OH)_3(H_2O)_3 + 4K^+ + 4OH^- \rightarrow 3Cl^- + 2K_2FeO_4 + 11H_2O$ $3H_2AsO_3^- + 2FeO_4^{2-} + 5H_2O \rightarrow 3H_2AsO_4^- + 2Fe(OH)_3 + 4OH^-$ $3HAsO_3^{2-} + 2FeO_4^{2-} + 5H_2O \rightarrow 3HAsO_4^{2-} + 2Fe(OH)_3 + 4OH^-$	Fan et al. (2002)

Several works have reported the adsorption of As(III) and As(V) on zirconium-loaded resins (Balaji et al., 2005; Suzuki et al., 2000; Zhu and Jyo, 2001), zirconium-loaded activated carbons (Daus et al., 2004; Peräiniemi et al., 1994) and zirconium nanoparticles (Sandoval et al., 2011). However, the methods of preparation of these resins, activated carbons, and nanoparticles, are not very easy.

2.1.2.2 Scope for Research

A critical review of the literature shows that very few studies have been reported on the use of ozone for oxidizing arsenite. The ozonation of arsenic using microbubbles is a promising technology. The effects of initial arsenic concentration, ozone generation rate, and solution pH on the efficiency of the ozonation system should be studied. The role of hydroxyl radicals should be investigated. In addition, the effect of carbonate ion radicals on ozonation of As(III) should be studied. The kinetics of oxidation of As(III) with ozone should be studied and the kinetic parameters need to be determined.

Since this work aims for developing a complete method for the removal of arsenic, the adsorption of As(V) on solid adsorbents should be studied. Zirconium-based adsorbents may be efficient and cost effective for the adsorption of As(V). These adsorbents need to be prepared using simple methods. Detailed characterization of these adsorbents has to be carried out. Besides this, the kinetics and mechanism of adsorption As(V) on these adsorbents should be studied at various concentrations of As(V). The experimental data need to be enunciated by various adsorption isotherms (e.g. Langmuir, Freundlich and Redlich–Peterson isotherms).

2.1.3 Removal of Dyestuff

2.1.3.1 Literature Survey

Cationic dyes are widely used in textile, tannery, food, paper and pulp, printing, cosmetics, plastic, pharmaceuticals, and dye industries (Srivastava et al., 2004). Among the various cationic dyes, Brilliant Green (BG, $C_{23}H_{26}N_2O$) is extensively used as a biocide, food coloring agent, food additive, medical disinfectant, and as a colorant in silk, wool, jute, leather, cotton and paper (Culp and Beland, 1996). It is a triphenylmethane dye, available in crystalline solid form, which is also known as Malachite Green, Basic Green-4 and Diamond Green-B. It is prepared by condensing benzaldehyde and dimethylaniline in 1:2 molar ratio in the presence of concentrated sulfuric acid or zinc chloride (Srivastava et al., 2004). It is available in the form of chloride or oxalate salt. The ionization constant (pKa) of BG is 6.90. It is 100% ionized at pH 4, 50% at pH 6.9, 25% at 7.4, and not ionized at pH > 10 (Goldacre and Philips, 1949). This dye, like other triphenylemethanes, can exist in two ionic forms, i.e. the dye salt and the carbinol or pseudobase. Due to its low cost, BG is extensively used for the control of fungal infections and ectoparasites in fish farming (Halme et al., 2007). In the past few decades, many health risks (e.g. its effects on the immune system, reproductive system as well as its genotoxic and carcinogenic properties) have been identified (Culp and Beland, 1996; Fernandes et al., 1991). Therefore, many processes such as biological (Ledakowicz et al., 2001), membrane based separation (Chakraborty et al., 2005; Purkait et al., 2006), adsorption (Purkait et al., 2005), photocatalysis (Chen and Lu, 2007), electro-Fenton (Oturan et al., 2008), Fenton (Gutowska et al., 2007), Fenton coupled with H_2O_2 photolysis (Modirshahla and Behnajady, 2006), and ozonation (Turhan and Turgut, 2009; Zhou et al., 2012) have been used for removal of this dye from wastewater.

Due to the stable chemical structure of BG, it is very difficult to remove it by using physical and biological processes (Voncina and Majcen-Le-Marechal, 2003). Therefore,

advanced oxidation processes are more efficient for treating the wastewater containing BG (Baek et al., 2010; Behnajady et al., 2008). Amongst all the oxidation methods, ozonation has attracted a lot of attention due to its high reactivity towards the organic pollutants (Meriç et al., 2005). Generally the ozonation processes have been carried out either in bubble column reactors or in small flasks in lab-scale experiments where ozone has been used as a dispersion of millibubbles. The bubble columns need a considerable amount of ozone, which requires high energy consumption. The excess ozone passed into the column remains unused, which is finally released into the atmosphere in either destructed or undestructed form. Therefore, a better gas−liquid contactor is required that can perform rapid decolorization and also decrease the ozone loss. Microbubbles can offer an alternative to millibubbles, which are conventionally used in the bubble column reactors.

2.1.3.2 Scope for Research

The oxidation of BG using ozone has been reported in a few works. However, in the absence of an efficient ozone contactor, the requirement of ozone is very high and the process is not cost effective. The existing ozonation systems are not efficient for commercial use. Partial oxidation of the dye by ozone may create organic intermediates, which might be more hazardous in nature than the dye. Ozonation of BG using the microbubbles might be a promising process. Hardly any work has been reported in the literature on decolorization of aqueous BG solutions using ozone microbubbles. Thus, the same should be studied in a microbubble ozonation system. This work would consist of the variation of concentration of BG with time, detection of the intermediate degradation products of BG, reaction mechanism, and the kinetics of the reaction. The degradation mechanism should be formulated by using the data constructed from the gas chromatography–mass spectrometry (GC–MS) and Fourier

transform infrared spectroscopy (FTIR) analyses. The TOC of the dye water should be analyzed to determine the extent of mineralization.

2.1.4 Measurement of Hydroxyl Radical Concentration

2.1.4.1 Literature Survey

The high reactivity of ozone towards many organic and inorganic pollutants, its affordability, and self-decomposition to oxygen make it more suitable than many other oxidants (Loeb et al., 2012). Ozone can directly participate in oxidation as well. Therefore, the oxidation of a compound by ozone may occur via two mechanisms. The reaction via molecular ozone is considered as the direct reaction, and when ozone reacts in the form of hydroxyl radical, it is termed indirect reaction (von Gunten, 2003).

The use of hydroxyl radicals in oxidation is known as Advanced Oxidation Process, which is an emerging method in the water and wastewater treatment (Legrini et al., 1993; Singer and Reckhow, 1999). The reaction with molecular ozone is selective to certain organic and inorganic compounds such as the compounds having C = C bonds, and the functional groups containing sulfur, phosphorous, nitrogen and oxygen (Oppenländer, 2003). The hydroxyl radicals readily react with many organic and inorganic compounds through hydrogen abstraction, radical–radical reactions, electrophilic addition and electron transfer. This often leads to the complete mineralization of the pollutant compounds (Ikehata et al., 2006; Oppenländer, 2003).

Prediction of the concentration of the hydroxyl radicals generated from ozone is important for determining the rate constant of the reaction. The concentration of ozone can be measured by electrochemical, optical, spectrophotometric or colorimetric techniques (Langlais et al., 1999). But the quantitative measurement of the hydroxyl radicals is rather difficult due to its low concentration. A few computer models have been developed for the

prediction of hydroxyl radical concentration (Chelkowska et al., 1992). Elovitz and von Gunten (1999) have developed an indirect method by using a probe compound (e.g. *p*-chlorobenzoic acid) to determine the concentration of hydroxyl radicals generated from ozone.

In conventional ozonation processes using millibubbles, hydroxyl radicals are generated from ozone under alkaline conditions, which is initiated by the hydroxyl ion (OH^-) (Tomiyasu et al., 1985). Generally, the amount of hydroxyl radicals generated under acidic conditions is neglected. However, ozone microbubbles act differently from the millibubbles. It is reported that the microbubbles are able to generate hydroxyl radicals even under acidic conditions (Takahashi et al., 2007). The reason behind this phenomenon has remained unclear although some possible mechanisms have been suggested (Takahashi et al., 2012).

2.1.4.2 Scope for Research

The concentration of hydroxyl radicals generated by ozone millibubbles at alkaline conditions has been reported in a few works (Elovitz and von Gunten, 2000; Meunier et al., 2006; Rosenfeldt et al., 2006). So far, hardly any work has reported the concentration of hydroxyl radicals generated from ozone microbubbles in the pH range 3−10. Therefore, the generation of hydroxyl radicals from ozone microbubbles needs to be studied. It may be verified by the indirect method proposed by Elovitz and von Gunten (1999). The effects of pH and carbonate ions on the generation of hydroxyl radicals have to be studied. The contribution of hydroxyl radicals on the degradation of the pollutants (e.g. phenol) should be studied at pH 3−10. The possible mechanism of the generation of hydroxyl radicals from ozone microbubbles under acidic and alkaline conditions would be explained in details.

2.2 OBJECTIVES OF THIS WORK

The research work presented in this thesis is divided into four parts, viz. (i) removal of ammonia, (ii) removal of arsenic, (iii) removal of dyestuff, and (iv) detection and measurement of hydroxyl radical concentration. Our work looks into the following aspects of the water/wastewater treatment.

- Design and develop a plant prototype for oxidation of pollutants using ozone microbubbles.
- Study the removal of ammonia from water using ozone microbubbles. Determine the volumetric mass transfer coefficient of ozone microbubbles at various pH and ozone generations rates.
- Study the oxidation of As(III) to As(V) using ozone microbubbles. Also, study the adsorption of As(V) on zirconium-based adsorbents. Analyze the data with adsorption isotherms and determine the thermodynamic parameters for adsorption.
- Study the oxidation of BG using ozone microbubbles. Analyze the oxidation mechanism, detect the intermediate products of reaction, and the kinetics of the overall oxidation.
- Measure the concentration of hydroxyl radicals generated from ozone microbubbles using an indirect method. Develop a mechanism for the generation of hydroxyl radicals from ozone microbubbles.

2.3 ORGANIZATION OF THESIS

This thesis is organized as follows. **Chapter 1** presents the summary of the properties of the microbubbles and their applications in water/wastewater treatment. **Chapter 2** presents the review of the literature, scope for research and the objectives of this work. **Chapter 3** presents the details of the experimental setup used in this work. The chemicals used in this

study are also given. The methods of measurement of concentrations of ammonia, arsenic, dyestuff, and the hydroxyl radicals are described in this chapter. The methods of preparation of adsorbents for arsenic removal are also described. The characterization of the adsorbents by SEM, energy dispersive EDX, XRD, FTIR, zeta potentiometer, and BET surface analyzer is described. The analysis of the intermediates formed during ozonation by using GC–MS and FTIR is also described in this chapter. **Chapter 4** presents the results obtained from the ozonation of ammonium salts in the pilot-plant. The effects of ozone feed rate, pH of the reaction medium, and the catalytic effect of bromide on oxidation have been discussed in this chapter. The mechanism of oxidation of ammonia by microbubbles has been investigated in detail. **Chapter 5** presents the results obtained from the ozonation of arsenic followed by the adsorption of As(V) on the zirconium-based adsorbents. The effects of initial As(III) concentration, ozone generation rate and pH of the reaction medium on the efficiency of ozonation have been reported. The effects of 2-propanol and the carbonate ion radicals on ozonation have also been reported in this chapter. The kinetics of oxidation of As(III) with ozone was studied and the kinetic parameters were evaluated. Two potential adsorbents of As(V) (i.e. zirconium–activated carbon and amorphous zirconium oxide) were prepared. These adsorbents were characterized, the charge on their surface at different pH was determined, adsorption isotherms were fitted to the data, and kinetic and thermodynamic parameters of the adsorbents were determined. **Chapter 6** presents the work on the decolorization of aqueous BG solutions using ozone microbubbles. This study includes the effect of variation of concentration of BG with time, intermediate degradation products of BG, reaction mechanism, and the kinetics of the reaction. The degradation mechanism was constructed from the data obtained from GC–MS and FTIR analyses. The mineralization of the dye was studied by the TOC analysis. **Chapter 7** presents the determination of the amount of hydroxyl radicals generated from ozone microbubbles. The effects of pH and

carbonate ions on the generation of hydroxyl radicals, and the contribution of hydroxyl radicals on the degradation of phenol at pH 3−10 have been reported in this chapter. The possible mechanism of the generation of hydroxyl radicals from ozone microbubbles under acidic and alkaline conditions has been explained. **Chapter 8** summarizes the inferences drawn from this work and provides some suggestions for future research.

ABBREVIATIONS

BET	Brunauer–Emmett–Teller
BG	Brilliant Green
BOD	biological oxygen demand
EDX	energy dispersive X-ray
FTIR	Fourier transform infrared
GC–MS	gas chromatography–mass spectrometry
SEM	scanning electron microscope
TOC	total organic carbon
WHO	World Health Organization
XRD	X-ray diffractometer

REFERENCES

Adams, C.E., 1974. Removing nitrogen from waste water. Environ. Sci. Technol. 7, 696−701.

Baek, M.H., Ijagbemi, C.O., Kim, D.S., 2010. Spectroscopic studies on the oxidative decomposition of Malachite Green using ozone. J. Environ. Sci. Health A 45, 630−636.

Balaji, T., Yokoyama, T., Matsunaga, H., 2005. Adsorption and removal of As(V) and As(III) using Zr-loaded lysine diacetic acid chelating resin. Chemosphere 59, 1169−1174.

Behnajady, M.A., Modirshahla, N., Shokri, M., Vahid, B., 2008. Effect of operational parameters on degradation of Malachite Green by ultrasonic irradiation. Ultrason. Sonochem. 15, 1009−1014.

Beltrán, F.J., 2004. Ozone Reaction Kinetics for Water and Wastewater System. CRC Press, Boca Raton, Florida, USA.

Chakraborty, S., De, S., Basu, J.K., DasGupta, S., 2005. Treatment of a textile effluent: application of a combination method involving adsorption and nanofiltration. Desalination 174, 73−85.

Chelkowska, K., Grasso, D., Fabian, I., Gordon, G., 1992. Numerical simulations of aqueous ozone decomposition. Ozone Sci. Eng. 14, 33−49.

Chen, C., Lu, C., 2007. Photocatalytic degradation of basic violet 4: degradation efficiency, product distribution, and mechanisms. J. Phys. Chem. C 111, 13922−13932.

Chu, L.B., Xing, X.H., Yu, A.F., Sun, X.L., Jurcik, B., 2008. Enhanced treatment of practical textile wastewater by microbubble ozonation. Process Saf. Environ. Prot. 86, 389−393.

Chuang, C.L., Fan, M., Xu, M., Brown, R.C., Sung, S., Saha, B., Huang, C.P., 2005. Adsorption of arsenic(V) by activated carbon prepared from oat hulls. Chemosphere 61, 478−483.

Culp, S.J., Beland, F.A., 1996. Malachite Green: a toxicological review. J. Am. Coll. Toxicol. 15, 219−238.

Daus, B., Wennrich, R., Weiss, H., 2004. Sorption materials for arsenic removal from water: a comparative study. Water Res. 38, 2948−2954.

Delwiche, C.C., 1981. Denitrification, Nitrification, and Atmospheric Nitrous Oxide. John Wiley & Sons, New York, USA.

DeSesso, J.M., Jacobson, C.F., Scialli, A.R., Farr, C.H., Holson, J.F., 1998. An assessment of the developmental toxicity of inorganic arsenic. Reprod. Toxicol. 12, 385−433.

Driehaus, W., Seith, R., Jekel, M., 1995. Oxidation of arsenate(III) with manganese oxides in water treatment. Water Res. 29, 297−305.

Elovitz, M.S., von Gunten, U., 1999. Hydroxyl radical/ozone ratios during ozonation processes. I. The R_{ct} concept. Ozone Sci. Eng. 21, 239−260.

Elovitz, M.S., von Gunten, U., 2000. Hydroxyl radical/ozone ratios during ozonation processes. II. The effect of temperature, pH, alkalinity, and DOM properties. Ozone Sci. Eng. 22, 123−150.

Fan, M., Brown, R.C., Huang, C.P., 2002. Preliminary studies of the oxidation of arsenic(III) by potassium ferrate. Int. J. Environ. Pollut. 18, 91−96.

Fernandes, C., Lalitha, V.S., Rao, V.K., 1991. Enhancing effects of malachite green on the development of hepatic preneoplastic lesions induced by N-nitrosodiethylamine in rats. Carcinogenesis 12, 839−845.

Ghurye, G., Clifford, D., 2001. Laboratory study on the oxidation of arsenic III to arsenic V. EPA/600/R-01/021, Houston, Texas, USA.

Ghurye, G., Clifford, D., 2004. As(III) oxidation using chemical and solid-phase oxidants. Am. Water Work. Assoc. 96, 84−96.

Goldacre, R.J., Philips, J.N., 1949. The ionization of basic triphenylmethane dyes. J. Chem. Soc. 1724−1732.

Gu, Z., Fang, J., Deng, B., 2005. Preparation and evaluation of adsorbents for arsenic removal. Environ. Sci. Technol. 39, 3833−3843.

Gutowska, A., Kaluzna-Czaplinska, J., Jozwiak, W.K., 2007. Degradation mechanism of reactive orange 113 dye by H_2O_2/Fe_2^+ and ozone in aqueous solution. Dyes Pigments 74, 41−46.

Haag, W., 1984. Improved ammonia oxidation by ozone in the presence of bromide ion during water treatment. Water Res. 18, 1125−1128.

Halme, K., Lindfors, E., Peltonen, K., 2007. A confirmatory analysis of malachite green residues in rainbow trout with liquid chromatography–electrospray tandem mass spectrometry. J. Chromatogr. B 845, 74−79.

Hoigné, J., Bader, H., 1978. Ozonation of water: kinetics of oxidation of ammonia by ozone and hydroxyl radicals. Environ. Sci. Technol. 12, 79−84.

Huang, C.P., Fu, P.L.K., 1984. Treatment of arsenic(V)-containing water by the activated carbon process. Water Pollut. Control Fed. 56, 233−242.

Huang, L., Li, L., Dong, W., Liu, Y., Hou, H., 2008. Removal of ammonia by OH radical in aqueous phase. Environ. Sci. Technol. 42, 8070−8075.

Ikehata, K., Naghashkar, N.J., Gamal El-Din, M., 2006. Degradation of aqueous pharmaceuticals by ozonation and advanced oxidation processes: a review. Ozone Sci. Eng. 28, 353−414.

Jain, C.K., Ali, I., 2000. Arsenic: occurrence, toxicity and speciation techniques. Water Res. 34, 4304−4312.

Juárez-Reyes, A., Jiménez-Capdeville, M.E., Delgado, J.M., Ortiz-Pérez, D., 2009. Time course of arsenic species in the brain and liver of mice after oral administration of arsenate. Arch. Toxicol. 83, 557−563.

Karim, M.M., 2000. Arsenic in groundwater and health problems in Bangladesh. Water Res. 34, 304−310.

Kim, K.W., Kim, Y.J., Kim, I.T., Park, G., Lee, E.H., 2006. Electrochemical conversion characteristics of ammonia to nitrogen. Water Res. 40, 1431−1441.

Kim, M.J., Nriagu, J., 2000. Oxidation of arsenite in groundwater using ozone and oxygen. Sci. Total Environ. 247, 71−79.

Kinniburgh, D.G., Smedley, P.L., 2000. Arsenic contamination of groundwater in Bangladesh, Final report summary. Keyworth, United Kingdom.

Kuo, C.H., Yuan, F., Hill, D.O., 1997. Kinetics of oxidation of ammonia in solutions containing ozone with or without hydrogen peroxide. Ind. Eng. Chem. Res. 36, 4108−4113.

Langlais, B., Reckhow, D.A., Brink, D.R., 1999. Ozone in Water Treatment: Applications and Engineering. Lewis Publishers, Boca Raton, Florida, USA.

Ledakowicz, S., Solecka, M., Zylla, R., 2001. Biodegradation, decolourisation and detoxification of textile wastewater enhanced by advanced oxidation processes. J. Biotechnol. 89, 175−184.

Lee, G., Song, K., Bae, J., 2011. Permanganate oxidation of arsenic(III): reaction stoichiometry and the characterization of solid product. Geochim. Cosmochim. Acta 75, 4713−4727.

Legrini, O., Oliveros, E., Braun, A.M., 1993. Photochemical processes for water treatment. Chem. Rev. 93, 671−698.

Leupin, O.X., Hug, S.J., 2005. Oxidation and removal of arsenic(III) from aerated groundwater by filtration through sand and zero-valent iron. Water Res. 39, 1729−1740.

Lin, S.H., Wu, C.L., 1996. Removal of nitrogeneous compounds from aqueous solution by ozonation and ion exchange. Water Res. 30, 1851−1857.

Lin, S.H., Yen, Y.L., 1996. Ozonation kinetics of ammonia and nitrite removal from aqueous solution. J. Environ. Sci. Health A 31, 797−809.

Lin, S.H., Yen, Y.L., 1997. Ammonia and nitrite removal from sea water by ozonation. Environ. Technol. 18, 65−73.

Loeb, B.L., Thompson, C.M., Drago, J., Takahara, H., Baig, S., 2012. Worldwide ozone capacity for treatment of drinking water and wastewater: a review. Ozone Sci. Eng. 34, 64−77.

Mandal, B.K., Suzuki, K.T., 2002. Arsenic round the world: a review. Talanta 58, 201−235.

Manning, B.A., Fendorf, S.E., Bostick, B., Suarez, D.L., 2002. Arsenic(III) oxidation and arsenic(V) adsorption reactions on synthetic birnessite. Environ. Sci. Technol. 36, 976−981.

Mass, M.J., Tennant, A., Roop, B.C., Cullen, W.R., Styblo, M., Thomas, D.J., Kligerman, A.D., 2001. Methylated trivalent arsenic species are genotoxic. Chem. Res. Toxicol. 14, 355−361.

Meriç, S., Selçuk, H., Belgiorno, V., 2005. Acute toxicity removal in textile finishing wastewater by Fenton's oxidation, ozone and coagulation−flocculation processes. Water Res. 39, 1147−1153.

Meunier, L., Canonica, S., von Gunten, U., 2006. Implications of sequential use of UV and ozone for drinking water quality. Water Res. 40, 1864−1876.

Modirshahla, N., Behnajady, M.A., 2006. Photooxidative degradation of malachite green (MG) by UV/H_2O_2: influence of operational parameters and kinetic modeling. Dyes Pigments 70, 54−59.

Mohan, D., Pittman Jr., C.U., 2007. Arsenic removal from water/wastewater using adsorbents–a critical review. J. Hazard. Mater. 142, 1−53.

Naraharisetti, S.B., Aggarwal, M., Sarkar, S.N., Malik, J.K., 2008. Concurrent subacute exposure to arsenic through drinking water and malathion via diet in male rats: effects on hepatic drug-metabolizing enzymes. Arch. Toxicol. 82, 543−551.

Neppolian, B., Celik, E., Choi, H., 2008. Photochemical oxidation of arsenic(III) to arsenic(V) using peroxydisulfate ions as an oxidizing agent. Environ. Sci. Technol. 42, 6179−6184.

Nishimura, T., Umetsu, Y., 2001. Oxidative precipitation of arsenic(III) with manganese(II) and iron(II) in dilute acidic solution by ozone. Hydrometallurgy 62, 83−92.

Obaid-ur-Rehman, S., Beg, S.A., 1990. Ammonia removal by air stripping–from origin to present state of technology. J. Environ. Sci. Health A 25, 343−365.

Oppenländer, T., 2003. Photochemical Purification of Water and Air. Wiley-VCH, Weinheim, Germany.

Oturan, M.A., Guivarch, E., Oturan, N., Sirés, I., 2008. Oxidation pathways of malachite green by Fe_3^+-catalyzed electro-Fenton process. Appl. Catal. B 82, 244−254.

Peräniemi, S., Hannonen, S., Mustalahti, H., Ahlgrén, M., 1994. Zirconium-loaded activated charcoal as an adsorbent for arsenic, selenium and mercury. Fresenius J. Anal. Chem. 349, 510−515.

Petrick, J.S., Ayala-Fierro, F., Cullen, W.R., Carter, D.E., Vasken, A.H., 2000. Monomethylarsonous acid (MMA^{III}) is more toxic than arsenite in Chang human hepatocytes. Toxicol. Appl. Pharmacol. 163, 203−207.

Pressley, T.A., Bishop, D.F., Roan, S.G., 1970. Ammonia-nitrogen removal by breakpoint chlorination. Environ. Sci. Technol. 6, 622−628.

Purkait, M.K., DasGupta, S., De, S., 2006. Micellar enhanced ultrafiltration of eosin dye using hexadecyl pyridinium chloride. J. Hazard. Mater. 136, 972−977.

Purkait, M.K., Gusain, D.S., DasGupta, S., De, S., 2005. Adsorption behavior of chrysoidine dye on activated charcoal and its regeneration characteristics using different surfactants. Sep. Sci. Technol. 39, 2419−2440.

Rajakovic, L.V., 1992. The sorption of arsenic onto activated carbon impregnated with metallic silver and copper. Sep. Sci. Technol. 27, 1423−1433.

Rakness, K.L., 2005. Ozone in Drinking Water Treatment: Process Design, Operation, and Optimization. American Water Works Association, Denver, USA.

Robertson, F.N., 1989. Arsenic in ground-water under oxidizing conditions, south-west United States. Environ. Geochem. Health 11, 171−185.

Rosenfeldt, E.J., Linden, K.G., Canonica, S., von Gunten, U., 2006. Comparison of the efficiency of ·OH radical formation during ozonation and the advanced oxidation processes O_3/H_2O_2 and UV/H_2O_2. Water Res. 40, 3695−3704.

Ruiz, G., Jeison, D., Chamy, R., 2003. Nitrification with high nitrite accumulation for the treatment of wastewater with high ammonia concentration. Water Res. 37, 1371−1377.

Sandoval, R., Cooper, A.M., Aymar, K., Jain, A., Hristovski, K., 2011. Removal of arsenic and methylene blue from water by granular activated carbon media impregnated with zirconium dioxide nanoparticles. J. Hazard. Mater. 193, 296−303.

Singer, P.C., Reckhow, D.A., 1999. Water Quality and Treatment: A Handbook of Community Water Supplies. American Water Works Association, McGraw-Hill, New York, USA.

Singer, P.C., Zilli, W.B., 1975. Ozonation of ammonia in wastewater. Water Res. 9, 127−134.

Smedley, P.L., Nicolli, H.B., Macdonald, D.M.J., Barros, A.J., Tullio, J.O., 2012. Hydrogeochemistry of arsenic and other inorganic constituents in groundwaters from La Pampa, Argentina. Appl. Geochem. 17, 259−284.

Srivastava, S., Sinha, R., Roy, D.S., 2004. Toxicological effects of malachite green. Aquat. Toxicol. 66, 319−329.

Suzuki, T.M., Bomani, J.O., Matsunaga, H., Yokoyama, T., 2000. Preparation of porous resin loaded with crystalline hydrous zirconium oxide and its application to the removal of arsenic. React. Funct. Polym. 43, 165−172.

Takahashi, M., Chiba, K., Li, P., 2007. Formation of hydroxyl radicals by collapsing ozone microbubbles under strongly acidic conditions. J. Phys. Chem. B 111, 11443–11446.

Takahashi, M., Ishikawa, H., Asano, T., Horibe, H., 2012. Effect of microbubbles on ozonized water for photoresist removal. J. Phys. Chem. C 116, 12578−12583.

Tanaka, J., Matsumura, M., 2002. Kinetic studies of removal of ammonia from seawater by ozonation. J. Chem. Technol. Biotechnol. 77, 649−656.

Tanaka, J., Matsumura, M., 2003. Application of ozone treatment for ammonia removal in spent brine. Adv. Environ. Res. 7, 835−845.

Tomiyasu, H., Fukutomi, H., Gordon, G., 1985. Kinetics and mechanism of ozone decomposition in basic aqueous solution. Inorg. Chem. 24, 2962−2966.

Tramper, J., Grootjen, D.R.J., 1986. Operating performance of *Nitrobacter agilis* immobilized in carrageenan. Enzyme Microb. Technol. 8, 477−480.

Turhan, K., Turgut, Z., 2009. Decolorization of direct dye in textile wastewater by ozonization in a semi-batch bubble column reactor. Desalination 242, 256−263.

Udeh, P.J., 2004. A Guide to Healthy Drinking Water. iUniverse, Bloomington, Indiana, USA.

von Gunten, U., 2003. Ozonation of drinking water : part I. Oxidation kinetics and product formation. Water Res 37, 1443–1467.

Voncina, D.B., Majcen-Le-Marechal, A., 2003. Reactive dye decolorization using combined ultrasound/H_2O_2. Dyes Pigments 59, 173−179.

Wang, A., Edwards, J.G., Davies, J.A., 1994. Photooxidation of aqueous ammonia with titania-based heterogeneous catalysts. Sol. Energy 52, 459−466.

Yang, M., Uesugi, K., Myoga, H., 1999. Ammonia removal in bubble column by ozonation in the presence of bromide. Water Res. 33, 1911−1917.

Yang, M., Uesugi, K., Myoga, H., 2000. Study on by-products of ozonation during ammonia removal under the existence of bromide: factors affecting formation and removal of the by-products. Ozone Sci. Eng. 22, 23−29.

Yoon, S.H., Lee, J.H., Oh, S., Yang, J.E., 2008. Photochemical oxidation of As(III) by vacuum-UV lamp irradiation. Water Res. 42, 3455−3463.

Zhou, X.J., Guo, W.Q., Yang, S.S., Ren, N.Q., 2012. A rapid and low energy consumption method to decolorize the high concentration triphenylmethane dye wastewater:

operational parameters optimization for the ultrasonic-assisted ozone oxidation process. Bioresour. Technol. 105, 40−47.

Zhu, X., Castleberry, S.R., Nanny, M.A., Butler, E.C., 2005. Effects of pH and catalyst concentration on photocatalytic oxidation of aqueous ammonia and nitrite in titanium dioxide suspensions. Environ. Sci. Technol. 39, 3784−3791.

Zhu, X., Jyo, A., 2001. Removal of arsenic(V) by zirconium(IV)-loaded phosphoric acid chelating resin. Sep. Sci. Technol. 36, 3175−3189.

CHAPTER 3

EXPERIMENTAL METHODS

CHAPTER 3

EXPERIMENTAL METHODS

This chapter presents the details of the experimental setup used for the oxidation ammonia, arsenic and dye. The materials used in this work and their source are given. The experimental methods employed for the detailed study of the ozonation of pollutants are described. The details of the instruments used for the detection of the pollutants are also given. The methods of preparation of the adsorbents and their characterization are also given.

3.1 EXPERIMENTAL SETUP

The pilot-plant setup used in this work was designed and developed by assembling several units. Oxygen was isolated from air by an oxygen concentrator [Oz-Air (India), model: HG 03]. It employs the pressure swing adsorption technique to generate high-purity oxygen (> 98% by volume) from air. This oxygen was fed to the ozonator [Oz-Air (India), model: ISM 10 Oxy EC], which converted oxygen to ozone by the corona-discharge method. The ozonator had a provision to control the rate of generation of ozone in the range of 0−3mg s^{-1}. The output flow rate of oxygen from the oxygen concentrator was controlled in the range of 120−240 dm^3h^{-1} for stable operation of the ozonator, as per the recommendation of the manufacturer. The flow rate of the gas mixture (i.e. oxygen and ozone) coming out of the ozonator was measured by a rotameter (31.2−312 dm^3h^{-1}). The percentage of ozone in the gas mixture was varied in the range of 0.7 to 2%. The photograph of the experimental setup is shown in Figure 3.1, and aschematic of the same is shown in Figure 3.2. Some experiments were performed with oxygen, in which the gas coming out of the oxygen concentrator was directly used.

Figure 3.1 Photograph of the experimental setup (1) microbubble generator, (2) ozonator, (3) oxygen contactor, (4) cooling water bath, (5) reactor, (6) water tank for cold water circulation, (7) step-down transformer, and (8) voltage stabilizer.

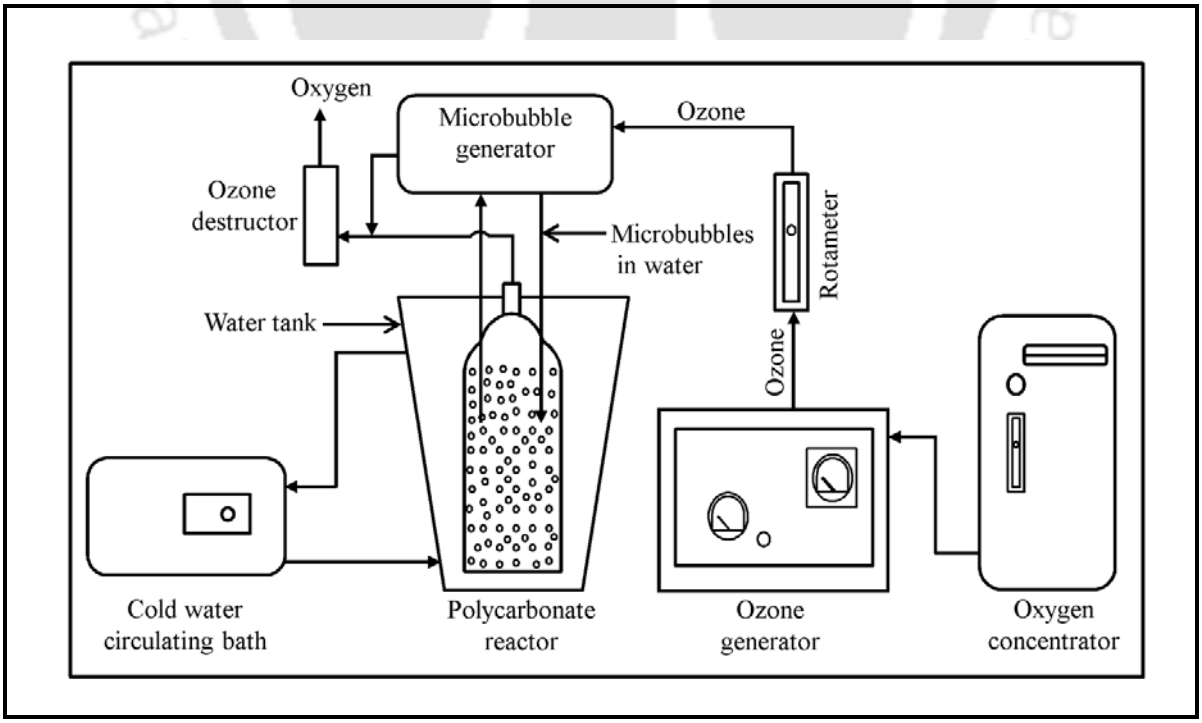

Figure 3.2 Schematic of the experimental setup.

The gas containing ozone and oxygen was passed into the microbubble generator [Riverforest Corporation (USA), model: AS MK-III]. The gas was dissolved in water by high pressure inside the microbubble generator. After dissolution, the microbubbles were generated by the release of pressure. The mean diameter of the microbubbles was 25 µm. The gas intake capacity of the microbubble generator was 1.7 cm^3s^{-1}. The microbubble generator operated in a recirculation mode and continuously generated the microbubbles. The aqueous phase reaction mixture, contained in a polycarbonate reactor of 20 dm^3 capacity, was recirculated through the microbubble generator, as illustrated in Figure 3.2. The excess gas, which was not dissolved in the aqueous phase, was passed through an ozone destructor [Oz-Air (India), model: Dest-50], which catalytically converted the ozone to oxygen and released it to atmosphere. The gas issuing from the reactor was also passed through this ozone destructor. The temperature of the reaction medium appreciably increased during ozonation of pollutants by the microbubbles (e.g. from 298 to 308 K). Tap water was filtered through an iron removal cartridge [Eureka Forbes (India), model: Iron-Nil]. All ammonium, arsenic and dye solutions were prepared by using this water.

3.2 MATERIALS

Oxygen (> 98% purity) was isolated from air. A portion of this oxygen was converted to ozone. The details of these procedures are described in Section 3.1. The chemicals used in this study are listed in Table 3.1.

Table 3.1 Materials used in this work.

Chemicals	Purity	Chemicals	Purity
Acetonitrile (Spectrochem, India)	99.9%	Phosphoric acid (Spectrochem, India)	85%
Activated charcoal (LobaChemie, India)	Granular	Potassium bromide (Merck, India)	99.9%
Ammonium chloride (Merck, India)	99.8%	Potassium indigo trisulfonate (Sigma Aldrich, India)	99%
Ammonia solution (Merck, India)	30%	Potassium iodide (Merck, India)	99.8%
Ammonium sulfate (Merck, India)	99.5%	Potassium nitrate (Merck, India)	> 98%
Arsenic (III) oxide (LobaChemie, India)	99.5%	2-propanol (Merck, India)	99.7%
Arsenic (V) oxide (Alfa Aesar, India)	99.9%	Sodium borohydride (Spectrochem, India)	96%
Arsenic standard solution (Merck, India)	995 ± 5 mg dm^{-3}	Sodium bromide (Titan Biotech, India)	99%
Brilliant Green dye (LobaChemie, India)	95%	Sodium carbonate anhydrous (Merck, India)	99.9%
Dowex 1×8 100–200 resin (Alfa Aesar, India)	Chloride form	Sodium dihydrogen phosphate (Merck, India)	99%
Hydrochloric acid (Merck, India)	> 35%	Sodium hydroxide (Rankem, India)	> 98%
Malonic acid (Spectrochem, India)	99%	Sodium sulfate (anhydrous) (Merck, India)	99.5%
Methanol (HPLC grade) (Spectrochem, India)	99.9%	Sodium thiosulfate pentahydrate (Merck, India)	99.9%
p-chlorobenzoic acid (Alfa Aesar, India)	98%	Zirconium dinitrate oxide hydrate (Alfa Aesar India)	99.9%
Phenol (Merck, India)	99.5%	Zirconium oxychlorideoctahydrate (LobaChemie, India)	98.5%

3.3 METHODS

The pH of the aqueous phase was measured by a pH meter [Eutech (Singapore), model: pH 2700, electrode: 93X218819]. The pH of the medium was maintained by using 0.1 mol dm^{-3}HCl and 0.1 mol dm^{-3}NaOH solutions. Standard solutions of precisely known pH were purchased from Oakton (USA).

3.3.1 Oxidation of Ammonia by using OzoneMicrobubbles

3.3.1.1 Measurement of Concentration of Ammonia

Standard solutions of ammonium salts were purchased from Eutech (Singapore). Aqueous solutions of the ammonium salts were prepared by using filtered tap-water, after removing iron from it.Samples were withdrawn from the reactor by pipette. The ammonium concentration in the reactor was analyzed by an ion meter [Eutech (Singapore), model: Ion Meter 2700] with ammonium-specific electrode [model: NH415XX], which was operable up to pH 10. In every sample, an ionic strength adjuster was added, which completely converted all ammonia to ammonium. Samples were taken out of the reactor and the total ammonia concentration was measured under continuous magnetic stirring at every 15 min interval. The concentration of ozone in the reactor was measured by a colorimeter [Eutech (Singapore), model: C 105] using the ozone-specific reagent (viz. the DPD method)(Eaton et al., 2005). Continuous circulation of the aqueous phase and the release of microbubbles in the reactor ensured a uniform concentration of the ammonium salt and ozone in the reactor. This was verified by randomly withdrawing samples from different parts of the reactor and measuring the ammonium and ozone concentrations.

3.3.1.2 Measurement of Concentration of Nitrate

The concentration of nitrate, which was formed by the oxidation of ammonia was determined by a UV-Visible spectrophotometer [Thermo Electron (India), model: UV 2300]. The absorbance was measured at 220 nm as described in the literature(Eaton et al., 2005). The calibration plot is shown in Figure 3.3. The NO_3^- calibration curve followed Beer's law up to 11 mg dm^{-3}. The higher concentrations (> 10 mg dm^{-3}) were measured by dilutingthe sample.

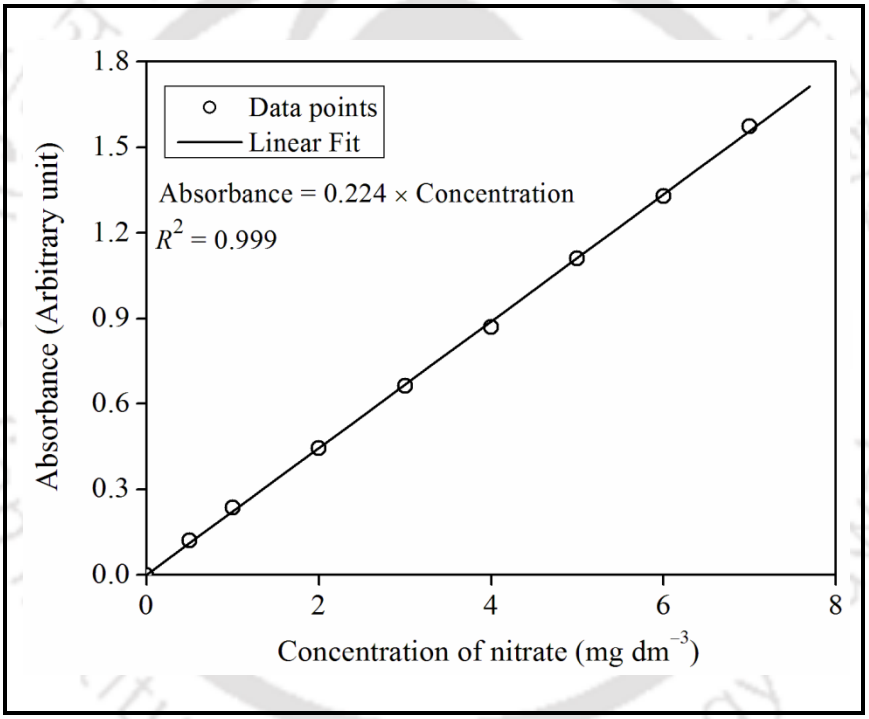

Figure 3.3 UV-Vis calibration curve for nitrate.

3.3.1.3 Mass Transfer of Ozone by Microbubbles

The determination of mass transfer coefficient was carried out in absence of ammonia. Gaseous ozone was introduced into the aqueous phase in the form of microbubbles at the required pH and ozone generation rate. The pH of the water was maintained before applying ozone. At time t = 0, the initial ozone concentration was zero. From the moment of ozone

supply, the concentration of ozone was measured using the ozone-specific reagent at the time interval of 2 min. The dissolved ozone concentration was measured asa function of time and continued until it reached steady state, which corresponds to the steady state ozone concentration.

3.3.2 Oxidation of As(III) by using Ozone Microbubbles

3.3.2.1 Separation of As(III) and As(V)

As(III) and As(V) were separated by using Dowex resin (chloride form) by the method described by Ficklin(1983). The resin was slurry-packed inside glass columns of 12.5 cm height and 12 mm diameter. The height of the resin bed inside the columns was 10 cm. The chloride form of resin was converted to the acetate form via the hydroxide form. About 3 $cm^3$of 1 mol dm^{-3} NaOH were passed through the resin, followed by 15 cm^3 water and 5 $cm^3$of 1 mol m^{-3} acetic acid. The excess acetic acid was removed by passing 10 cm^3 water. The resin column was ready for use after these steps.

Samples were withdrawn from the reactor by a glass pipette. At particular time intervals, 25 cm^3 samples were taken out of the reactor and acidified with 0.25 cm^3 concentrated HCl. About 5 cm^3acidified solution were passed through the resin bed and the effluent liquid was collected in clean sample bottles. The resin allowed As(III) to pass through it, but completely retained the As(V). Therefore, the effluent contained As(III) only.

3.3.2.2 Measurement of Concentration of Arsenic

Aqueous solutions required for the analysis of standards were prepared by using water that was purified by a Millipore water purification system [Millipore (USA), model: Elix-3]. The concentration of arsenic was measured by using an atomic adsorption spectrophotometer (AAS) [Varian (The Netherlands), model: Spectra AA 220FS] equipped with vapor

generation assembly (which operated at 1198 K). The procedure reported by Behari and Prakash (2006) was followed. The sample was acidified by using 7 mol dm^{-3} HCl. The generation of hydride was achieved by continuous-flow mixing of the acidified sample using potassium iodide and sodium borohydride (viz. 0.6% $NaBH_4$ dissolved in 0.5% aqueous NaOH solution).Fresh arsenic standards were prepared 1 h before the detection of sample. A calibration plot was prepared at the time of sample analysis.The calibration curve is shown in Figure 3.4. The higher concentrations of arsenic (> 100 μg dm^{-3}) were measured by diluting the samples by 2−50 fold. The minimum measurable arsenic concentration was 0.1 μg dm^{-3}.

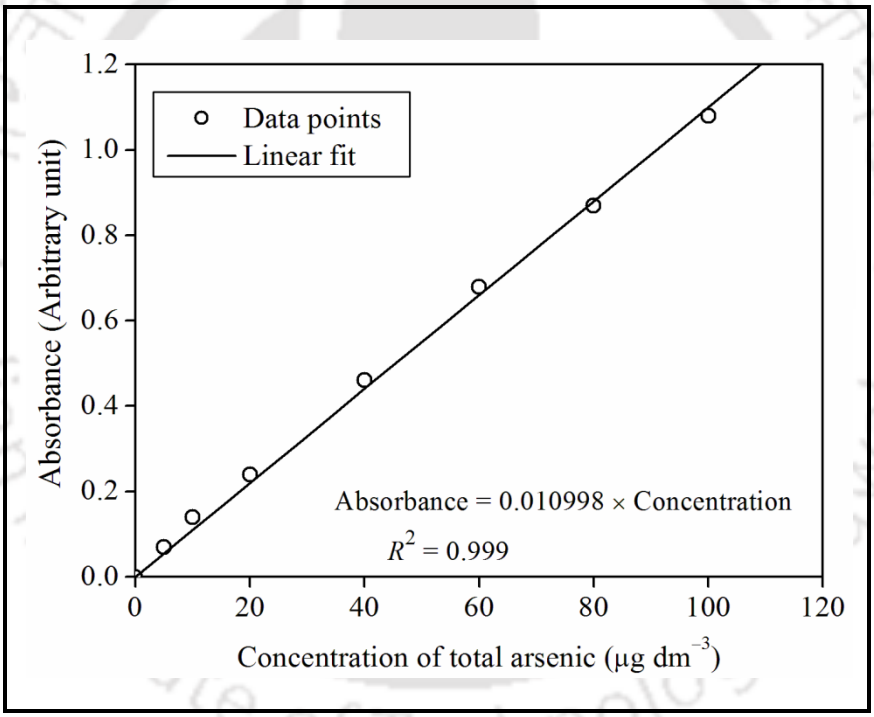

Figure 3.4 Calibration curve for total arsenic analysis by AAS.

3.3.3 Adsorption of As(III) and As(V)

3.3.3.1 Preparation of Adsorbents

Activated carbon was impregnated with zirconium by the method given by Okumura et al.(1998). Aqueous zirconyl nitrate solution (5.9%) was prepared by dissolving zirconyl nitrate dihydrate in water. The activated carbon was crushed and sieved to prepare 200 μm

size, washed with deionized water several times and dried in an oven at 398 K for 24 h. The purified activated carbon (50 g) was mechanically mixed with 500 cm^3zirconyl nitrate solution for 3 d at 398 K.

The amorphous zirconium oxide particles were prepared by the method described by Cui et al. (2012). Aqueous zirconium oxychloride solution (0.035 mol dm^{-3}) was prepared by dissolving zirconium octahydrate in water. The solution was magnetically stirred for 5 min. Thereafter, 50 cm^3 aqueous ammonia solution were slowly added to 20 cm^3 zirconium oxychloride solution with rigorous stirring. The stirring was continued for 5 min. The amorphous zirconium oxide precipitate was then dried in a hot air oven for 4 h at 423 K. The precipitate was subsequently cooled at room temperature, thoroughly washed with water to remove chloride, and then dried in the oven for 8 h at 383 K. It was then crushed to the desired size. The average diameter of the particles was ~50 μm. The particle size was determined by a laser particle size analyzer [Malvern (UK), model: Master Sizer 2000].

3.3.3.2 Characterization of Adsorbents

The scanning electron microscope (SEM) [Leo (England), model: 1430vp] was used to image the surface of the adsorbents. The chemical composition of zirconium–activated carbon was analyzed by using EDX [Oxford instruments (England), model: 7353], which was connected to the SEM. The crystal structure of the adsorbents was analyzed by a XRD [Bruker (Germany), model: D8 Advance] at a step-size of 0.1 s^{-1}.

FTIR spectroscopy was used to analyze the functional groups of the adsorbents. A FTIR spectrophotometer [Shimadzu (Japan), model: IRAffinity-1] was used for this purpose. Dried adsorbents were ground with KBr in a fixed weight ratio (viz. sample : KBr = 1:100). All infrared spectra were generated at room temperature in transmission mode.

Zeta potential on the surface of the adsorbents was measured by the electrophoretic mobility of the fine particles of the adsorbents in a zeta potentiometer [Beckman Coulter (Switzerland), model: Delsa Nano]. 0.1 g of adsorbent was dispersed in 50 cm^3 water at different pH and shaken for 12 h. The zeta potential at the surface of the dispersed adsorbent was measured thereafter.

A BET surface analyzer [Beckman Coulter (Switzerland), model: SA 3100] was used to measure the surface area and pore volume of the adsorbents. The samples were degassed by using helium at 473 K for 2 h. The parameters mentioned above were obtained from the nitrogen adsorption isotherms.

3.3.3.3 Batch Adsorption Studies of As(III) and As(V)

All batch experiments on adsorption of As(III) and As(V) were carried out in 250 cm^3 Erlenmeyer flasks at different temperatures. The working volume of the heterogeneous mixture was 200 cm^3 and the adsorbent dose was 1 gdm^{-3}. Stock solutions of 100 $mgdm^{-3}$ arsenic trioxide and arsenic pentoxide were prepared by dissolving the respective compounds in water at the required pH. The concentration of the solutions was varied by successive dilution of the stock solution.

Kinetics of adsorption was studied by taking different initial concentrations of As(V) (viz. 25, 50 and 100 μgdm^{-3}) at a constant adsorbent dose (viz. 1 g dm^{-3}). At a particular time interval, samples were withdrawn and filtered through Whatman filter paper no. 1 (particle retention: 11 μm), and the concentration of As(V) was measured.The adsorbent particles settled quickly. Thesize of the adsorbent particles was > 20 μm.

100 cm^3 As(V) solutions (having concentration in the range of 0.05−5 mg dm^{-3}) were kept in contact with 0.1 g of adsorbent for 24 h at 298 K, and were shaken at a speed of 200 rpm. The pH of the solution was 6. The equilibrium concentration of As(V) was measured

after 24 h of contact time. The amount ofarsenic adsorbed on the surface of the adsorbent was calculated as the difference between the initial and equilibrium concentrations.

To determine the thermodynamic parameters for the adsorption of As(V), 100 $cm^3$of 1 mg dm^{-3}As(V) solution was contacted with 0.1 g of the adsorbent at temperatures in the range of 298 to 318 K at pH 6. The shaking speed was 200 rpm. The equilibrium concentration of As(V) was measured after 24 h of contact time.

3.3.4Oxidation of Dye using Ozone Microbubbles

3.3.4.1 Measurement of Concentration of Dye

The dye concentration was varied in the range of 0.0274−0.164 mmoldm^{-3}.The ozonation reactions were carried out for 1 h. 15 cm^3 of samples were withdrawn from the reactor at 5 min intervals.

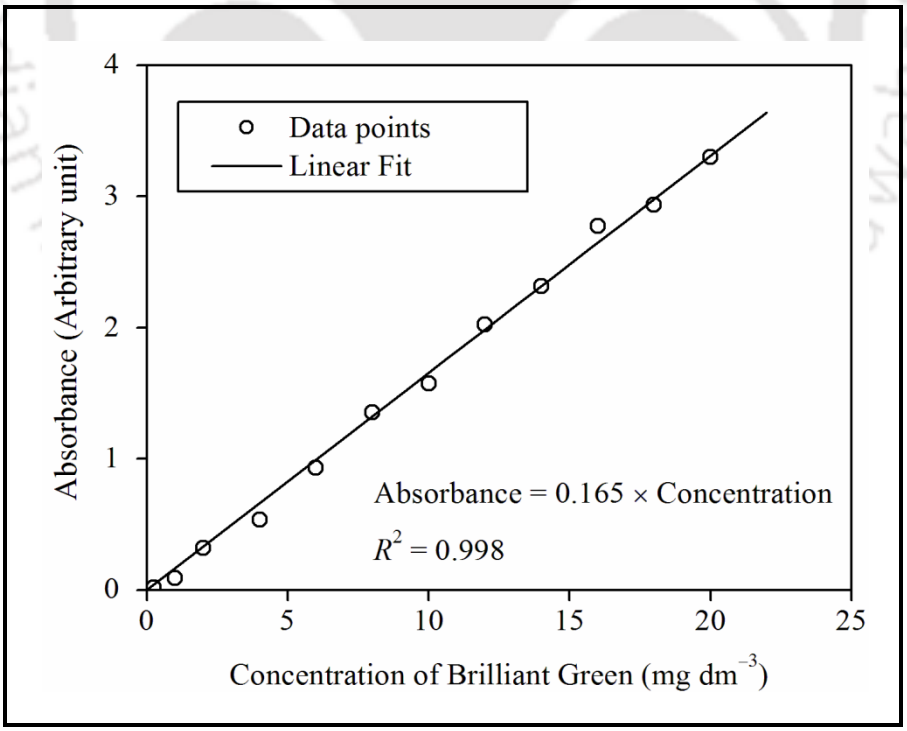

Figure 3.5 UV-Vis calibration curve for BG.

2 gof sodium thiosulfate pentahydrate was added to the sample under continuous stirring to quench the reaction. The absorbance of the dye was measured at the maximum absorption wavelength of 625 nm using a UV−Visible spectrophotometer [Perkin Elmer (Switzerland), model: Lambda 35]. The ozone concentration was measured by using the Indigo Colorimetric Method (Eaton et al., 2005)using potassium indigo trisulfonate as the indicator. The calibration curve for concentration of Brilliant Green (BG) is shown in Figure 3.5.

3.3.4.2 Analysis of Dye Intermediates

The reaction intermediates were analyzed by a gas chromatography (GC)[Varian (The Netherlands), model: 450-GC] connected to a mass spectrometer (MS) [Varian (The Netherlands), model: 240-MS]. It is reported that the sulfonated azo dyes are non-volatile and difficult to detect by using GC–MS (Poiger et al., 2000). However, the intermediates formed by dye degradation can be easily detected by GC–MS (Feng et al., 2000). The sample for GC–MS analysis was prepared as follows (Diao et al., 2013; Muruganandham and Swaminathan, 2006). 10 cm^3 sample was evaporated in an air oven at 323 Kfor 40 h followed by drying in air to attain a constant weight. The remaining mass (i.e. about 1−2 g) was dissolved in 10 cm^3 methanol. Anhydrous sodium sulfate (3−5 g) was added to dehydrate the sample. The liquid mixture was collected in a 5 cm^3glass vial for analysis.

The GC conditions were as follows. The split/splitless injector was operated at 533 K with the split closed for 5 min. Helium (> 99.999% pure) was used as the carrier gas at a flow rate of 1 cm^3min^{-1}. The column used for the analysis was VF-5ms [Varian (The Netherlands)] and its dimensions were 30 m × 0.25 mm. The thickness of the column film of the stationary phase was 0.25 μm. The temperature program was set as follows. The initial column oven temperature was 333 K for 4 min, and the temperature was then increased to 423 K at a rate of 5 K min^{-1}. After that, the temperature was raised from 423 K to 553K at a

rate of 15 K min^{-1}. The temperature was then maintained at 553 K for 5 min. The MS conditions were as follows. The temperature of the ion source was set at 573 K. The detector voltage was 1 kV. The electron impact (70 eV) ionization mode was used. The data were acquired in the full scan detection mode from 35 to 350 amu at a rate of 0.5 $scans^{-1}$.the products were identified bycomparing the mass spectra with NIST 98 Library providedwith the GC−MS instrument.

FTIR spectroscopy was used to analyze the functional groups of the compounds present in the samples. 25 cm^3 samples were withdrawn from the reactor at 0, 5, 15 and 30 min intervals and evaporated at 323 K until a small amount of the liquid was left. The sample was then dried in air until the weight attained a constant value. The sample was then ground with KBr to make pellets for FTIR analysis. For FTIR and GC–MS analyses, the experiments were performed at 0.164 $mmoldm^{-3}$ concentration of BG.

3.3.4.3 Analysis of Total Organic Carbon (TOC)

The total organic carbonwas measured by using a TOC analyzer [O.I. Analytical (USA), model: Aurora 1030]. 15 cm^3 samples were withdrawn from the reactor at different time intervals and the TOC was measured.

3.3.5Measurement of Concentration of Hydroxyl Radicals

3.3.5.1 Measurement of Concentration of PCBA and Phenol

The concentration of PCBA was detected by using a HPLC [Shimadzu (Japan), model:LC-20AD]equipped with a ternary pump delivery system and ultra violet (UV) detector. 0.3cm^3 sample was injected into the C18 column [Varian(The Netherlands),model: Hypersil ODS, 250 mm length, 4.6 mm ID, 5 µm particle size]. The mobile phase consisted of 55% methanol and 45% water containing 10 $molm^{-3}$ phosphoric acid.

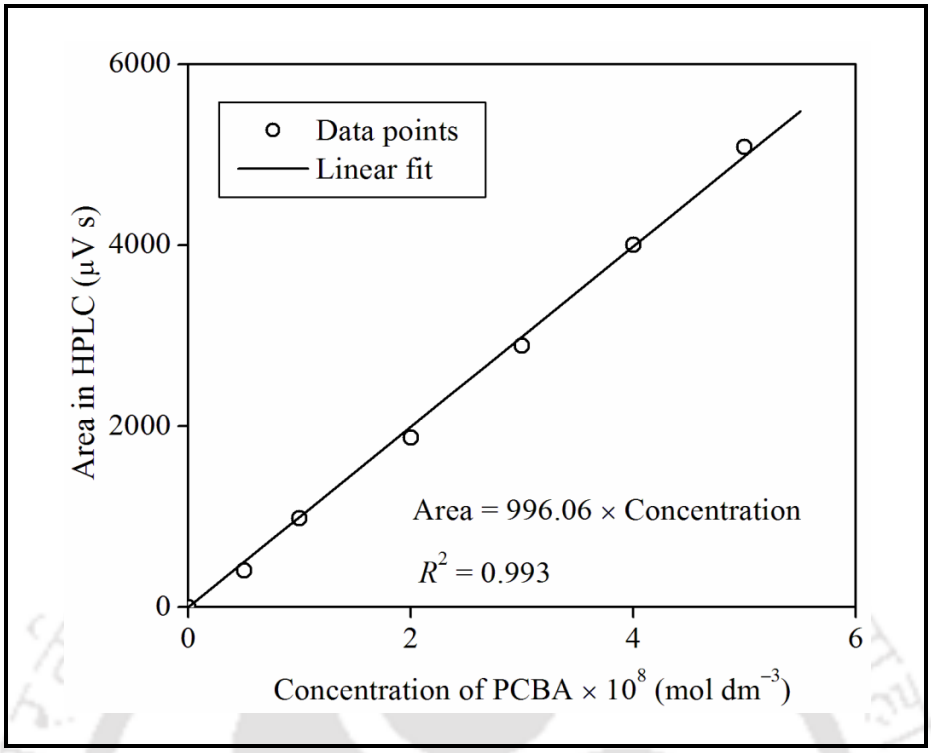

Figure 3.6 HPLC calibration curve for PCBA.

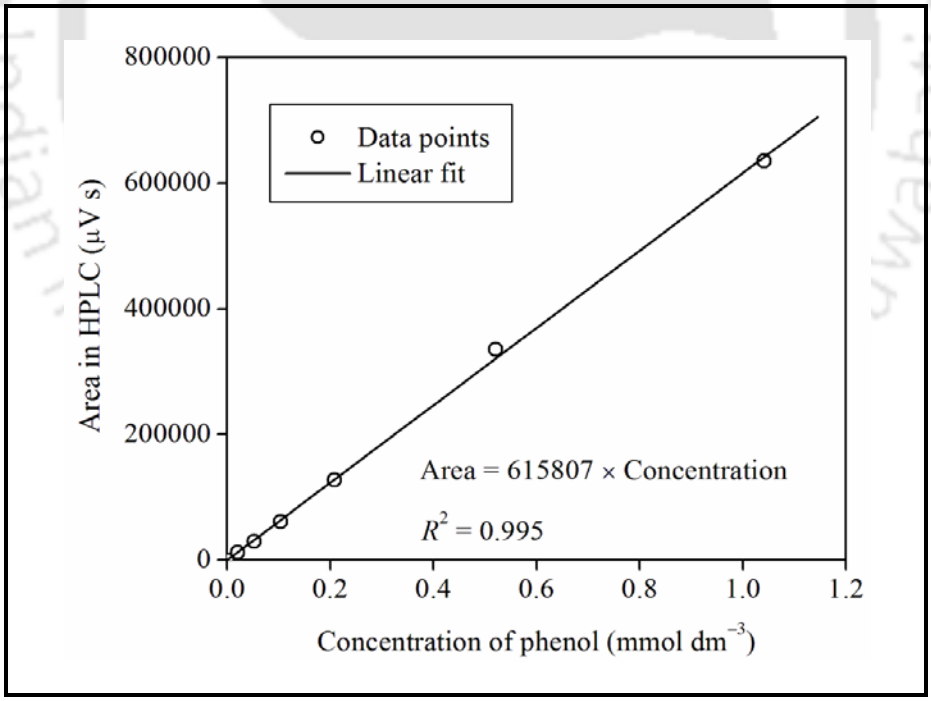

Figure 3.7 HPLC calibration curve for phenol.

PCBA was detected at 234 nm. With 0.3 cm^3 injection, the detection limit was 0.05 μmol dm^{-3}. The concentration of phenol was measured by HPLC using the same C18 column at

280 nm. The mobile phase was constituted of water and acetonitrile (with 0.2% phosphoric acid, pH ~3) in 50:50 volume%. The calibration curves for PCBA and phenol are shown in Figures 3.6 and Figure 3.7, respectively.

3.3.5.2 Indirect Measurement of Hydroxyl Radicals

The concentration of hydroxyl radical was measured by using PCBA as the radical probe. 0.05 μmoldm^{-3}PCBA was added after the aqueous phase in the reactor was saturated withozone. At certain time intervals, 20 cm^3 samples were withdrawn, out of which 2 cm^{3}was used for measuring the concentration of PCBA and the rest was used for measuring the ozone concentration. Effect of carbonate on the generation of hydroxyl radicals was studied by adding 1 and 2 mmoldm^{-3}sodium carbonate. After the saturation of water by ozone, PCBA was added followed by calcium carbonate. All the experiments were performed at 298 K.

The contribution of hydroxyl radical on phenol degradation was determined at pH 3−10. 0.53 mmoldm^{-3} phenol and 0.05 μmoldm^{-3}PCBA were added after the saturation of the aqueous phase by ozone. The procedure for determining the concentrations of PCBA and phenol was similar to that described earlier in this chapter (section 3.3.5.1).

3.4 EXPERIMENTAL CONDITIONS

All experiments were carried out in an air-conditioned room. The oxidation of ammonia, arsenic, dye, PCBA and phenol was done at 298 K. The variation of temperature in the room was within 0.5 K. To keep the temperature of the reaction mass under control, the reactor was placed in a water bath and the temperature of the bath was controlled by an external circulator [Jeio Tech (Korea), model: RW-2025G]. The temperature of the aqueous phase within the reactor was controlled at 298 ± 1 K by this method. The thermodynamic study and the

adsorption of As(V) were done at 298−318 K.Most of the experiments were repeated for 3−4 times to check the variation in the experimental results.

NOTATIONS

R^2	coefficient of determination

Abbreviations	
AAS	atomic adsorption spectrophotometry
BET	Brunauer–Emmett–Teller
EDX	energy dispersive X-ray
FTIR	Fourier transform infrared
GC	gas chromatography
GC–MS	gas chromatography–mass spectrometry
HPLC	high-performance liquid chromatography
PCBA	*p*-chlorobenzoic acid
SEM	scanning electron microscope
TOC	total organic carbon
XRD	X-ray diffractometry

REFERENCES

Behari, J.R., Prakash, R., 2006. Determination of total arsenic content in water by atomic absorption spectroscopy (AAS) using vapour generation assembly (VGA). Chemosphere 63, 17−21.

Cui, H., Li, Q., Gao, S., Shang, J.K., 2012. Strong adsorption of arsenic species by amorphous zirconium oxide nanoparticles. J. Ind. Eng. Chem. 18, 1418−1427.

Diao, Z., Li, M., Zeng, F., Song, L., Qiu, R., 2013. Degradation pathway of malachite green in a novel dual-tank photoelectrochemical catalytic reactor. J. Hazard. Mater. 260, 585−592.

Eaton, A.D., Clesceri, L.S., Rice, E.W., Greenberg, A.E., 2005. Standard Methods for the Examination of Water & Wastewater. American Public Health Association, New York, USA.

Feng, W., Nansheng, D., Helin, H., 2000. Degradation mechanism of azo dye C. I. reactive red 2 by iron powder reduction and photooxidation in aqueous solutions. Chemosphere 41, 1233−1238.

Ficklin, W.H., 1983. Separation of arsenic(III) and arsenic(V) in ground waters by ion-exchange. Talanta 30, 371−373.

Muruganandham, M., Swaminathan, M., 2006. Photocatalytic decolourisation and degradation of Reactive Orange 4 by TiO_2-UV process. Dyes Pigments 68, 133−142.

Okumura, M., Fujinaga, K., Seike, Y., Hayashi, K., 1998. A simple in-situ preconcentraion method for phosphate phosphrous in environmental waters by column solid phase extraction using activated carbon loaded with zirconium. Anal. Sci. 14, 417−419.

Poiger, T., Richardson, S.D., Baughman, G.L., 2000. Identification of reactive dyes in spent dyebaths and wastewater by capillary electrophoresis–mass spectrometry. J. Chromatogr. A 886, 271−282.

CHAPTER 4

REMOVAL OF AMMONIA FROM WATER

CHAPTER 4

REMOVAL OF AMMONIA FROM WATER

This chapter presents the work on the removal of ammonia from water using ozone microbubble. The effects of ozone feed rate and pH of the reaction medium on ozonation have been studied. Removal of ammonia using oxygen microbubbles has also been carried out and compared with that of ozone microbubbles. The mechanism of oxidation of ammonia by microbubbles has been investigated in detail. The catalytic effect of bromide ions on ozonation efficiency has also been studied.

4.1 EFFECT OF pH ON OZONATION OF AMMONIA

The dissociation of NH_4Cl in water results in an equilibrium between the ammonium ion $\left(NH_4^+\right)$ and free ammonia $\left(NH_3\right)$, which can be expressed as

$$NH_3 + H_2O \Leftrightarrow NH_4^+ + OH^- \tag{4.1}$$

The existence of these two species in aqueous solution is dependent on the pH of the solution. At pH < 7, the ammonium form $\left(NH_4^+\right)$ dominates whereas at pH > 7, the amount of free ammonia $\left(NH_3\right)$ increases(Lin and Wu, 1996). The fraction of free ammonia at a given pH can be calculated from the following equation(Kuo et al., 1997).

$$\frac{c_{NH_3}}{c_{NH_4^+} + c_{NH_3}} = \frac{10^{pH-14}}{K_b + 10^{pH-14}} \tag{4.2}$$

where K_b= 1.774 × 10^{-5} at 298 K. Equation (4.2) indicates that the fraction of free ammonia drastically increases with increasing pH. For example, the fraction of free ammonia at pH 6 is 6 × 10^{-4}, which increases to 0.4 at pH 9. According to Hoigné and Barder(1978), ozone

cannot oxidize NH_4^+, but it can oxidize free ammonia directly or indirectly. A similar phenomenon has been observed by Kuo et al.(1997).

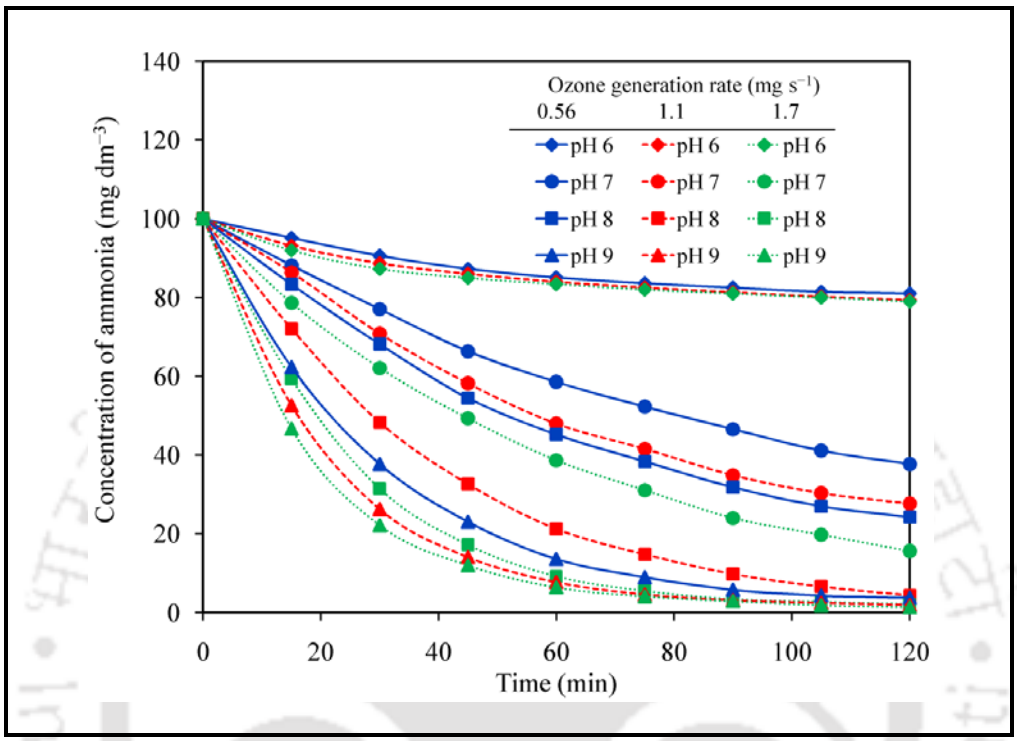

Figure 4.1 Effect of pH on oxidation of ammonia by ozone microbubbles at different ozone generation rates.

The effect of pH on the ozonation of ammonia at different ozone generation rates is shown in Figure4.1. It was observed that the increase in pH from 6 to 9 favored the removal of ammonia. With increasing pH, the percentage of ammonia in the ammonia/ammonium mixture increased. At pH 6, only 19% ammonia could be removed in 120 min. However, a remarkable increase in the removal of ammonia was observed at pH 9, at all the ozone generation rates. The oxidation of ammonia can be very fast when pH > 9, because of the conversion of ammonium to free ammonia. However, the microbubble generator used in this work is operable in the pH range of 6 to 9 (as per the recommendation of its manufacturer), and therefore, the experiments were conducted in the aforementioned pH range. The pH of

the industrial effluents containing ammonia lies in the range 7−8.5 (Table 4.1). It is noticed that under this pH range the ammonia oxidation can be done, although for some effluents further addition of alkali is required. However the addition of alkali can be considered as the additional pollution, but it was observed that after the oxidation the pH of the medium decreases, which will be discussed in this section later.

Table 4.1 pH of various effluents containing ammonia.

Source of ammonia	pH	Reference
Spent brine	7	Tanaka and Matsumura (2003)
Diluted chemical industrial wastewater	7.32 ± 0.17	Ramos et al. (2007)
Raw leachate	8.22	Li et al. (1999)
	7.53 ± 0.5	Wang et al. (2006)
Mine effluents	7−8	Koren et al. (2000)
Anaerobic digestion effluent wastewater	8.5	Park et al. (2010)
Aquaculture system	7.49–7.77	Gendel and Lahav (2013)

pH plays an important role in the decomposition of ozone into hydroxyl radicals(Beltrán, 2004).Formation of these radicalstakes place via a series of initiation, propagation and termination steps. Takahashi et al. (2007)have shown that hydroxyl radicals can form from ozone microbubbles under strongly-acidic conditions in the presence of mineral acids (i.e. HCl, H_2SO_4, and HNO_3). According to them, the extreme accumulation of ions around the surface of the collapsing microbubbles transforms ozone to the ·OH radicals. The hydroxyl radicals are strongeroxidizing species as compared to ozone, which is reflected by their standard redox potentials (viz. 2.8 and 2.07 V for ·OH and O_3 respectively)(Beltrán, 2004). However, as their occurrence depends on the pH of the medium, the mechanism of

oxidation of ammonia can occur either by direct oxidation or via the hydroxyl radicals. According to Hoigné and Bader(1978), direct oxidation of ammonia occurs at pH < 9. In thiswork, pH of the solution was varied from 6 to 9. Direct oxidation is likely to occur in this range of pH. At low pH, the concentration of free ammonia is practically negligible, and therefore, the rate of oxidation of ammonia is very slow. As the pH was increased, more free ammonia is formed, and the availability of free ammonia enhances the rate of oxidation.

There are a few methods for detecting the role of hydroxyl radicals in ammonia oxidation. Carbonate ions, whenever present in a concentration comparable to that of NH_3, may protect it from oxidation by reducing the hydroxyl radical(Hoigné and Bader, 1978). The carbonate ions become oxidized to $HCO_3\cdot$ by the hydroxyl radicals according to the reaction

$$\cdot OH \xrightarrow{+CO_3^{2-}} HCO_3\cdot \qquad (4.3)$$

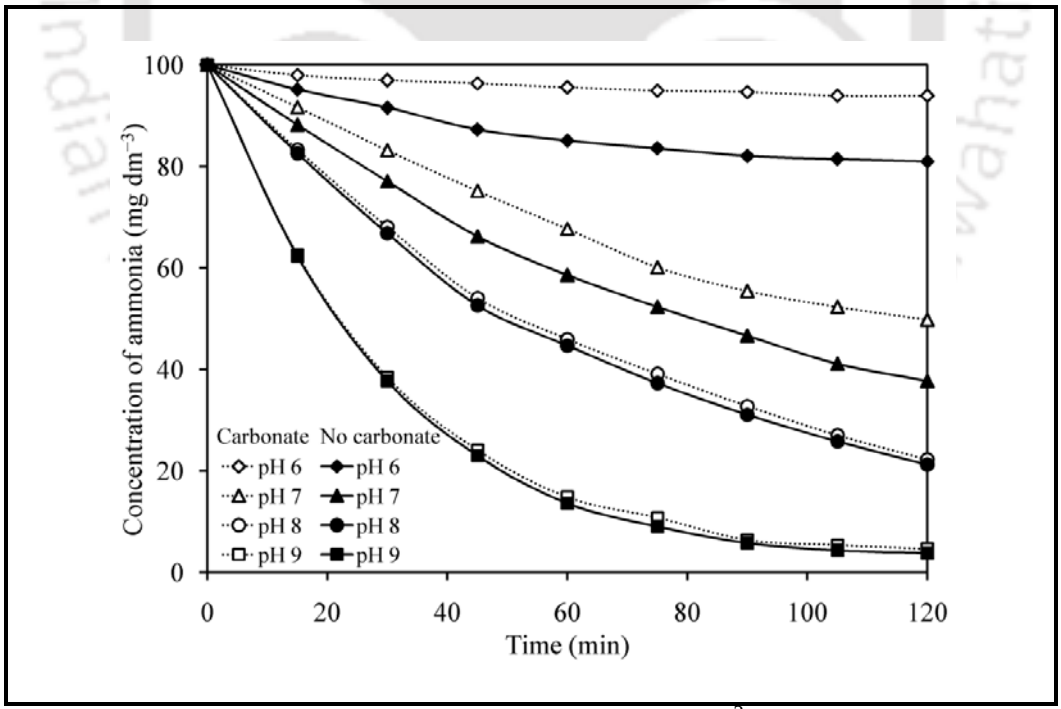

Figure 4.2 Effect of sodium carbonate (100 mg dm^{-3})on the oxidation of ammonia at different pH (ozone generation rate = 0.56 mg s^{-1}).

Figure 4.2 shows the effect of carbonate on the oxidation of ammonia in the pH range of 6 to 9. At pH 6, the oxidation of ammonia was very small. However, the addition of carbonate inhibited the reaction almost completely. At pH 7, the rate of oxidation decreased due to the protective effect of carbonate. At pH 8 and 9, the effect of addition of carbonate was negligible, and the concentration profiles of ammonia were unaltered. This shows that, at pH 6 and 7, there was generation of free radicals, which oxidized ammonia. At such low pH, where the fraction of free ammonia was small, the oxidation was due to both direct reaction of ammonia with ozone as well as by the reaction with hydroxyl radicals. This also shows that at pH 8 and 9, oxidation of ammonia was mainly due to the direct reaction with molecular ozone. A similar effect of carbonate ions was observed at the other ozone generation rates.

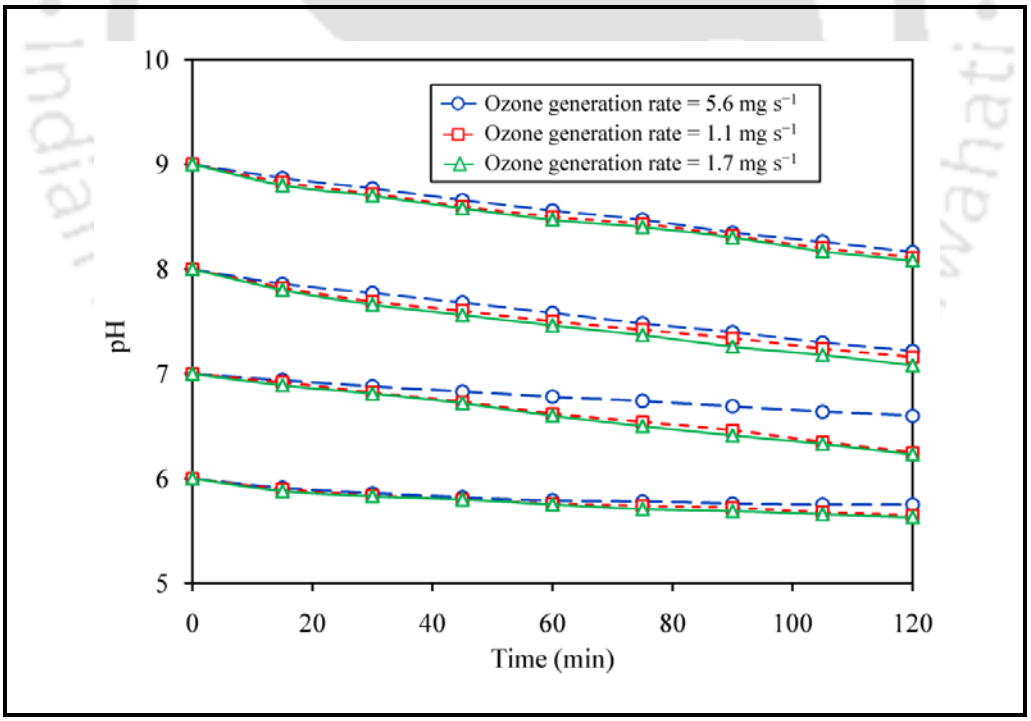

Figure 4.3 Variation of pH during ozonation of ammonia in the reactor.

The pH of the aqueous solution inside the reactor slightly decreased with time, as shown in Figure 4.3, due to the conversion of ammonia to nitrate and formation of H^+ ion. Because pH

plays such an important role in the ozonation of ammonia, this reduction in pH would slow down the rate of reaction by lowering the amount of free ammonia. The allowable limit of ammonia in water is usually below 1 mg dm^{-3}. Therefore, a study was undertaken using a 1 mg dm^{-3} feed solution of ammonium chloride, and the concentration profiles of total ammonia with time were developed (shown in Figure 4.4). It is observed from this figure that the ozone microbubbles effectively oxidized ammonia and the total ammonia concentration was considerably reduced.

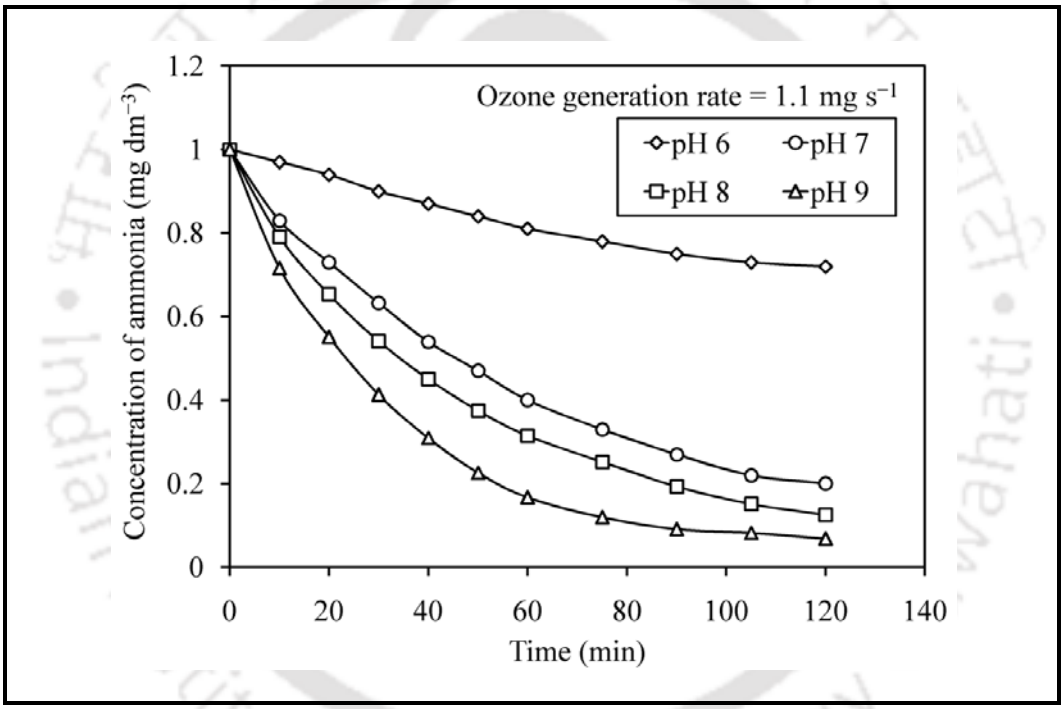

Figure 4.4 Effect of pH on oxidation of ammonia by ozone microbubbles

4.2 EFFECT OF OZONE GENERATION RATE ON OXIDATION OF AMMONIA

In this pilot-plant study of removal of ammonia by ozone, the concentration of ozone in the gas mixture (i.e. mixture of oxygen and ozone) was small (0.7−2% by volume). This was necessary as per the design of the ozonator so that a continuous stable operation was possible.

Many commercial ozonation plants for water treatment use a similar concentration of ozone in the feed gas. Increase in the concentration of ozone in the gas fed to the microbubble generator increased the rate of oxidation of ammonia due to the enhanced concentration of ozone in the aqueous phase.

The solubility of ozone in water is several times higher than that of oxygen. To illustrate, the mole fraction solubility of oxygen in water is 2.3×10^{-5} and the same for ozone is 9.1×10^{-5} at 298 K and atmospheric pressure(Scharlin et al., 1998). Therefore, when a mixture of ozone and oxygen is passed into water in the form of microbubbles, ozone preferentially dissolves in water. The concentration of ozone in the aqueous phase can be described by the Henry's law: $\tilde{p} = Hc$. The Henry's law constant, *H*, depends on pH and temperature. The equilibriumconcentration of ozone in the aqueous phase is given by (Roth and Sullivan, 1981)

$$c^{*}_{O_3} = \left(\frac{\rho RT}{M}\right)\frac{c_g}{H} \tag{4.4}$$

The Henry's law constant, *H*, depends on pH andtemperature, which is given by (Roth and Sullivan, 1981)

$$H = 3.84\times10^{7} c_{OH^-}^{0.035} \exp(-2428/T) \tag{4.5}$$

At low ozone generation rate, the partial pressure of ozone in the gas mixture that formed the microbubbles was low due to the presence of a large percentage of oxygen in the gas. Therefore, the concentration of ozone in the aqueous phase was low.The effect of ozone generation rate on ammonia oxidation can be observed from Figure 4.1. When the ozone production rate was high (e.g. 1.7 mg s^{-1}), the concentration of ozone in the aqueous phase was high, due to which the rate of reaction considerably increased. The concentration profiles of ozone in the reactor at pH 9 is shown in the Figure4.5. Ozone has a short lifetime in water, and decomposes readily(Rakness, 2005). Therefore, the profiles shown in Figure4.5 depict

the amount of ozone, which was available in the reactor after reacting with ammonia, and after its self-decomposition. Effect of ozone generation rate on ozonation of ammonia at pH 6−9 is given in Figure 4A.1 (Appendix 4A). The ozone concentration profiles at pH 6−8 are given in Figure 4A.2.

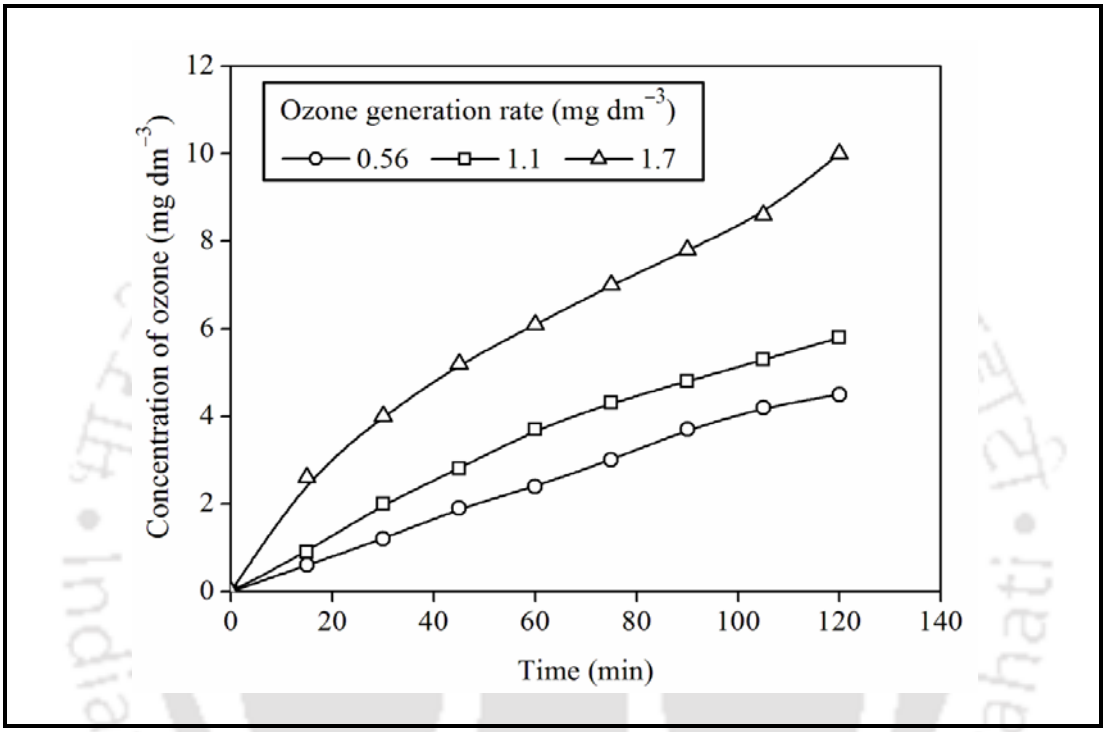

Figure 4.5 Ozone concentration profiles in the reactor in presence of ammonia.

4.3 OZONATION USING AMMONIUM SULFATE

Ammonium chloride was used as the source of ammonia in the works described in Sections 4.1 and 4.2. Ozone has the potential to oxidize chloride to chlorine, which is also capable of oxidizing ammonia. To investigate whether the chloride ion had any role in the ammonia oxidation process, another ammonium salt (i.e. ammonium sulfate) was used. Figure 4.6 shows the comparison of oxidation of ammonia at pH 8 using ammonium chloride and ammonium sulfate. It can be observed from this figure that ozonation of ammonia was practically the same for both the ammonium salts. No significant variation was observed at

other pH as well. This confirms that chloride or sulfate had no role in the ozonation of ammonia. The comparison of ozonation of NH_4Cl and $(NH_4)_2SO_4$ at pH 6, 7 and 9 at three ozone generation rates are given in Figure 4A.3.

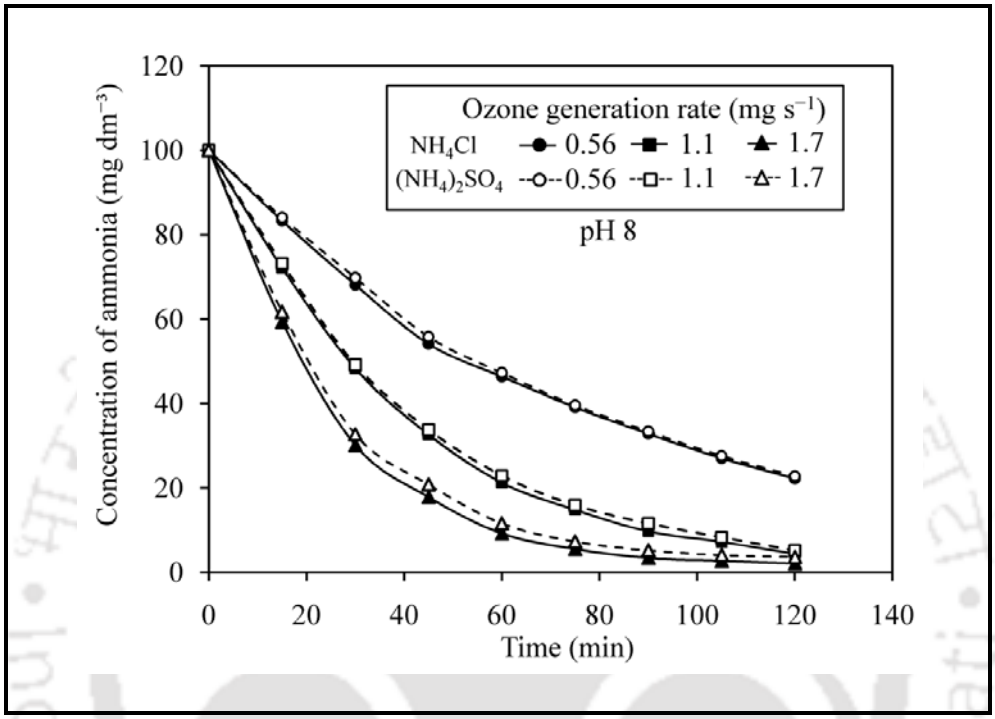

Figure 4.6 Comparison of ozonation of NH_4Cl and $(NH_4)_2SO_4$ at pH 8.

4.4 OXIDATION OF AMMONIA USING OXYGEN MICROBUBBLES

It has been reported in the literature that free hydroxyl radicals are generated from collapsing oxygen microbubbles under strongly acidic conditions(Li et al., 2009; Takahashi et al., 2007). These free radicals have been detected using the electron spin-resonance method. Therefore, the possibility of oxidation of ammonia by the free radicals generated from oxygen microbubbles was explored. Experiments were conducted at pH 6, 7, 8 and 9. The concentration profiles of ammonia at these pH are shown in Figure4.7. It is observed that there was a small amount of oxidation of ammonia at pH 7. However, there was hardly any oxidation at pH 9, and practically no change in the concentration of ammonia with time at

this pH. On the other hand, at pH 6 and 8, there was a small decrease in the ammonia concentration.

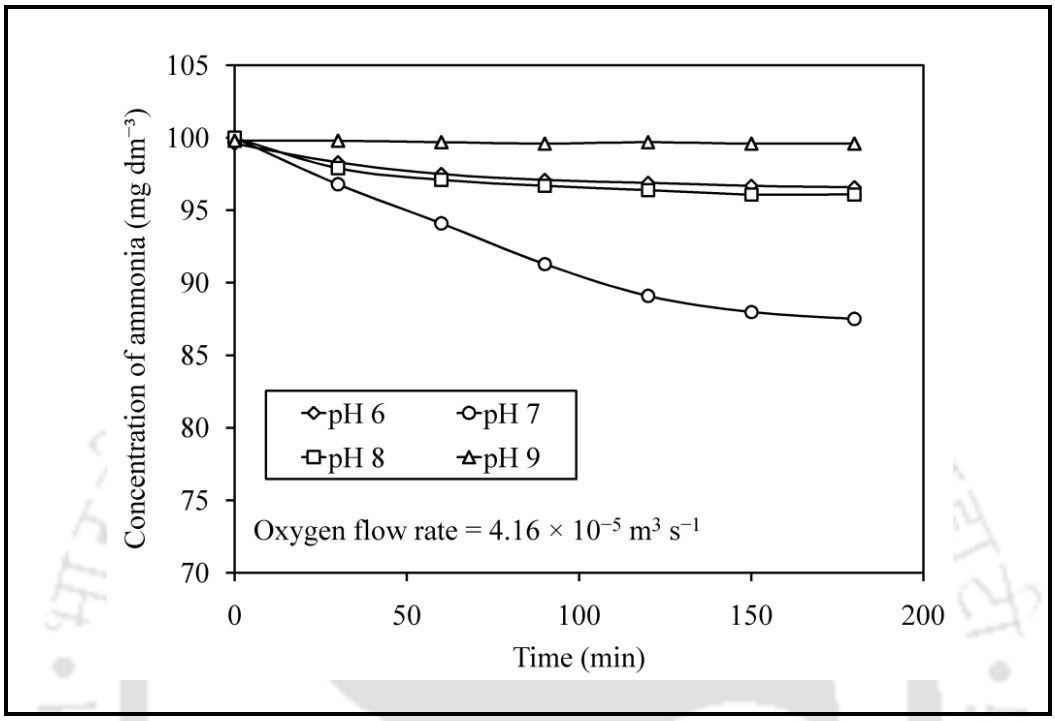

Figure 4.7 Effect of pH on oxidation of ammonia by oxygen microbubbles.

These results indicate the possibility of oxidation of ammonia by the hydroxyl radicals at low pH. At pH 6, the amount of free radical is likely to be more than that at pH 8, but the free ammonia available for oxidation is very small. It appears that the most favorable condition was attained at pH 7. The oxidation of ammonia using oxygen microbubbles, therefore, cannot be considered as an effective process. For oxidation of ammonia, the pH of the medium needs to be increased for the availability of free ammonia.However, this would diminish the generation of ·OH radicals from the oxygen microbubbles. The results presented in this section clearly indicate that the oxidation of ammonia in natural water by oxygen would be very slow, and practically unimportant. Therefore, the oxygen demand exerted by ammonia would be insignificant.

4.5 OZONATION OF AMMONIA USING BROMIDE CATALYST

It isseenfrom Eq. (2.1) that ammonia reacts with ozone and forms nitrate. Nitrate is also hazardous for humans as well as for the animals(Ghafari et al., 2008). According to Yang et al.(2000), there is a possibility of the formation of nitrite by direct reaction of ammonia with ozone. Also, the United States Environmental Protection Agency(EPA) and WHO have set the maximum contaminant of 10 mg dm^{-3}(Ghafari et al., 2008). However, nitrite further reacts with ozone, and finally nitrate is formed. These reactions are shown below.

$$NH_3 + 3O_3 \rightarrow NO_2^- + 3O_2 + H^+ + H_2O \quad (4.6)$$

$$NO_2 + O_3 \rightarrow NO_3^- + O_2 \quad (4.7)$$

Several works have demonstrated that nitrate, thus formed, can be converted to nitrogen in the presence of a bromide salt(Haag and Hoigné, 1983; Lin and Yen, 1996; Tanaka and Matsumura, 2002; Yang et al., 1999, 2000). Many types of water that are subjected to ozonation often contain some bromide. The reaction of bromide ion with ozone follows the following sequence of reactions(Masschelein and Denis, 1981).

$$O_3 + Br^- \rightarrow OBr^- + O_2 \quad (4.8)$$

$$O_3 + OBr^- \rightarrow Br^- + 2O_2 \quad (4.9)$$

$$2O_3 + OBr^- \rightarrow BrO_3^- + 2O_2 \quad (4.10)$$

$$HOBr \Leftrightarrow H^+ + OBr^- \quad (4.11)$$

It is observed from Eq. (4.10) that ozonation of bromide yields BrO_3^-, which is carcinogenic in nature. The concentration of bromide found in surface water is quite small (0−0.8 $mgdm^{-3}$)(Masschelein and Denis, 1981), whereas in ground water it is only 0−2 mg dm^{-3}(Sweetman and Simmons, 1980). A guideline value of 25 µg dm^{-3} of bromate is recommended by WHO(Haag and Hoigné, 1983). Haag and Hoigné (1983)have reported that

even though ozonation of Br^- forms BrO_3^-, however, this conversion is inefficient due to the cyclic regeneration of Br^-, which is formed by an intermediate, OBr^-, as shown by Eqs. (4.8) and (4.9). HOBr (sometimes termed "active bromine") is the important intermediate, which can brominate ammonia. The active bromine forms slowly in common drinking water treatment practice. Further oxidation of OBr^- to BrO_3^- is slow at low pH. According to Tanaka and Matsumura(2002), formation of BrO_3^- does not occur if ammonia is present in water. However, the production of bromate increases with increasing pH because a higher pH favors the formation of OBr^-, a part of which oxidizes to BrO_3^-, as shown by Eq. (4.10). The following reactions are involved when ammonia reacts with ozone in presence of bromide(Tanaka and Matsumura, 2002, 2003).

$$HOBr + NH_3 \rightarrow NH_2Br + H_2O \quad (4.12)$$

$$HOBr + NH_2Br \rightarrow NHBr_2 + H_2O \quad (4.13)$$

$$HOBr + NHBr_2 \rightarrow NBr_3 + H_2O \quad (4.14)$$

$$2H_2O + NHBr_2 + NBr_3 \rightarrow N_2 + 3Br^- + 3H^+ + 2HOBr \quad (4.15)$$

Tanaka and Matsumura(2003) have suggested three pathways of ozonation of ammonia. The first pathway is described by Eqs. (4.12)−(4.15), in which hypobromous acid reacts with ammonia and intermediates such as NH_2Br, $NHBr_2$ and NBr_3 are formed. Finally, these compounds are converted to nitrogen, as depicted by Eq. (4.15). A different reaction for the formation of N_2 [which may be viewed as an alternative of Eq. (4.15)] has been proposed by Yang et al.(1999). This is given by

$$NH_3Br + NHBr_2 \rightarrow N_2 + 3Br^- + 3H^+ \quad (4.16)$$

The overall reaction of ammonia with active bromine, as per Eqs. (4.12)−(4.15), is given by(Tanaka and Matsumura, 2002)

$$3HOBr + 2NH_3 \rightarrow N_2 + 3Br^- + 3H^+ + H_2O \quad (4.17)$$

The second pathway is described by the following reaction, in which nitrate is formed by the reaction of NH_2Br with ozone.

$$3O_3 + NH_2Br \rightarrow NO_3^- + Br^- + 2H^+ + 3O_2 \quad (4.18)$$

The third pathway involves direct reaction of ammonia with ozone, and the formation of nitrate, as given by Eqs. (4.6) and (4.7). Ozonation transforms bromide into hypobromous acid (HOBr) and hypobromite (OBr^-), which are in equilibrium with each other. Hypobromous acid is a weak acid which reacts very slowly with ozone and does not contribute significantly to bromate formation. It has been reported by von Gunten and Hoigné (1994)that, $NHBr_2$ is formedfor molar ratios of $c_{HOBr}/c_{NH_4^+} > 1$, which reacts four times more slowly that NH_2Br. The reaction given in Eq. (4.15) leads to a further delay in bromate formation.

In this work, ozonation of ammonia in presence of bromide was carried out by keeping the concentrations of the ammonium and bromide salts in the 4:1 weight ratio (i.e. 18:1 molar ratio). The molar ratio of ammonia and bromide for complete reaction is 2:3, as shown in Eq. (4.17). However, after the oxidation of ammonia is completed, the bromate formation can be significant at high bromide concentrations. To avoid this additional bromate formation, the experiments were carried out at a very low bromide and ammonia ratio. Figure 4.8 shows the depletion of ammonia with time in presence of bromide. The concentration of nitrate first increased, and then decreased because it was converted to nitrogen. At lower pH and lower ozone generation rates, the concentration of nitrate was higher, which indicates that the conversion to nitrogen was less. Furthermore, the maxima of the nitrate concentration profiles shifted to the higher times under these conditions. Such a low bromide/ammonia molar ratio was also effective to oxidize ammonia into nitrate, and

further into nitrogen. The complete conversion of ammonia to nitrogen was fast. The depletion of ammonia with and without the bromide catalyst is shown in Figure 4A.4. The concentration profiles of ammonia and nitrate in presence of bromide at pH 7 and 8 are shown in Figure 4A.5.

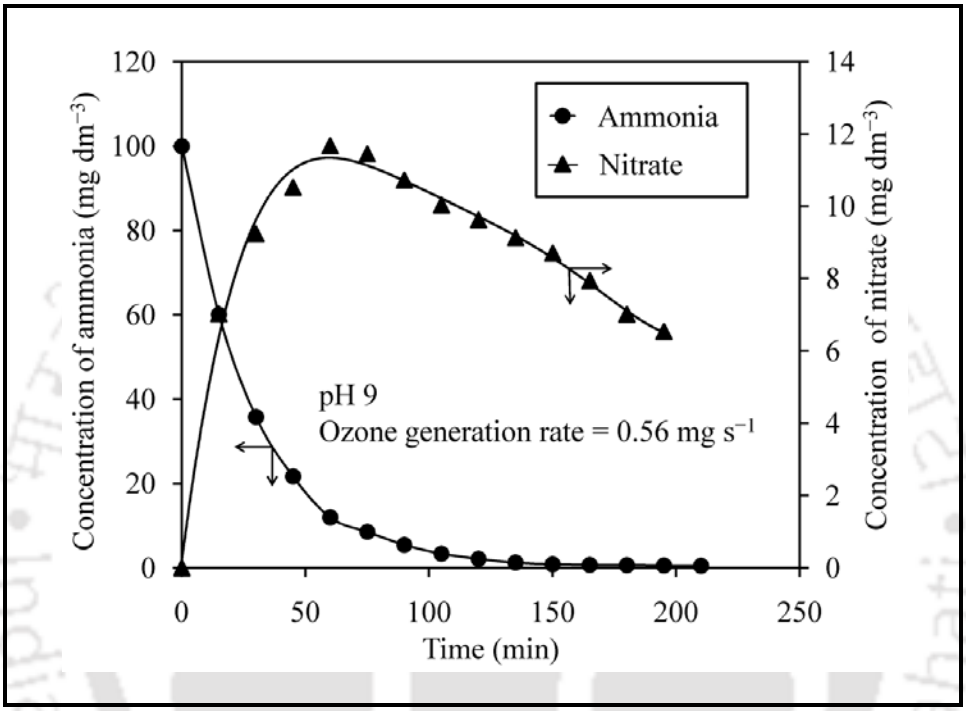

Figure 4.8 Concentration profiles of ammonia and nitrate in the reactor in presence of bromide.

4. 6 MASS TRANSFER OF OZONE BY MICROBUBBLES

The volumetric mass transfer coefficient, $k_l a$,for ozone absorption using microbubbles was studied at different pH (viz. pH 6, 7, 8 and 9) and ozone generation rates. The concentration of ozone dissolved in water, increased with time, and became constant, which corresponds to the steady state concentration of ozone dissolved in water, c_{ss} at $t \rightarrow \infty$. The steady-state concentration is reached when the solute concentrations in the gas and the liquid are constant. For the determination of the volumetric mass transfer coefficient of ozone, two phenomena

are important,i.e. the mass transfer of the gaseous ozone into the aqueous phase and the rate of self-decomposition of ozone absorbed into solution. Many researchers have reported that decomposition of ozone in water is a function of pH and temperature, which follows a first-order reaction rate(Gendel and Lahav, 2013; Roth and Sullivan, 1981; Sotelo et al., 1987). When ozone in the gas phase is absorbed into water and it simultaneously undergoes decomposition reaction in a completely mixed semi-batch reactor, a mass balance equation can be written as

$$\frac{dc_{O_3}}{dt} = k_l a\left(c^*_{O_3} - c_{O_3}\right) - k_d c_{O_3} \tag{4.19}$$

The diffusivity of ozone in gas is much larger than that in water, so the resistance to mass transfer in the gas phase is negligible, compared to that in the liquid phase. The equilibrium concentration of ozone in water can be calculated from the following equation.

$$c_{ss} = \left(\frac{k_l a}{k_l a + k_d}\right) c^*_{O_3} \tag{4.20}$$

From Eqs. (4.19) and(4.20), the mass balance equation for ozone can be written as

$$\frac{dc_{O_3}}{dt} = \left(k_l a + k_d\right)\left(c_{ss} - c_{O_3}\right) \tag{4.21}$$

Integration of Eq. (4.21) with the boundary condition, at t = 0, c_{O_3} = 0, gives the following equations.

$$c_{O_3} = c_{ss}\left[1 - \exp\left\{-\left(k_l a + k_d\right)t\right\}\right] \tag{4.22}$$

$$\ln\left(\frac{c_{ss}}{c_{ss} - c_{O_3}}\right) = \left(k_l a + k_d\right)t \tag{4.23}$$

The concentration of ozone in water increases with time and attains equilibrium after a certain time. The solubility profile of ozone in water is depicted in Figure4.9. The ozone concentration profiles at pH 6–9 at different ozone generation rates are shown in Figure 4A.6.

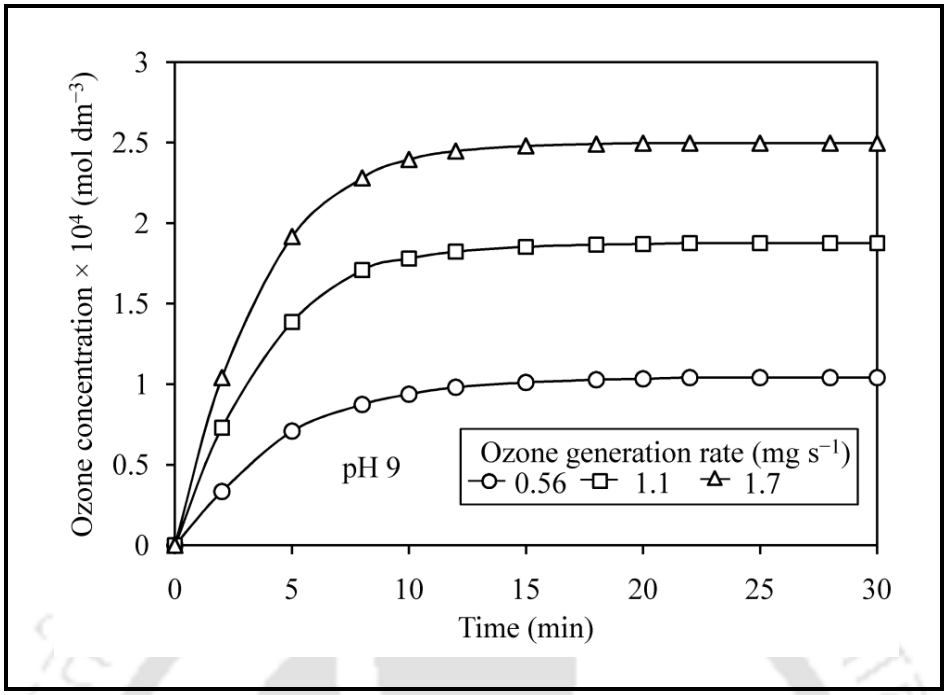

Figure 4.9 Concentration profiles of ozone in water at different ozone generation rates (without ammonia).

A plot of $\ln\left(\frac{c_{ss}}{c_{ss}-c_{O_3}}\right)$ versus *t*, gives a straight line with a slope of $(k_l a + k_d)$ as shown in Figure4.10. The values of k_d at different pH was taken from Sotelo et al.(1987). Same procedure was followed for all pH and ozone generation rates, and the values of volumetric mass transfer coefficients were calculated. These are given in Table 4.2.These values agree well with those reported in the literature for similar systems(Chu et al., 2007, 2008; Kukuzaki et al., 2010).It was observed from Table 4.2 that $k_l a$ increased with increasing ozone generation rate. Increase in the ozone generation rate increased the rate of mass transfer from the gas phase to the aqueous phase, which is evident from the concentration profiles shown in Figure 4.9. Increase in pH also increased the value of $k_l a$. With the increasing pH, the rate of decomposition of ozone increased, which enhanced the rate of mass transfer of ozone. The time taken to reach the steady state concentration decreased with increasing pH.

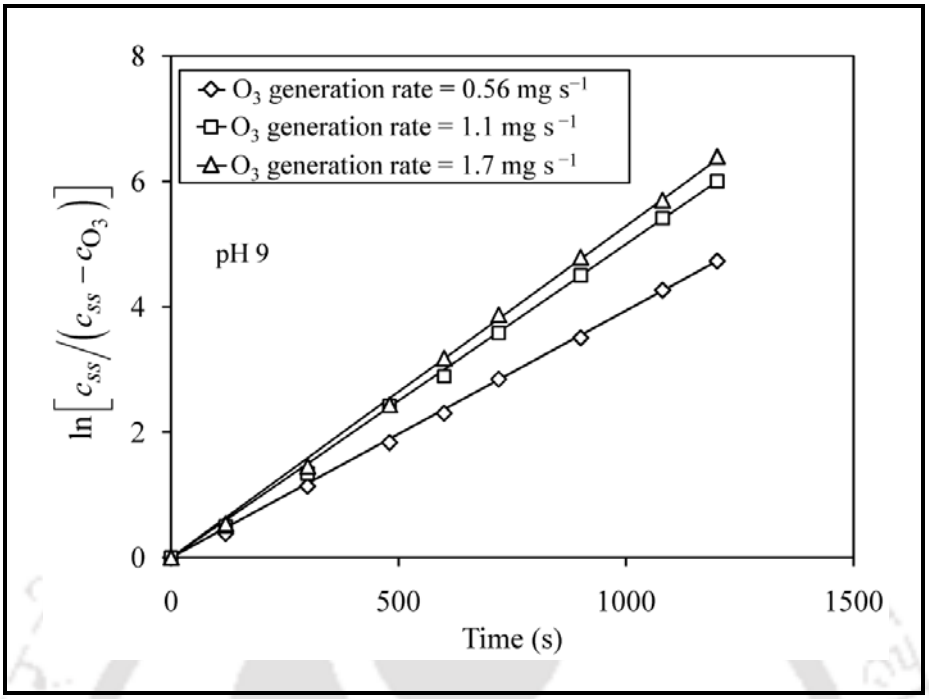

Figure 4.10 Plot of $\ln\left[c_{ss}/\left(c_{ss}-c_{O_3}\right)\right]$ versus*t* at different ozone generation rates.

Table 4.2 Values of volumetric mass transfer coefficient ($k_l a$).

pH	Volumetric mass transfer coefficient, $k_l a \times 10^3$ (s^{-1})			$k_d \times 10^4$ (s^{-1}) (Sotelo et al., 1987)
	O_3 generation rate= 0.56 mg s^{-1}	O_3 generation rate= 1.1 mg s^{-1}	O_3 generation rate= 1.7 mg s^{-1}	
6	1.690	1.928	2.366	2.50
7	1.940	2.183	2.849	3.16
8	2.054	3.196	3.637	7.83
9	2.612	3.674	3.964	13.3

NOTATIONS

c	concentration of ozone in the gas phase, mol m^{-3}
c_{HOBr}	concentration of hypobromous acid in the aqueous phase, mol m^{-3}
c_{NH_3}	concentration of ammonia in the aqueous phase,mol m^{-3}
$c_{NH_4^+}$	concentration of ammonium salt in the aqueous phase,mol m^{-3}
c_{O_3}	concentration of dissolved ozone in aqueous phase at time t, mol m^{-3}
$c^*_{O_3}$	equilibrium ozone concentration in aqueous phase,mol m^{-3}
$C_{[OH^-]}$	concentration of hydroxide ion in aqueous phase, mol dm^{-3}
C_{ss}	steady state ozone concentration in aqueous phase at $t \to \infty$, mol m^{-3}
H	Henry's law constant, Pa molfraction^{-1}
k_d	first-order decomposition rate constant of ozone, s^{-1}
$k_l a$	volumetric mass transfer coefficient of ozone, s^{-1}
K_b	ionization constant of ammonia
M	molecular weight of water,kg mol^{-1}
$\tilde{p}$	partial pressure of ozone in the gas phase, Pa
R	gas constant, J mol^{-1} K^{-1}
t	time, s
T	temperature, K

Greek Letters

ρ	density of water, kg m^{-3}

Abbreviations

WHO	World Health Organization

REFERENCES

Beltrán, F.J., 2004. Ozone Reaction Kinetics for Water and Wastewater Systems. CRC Press, Boca Raton, Florida, USA.

Chu, L.B., Xing, X.H., Yu, A.F., Zhou, Y.N., Sun, X.L., Jurcik, B., 2007. Enhanced ozonation of simulated dyestuff wastewater by microbubbles. Chemosphere 68, 1854−1860.

Chu, L.B., Xing, X.H., Yu, A.F., Sun, X.L., Jurcik, B., 2008. Enhanced treatment of practical textile wastewater by microbubble ozonation. Process Saf. Environ. Prot. 86, 389−393.

Gendel, Y., Lahav, O., 2013. A novel approach for ammonia removal from fresh-water recirculated aquaculture systems, comprising ion exchange and electrochemical regeneration. Aquac. Eng. 52, 27−38.

Ghafari, S., Hasan, M., Aroua, M.K., 2008. Bio-electrochemical removal of nitrate from water and wastewater–a review. Bioresour. Technol. 99, 3965−3974.

Haag, W.R., Hoigné, J., 1983. Ozonation of bromide-containing waters: kinetics of formation of hypobromous acid and bromate. Environ. Sci. Technol. 17, 261−267.

Hoigné, J., Bader, H., 1978. Ozonation of water: kinetics of oxidation of ammonia by ozone and hydroxyl radicals. Environ. Sci. Technol. 12, 79−84.

Koren, D.W., Gould, W.D., Bedard, P., 2000. Biological removal of ammonia and nitrate from simulated mine and mill effluents. Hydrometallurgy 56, 127−144.

Kukuzaki, M., Fujimoto, K., Kai, S., Ohe, K., Oshima, T., Baba, Y., 2010. Ozone mass transfer in an ozone–water contacting process with Shirasu porous glass (SPG) membranes–a comparative study of hydrophilic and hydrophobic membranes. Sep. Purif. Technol. 72, 347−356.

Kuo, C.H., Yuan, F., Hill, D.O., 1997. Kinetics of oxidation of ammonia in solutions containing ozone with or without hydrogen peroxide. Ind. Eng. Chem. Res. 36, 4108−4113.

Li, P., Takahashi, M., Chiba, K., 2009. Enhanced free-radical generation by shrinking microbubbles using a copper catalyst. Chemosphere 77, 1157−1160.

Li, X.Z., Zhao, Q.L., Hao, X.D., 1999. Ammonium removal from landfill leachate by chemical precipitation. Waste Manage. 19, 409−415.

Lin, S.H., Wu, C.L., 1996. Removal of nitrogeneous compounds from aqueous solution by ozonation and ion exchange. Water Res. 30, 1851−1857.

Lin, S.H., Yen, Y.L., 1996. Ozonation kinetics of ammonia and nitrite removal from aqueous solution. J. Environ. Sci. Health A 31, 797−809.

Masschelein, W.J., Denis, M., 1981. The specific determination of bromide in natural waters. Water Res. 15, 857−861.

Park, J., Jin, H.F., Lim, B.R., Park, K.Y., Lee, K., 2010. Ammonia removal from anaerobic digestion effluent of livestock waste using green alga *Scenedesmus* sp. Bioresour. Technol. 101, 8649−8657.

Rakness, K.L., 2005. Ozone in Drinking Water Treatment: Process Design, Operation, and Optimization. American Water Works Association, Denver, USA.

Ramos, A.F., Gomez, M.A., Hntoria, E., Lopez, G.J., 2007. Biological nitrogen and phenol removal from saline industrial wastewater by submerged fixed-film reactor. J. Hazard. Mater. 142, 175−183.

Roth, J.A., Sullivan, D.E., 1981. Solubility of ozone in water. Ind. Eng. Chem. Res. 20, 137−140.

Scharlin, P., Battino, R., Silla, E., Tunon, I., Pascual-Ahuir, J.L., 1998. Solubility of gases in water: correlation between solubility and the number of water molecules in the first solvation shell. Pure Appl. Chem. 70, 1895−1904.

Sotelo, J.L., Beltran, F.J., Benitez, F.J., Beltran-Heredia, J., 1987. Ozone decomposition in water: kinetic study. Ind. Eng. Chem. Res. 26, 39−43.

Sweetman, J.A., Simmons, M.S., 1980. The production of bromophenols resulting from the chlorination of waters containing bromide ion and phenol. Water Res. 14, 287−290.

Takahashi, M., Chiba, K., Li, P., 2007. Free-radical generation from collapsing microbubbles in the absence of a dynamic stimulus. J. Phys. Chem. B 111, 1343−1347.

Tanaka, J., Matsumura, M., 2002. Kinetic studies of removal of ammonia from seawater by ozonation. J. Chem. Technol. Biotechnol. 77, 649−656.

Tanaka, J., Matsumura, M., 2003. Application of ozone treatment for ammonia removal in spent brine. Adv. Environ. Res. 7, 835−845.

von Gunten, U., Hoigne, J., 1994. Bromate formation during ozonation of bromide-containing waters: interaction of ozone and hydroxyl radical reactions. Environ. Sci.Technol. 28, 1234−1242.

Wang, Y., Liu, S., Xu, Z., Han, T., Chuan, S., Zhu, T., 2006. Ammonia removal from leachate solution using natural Chinese clinoptilolite. J. Hazard. Mater. 136, 735−740.

Yang, M., Uesugi, K., Myoga, H., 1999. Ammonia removal in bubble column by ozonation in the presence of bromide. Water Res. 33, 1911−1917.

Yang, M., Uesugi, K., Myoga, H., 2000. Study on by-products of ozonation during ammonia removal under the existence of bromide: factors affecting formation and removal of the by-products. Ozone Sci. Eng. 22, 23−29.

APPENDIX 4A

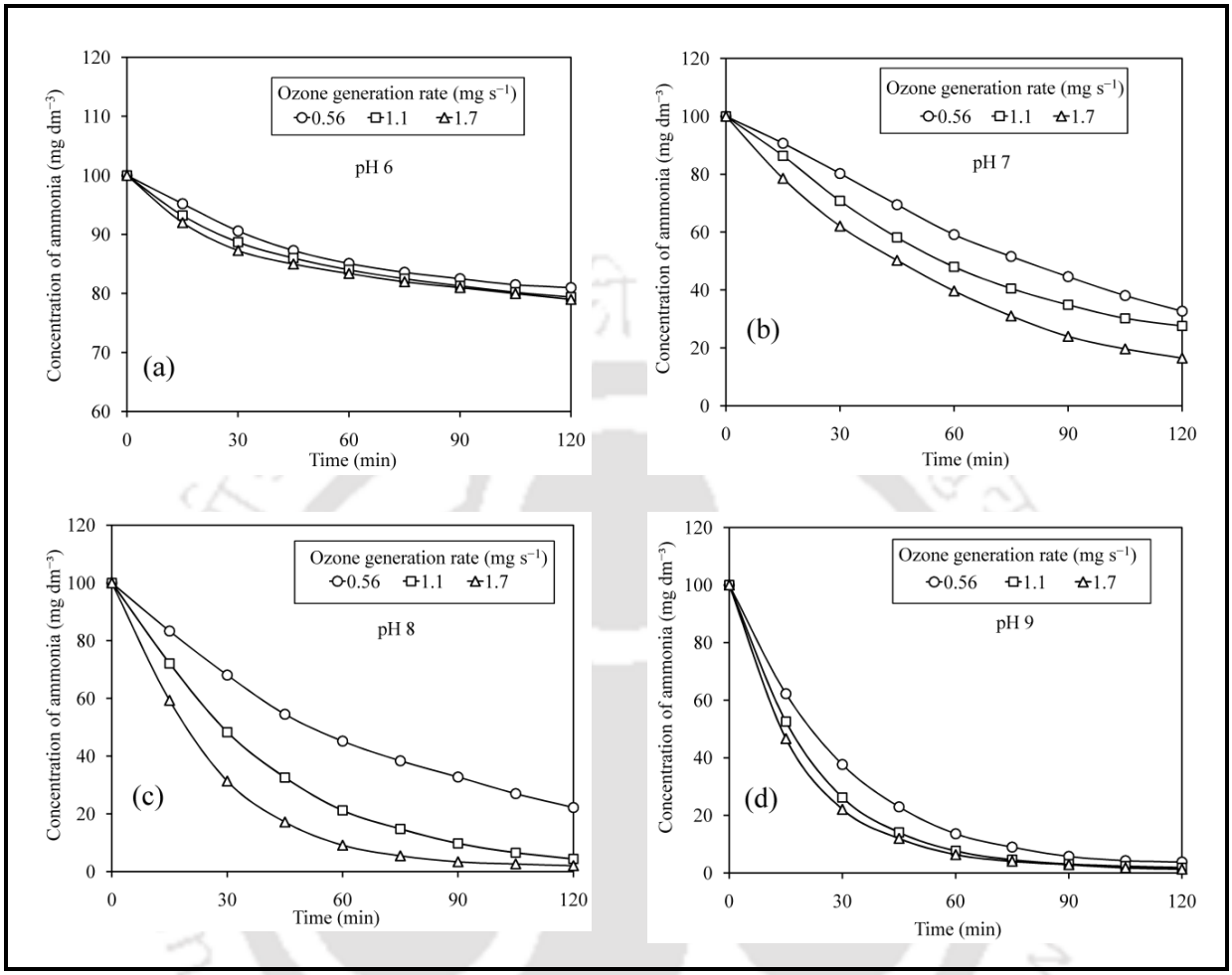

Figure 4A.1 Effect of ozone generation rate on concentration of ammonia at (a) pH 6, (b) pH 7, (c) pH 8, and (d) pH 9.

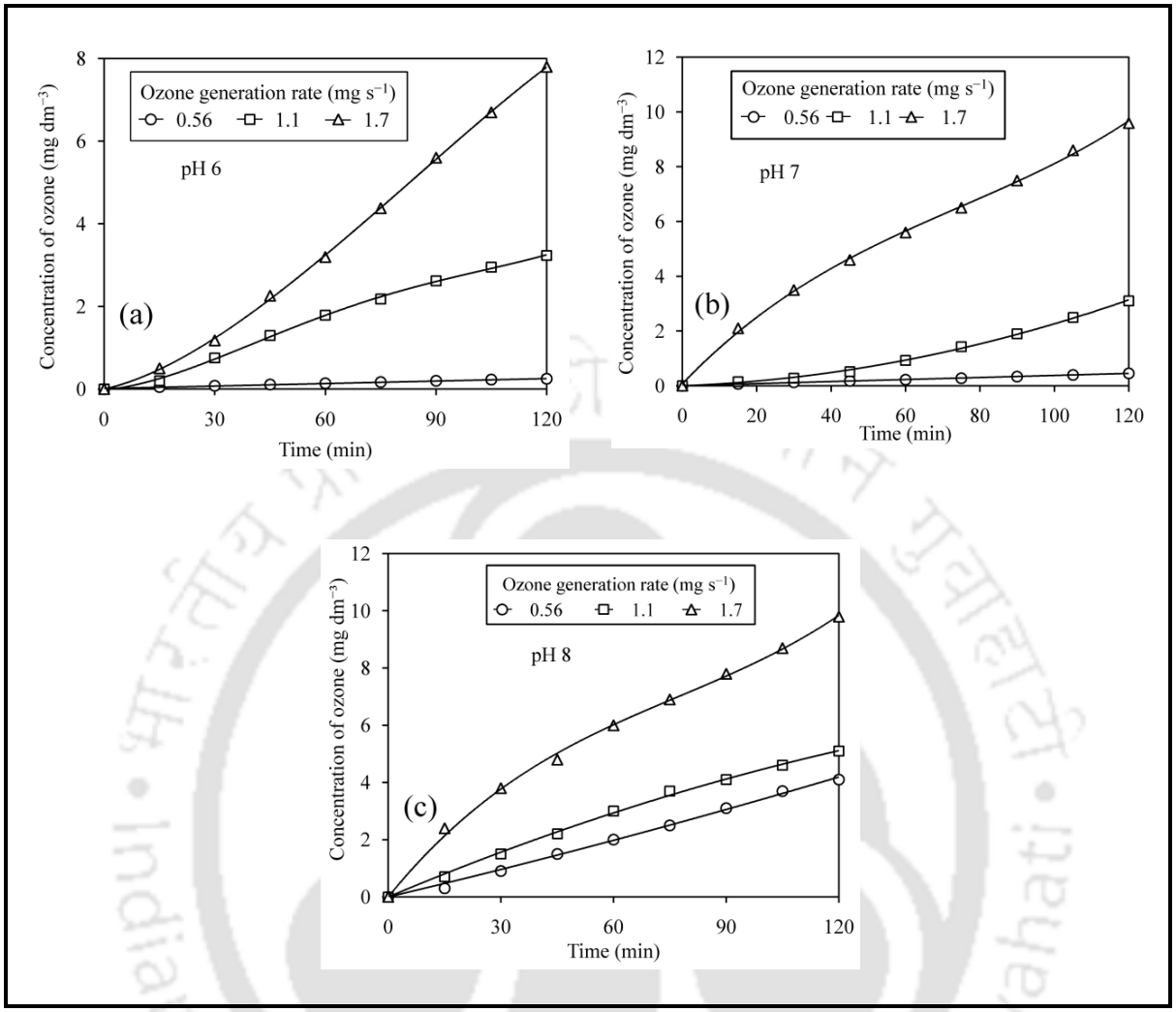

Figure 4A.2 Ozone concentration profiles in the reactor at different ozone generation rates in presence of ammonia at (a) pH 6, (b) pH 7, and (c) pH 8.

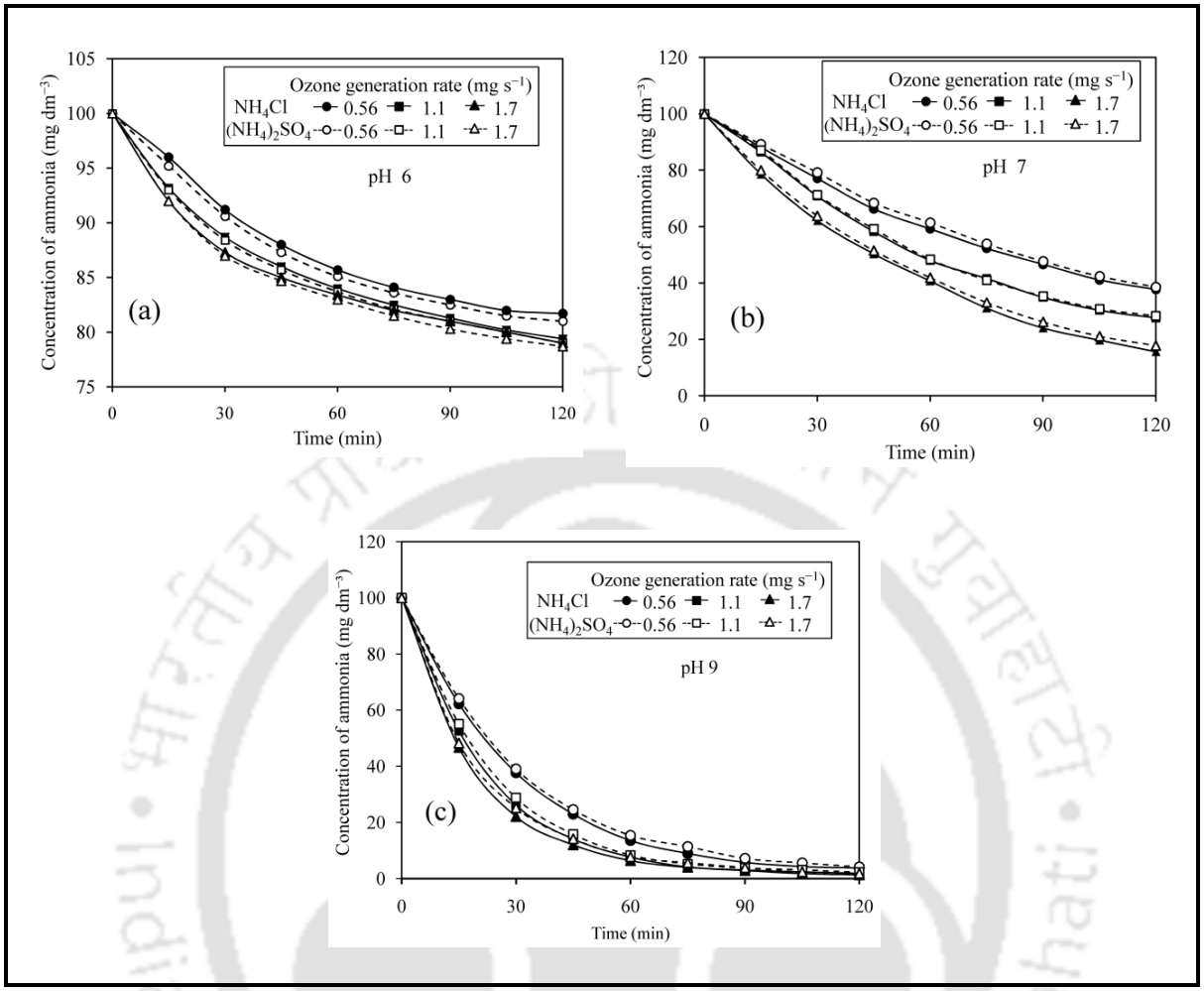

Figure 4A.3 Comparison of ozonation of NH_4Cl and $(NH_4)_2SO_4$ at (a) pH 6, (b) pH 7, and (c) pH 9.

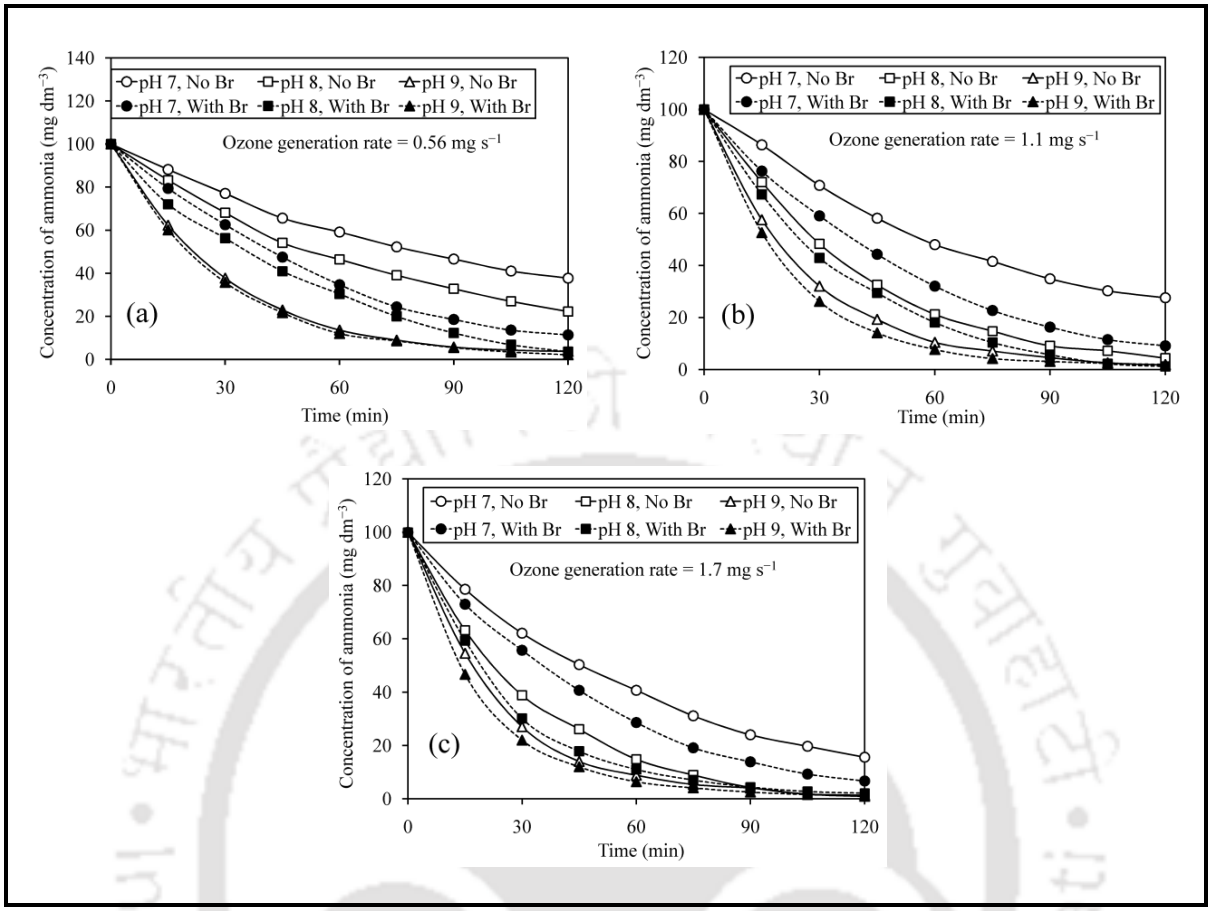

Figure 4A.4 Concentration profiles of ammonia with and without bromide catalyst: (a) ozone generation rate 0.56 mg s^{-1}, (b) ozone generation rate 1.1 mg s^{-1}, and (c) ozone generation rate 1.7 mg s^{-1}.

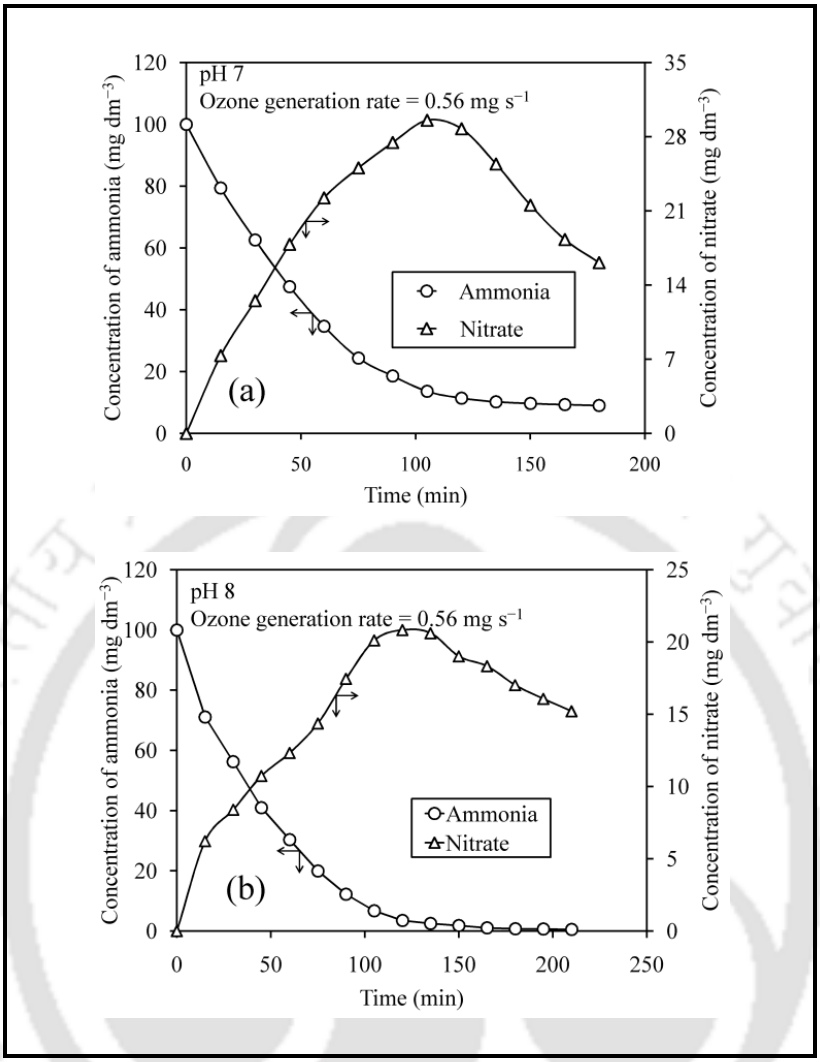

Figure 4A.5 Concentration profiles of ammonia and nitrate in the reactor in presence of bromide: (a) at pH 7, and (b) at pH 8.

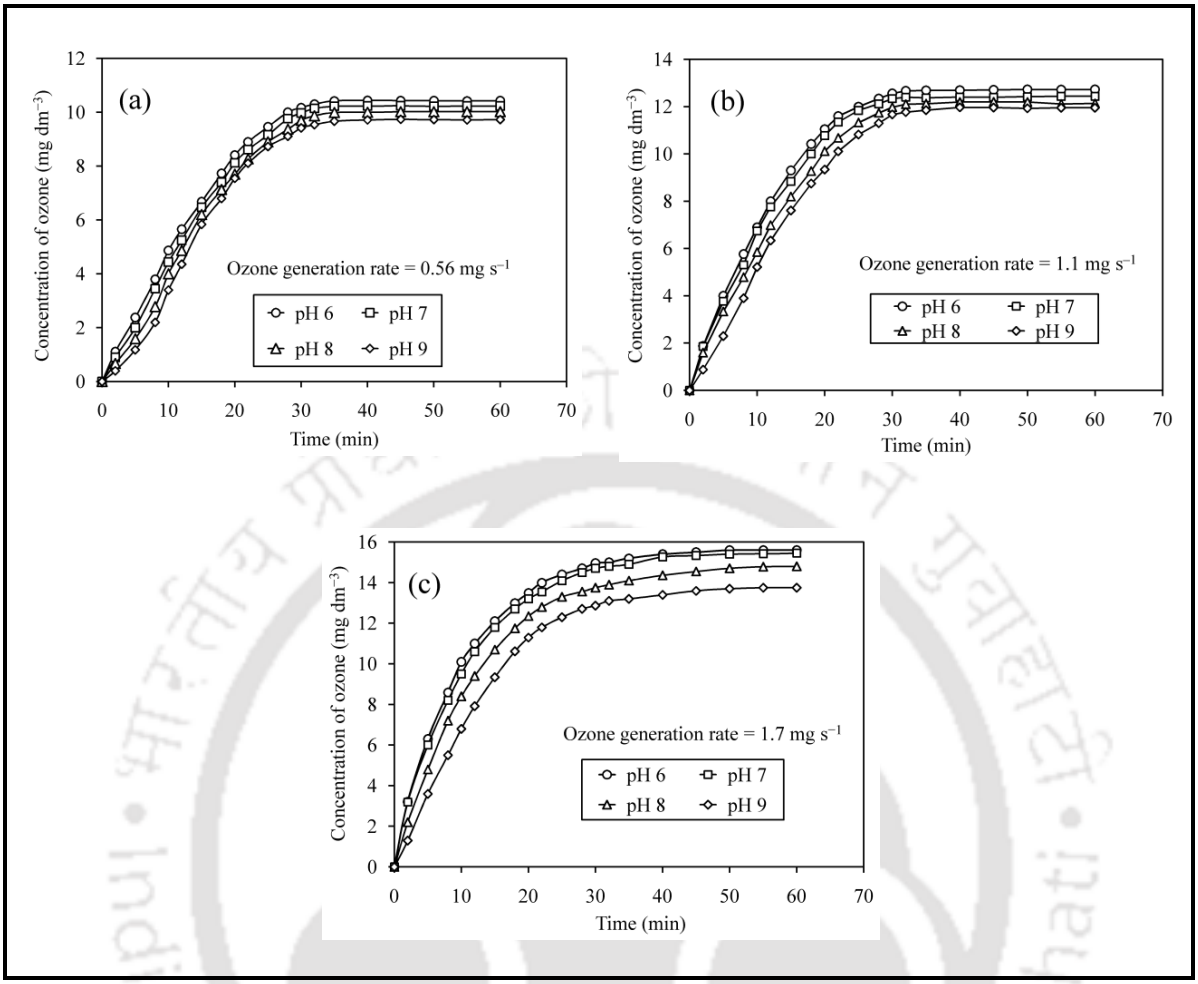

Figure 4A.6 Concentration profiles of ozone in water at different pH: (a) ozone generation rate 0.56 mg s^{-1}, (b) ozone generation rate 1.1 mg s^{-1}, and (c) ozone generation rate 1.7 mg s^{-1}.

CHAPTER 5

REMOVAL OF ARSENIC FROM WATER

CHAPTER 5

REMOVAL OF ARSENIC FROM WATER

In this chapter, the work on oxidation of arsenic using ozone microbubbles has been reported. A wide range of initial arsenic concentrations has been used in this study. The effects of ozone generation rate and pH of the aqueous medium on efficiency of ozonation have been studied. The use of 2-propanol as the ·OH radical scavenger and the effect of carbonate ion radicals on the ozonation of arsenic have been reported. The kinetics of oxidation of As(III) with ozone was studied and the kinetic parameters were evaluated. The second part of this study deals with the adsorption of As(V) by using two adsorbents i.e. zirconium–activated carbon (Zr–AC) and amorphous zirconium oxide (Am-Zr). The preparation of these adsorbents has been described in Chapter 3. This chapter contains the characterization of these adsorbents, determination of charge on their surface in aqueous solutions at different pH, development of adsorption isotherms, and evaluation of kinetic and thermodynamic parameters. The experimental data are enunciated by Langmuir, Freundlich and Redlich–Peterson adsorption isotherms. Changes in Gibbs free energy, enthalpy and entropy during adsorption are also calculated at different temperatures.

5.1 OXIDATION OF As(III) USING OZONE MICROBUBBLES

5.1.1 Oxidation of As(III) to As(V)

The oxidation of As(III) using ozone microbubbles at different initial arsenic concentrations is shown in Figure 5.1. It is observed from this figure that even at a low ozone generation rate (e.g. 0.56 mg s^{-1}) and a low arsenic concentration (e.g. 50−200 μg dm^{-3}), the oxidation of As(III) was fast and effective at pH 7.

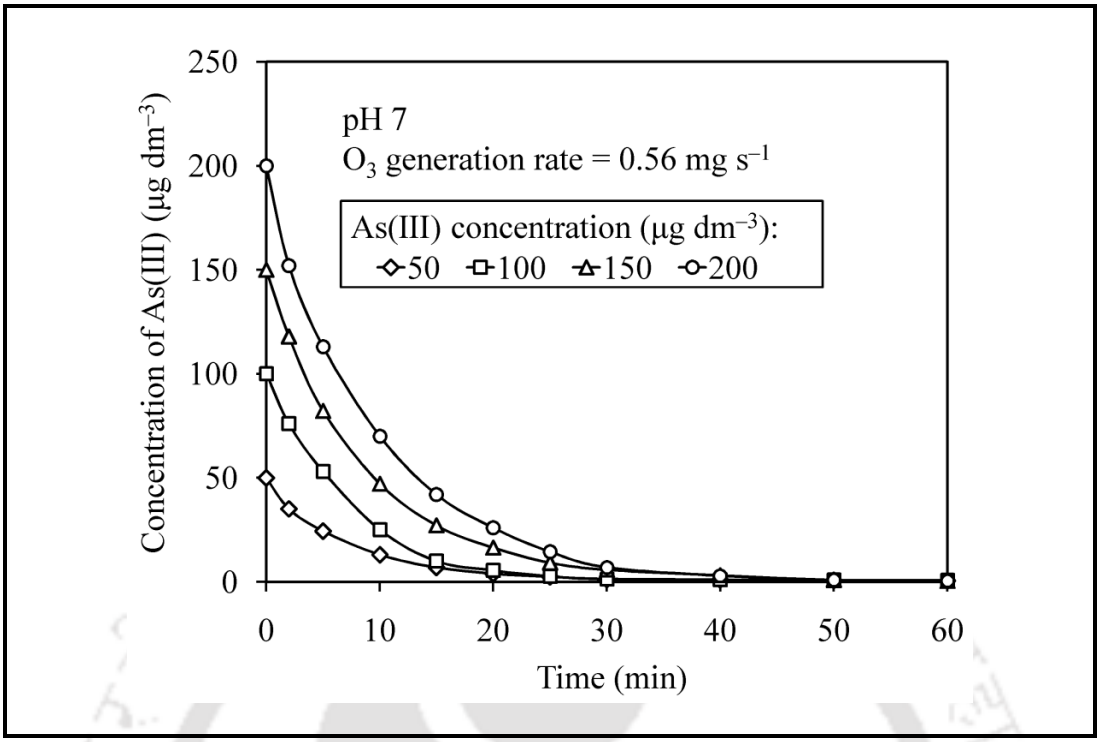

Figure 5.1 Oxidation of As(III) to As(V) at different initial As(III) concentrations.

The time required to reach the half of the initial concentration of arsenic was below 15 min in all the four cases shown in Figure 5.1. More than 90% of As(III) was oxidized in just 25 min. The products of the reaction between As(III) and ozone change with pH, which are described by the following reactions (Ghurye and Clifford, 2001, 2004)

$$\text{At pH 6.5: } H_3AsO_3 + O_3 \rightarrow H_2AsO_4^- + O_2 + H^+ \quad (5.1)$$

$$\text{At pH 8.5: } H_3AsO_3 + O_3 \rightarrow HAsO_4^- + O_2 + 2H^+ \quad (5.2)$$

As more and more of As(III) was oxidized, the concentration of As(V) in the reactor increased. The total arsenic concentration was constant throughout the experiment, which therefore satisfied the overall material balance as shown in Figure 5.2. The increase in ozone generation rate increased the rate of oxidation of As(III) at all pH (viz. 5–9), as shown in Figure 5.3 and Figure 5A.1.

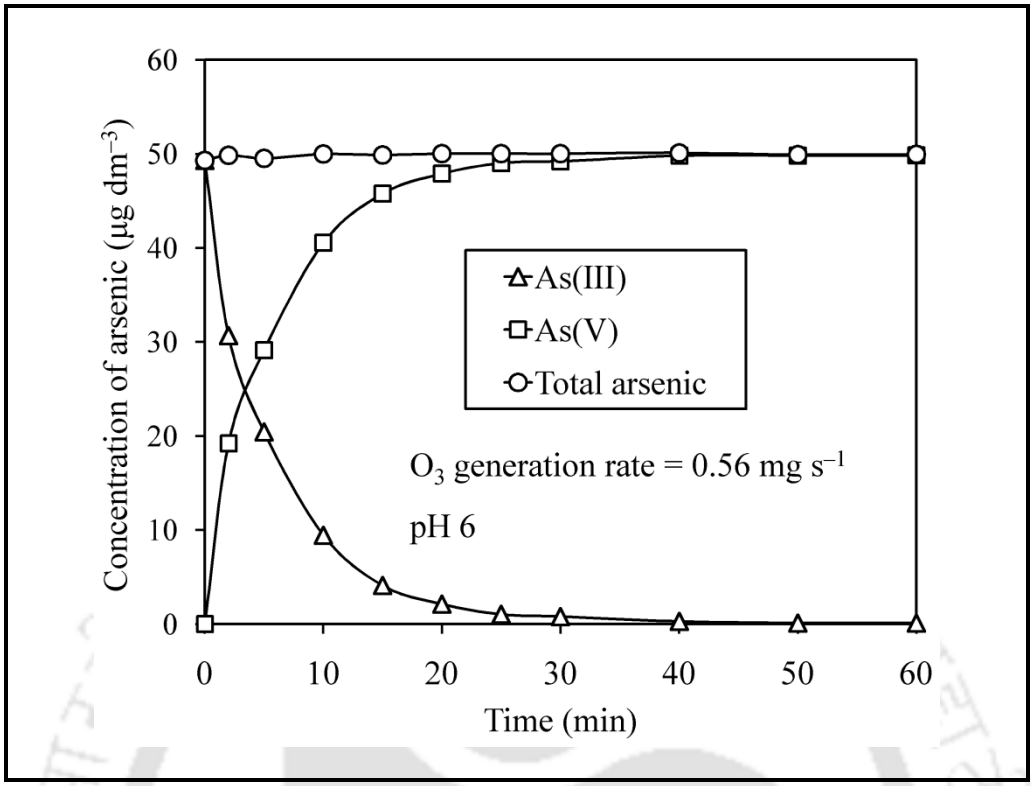

Figure 5.2 Concentration profiles of As(III) and As(V) in the reactor.

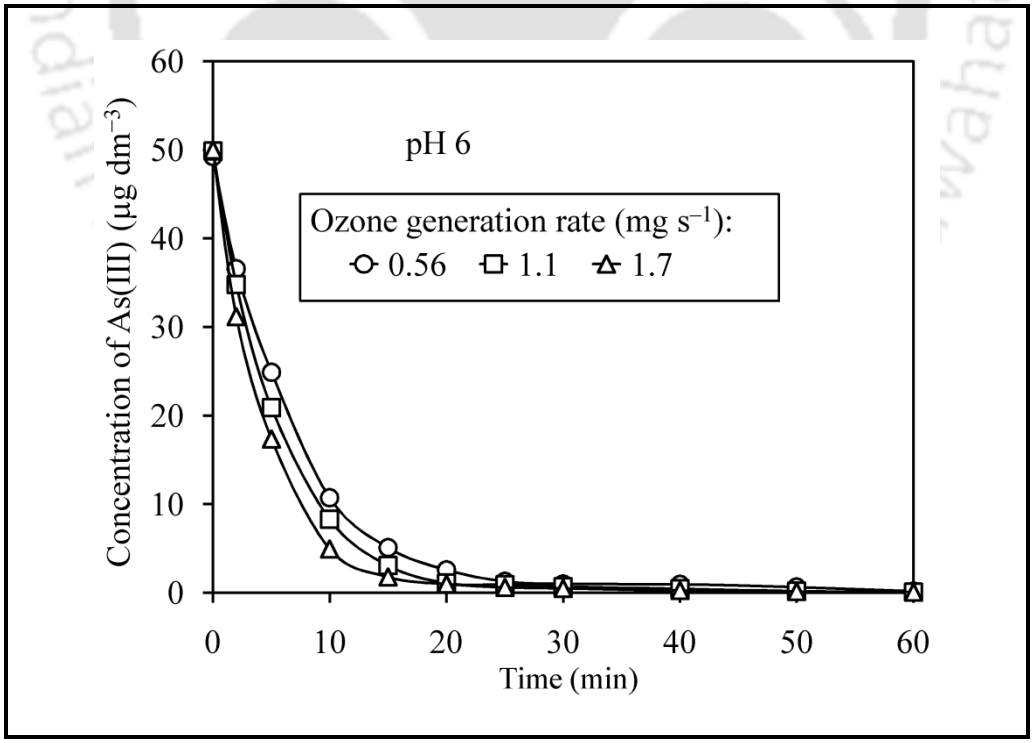

Figure 5.3 Effect of ozone generation rate on oxidation of As(III).

At the ozone generation rate of 1.7 mg s^{-1}, the concentration of As(III) reduced to 10 μg dm^{-3} within 8 min. During the continuous supply of ozone in water in the form of microbubbles, the concentration of dissolved ozone went on increasing and attained equilibrium. It was observed that most of the oxidation took place within the first 15 min, after which the oxidation slowed down. However, by this time, most of As(III) was oxidized to As(V). The effects of ozone generation rate on oxidation of As(III) at pH 5, 7, 8, and 9 are depicted in Figure 5A.1.

5.1.2 Effect of pH on As(III) Oxidation

In most of the works reported in the literature, oxidation of As(III) has been carried out in the pH range of 3−9. Driehaus et al. (1995) have oxidized As(III) using manganese oxide in the pH range of 5−10. They did not observe any effect of pH on the rate of oxidation of As(III). On the other hand, Sorlini and Gialdini (2010) have reported variations in the rate of oxidation in the pH range of 5.7−8 by using chlorine dioxide, hypochlorite, potassium permanganate and monochloramine as oxidants. Hug and Leupin (2003) have reported that the oxidation of As(III) by H_2O_2 was slow at neutral and acidic pH.

In our experiments with ozone microbubbles, the pH of the solution was varied from 5 to 9. Figure 5.4 shows the effect of pH on the oxidation of As(III). It is observed from this figure that 98% oxidation of As(III) was completed within 30 min at all pH for 0.56 mg s^{-1} ozone generation rate. The oxidation was slower at pH 7 at all As(III) concentrations. The oxidation was fast at pH 6 and 9. The oxidation rates were similar at pH 5 and 8. Similar results were observed for other ozone generation rates (e.g. 1.1 and 1.7 mg s^{-1}) as given in Figure 5A.2.

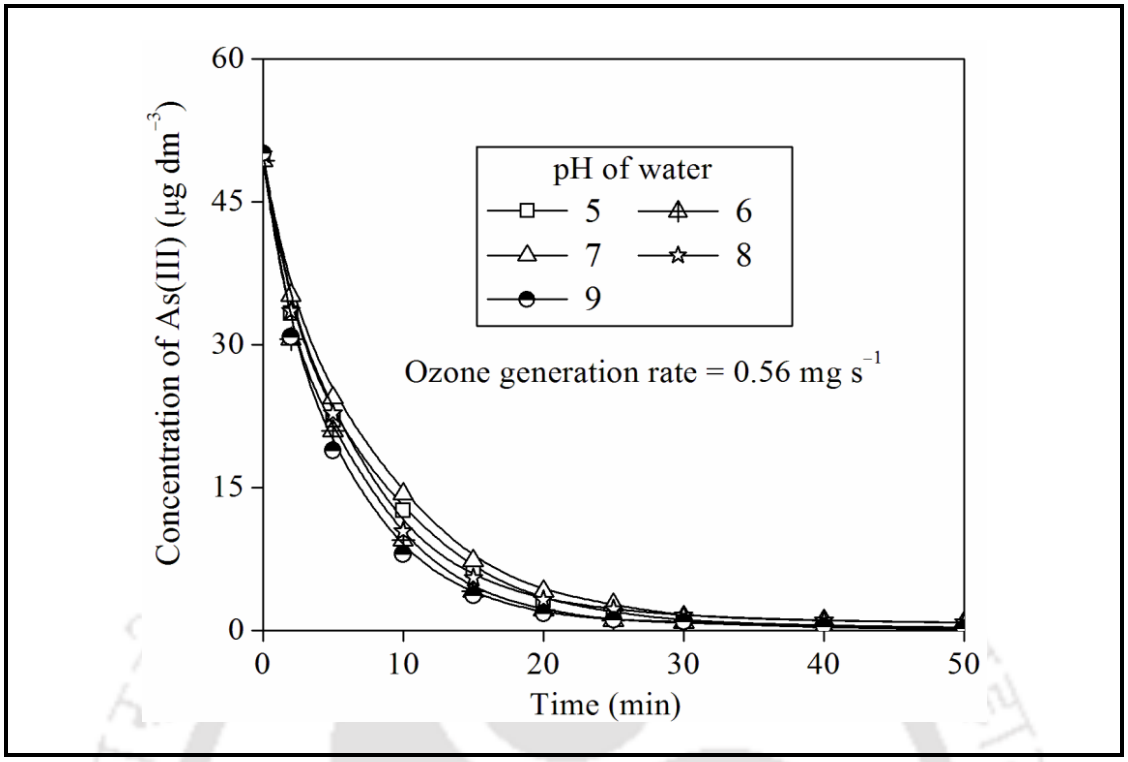

Figure 5.4 Effect of pH on oxidation of As(III).

5.1.3 Study of the Direct/Indirect Oxidation Mechanism

It has been reported in the literature that ozone, under certain conditions, produces hydroxyl radicals (·OH) in aqueous medium (Beltrán, 2004). The generation of hydroxyl radicals from ozone is an important phenomenon for the oxidation of any organic or inorganic compound. Because of its high standard redox potential, the ·OH radical is capable of reacting with many compounds that are otherwise resistant towards oxidation by ozone. The oxidation of As(III) in presence of ozone may occur by molecular ozone, by hydroxyl radicals, or by both. Li et al. (2009) have investigated the generation of hydroxyl radicals by microbubbles at acidic pH. They have confirmed the generation of hydroxyl radicals at pH 2. The presence of ·OH radicals at slightly acidic pH (e.g. 5 and 6) and the comparative roles of molecular ozone and these radicals in the oxidation of As(III) can be confirmed by using 2-propanol as the ·OH radical scavenger. Figures 5.5 (a) and (b) depict the effect of 2-propanol at pH 5 and 6,

respectively. At pH 6, the presence of 2-propanol at 10 mol m^{-3} concentration had hardly any effect on the oxidation of As(III).

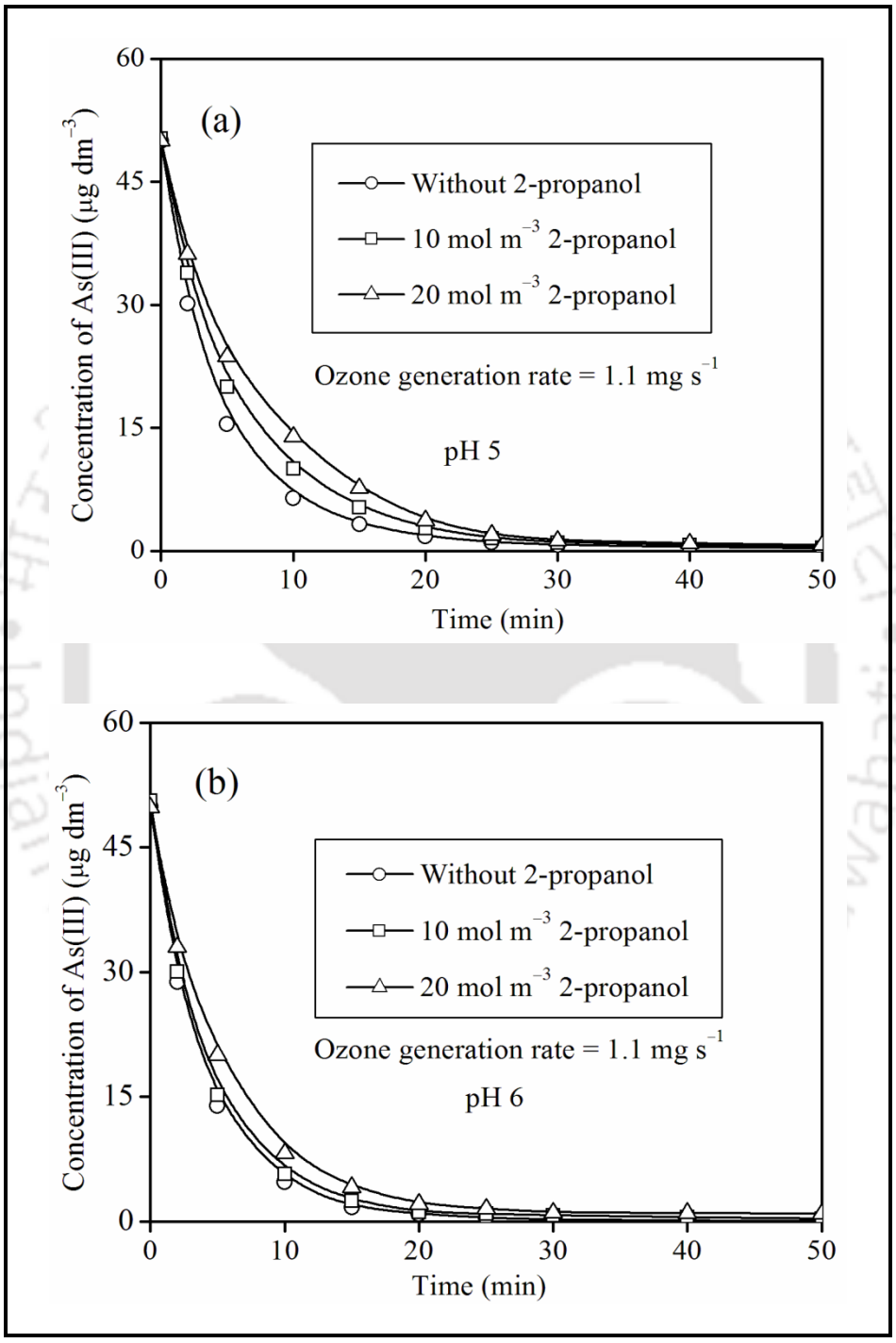

Figure 5.5 Effect of 2-propanol on oxidation of As(III) at (a) pH 5, and (b) pH 6.

However, when the concentration of 2-propanol was increased to 20 mol m^{-3}, the reaction was slightly slowed. At pH 5, the conversion of As(III) to As(V) was reduced from 70% to 60% at 10 mol m^{-3} concentration of 2-propanol after a reaction time of 5 min. The conversion was reduced to 52% in presence of 20 mol m^{-3} 2-propanol after the same reaction time. This appreciable effect of 2-propanol on the oxidation of As(III) by ozone microbubbles confirms the participation of hydroxyl radicals at acidic pH. Because 2-propanol acts as a scavenger of these radicals, it is apparent that ·OH radicals play the role of an effective oxidant for As(III).

Hug and Leupin (2003), and Kläning et al. (1989) have reported that the reaction of As(III) with ·OH radicals forms an As(IV) intermediate, which further oxidizes to As(V). Four different species of As(IV) [viz. $As(OH)_4$, $As(OH)_3O^-$, $HAsO_3^-$ and AsO_3^{2-}] are formed by the reaction between As(III) and ·OH, as shown below.

$$As(OH)_3 + \cdot OH \rightarrow As(OH)_4 \quad (5.3)$$

$$As(OH)_2O^- + \cdot OH \rightarrow As(OH)_3O^- \quad (5.4)$$

$$As(OH)_4 \rightarrow H_2AsO_3 + H_2O \quad (5.5)$$

$$As(OH)_4 \rightarrow HAsO_3^- + H^+ + H_2O \quad (5.6)$$

$$H_2AsO_3 \rightarrow HAsO_3^- + H^+ \quad (5.7)$$

$$As(OH)_2O^- + O^- \rightarrow AsO_3^{2-} + H_2O \quad (5.8)$$

The generation of the four As(IV) species depends on the pH. The species, $As(OH)_4$, was observed at pH < 6, whereas $As(OH)_3O^-$ was found in the pH range of 8.5 to 10. The species, $HAsO_3^-$ and AsO_3^{2-}, were formed at pH > 3. Therefore, in the case of the generation of ·OH radicals from ozone microbubbles under acidic conditions, As(IV) would exist as $As(OH)_4$, $HAsO_3^-$ and AsO_3^{2-}. The species, $As(OH)_3O^-$, is not expected to form under these conditions. All the four As(IV) species further oxidize to As(V).

5.1.4 Effect of Carbonate Ions/Radicals on Oxidation of As(III)

The presence of carbonates and bicarbonates in water is quite common. These may form the reactive carbonate ion radical (viz. $CO_3^{-}\cdot$) by the reaction with ·OH radicals given in Eq. (4.3) (Beltrán, 2004). The carbonate radical anion is a powerful one-electron oxidant (Cope et al., 1978). The role of carbonate/carbonate ion radical on ozonation of As(III) was investigated at pH 5 and 6. The concentration of carbonate was 1 mg dm^{-3}. The effect of carbonate on oxidation of As(III) is shown in Figure. 5.6.

From this figure, it is apparent that the generation of $CO_3^{-}\cdot$ radicals increased the rate of oxidation of As(III). As a result, the conversion of As(III) to As(V) became faster at both pH 5 and 6. The amount of ·OH radicals generated at pH 6 was small. Therefore, a small amount of carbonate ions was converted to the carbonate ion radicals. However, at pH 5, the amount of carbonate ion radical was more due to a larger amount of hydroxyl radicals present in the reaction medium. Therefore, the carbonate ion radicals were more effective for the oxidation of As(III) at pH 5 than at pH 6, which may be attributed to the greater concentration of ·OH radicals at the former pH. The reaction between the $CO_3^{-}\cdot$ radical and As(III) is given by (Kläning et al., 1989)

$$As(OH)_2O^- + CO_3^{-}\cdot + 2OH^- \rightarrow AsO_3^{2-} + CO_3^{2-} + 2H_2O \qquad (5.9)$$

It was observed from Figure 5.6 that the oxidation of As(III) by the carbonate ion radicals is faster than either the hydroxyl radicals or ozone. Yoon et al. (2008) have observed similar results and reported that the carbonate ion radicals act as a minor oxidant for the oxidation of As(III). This may be due to a different pathway for the reaction between carbonate ion radical and As(III). There is some mismatch among the results reported in the literature regarding the value of the standard redox potential of the carbonate ion radical. The values reported by Cope et al. (1978), Huie et al. (1991) and Augusto et al. (2002) are 2.1, 1.5

and 1.8 V, respectively. Apparently, there is an uncertainty in the value of the standard redox potential of the carbonate ion radical. Further studies are necessary for confirming the role of carbonate ion radicals in augmenting the rate of oxidation of As(III) by ozone microbubbles.

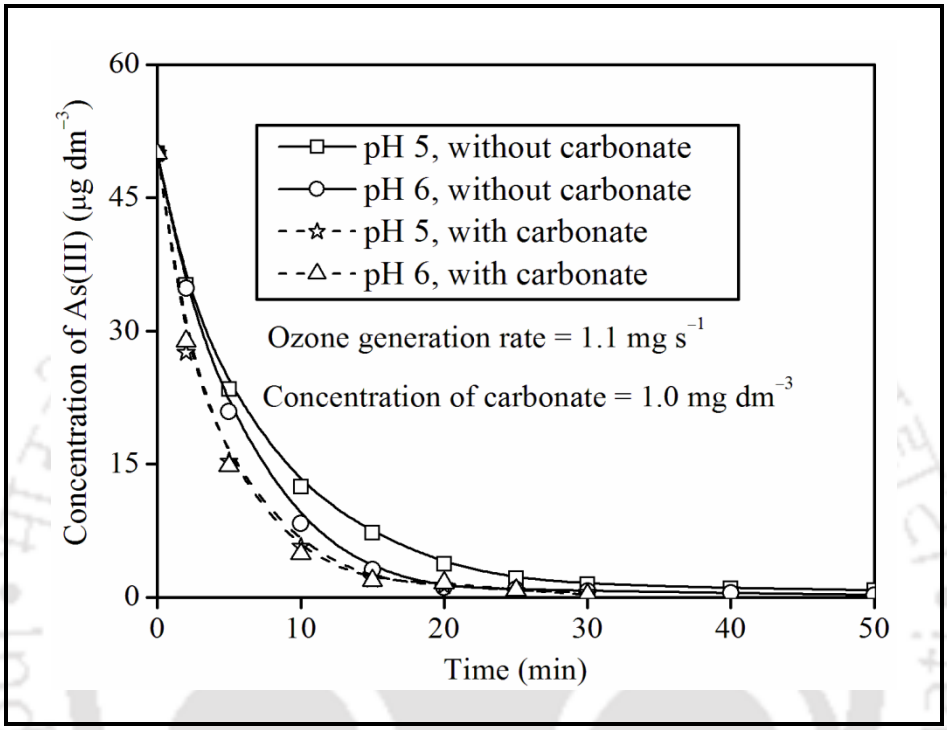

Figure 5.6 Effect of carbonate ion radicals on oxidation of As(III).

5.1.5 Kinetics of Oxidation of As(III) by Ozone

The solubility of ozone in water is higher than that of oxygen due to the high rate of transfer of ozone from the gas phase to water. Therefore, the concentration of ozone in water was much higher than the concentration of As(III) a few minutes after the ozonation started. Thus, the concentration of ozone can be assumed as constant, and the conversion of As(III) to As(V) can be taken as the rate-limiting step. The oxidation of As(III) by ozone can be described by a modified pseudo first-order kinetics as (Kim and Nriagu, 2000)

$$\frac{\mathrm{d[As(III)]}}{\mathrm{d}t} = -k[\mathrm{As(III)}] \tag{5.10}$$

Integration of Eq. (5.10) gives

$$[\text{As(III)}] = [\text{As(III)}]_0 \exp(-kt) \tag{5.11}$$

Kim and Nriagu (2000) have reported that the experimental data can be fitted in a better manner by using a modified form of Eq. (5.11) in which an exponent, *m*, is introduced on time, *t*, as

$$[\text{As(III)}] = [\text{As(III)}]_0 \exp(-kt^m) \tag{5.12}$$

The value of *m* is less than unity. The reaction of As(III) with ozone was fast and a large portion of As(III) was quickly oxidized to As(V). The time taken for the reduction of concentration of As(III) to half of its initial concentration is termed the half-life of the reaction $(t_{0.5})$. This value was used to normalize the time (*t*), and Eq. (5.12) was modified to

$$[\text{As(III)}] = [\text{As(III)}]_0 \exp\left[-k'(t/t_{0.5})^m\right] \tag{5.13}$$

The rate constant, k', in Eq. (5.13) is dimensionless. The half-life was obtained from the experimental data. The values of *m* and k' are shown in Table 5.1. It was observed that the initial concentration of As(III) had no effect on the rate of reaction. However, there was a small decrease in the rate constant at pH 7 as compared to other pH.

The true kinetics of oxidation of As(III) with ozone was studied by using the mass balance. The concentration of As(III) in water was very small as compared to ozone. However, the self-decomposition of ozone occurs simultaneously. The kinetic equation for the reaction of ozone and As(III) is expressed as

$$\frac{\mathrm{d}[\text{As(III)}]}{\mathrm{d}t} = -k[\text{As(III)}]^m[\text{O}_3]^n \tag{5.14}$$

In Chapter 4, it was observed that the decomposition of ozone in water plays an important role in the mass transfer ozone. Sotelo et al. (1987) have reported that ozone decomposition follows first-order kinetics with respect to ozone concentration. Therefore the decomposition rate can be expressed as.

$$\frac{d[O_3]}{dt} = -k_d[O_3] \quad (5.15)$$

Table 5.1 Kinetic parameters for oxidation of As(III) with ozone calculated as per Eq. (5.13).

O_3 generation rate (mg s^{-1})		0.56			1.1			1.7		
$[As(III)]_0$ (μg dm^{-3})	pH	k'	m	$t_{0.5}$ (min)	k'	m	$t_{0.5}$ (min)	k'	m	$t_{0.5}$ (min)
50	5	0.74	0.71	4.2	0.74	0.70	2.8	0.73	0.71	2.0
	6	0.75	0.72	3.5	0.75	0.71	2.5	0.75	0.70	1.7
	7	0.73	0.73	4.6	0.73	0.72	3.5	0.74	0.68	2.3
	8	0.76	0.73	4.2	0.75	0.69	2.6	0.75	0.72	2.2
	9	0.76	0.72	3.5	0.76	0.68	2.4	0.75	0.71	2
100	5	0.73	0.71	4.6	0.73	0.73	4.0	0.74	0.71	3.8
	6	0.75	0.70	3.8	0.75	0.72	3.5	0.75	0.70	2.8
	7	0.73	0.72	4.6	0.73	0.73	4.2	0.75	0.71	3.8
	8	0.75	0.71	4.0	0.75	0.73	3.8	0.75	0.71	3.6
	9	0.76	0.73	3.8	0.76	0.71	3.3	0.76	0.70	2.8

The hydroxyl radicals react with many species in chain reactions. So the expressions for the depletion rates of ozone are derived by using the steady-state approximations for the generation of ·OH, O^-, O_2^-, and O_3^- (Kuo et al., 1997). Therefore the self-decomposition of ozone cannot be neglected in the ozone depletion rate. Thus the depletion rate of ozone contains three terms i.e. the mass transfer of ozone from gas to liquid, the decomposition of ozone and the reaction of As(III) with ozone. So the depletion rate of ozone is expressed as

$$\frac{d[O_3]}{dt} = k_l a\left([O_3]^* - [O_3]\right) - k_d[O_3] - k[As(III)]^m[O_3]^n \quad (5.16)$$

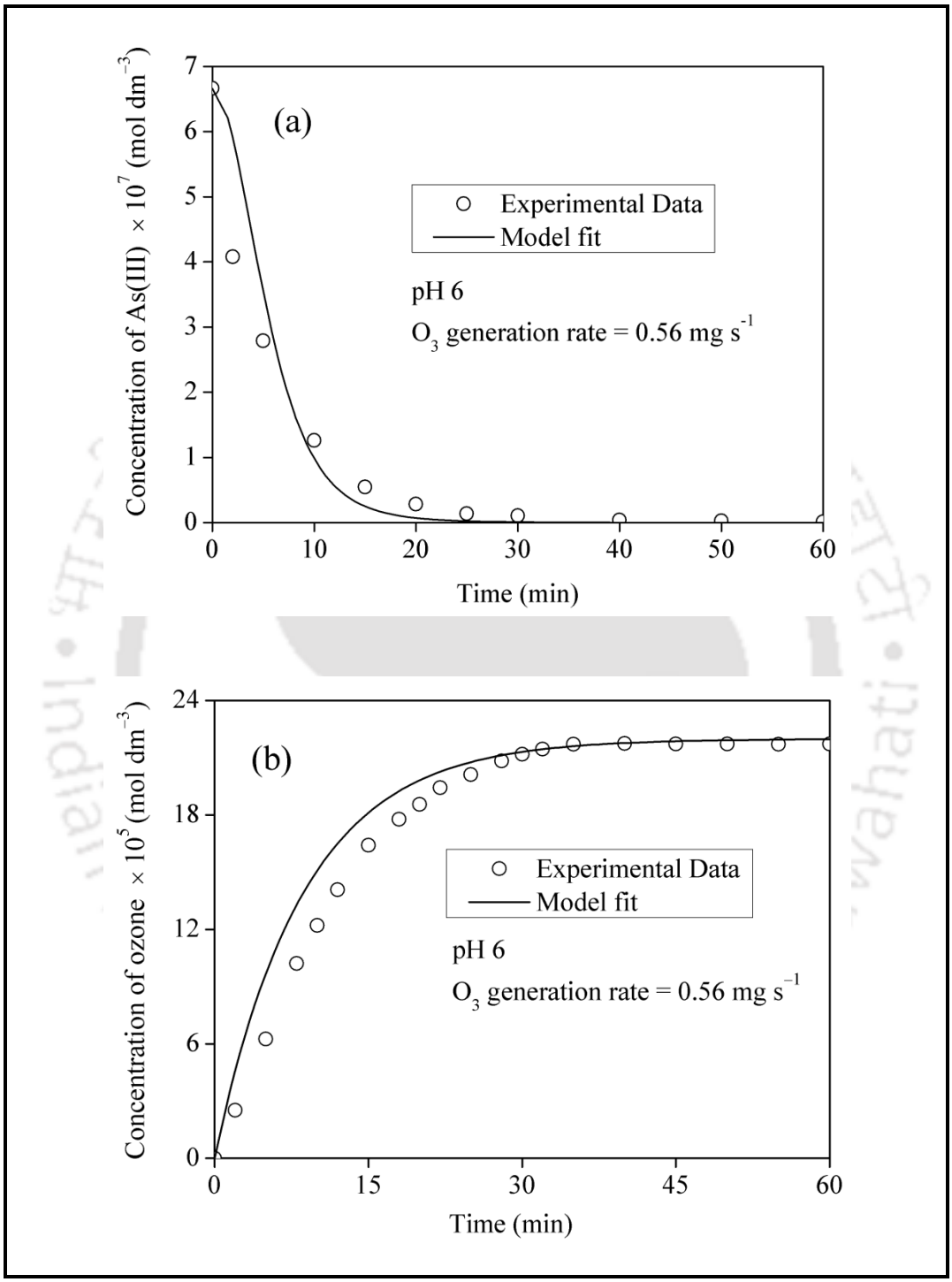

Figure 5.7 Variation of (a) As(III) concentration, and (b) O_3 concentration with time. The parity of the kinetic model with the experimental data is shown.

The calculation of $[O_3]^*$ is discussed in Chapter 4, and the values of k_d are adopted from Sotelo et al. (1987). The value of k can be calculated by solving Eqs. (5.14) and (5.16) simultaneously by using Runge–Kutta method. The kinetic model parameters are given in Table 5.2. The comparison of the kinetic model and the experimental data for the concentration of As(III) and ozone at pH 6 is shown in Figure 5.7. The comparison of the model and the experimental data for the concentration of As(III) and ozone at pH 5, 7, 8, and 9 are given in Figure 5A.3. It is observed that the values of m and n are close to unity and nearly the same for all pH. The value of rate constant lies between 436−442 in the pH range of 5−9.

Table 5.2 Kinetic parameters for oxidation of As(III) with ozone using Eqs. (5.14) and (5.16) (ozone generation rate = 0.56 mg s^{-1}).

pH	k $(mol\ dm^{-3})^{1-m-n}\ s^{-1}$	m	n	$k_l a \times 10^3$ $(s^{-1})^{\dagger}$	$k_d \times 10^4$ (s^{-1})
5	437	1.18	1.02	1.57	2.33
6	440	1.17	1.01	1.70	2.50
7	436	1.20	1.02	1.90	3.20
8	438	1.21	0.98	2.10	7.80
9	442	1.17	1.02	2.60	13.3

†From Table 4.2

5.2. ADSORPTION OF ARSENIC (V) ON ZIRCONIUM-BASED ADSORBENTS

5.2.1 Characterization of Zirconium−Activated Carbon (Zr–AC) and Amorphous Zirconium Oxide (Am-Zr)

The SEM images of the activated carbon and zirconium–activated carbon (Zr–AC) before the adsorption of As(V) are shown in Figures 5.8 (a) and (b), respectively. It is observed from these micrographs that the activated carbon and Zr–AC have different textures. The activated carbon surface has porous structure. However, after the zirconium impregnation, these pores were filled-up with the zirconium nanoparticles [Figure 5.8 (b)]. This makes the adsorbent efficient in the water treatment process, as it can be used repeatedly without losing the zirconium nano particles from the pores of the activated carbon. The distribution of pores was, however, not uniform along the surface.

From the EDX spectrum of the Zr–AC it was observed that the surface of the activated carbon was loaded with 2.9 atomic% (viz. 18.6 weight%) of zirconium [Figure 5.8 (c)]. After the adsorption of As(V), the EDX spectrum showed another peak for arsenic. Figure 5.8 (d) depicts that the adsorption of As(V) on the Zr–AC was effective and the impregnated zirconium nanoparticles did not come out after the adsorption was carried out. The XRD pattern of Zr–AC before and after As(V) adsorption shows the wide diffraction peak and weak peak intensity [Figure 5.8 (e)]. This indicates that the Zr–AC was amorphous in nature. From the XRD pattern, it was observed that neither the impregnation of zirconium on activated carbon, nor the adsorption of As(V) on it changed the morphology of these adsorbents. The SEM image of zirconium oxide showed that the surface morphology of the sorbent was amorphous and formed a tooth-like structure [Figure 5.9 (a)]. The surface of the adsorbent was rough and porous.

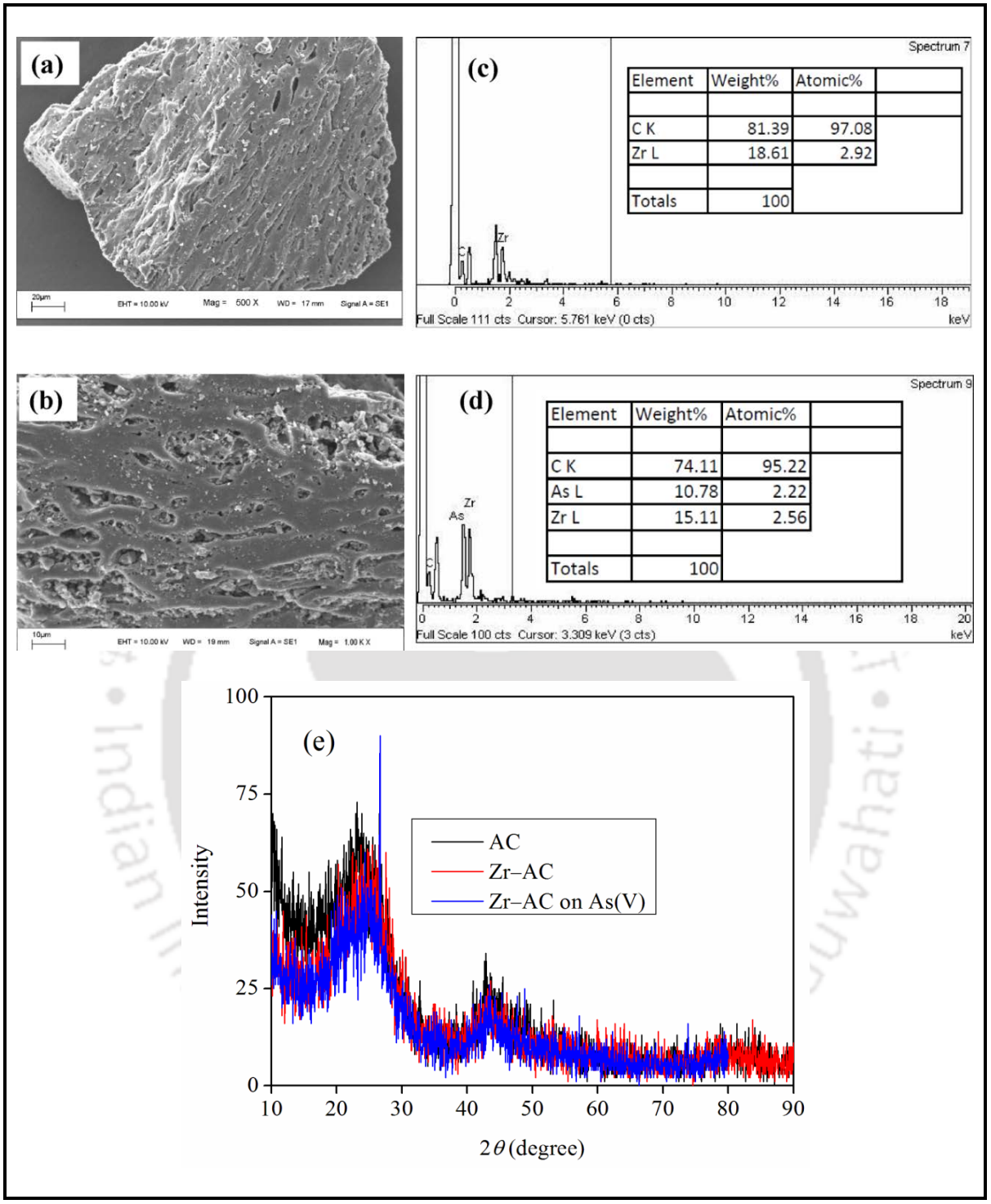

Figure 5.8 SEM of (a) activated carbon (AC), and (b) Zr–AC before adsorption of As(V); (c) EDX of Zr–AC before As(V) adsorption, and (d) EDX of the same after As(V) adsorption; (e) XRD of Zr–AC before and after As(V) adsorption.

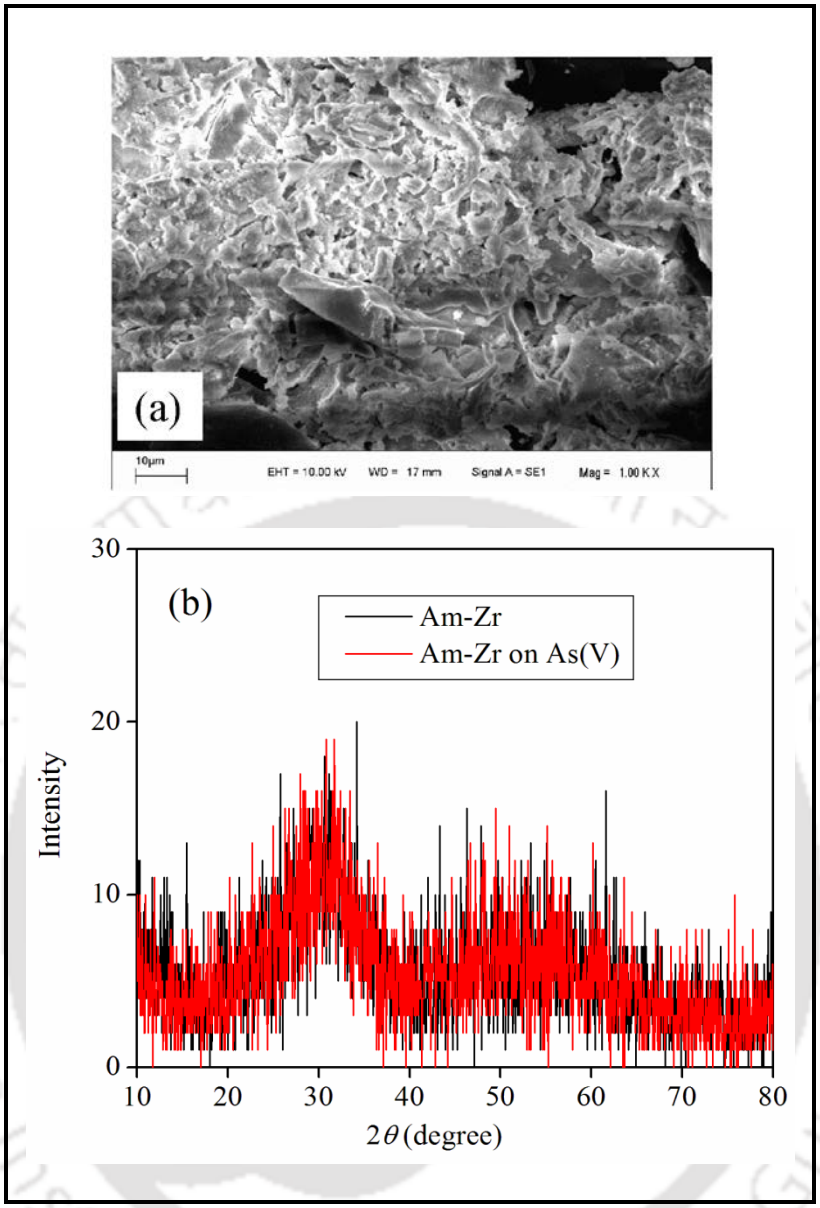

Figure 5.9 (a) SEM of Am-Zr, and (b) XRD of Am-Zr.

The XRD pattern of Am-Zr shows two major diffraction peaks of the tetragonal ZrO_2 phase at $2\theta = 30^o$ and 50^o. However, the wide diffraction peak and the weak peak intensity [Figure 5.9 (b)] showed that the prepared zirconium oxide was amorphous in nature. The specific surface area of Zr–AC, determined from the BET surface area analyzer, was 737 $m^2\ g^{-1}$. About 70.8% of total pores were in the range of 6−40 nm diameter, with the total pore volume of 0.45 $cm^3\ g^{-1}$. This indicates a very high mesopore volume. The specific surface

area of Am-Zr was 478 m^2 g^{-1}. About 86% pores had diameter in the range of 6−40 nm, and the total pore volume was 0.52 cm^3 g^{-1} as shown in Figure 5.10 (a) and (b). The various parameters obtained from BET are given in Table 5.3.

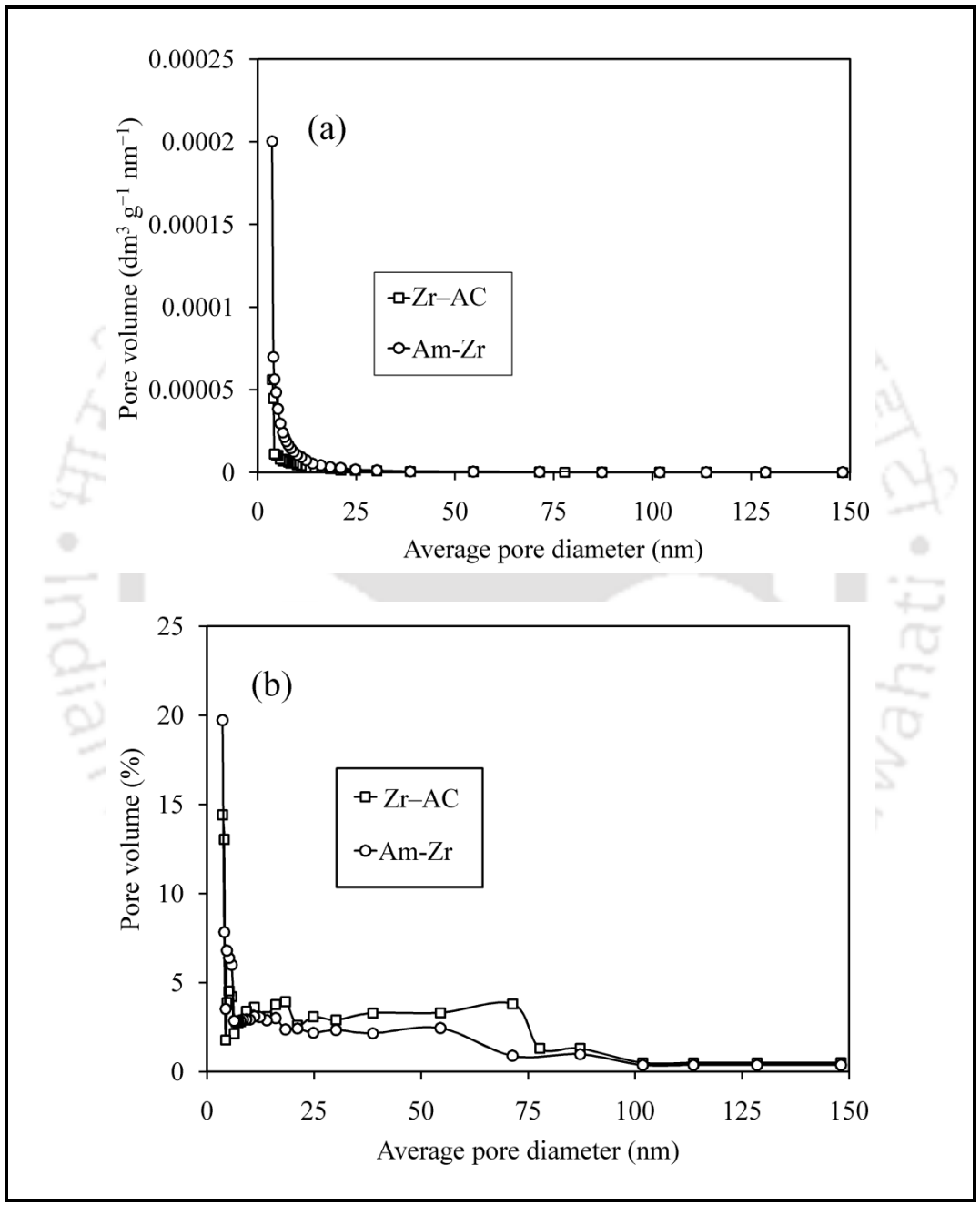

Figure 5.10 The variation of average pore diameter of the adsorbents with (a) pore volume (dm^3 g^{-1} nm^{-1}) and (b) pore volume (%).

Table 5.3 The values of different adsorbent parameters determined from BET analysis.

BET values	Zr–AC	Am-Zr
Particle size (μm)	150−200	50
BET surface area ($m^2\ g^{-1}$)	737.25	478.16
Langmuir surface area ($m^2\ g^{-1}$)	897.14	463.23
Total surface area ($m^2\ g^{-1}$)	764.33	477.53
Micropore volume ($dm^3\ g^{-1}$)	0.00026	0.00004
Mesopores (%)	70.8	86
Mesopore volume ($dm^3\ g^{-1}$)	0.00019	0.00048
Total pore volume ($dm^3\ g^{-1}$)	0.00045	0.00052

5.2.2 Effect of pH on Adsorption of As(III) and As(V)

In order to determine the effective pH ranges for adsorption of As(III) and As(V), 50 μg dm^{-3} of As(V) and 1 g dm^{-3} of the adsorbent were stirred at 298 K at different pH. The adsorption profiles of As(V) on Zr–AC and Am-Zr are shown in Figure 5.11 (a). It was observed that As(V) was adsorbed more on Am-Zr at all As(V) concentrations.

Figure 5.11 (b) illustrates the effect of pH on adsorption of As(III) and As(V). The untreated granular activated carbon shows a poor adsorption for both As(III) and As(V). The effective pH range for adsorption of As(III) on Zr–AC carbon was found to be 5−8, and the same for As(V) was 4−9. For Am-Zr, the effective adsorption of As(III) was observed at pH 3−8, and for As(V) the range was 3−9. However for both the adsorbents, it was observed that the adsorption of As(V) was more than that of As(III) at pH in the range 4−9. From these results, it can be concluded that Zr–AC and Am-Zr can be used as suitable adsorbents in the aforesaid range of pH for As(V) adsorption. The value of zeta potential was measured at different pH to determine the surface charge of the adsorbents and its role in the adsorption of

As(V). The adsorption of As(III) and As(V) depends on the surface charge of the adsorbents as well as the speciation of arsenic at different pH.

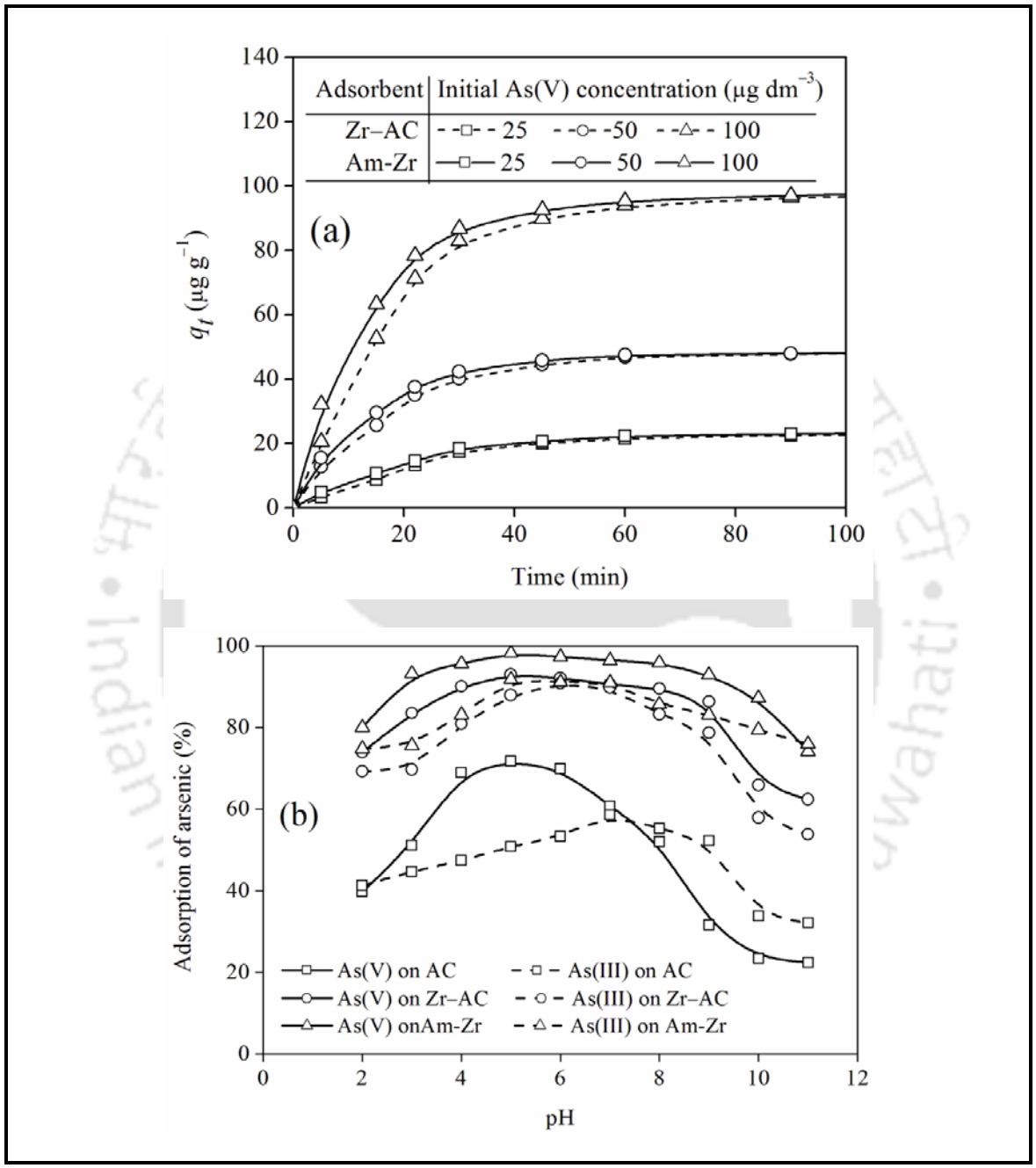

Figure 5.11 (a) Adsorption profile of As(V) on Am-Zr and Zr–AC, (b) Effect of pH on adsorption of arsenic on AC, Zr–AC, and Am-Zr at $[As(III)]_0$ = 50 μg dm^{-3}, $[As(V)]_0$ = 50 μg dm^{-3}: shaking speed = 200 rpm, contact time = 3 h, T = 298 K, and adsorbent dose = 1 g dm^{-3}.

In aqueous solution, As(V) exhibits anionic behavior in the pH range of 2−11 (Ansari and Sadegh, 2007). The variation of zeta potential with pH is shown in Figure 5.12. It is observed from this figure that the surface charge of the adsorbents is positive in acidic conditions, and it becomes negative in the alkaline media.

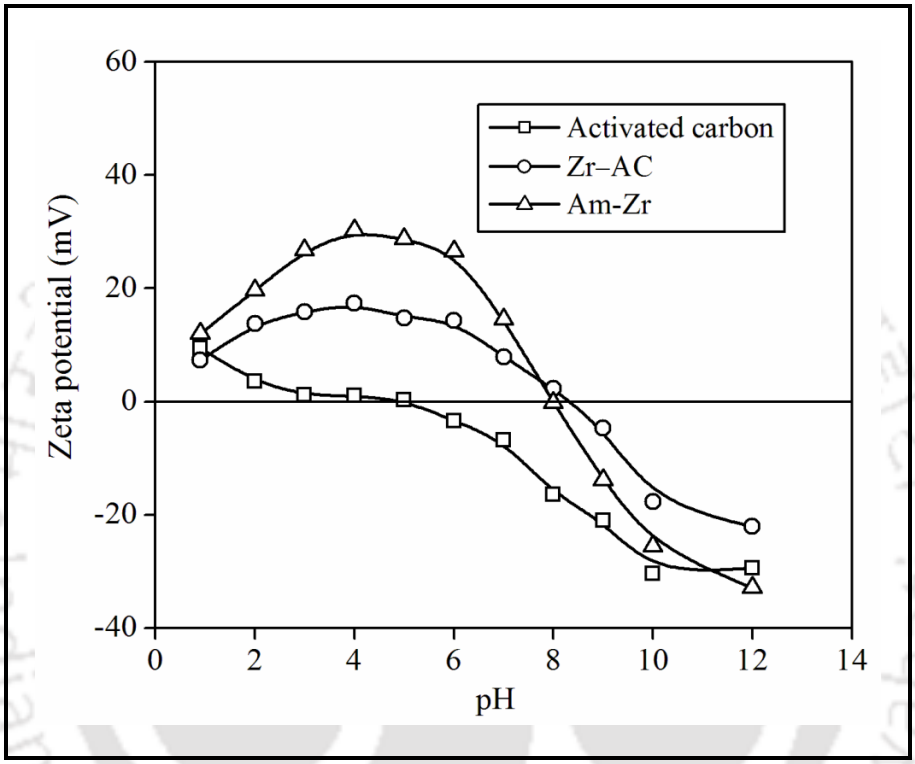

Figure 5.12 Variation of zeta potential of the adsorbents with the pH of the medium.

The point of zero charge was observed at pH 5 for activated carbon, and the same was observed at higher values of pH for the other adsorbents. The adsorption of negatively charged As(V) species was stronger in the acidic condition, which has been depicted in Figure 5.11 (b). The value of zeta potential at the Zr–AC surface was positive at pH in the range of 1−8. This suggests that As(V) can be efficiently adsorbed at this pH range. At pH 8.5, the value of zeta potential was zero. The Am-Zr surface showed positive charge at the acidic pH. The highest value of zeta potential was observed at about pH 4, and the magnitude

of zeta potential was higher than that of the Zr–AC, for which the value of zeta potential was zero at pH 8.

5.2.3 Kinetics of Adsorption

Three kinetic models (viz. pseudo first-order, pseudo second-order, and intra-particle-diffusion model) were used to study the adsorption of As(V) on Zr–AC and Am-Zr. The amount of As(V) adsorbed per unit mass of adsorbent, q_t , at time *t*, is given by,

$$q_t = \frac{(C_0 - C_t)V}{M} \tag{5.17}$$

The variation of q_t with time is shown in Figure 5.11 (a). The adsorption was faster for a higher initial As(V) concentration, although, the time required to attain the equilibrium was longer. For example, the time required to attain equilibrium was 1.5 h for 100 μg dm^{-3} initial As(V) concentration whereas, the same for 25 μg dm^{-3} initial As(V) concentration was 1 h.

5.2.3.1 Pseudo First-Order Kinetic Model

The assumption behind the pseudo first-order kinetic model is that the rate of change of adsorbate uptake with time is directly proportional to the difference between the saturation concentration and the amount of adsorbate uptake with time. The first-order rate expression of adsorption is expressed as (Hameed et al., 2007)

$$\frac{dq_t}{dt} = k_1 t (q_e - q_t) \tag{5.18}$$

Integrating Eq. (5.18), one gets,

$$\ln(q_e - q_t) = \ln(q_e) - k_1 t \tag{5.19}$$

Equation (5.19) suggests that the plot of $\ln(q_e - q_t)$ versus *t* is linear. This is shown in Figures 5.13 (a) and (b). The adsorption rate constant, k_1, and the equilibrium adsorption

capacity, q_e, were calculated from the slope and intercept, respectively. These values are presented in Table 5.4. The coefficient of determination (ρ^2) for Zr–AC carbon and Am-Zr were found to be 0.94 and 0.98 respectively.

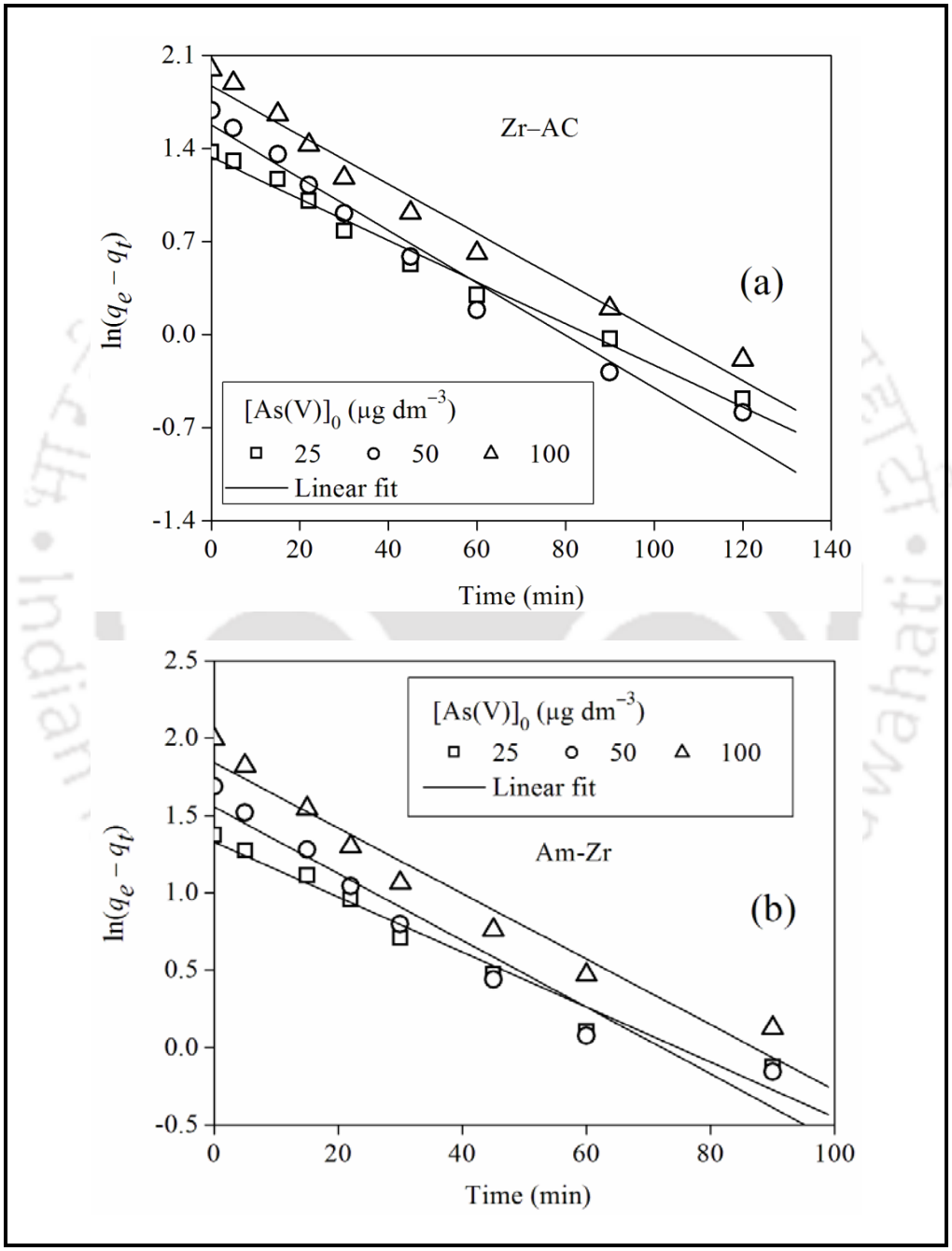

Figure 5.13 Pseudo first-order kinetic model for the adsorption of As(V) on (a) Zr–AC, and (b) Am-Zr.

5.2.3.2 Pseudo Second-Order Kinetic Model

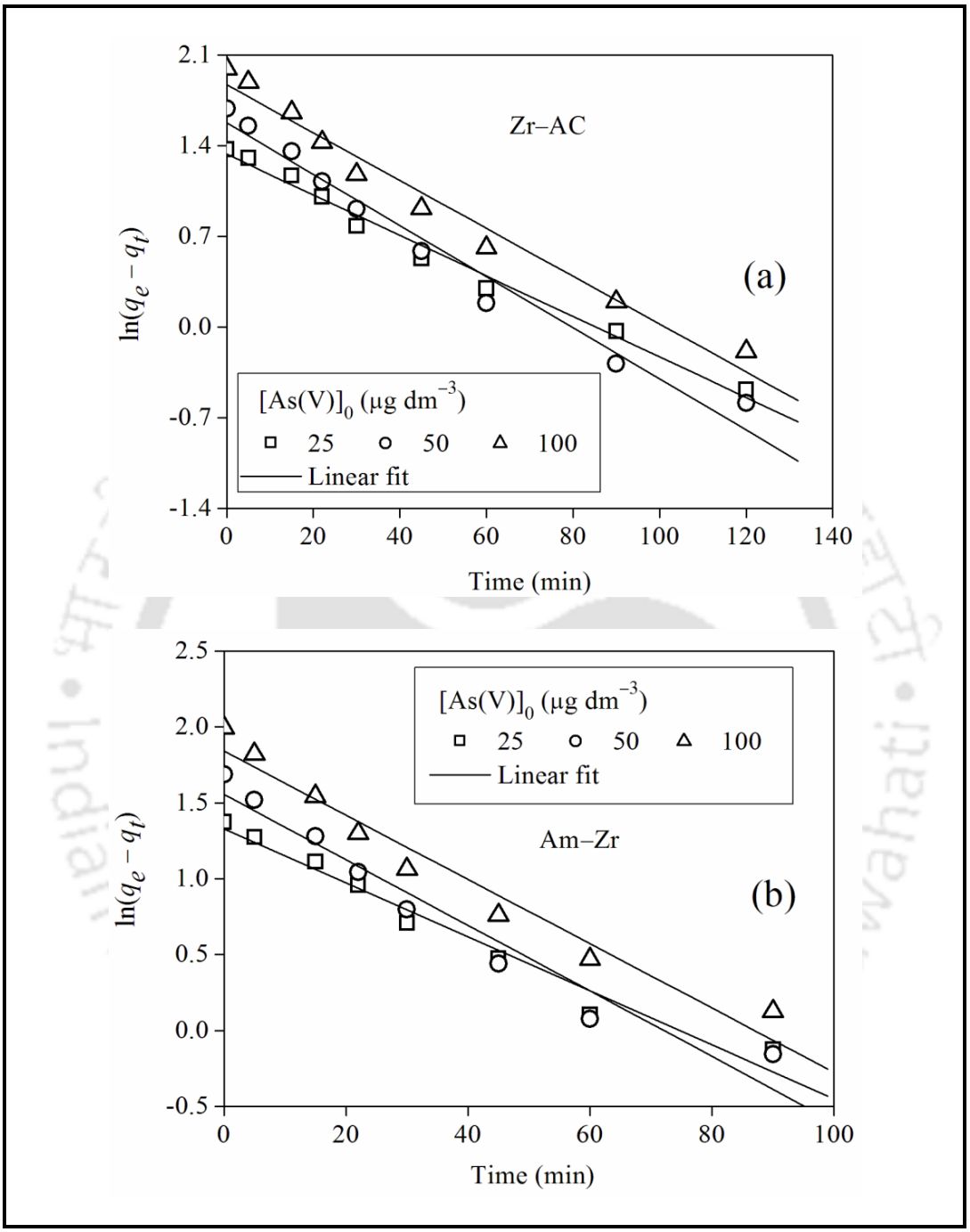

Figure 5.14 Pseudo second-order kinetic model for the adsorption of As(V) on (a) Zr–AC, and (b) Am-Zr.

Although Eq. (5.19) fitted the experimental data reasonably well, the second-order model was explored to determine the best kinetic model to describe the mechanism of As(V) adsorption

on these adsorbents. The equation for pseudo second-order kinetic model is given by (Hameed et al., 2007)

$$\frac{t}{q_t} = \frac{1}{k_2 q_e^2} + \frac{t}{q_e} \tag{5.20}$$

Equation (5.20) suggests that a plot of t/q_t with t would be a straight line. From the slope and the intercept, the values of q_e and k_2 can be determined. These plots are shown in Figures 5.14 (a) and (b). The values of q_e and k_2 are presented in Table 5.4. The coefficient of determination (ρ^2) for both the adsorbents were ~0.99 for all As(V) concentrations.

Table 5.4 Pseudo first-order and pseudo second-order kinetic parameters for adsorption of As(V) at 298 K.

Kinetic model	Adsorbent	Zr–AC			Am-Zr		
	C_0 (μg dm^{-3})	25	50	100	25	50	100
Pseudo first-order	q_e^{cal} (μg g^{-1})	17.9	37.7	72.6	19.6	30.4	72.8
	q_e^{expt} (μg g^{-1})	23.5	48.4	98.0	23.7	48.7	98.4
	k_1 (min^{-1})	0.013	0.019	0.018	0.016	0.018	0.022
	ρ^2	0.97	0.99	0.99	0.97	0.95	0.98
Pseudo second-order	q_e^{cal} (μg g^{-1})	26.3	52.6	111.1	25.6	52.7	110.6
	q_e^{expt} (μg g^{-1})	23.5	48.4	98.0	23.7	48.7	98.4
	$k_2 \times 10^3$ (g μg^{-1} min^{-1})	1.90	1.99	0.82	2.80	2.80	1.30
	ρ^2	0.99	0.99	0.99	0.99	0.99	0.99

5.2.3.3 Intra-Particle-Diffusion Model

According to the intra-particle-diffusion model, q_t varies with t as (Nandi et al., 2009)

$$q_t = k_i\sqrt{t} + I \tag{5.21}$$

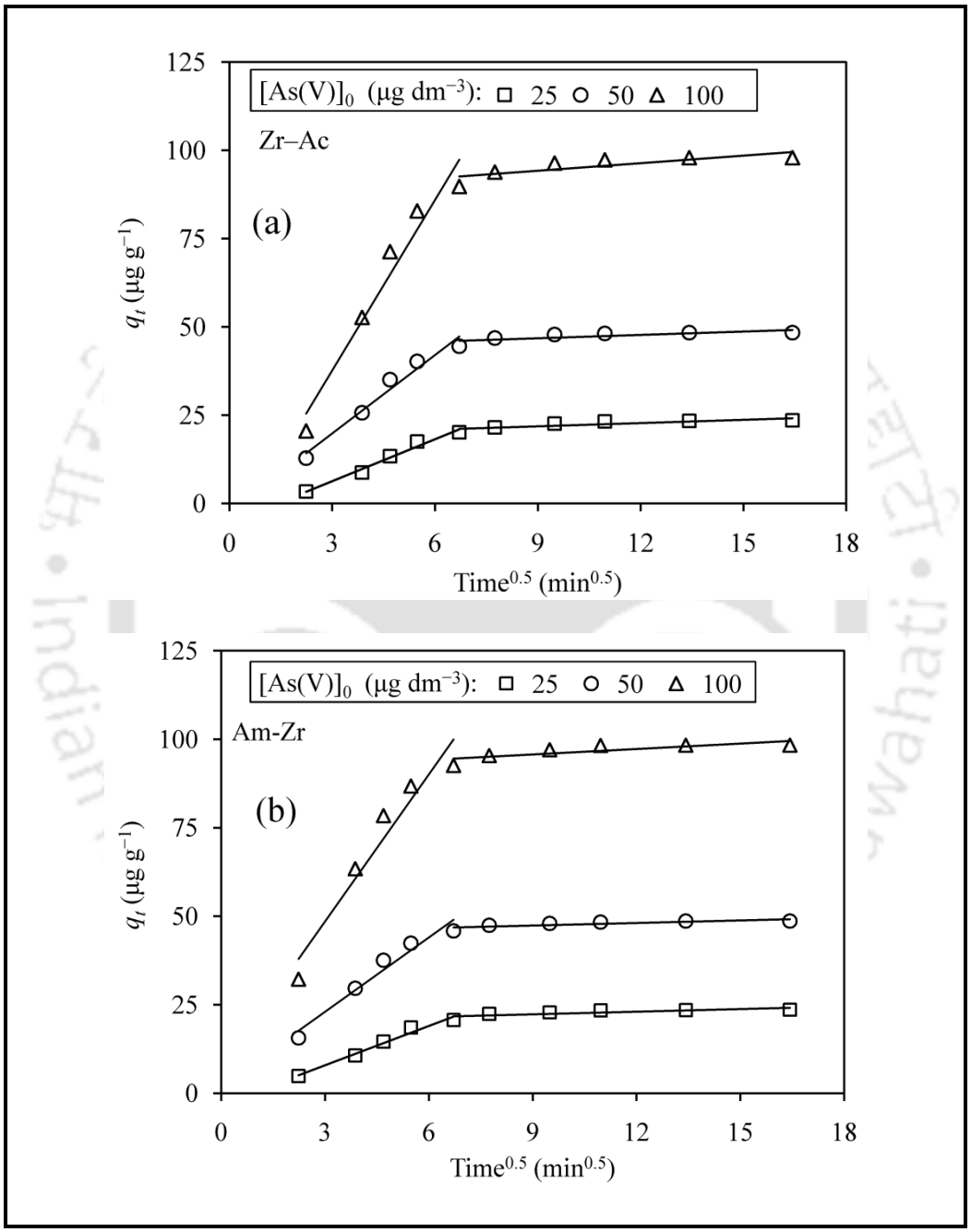

Figure 5.15 Intra-particle-diffusion model for adsorption of As(V) on (a) Zr–AC, and (b) Am-Zr (adsorbent dose = 1 g dm^{-3}, temperature = 298 K, shaking speed = 200 rpm and pH 6 ± 0.2).

As per this adsorption model, the adsorption process takes place via four steps, viz. (i) movement of adsorbate molecules from bulk solution to the surface of the adsorbent through bulk diffusion, (ii) diffusion of adsorbate molecules through the boundary layer to the surface of the adsorbent via film diffusion, (iii) transport of the adsorbate molecules from the surface to the interior pores of the particle due to intra-particle-diffusion or pore-diffusion mechanism, and, (iv) adsorption of adsorbate at an active site on the surface of the material via ion-exchange, complexation and/or chelation.

Table 5.5 Intra-particle-diffusion model parameters for adsorption of As(V) at 298 K.

	Adsorbent	Zr–AC			Am-Zr		
	C_0 (μg dm^{-3})	25	50	100	25	50	100
First linear segment	k_i^1 $\left(\mu g\ g^{-1}\ min^{-0.5}\right)$	3.96	7.40	16.10	3.71	7.00	13.87
	I_1 (μg g^{-1})	5.60	2.34	10.52	3.18	2.05	6.90
	ρ^2	0.98	0.97	0.95	0.98	0.96	0.94
Second linear segment	k_i^2 $\left(\mu g\ g^{-1}\ min^{-0.5}\right)$	0.31	0.32	0.71	0.25	0.24	0.52
	I_2 (μg g^{-1})	19.02	43.84	87.78	20.10	45.30	91.10
	ρ^2	0.97	0.95	0.94	0.97	0.97	0.95

Figures 5.15 (a) and (b) depict the variation of q_t with time. The experimental data clearly depict two linear segments in as many time zones. The plots indicate that two steps are involved in the adsorption process. The initial sudden increase in the slope (i.e. the first linear segment) indicates that As(V) was transported to the external surface of the adsorbent

through film diffusion and the rate was very fast. The second linear segment (i.e. at higher times) indicates a gradual adsorption, where intra-particle-diffusion was the rate-limiting step. Both the lines do not pass through the origin, which means both film diffusion and intra-particle-diffusion took place simultaneously during the adsorption of As(V) on Zr–AC and Am-Zr. The values of k_i^1, k_i^2, I_1, I_2 and ρ^2 are given in Table 5.5.

5.2.4 Adsorption Isotherms

Three adsorption isotherms (viz. Langmuir, Freundlich and Redlich–Peterson) were used for studying the adsorption of As(V). The Langmuir isotherm is given by

$$\frac{q_e}{q_{\max}} = \frac{K_L C_e}{1 + K_L C_e} \tag{5.22}$$

where $q_{\max}$ is the maximum adsorption capacity corresponding to a complete monolayer coverage on the surface, and K_L is the Langmuir constant, which corresponds to the adsorption energy. K_L and $q_{\max}$ are determined by a linear plot of C_e/q_e vs C_e. A dimensionless separation factor, *r*, describes the adsorption efficiency. It is defined as

$$r = \frac{1}{1 + K_L C_0} \tag{5.23}$$

The process is irreversible if $r = 0$, linear if $r = 1$, and unfavorable if $r > 1$. For a favorable adsorption, the value of *r* should lie between 0 and 1 (Tuna et al., 2013).

According to the Freundlich adsorption isotherm, the adsorption energy decreases exponentially. This isotherm describes reversible adsorption and it is not restricted to the formation of a monolayer. The Freundlich isotherm is given by

$$q_e = K_F C_e^N \tag{5.24}$$

where K_F reflects the adsorption capacity. The value of *n* greater than unity represents favorable adsorption conditions. Redlich and Peterson (Redlich and Peterson, 1959) incorporated three parameters into an empirical isotherm. This model combines elements from both the Langmuir and Freundlich equations, and the mechanism of adsorption is not restricted to the formation of a monolayer. The Redlich–Peterson isotherm is given by (Redlich and Peterson, 1959)

$$q_e = \frac{AC_e}{1 + B(C_e)^g} \tag{5.25}$$

The constants of Langmuir isotherm were calculated by regression analysis. These values are presented in Table 5.6. The maximum adsorption capacity, $q_{\max}$, of the adsorbent increased with increasing temperature. This indicates that the adsorption of As(V) on Zr–AC and Am-Zr was endothermic in nature. The value of K_L remained almost constant with increasing temperature from 298 to 308 K. However, it decreased at 318 K. The As(V) adsorption capacity of Am-Zr was found to be more than that of Zr–AC at all temperatures. The values of *r* for different initial concentrations of As(V) (i.e. C_0) were between 0 and 1 for both the adsorbents (viz. 0.26−0.98 for Zr–AC and 0.17−0.96 for Am-Zr) in the temperature range of 298 to 308 K. These values indicate a favorable adsorption system, and show that the data obeyed the Langmuir isotherm. The Freundlich isotherm constants were calculated from the linear plot of $\ln q_e$ versus $\ln C_e$. For both the adsorbents, Freundlich isotherm gave a better fit than the Langmuir isotherm as shown in Figure 5.16.

The value of K_F increased with increasing temperature, which indicates that the adsorption efficiency of As(V) on both the adsorbents increased with temperature. The value of *N* was very close to unity, which represents favorable adsorption conditions. The

Redlich–Peterson isotherm was found to fit the data in the best manner, as shown in Figure 5.16.

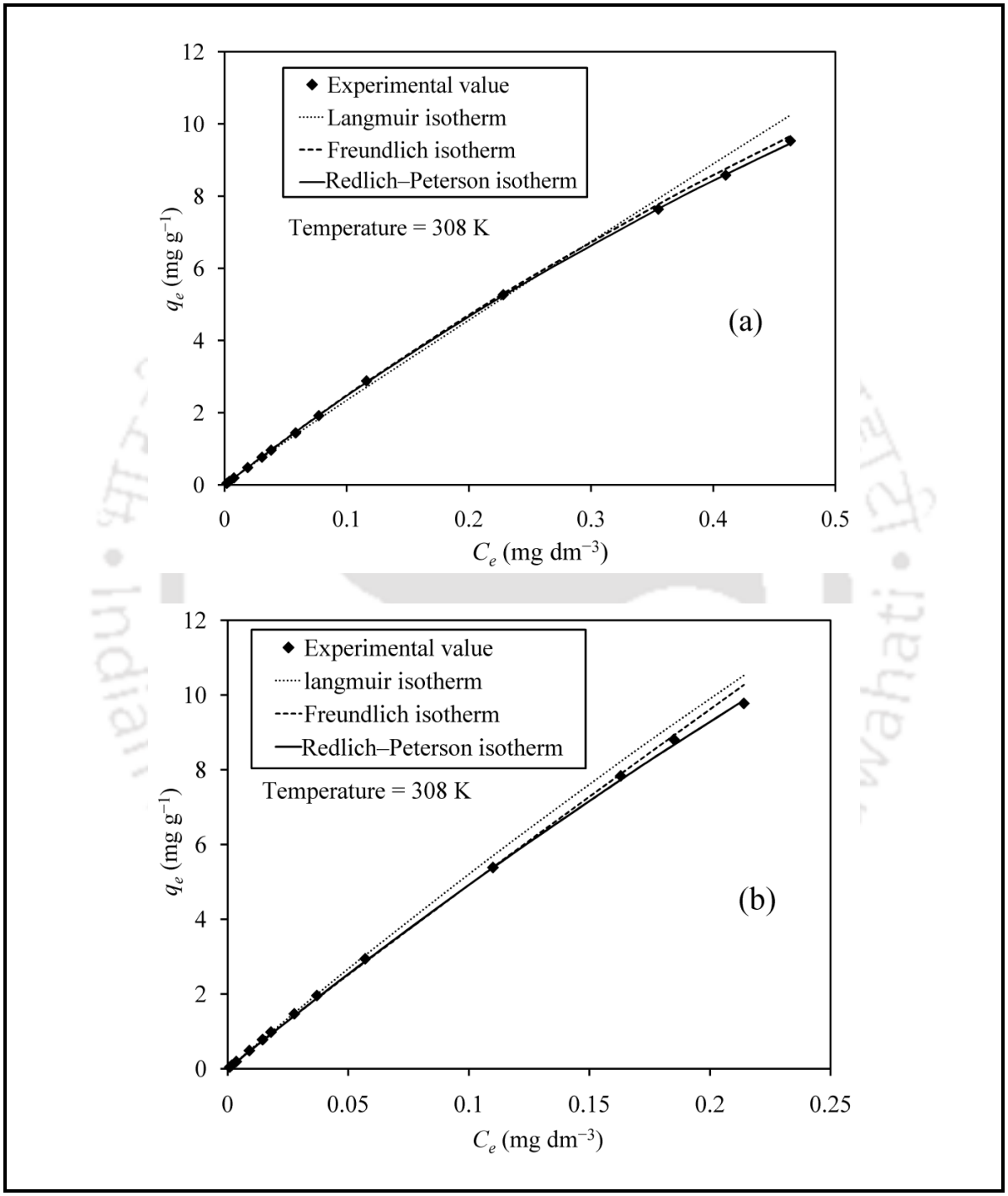

Figure 5.16 The fit of Langmuir, Freundlich and Redlich–Peterson adsorption isotherms to the experimental data (at 308 K) for adsorption of As(V) on (a) Zr–AC, and (b) Am-Zr.

The constants of Redlich–Peterson isotherm were determined by non-linear regression. These values are given in Table 5.6. The Redlich–Peterson constant, *A*, increased whereas the value of the constant, *B*, decreased with increasing temperature. The exponent, *g*, was found to lie between 0 and 1. The isotherms are depicted in Figure 5A.4 at 298− 318 K.

Table 5.6 Langmuir, Freundlich and Redlich–Peterson isotherm constants for adsorption of As(V) on Zr–AC and Am-Zr.

Isotherm	Adsorbents	Zr–AC			Am-Zr		
	Temperature (K)	298	308	318	298	308	318
Langmuir	q_{max} (mg g^{-1})	42.60	47.60	58.80	50.30	55.60	66.70
	K_L (dm^3 mg^{-1})	0.55	0.55	0.51	0.99	0.99	0.88
	ρ^2	0.98	0.98	0.99	0.96	0.96	0.97
Freundlich	K_F (mg g^{-1})(dm^3 mg^{-1})$^{1/n}$	19.30	21.50	25.90	40.90	45.70	49.90
	N	1.04	1.04	1.03	1.04	1.03	1.03
	ρ^2	0.99	0.99	0.99	0.99	0.99	0.99
Redlich–Peterson	A (dm^3 g^{-1})	23.70	26.30	30.30	52.20	53.20	58.63
	B (dm^3 mg^{-1})^g	0.55	0.59	0.41	0.62	0.62	0.53
	g	1.00	0.96	0.93	0.62	1.00	0.78
	ρ^2	1.00	1.00	1.00	1.00	1.00	0.99

From the adsorption isotherm studies, it was found that Langmuir, Freundlich and Redlich–Peterson models fitted the data well for both the adsorbents. The monolayer adsorption capacity, q_{max}, for these adsorbents was much higher than the zirconium-loaded activated carbon prepared by Daus et al. (2004), and close to the zirconium-based magnetic sorbent prepared by Zheng et al. (2009), and zirconium resins (Balaji et al., 2005; Suzuki et

al., 2000). However, Freundlich and Redlich–Peterson models fitted the data better than the Langmuir model. This indicates that multilayer adsorption of As(V) on Zr–AC and Am-Zr took place via the surface functional groups (Tuna et al., 2013).

5.2.5 Determination of Thermodynamic Parameters for As(V) Adsorption

The changes in standard Gibbs free energy (ΔG^0), standard enthalpy (ΔH^0) and standard entropy (ΔS^0) for the adsorption of As(V) were determined as follows (Rodrigues et al., 2010).

$$\ln K_C = \frac{\Delta S^0}{R} - \frac{\Delta H^0}{RT} \tag{5.26}$$

$$\Delta G^0 = \Delta H^0 - T\Delta S^0 \tag{5.27}$$

where K_c is defined as q_e/C_e. From the linear plot of $\ln K_C$ versus $1/T$, as shown in Figure 5.17, the values ΔH^0 and ΔS^0 were calculated. These values are given in Table 5.7.

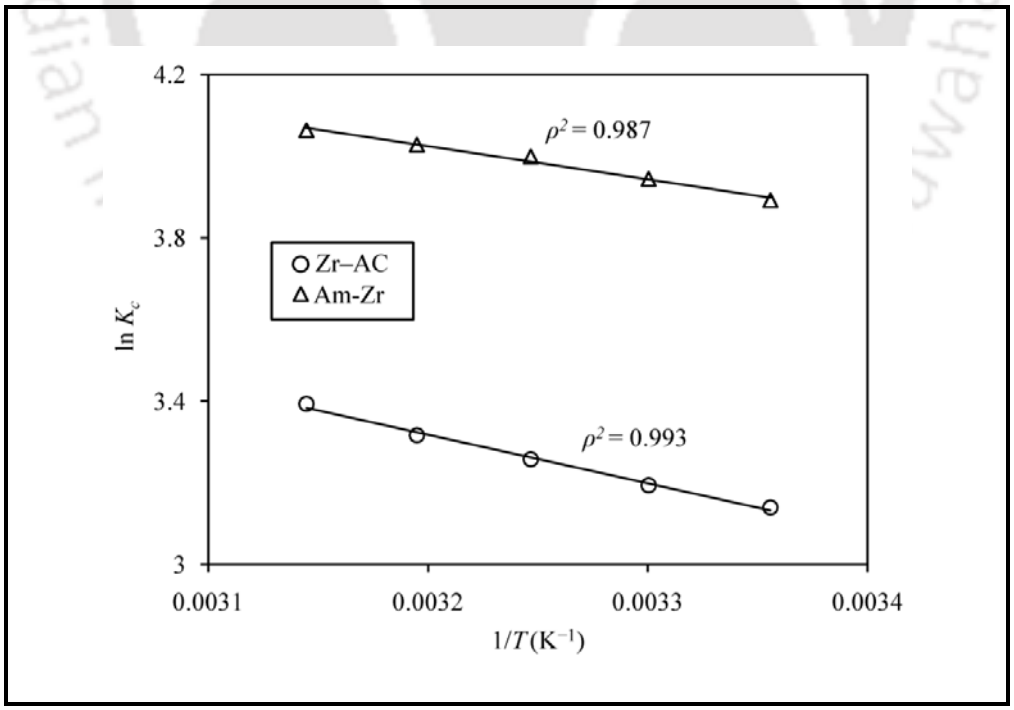

Figure 5.17 The fit of Redlich–Peterson adsorption isotherm to the experimental data for adsorption of As(V).

The positive values of ΔH^0 indicate that adsorption of As(V) on both of these adsorbents was endothermic in nature. The heat of adsorption was found to be about 6−10 kJ mol^{-1}, which indicates that the adsorption was physical rather than chemical (Du and Yuan 2008). The negative values of ΔG^0 indicate the spontaneity of the adsorption process. The positive values of ΔS^0 indicate an increase in the randomness during adsorption. They reflect the affinity of the adsorbent for As(V). This is likely due to some structural changes in the arsenic species and the adsorbent (Zeng, 2004). Similar results have been reported in the literature (Hameed et al., 2007; Mandal et al., 2011; Tuna et al., 2013).

Table 5.7 Thermodynamic parameters for adsorption of As(V) on Zr–AC and Am-Zr.

Adsorbents	Temperature (K)	298	303	308	313	318
Zr–AC	ΔH^0 (kJ mol^{-1})	9.9	9.9	9.9	9.9	9.9
	ΔS^0 (kJ K^{-1} mol^{-1})	0.06	0.06	0.06	0.06	0.06
	$-\Delta G^0$ (kJ mol^{-1})	7.98	8.28	8.58	8.88	9.18
Am-Zr	ΔH^0 (kJ mol^{-1})	6.7	6.7	6.7	6.7	6.7
	ΔS^0 (kJ K^{-1} mol^{-1})	0.06	0.06	0.06	0.06	0.06
	$-\Delta G^0$ (kJ mol^{-1})	11.18	11.48	11.78	12.08	12.38

5.2.6 FTIR Studies of the Adsorbents Before and After As(V) Adsorption

The mechanism of adsorption of As(V) on Zr–AC and Am-Zr was investigated by FTIR spectroscopy. Figure 5.18 (a) shows the FTIR spectra of untreated activated carbon and Zr–AC before and after the adsorption of As(V). The hydroxyl stretching was found to be very poor for the untreated activated carbon (which is generally found at 3100−3700 cm^{-1}). However, Zr–AC showed a broad region of hydroxyl functional group with a very prominent

peak at 3441 cm^{-1}, which is usually derived from the carboxylic and phenolic groups, and adsorbed H_2O molecules (Wu et al., 2013). The small absorption bands present at 2924 and 2850 cm^{-1} were due to the symmetric and asymmetric C–H stretching vibrations (Wu et al., 2013). The peak at 1589 cm^{-1} shows the vibrations of physically adsorbed H_2O (Cui et al., 2012). The disappearance of the hydroxyl group (i.e. 3441 cm^{-1}) after As(V) adsorption implies that the hydroxyl groups were involved in the adsorption of As(V).

The broad bands appearing for activated carbon at 949 and 1168 cm^{-1} are mainly related to the C–O stretching vibration of alcoholic, phenolic and carboxylic groups. These bands disappeared after zirconium impregnation. This peak was replaced by the Zr–O bond and a strong peak appeared at 1018 cm^{-1}. After adsorption of As(V), the peak at 1018 cm^{-1} disappeared. This happened due to the formation of the As–OZr bond (Cui et al., 2012). It was observed that the shape of the spectrum from 600 to 1000 cm^{-1} of Zr–AC after As(V) adsorption was different from that before adsorption. This change might be due to the formation of the complex of the arsenate ion with the ZrO group (Zheng et al., 2009).

Figure 5.18 (b) depicts the FTIR spectra of Am-Zr before and after the adsorption of As(V). Before the adsorption of As(V), the FTIR spectra of Am-Zr had a strong and prominent hydroxyl stretching at 3221 cm^{-1}. The peaks at 1628 and 1404 cm^{-1} represent the adsorbed H_2O molecules and the Zr–OH group, respectively (Cui et al., 2012). The broadening of the peak corresponding to the hydroxyl group after As(V) adsorption suggests the involvement of the hydroxyl group in the adsorption process. Furthermore, the peak at 1404 cm^{-1} disappeared after adsorption and two smaller peaks at 1357 and 1520 cm^{-1} appeared due to the formation of Zr–As bond by the replacement of the Zr–O bond.

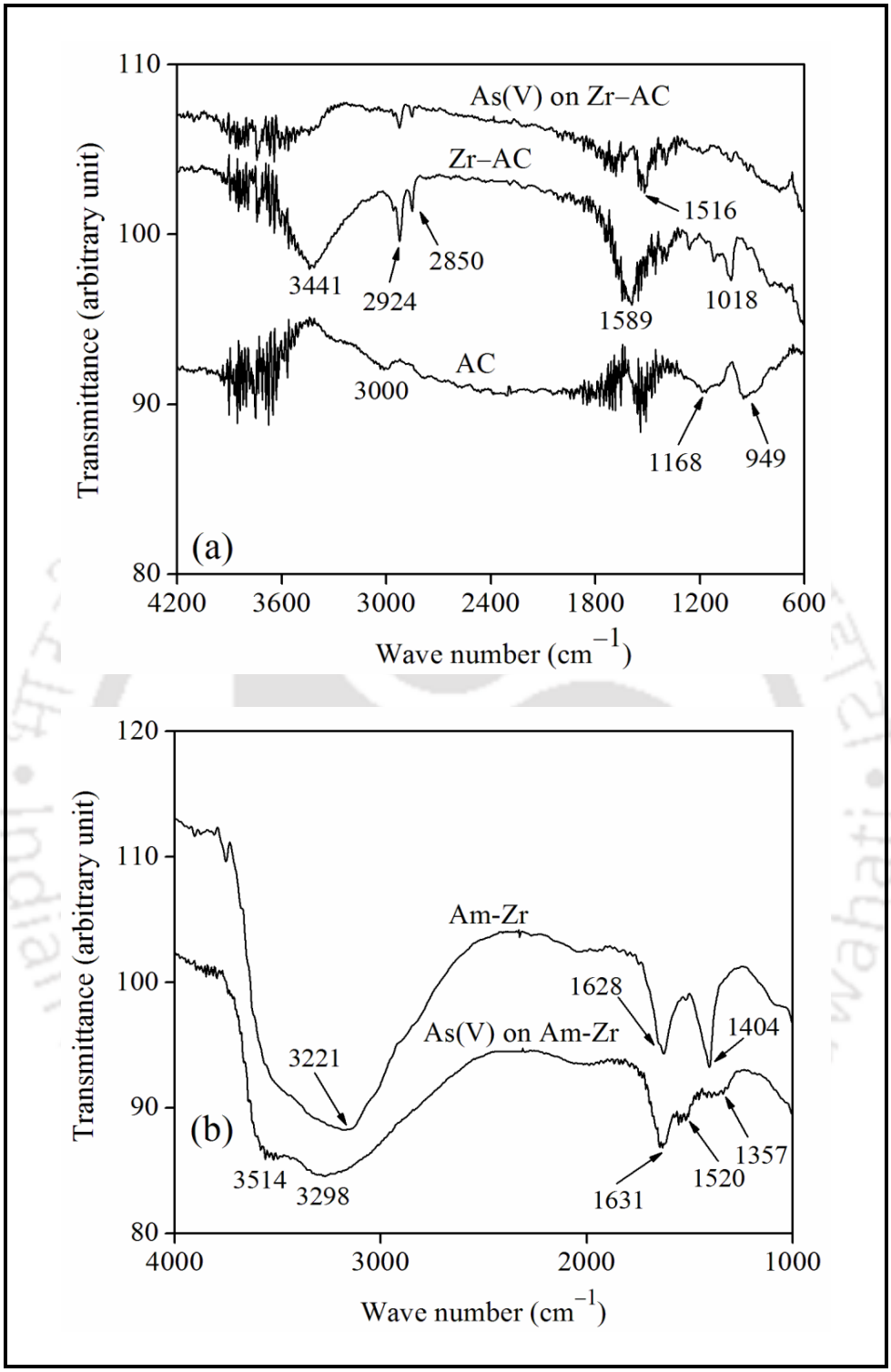

Figure 5.18 FTIR spectra of (a) Zr–AC and (b) Am-Zr before and after As(V) adsorption.

NOTATIONS

A	Redlich–Peterson constant, $dm^3\ g^{-1}$
[As(III)]	arsenite concentration at time t, mol dm^{-3}
$[As(III)]_0$	arsenite concentration at $t = 0$, mol dm^{-3}
B	Redlich–Peterson constant, $(dm^3\ mg^{-1})^g$
C_0	initial concentrations of As(V), μg dm^{-3}
C_e	concentration of adsorbate at equilibrium, mg dm^{-3}
C_g	ozone generation rate, mg s^{-1}
C_t	concentrations of As(V) after time t, μg dm^{-3}
g	Redlich–Peterson constant, dimensionless
ΔG^0	standard Gibbs free energy, kJ mol^{-1}
ΔH^0	standard enthalpy, kJ mol^{-1}
I	intercept of intra-particle-diffusion model, μg g^{-1}
k	the rate constant of As(III) oxidation with O_3, $(mol\ dm^{-3})^{1-m-n}\ s^{-1}$
k'	rate constant with respect to $t/t_{0.5}$, dimensionless
k_1	pseudo first-order rate constant for adsorption, min^{-1}
k_2	pseudo second-order rate constant for adsorption, g μg^{-1} min^{-1}
k_d	rate constant for self-decomposition of ozone, s^{-1}
k_i	intra-particle-diffusion rate constant, μg g^{-1} $min^{-0.5}$
k_i^1, k_i^2	intra-particle-diffusion rate constants for first and second linear segment respectively, μg g^{-1} $min^{-0.5}$
$k_l a$	volumetric mass transfer coefficient, s^{-1}
K_c	ratio of q_e and C_e, $dm^3\ g^{-1}$
K_F	Freundlich constant, (mg g^{-1}) (L^{-n} mg^n)

K_L	Langmuir constant, L mg^{-1}
m	order with respect to As(III), dimensionless
M	mass of the adsorbent, g
n	order with respect to ozone, dimensionless
N	heterogeneity factor, dimensionless
$[O_3]$	concentration of ozone, mol dm^{-3}
$[O_3]^*$	equilibrium concentration of ozone in the aqueous phase, mol dm^{-3}
q_e	amounts of As(V) adsorbed at equilibrium, μg g^{-1}
q_{max}	maximum adsorption capacity, mg g^{-1}
q_t	amount of As(V) adsorbed per unit mass of adsorbent at time t, μg g^{-1}
r	separation factor, dimensionless
R	the gas constant, J K^{-1} mol^{-1}
ΔS^0	standard entropy, kJ K^{-1} mol^{-1}
t	time, s
$t_{0.5}$	half-life of the reaction, min
T	temperature, K
V	volume of solution, dm^3
ρ^2	coefficient of determination, dimensionless

Abbreviations

AC	activated carbon
Am-Zr	amorphous zirconium oxide
BET	Brunauer–Emmett–Teller
EDX	energy dispersive X-ray
FTIR	Fourier transform infrared

SEM	scanning electron microscope
XRD	X-ray diffractometry
Zr–AC	Zirconium–activated carbon

REFERENCES

Ansari, R., Sadegh, M., 2007. Application of activated carbon for removal of arsenic ions from aqueous solutions. E-Journal Chem. 4, 103−108.

Augusto, O., Bonini, M.G., Amanso, A.M., Linares, E., Santos, C.C.X., Menezes, S.L.D., 2002. Nitrogen dioxide and carbonate radical anion: two emerging radicals in biology. Free Radic. Biol. Med. 32, 841−859.

Balaji, T., Yokoyama, T., Matsunaga, H., 2005. Adsorption and removal of As(V) and As(III) using Zr-loaded lysine diacetic acid chelating resin. Chemosphere 59, 1169−1174.

Beltrán, F.J., 2004. Ozone Reaction Kinetics for Water and Wastewater System. CRC Press, Boca Raton, Florida, USA.

Cope, V.W., Hoffman, M., Chen, S., 1978. Reactivity of the carbonate radical toward metal complexes in aqueous solution. J. Phys. Chem. 82, 2665−2669.

Cui, H., Li, Q., Gao, S., Shang, J.K., 2012. Strong adsorption of arsenic species by amorphous zirconium oxide nanoparticles. J. Ind. Eng. Chem. 18, 1418−1427.

Daus, B., Wennrich, R., Weiss, H., 2004. Sorption materials for arsenic removal from water: a comparative study. Water Res. 38, 2948−2954.

Driehaus, W., Seith, R., Jekel, M., 1995. Oxidation of arsenate(III) with manganese oxides in water treatment. Water Res. 29, 297−305.

Ghurye, G., Clifford, D., 2001. Laboratory study on the oxidation of arsenic III to arsenic V, EPA/600/R-01/021. Houston, Texas, USA.

Ghurye, G., Clifford, D., 2004. As(III) oxidation using chemical and solid-phase oxidants. Am. Water Work. Assoc. 96, 84−96.

Hameed, B.H., Ahmad, A.A., Aziz, N., 2007. Isotherms, kinetics and thermodynamics of acid dye adsorption on activated palm ash. Chem. Eng. J. 133, 195−203.

Hug, S.J., Leupin, O., 2003. Iron-catalyzed oxidation of arsenic(III) by oxygen and by hydrogen peroxide: pH-dependent formation of oxidants in the Fenton reaction. Environ. Sci. Technol. 37, 2734−2742.

Huie, R.E., Clifton, C.L., Neta, P., 1991. Electron transfer reaction rates and equilibria of the carbonate and sulfate radical anions. Radiat. Phys. Chem. 38, 477−481.

Kim, M.J., Nriagu, J., 2000. Oxidation of arsenite in groundwater using ozone and oxygen. Sci. Total Environ. 247, 71−79.

Kläning, U.K., Bielski, B.H.J., Sehested, K., 1989. Arsenic(IV). A pulse-radiolysis study. Inorg. Chem. 28, 2717−2724.

Kuo, C.H., Yuan, F., Hill, D.O., 1997. Kinetics of oxidation of ammonia in solutions containing ozone with or without hydrogen peroxide. Ind. Eng. Chem. Res. 36, 4108−4113.

Li, P., Takahashi, M., Chiba, K., 2009. Enhanced free-radical generation by shrinking microbubbles using a copper catalyst. Chemosphere 77, 1157−1160.

Mandal, S., Padhi, T., Patel, R.K., 2011. Studies on the removal of arsenic (III) from water by a novel hybrid material. J. Hazard. Mater. 192, 899−908.

Nandi, B.K., Goswami, A., Purkait, M.K., 2009. Adsorption characteristics of brilliant green dye on kaolin. J. Hazard. Mater. 161, 387−395.

Redlich, O., Peterson, D.L., 1959. A useful adsorption isotherm. J. Phys. Chem. 63, 1024−1024.

Rodrigues, L.A., Maschio, L.J., da Silva, R.E., da Silva, M.L.C.P., 2010. Adsorption of Cr(VI) from aqueous solution by hydrous zirconium oxide. J. Hazard. Mater. 173, 630−636.

Sorlini, S., Gialdini, F., 2010. Conventional oxidation treatments for the removal of arsenic with chlorine dioxide, hypochlorite, potassium permanganate and monochloramine. Water Res. 44, 5653−5659.

Sotelo, J.L., Beltran, F.J., Benitez, F.J., Beltran-Heredia, J., 1987. Ozone decomposition in water: kinetic study. Ind. Eng. Chem. Res. 26, 39−43.

Suzuki, T.M., Bomani, J.O., Matsunaga, H., Yokoyama, T., 2000. Preparation of porous resin loaded with crystalline hydrous zirconium oxide and its application to the removal of arsenic. React. Funct. Polym. 43, 165−172.

Tuna, A.Ö.A., Özdemir, E., Şimşek, E.B., Beker, U., 2013. Removal of As(V) from aqueous solution by activated carbon-based hybrid adsorbents: impact of experimental conditions. Chem. Eng. J. 223, 116−128.

Wu, G.Q., Sun, X.., Hui, H., Zhang, X., Yan, J., Zhang, Q.S., 2013. Adsorption of 2,4-dichlorophenol from aqueous solution by activated carbon derived from moso bamboo processing waste. Desalin. Water Treat. 51, 4603−4612.

Yoon, S.H., Lee, J.H., Oh, S., Yang, J.E., 2008. Photochemical oxidation of As(III) by vacuum-UV lamp irradiation. Water Res. 42, 3455−3463.

Zeng, L., 2004. Arsenic adsorption from aqueous solutions on an Fe(III)-Si binary oxide adsorbent. Water Qual. Res. J. Can. 39, 267−275.

Zheng, Y.M., Lim, S.F., Chen, J.P., 2009. Preparation and characterization of zirconium-based magnetic sorbent for arsenate removal. J. Colloid Interface Sci. 338, 22−29.

APPENDIX 5A

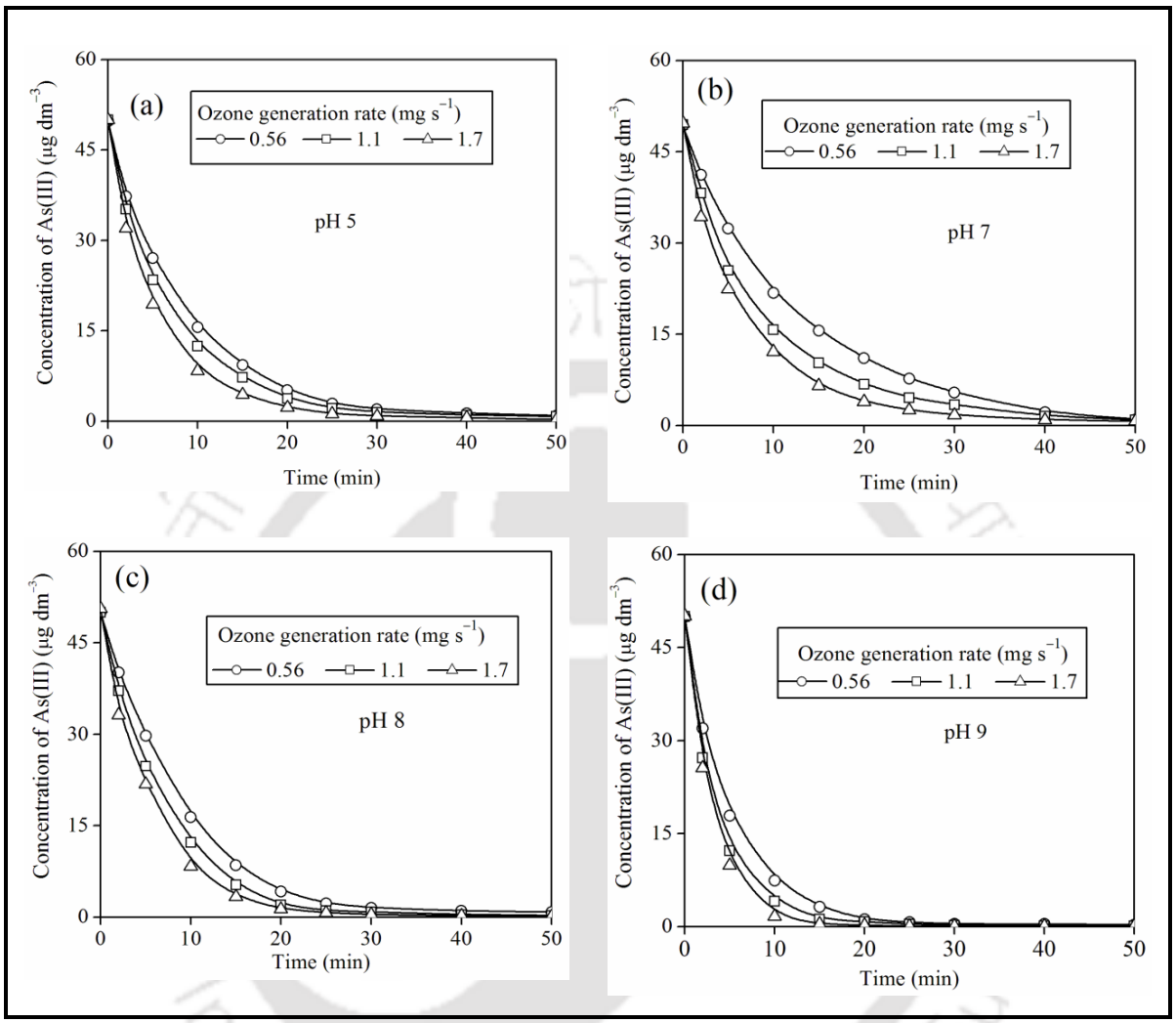

Figure 5A.1 Effect of ozone generation rate on oxidation of As(III) (a) pH 5, (b) pH 7, (c) pH 8, and (d) pH 9.

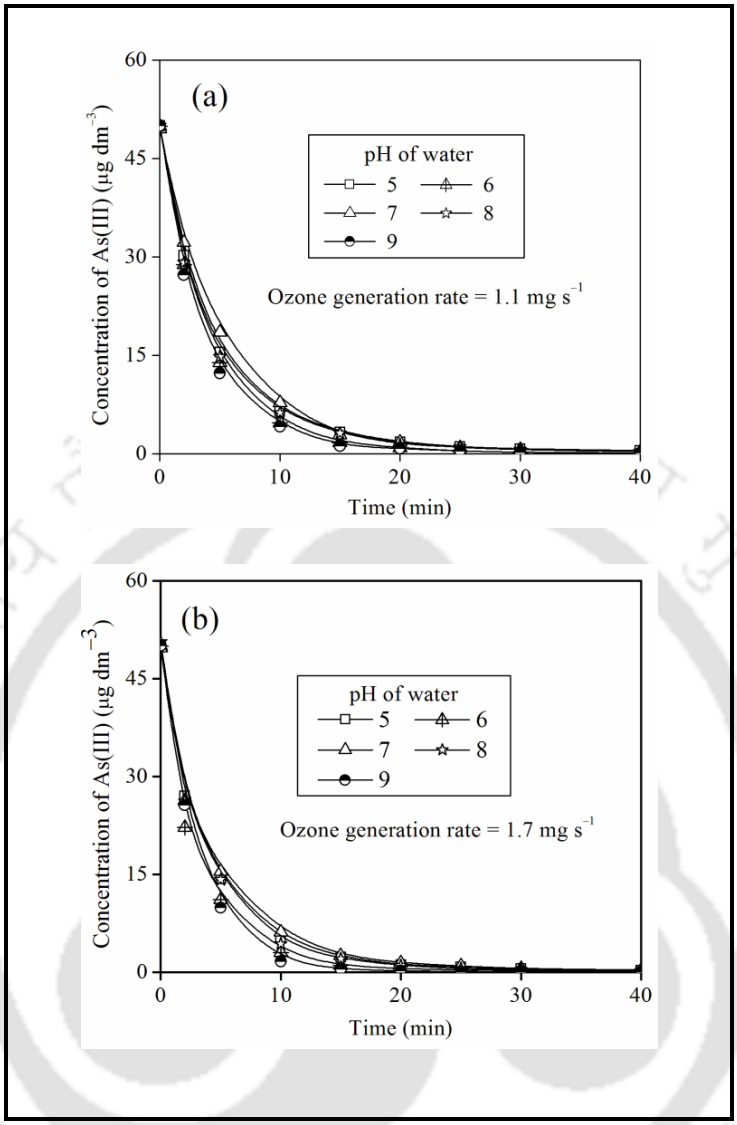

Figure 5A.2 Effect of pH on oxidation of As(III) (a) ozone generation rate 1.1 mg s^{-1}, and (b) ozone generation rate 1.7 mg s^{-1}.

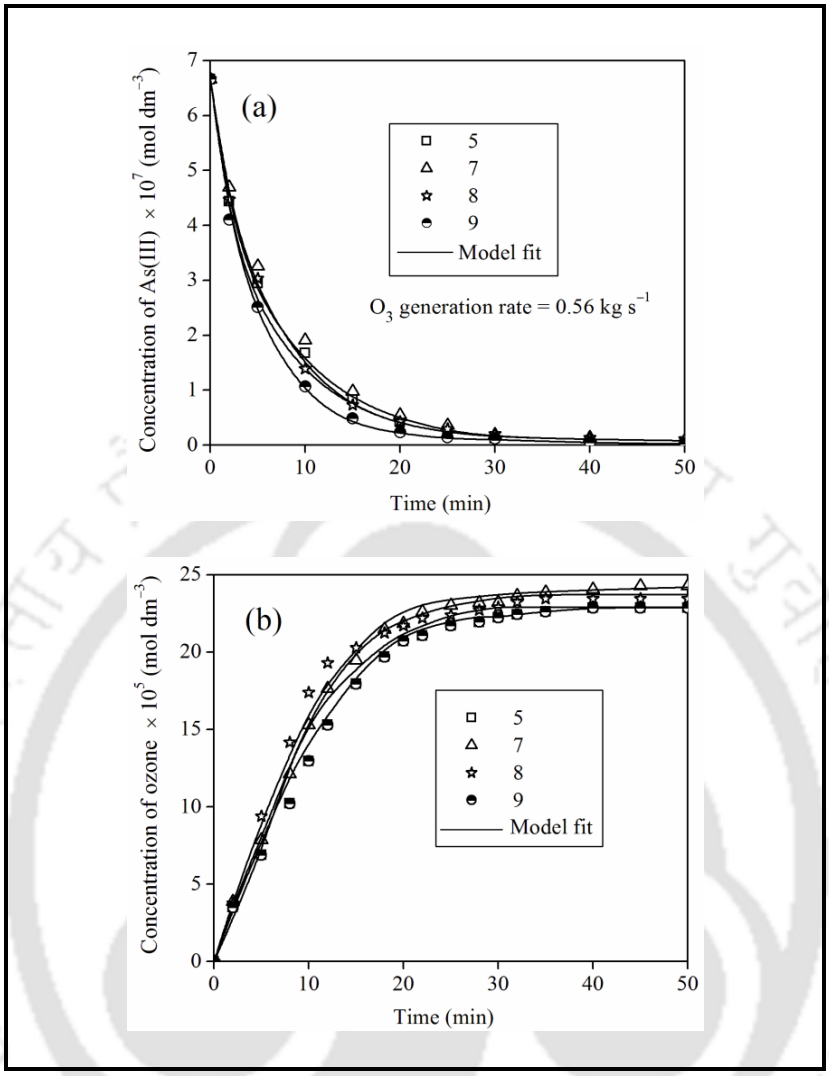

Figure 5A.3 Variation of (a) As(III) concentration, and (b) O_3 concentration with time. The parity of the kinetic model with the experimental data at pH 5, 7, 8, and 9 are shown.

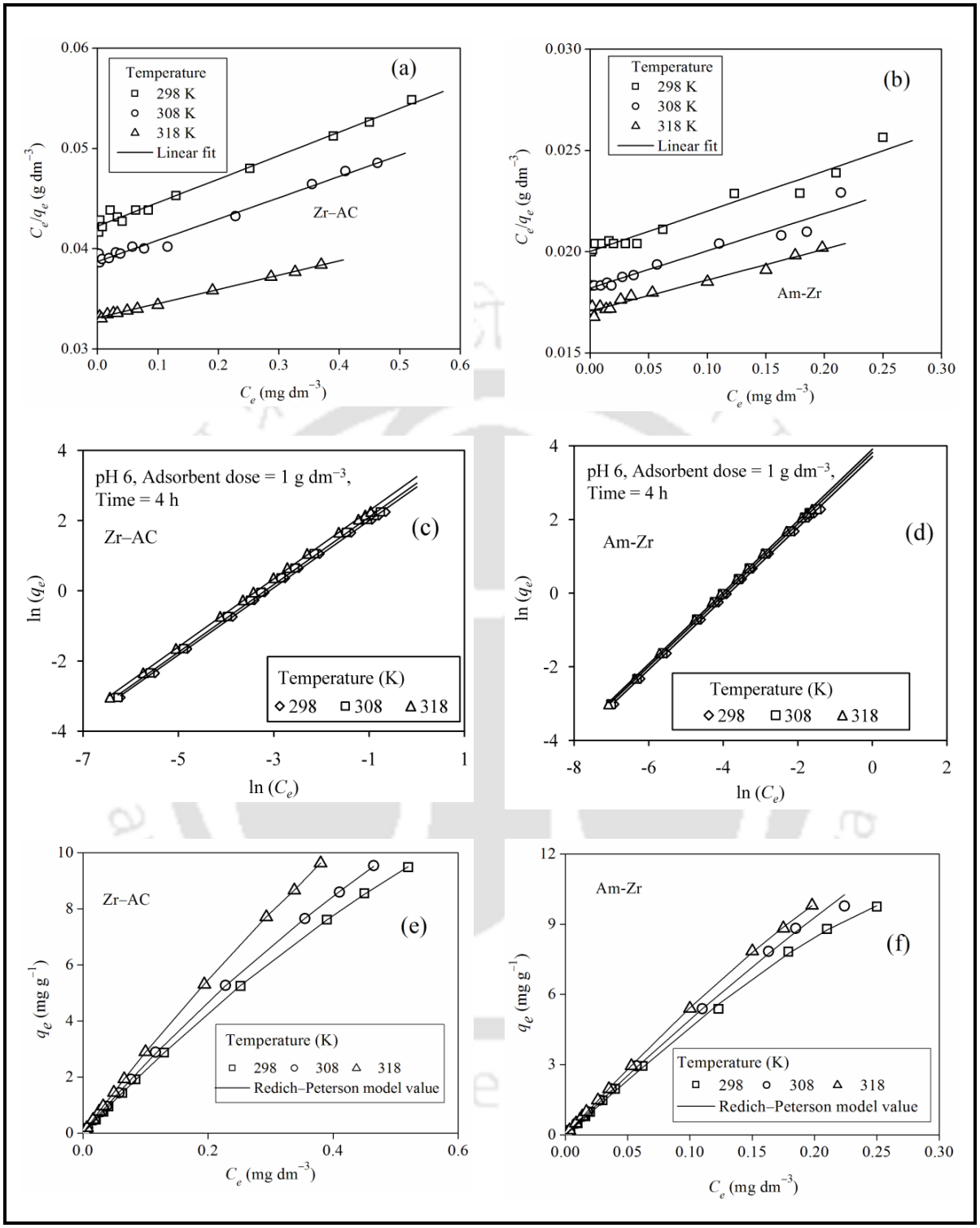

Figure 5A.4 (a) Langmuir isotherm for Zr–AC, (b) Langmuir isotherm for Am-Zr, (c) Freundlich isotherm for Zr–AC, (d) Freundlich isotherm for Am-Zr, (e) Redlich-Peterson isotherm for Zr–AC, and (f) Redlich–Peterson isotherm for Am-Zr.

CHAPTER 6

REMOVAL OF DYESTUFFS FROM WATER

CHAPTER 6

REMOVAL OF DYESTUFFS FROM WATER

This chapter presents the oxidation of Brilliant Green (BG) dye using ozone microbubbles. This work focused on the variation of concentration of BG with time, degradation products of BG, reaction mechanism, and the kinetics of the reaction. The variation of concentration of BG with time was investigated by UV–Visible spectrophotometry. The degradation mechanism was constructed from the data obtained from GC–MS and FTIR analyses. The TOC of the dye water was analyzed to find out the extent of mineralization.

6.1 DECOLORIZATION OF BG USING OZONE

The UV-Visible spectrum of BG was generated at 200−800 nm. The absorbance as well as the spectrum rapidly changed with time due to the fast decolorization and the formation of the intermediates. It was observed that more than 90% of the color of the dye was removed within 20 min. The fast decrease in absorbance of BG at the maximum peak (i.e. 625 nm) indicates a rapid decomposition of the dye as shown in Figure 6.1 (a). The strong oxidizing power of ozone was effective in the degradation of BG. About 99% of BG was oxidized in 30 min and the absorbance was below the detection limit at 40 min. The rapid decolorization of BG was also visible with naked eye within 15 min for 10−20 mg dm^{-3} initial BG concentration, as shown in Figure 6.1 (b). The spectral band changed (after ~5 min) due to the destruction of the structure of BG by ozone. The change of spectral band position in the absorbance (i.e. hypsochromic shift) is due to the N-demethylation of the dye molecule (Behnajady et al., 2008). The degradation intermediates were identified by GC–MS and the mechanism of degradation is discussed later in Section 6.4.

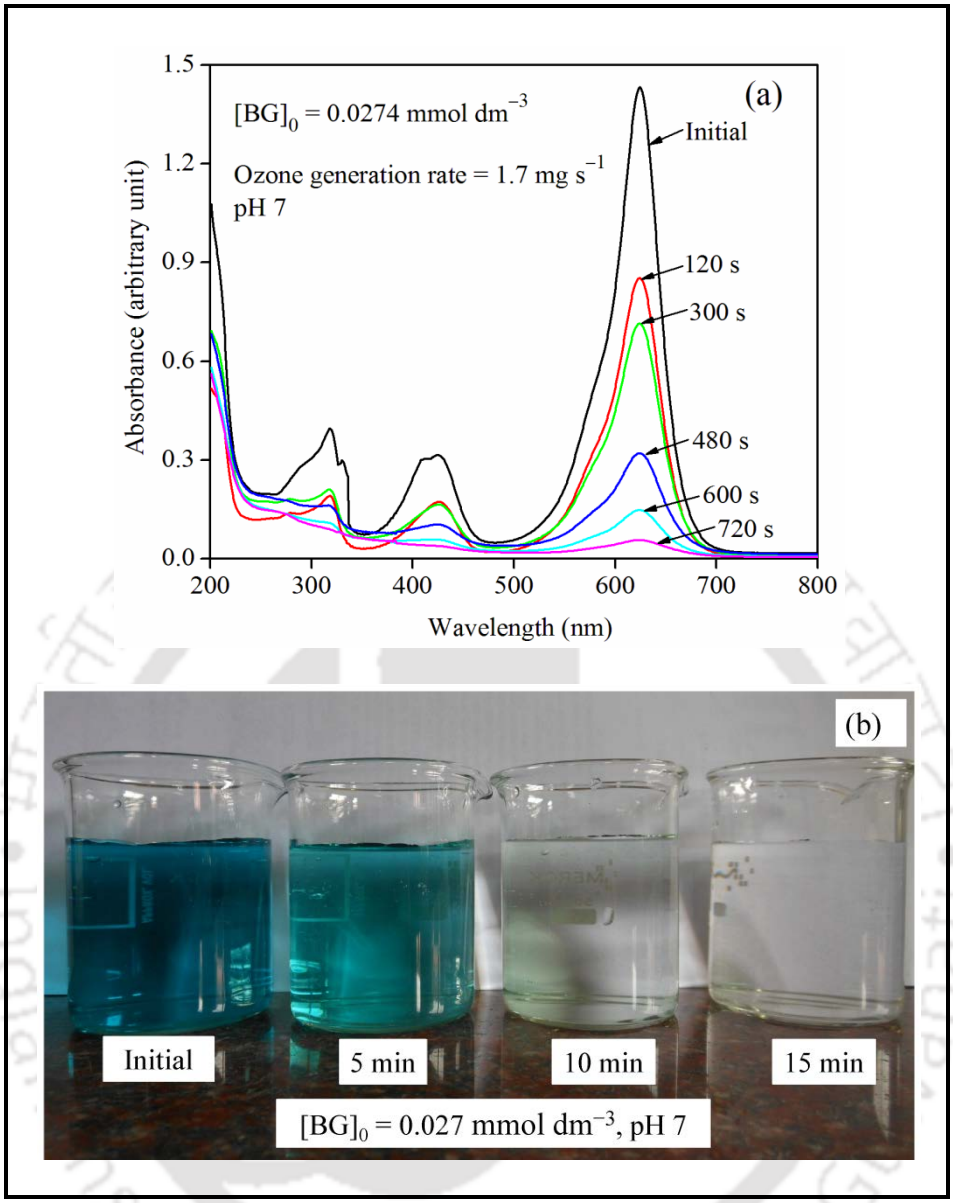

Figure 6.1 (a) Spectroscopic detection, and (b) photographic view of BG degradation with time.

6.2 EFFECT OF pH

The decolorization experiments were carried out with 0.028 mmol dm^{-3} dye concentration at pH 4−10 for 30 min. The oxidation of BG was effective in both acidic and alkaline conditions at all ozone generation rates (Figure 6.2). The effect of pH at other ozone generation rates (i.e. 0.56 and 1.1 mg s^{-1}) is given in Figure 6A.1.

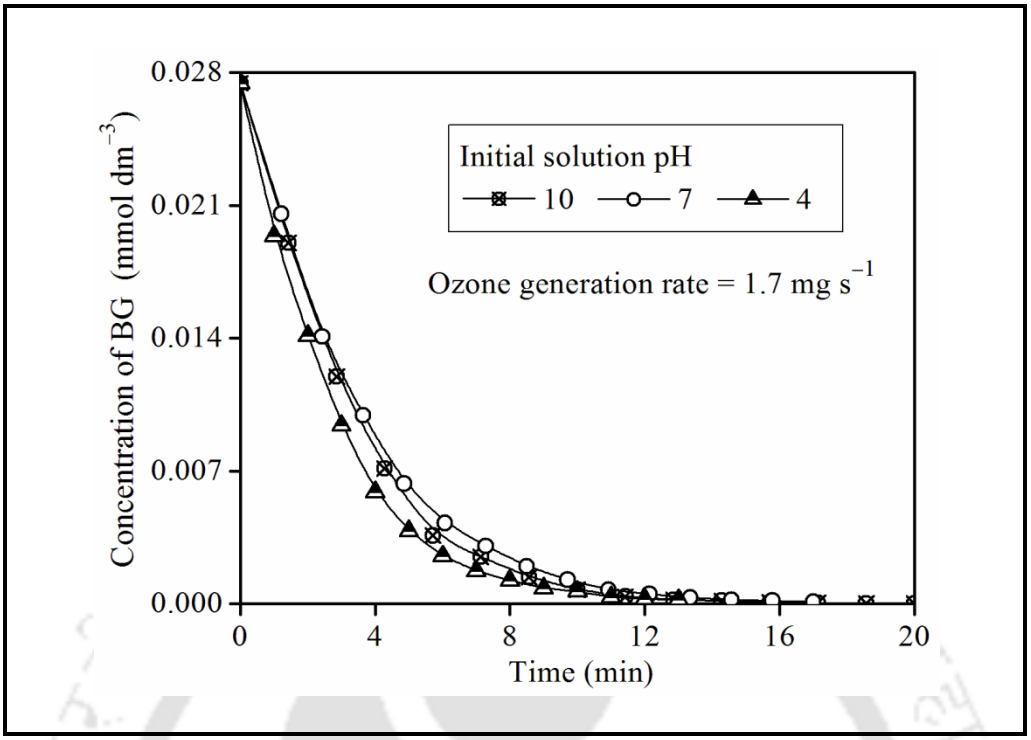

Figure 6.2 Effect of pH on oxidation of BG.

The half-life of BG was higher at neutral pH as shown in Figure 6.3 (a). For 0.028 mmol dm^{-3} initial dye concentration, the half-life was 2−7 min for the ozone generation rates in the range of 0.56−1.7 mg s^{-1}, at pH 4−10. With progress in oxidation of the dye, there was a corresponding decrease in the pH of the dye solution. A similar behavior was observed by Shu and Chang (2005). The generation of some partial oxidation products of BG (such as organic and inorganic acids, aldehydes and ketones) is expected during ozonation. Therefore, a decrease in the solution pH indicates that BG degraded into some more acidic intermediates, which were responsible for the decrease of the solution pH [Figure 6.3 (b)]. It is reported that BG can exist in two ionic forms in water (Mitrowska et al., 2008). At acidic pH, BG gets protonated to form the stable and colored form of the dye. On the other hand, at alkaline pH, BG gets deprotonated to form the colorless leuco-form, which is less stable (Mitrowska et al., 2008).

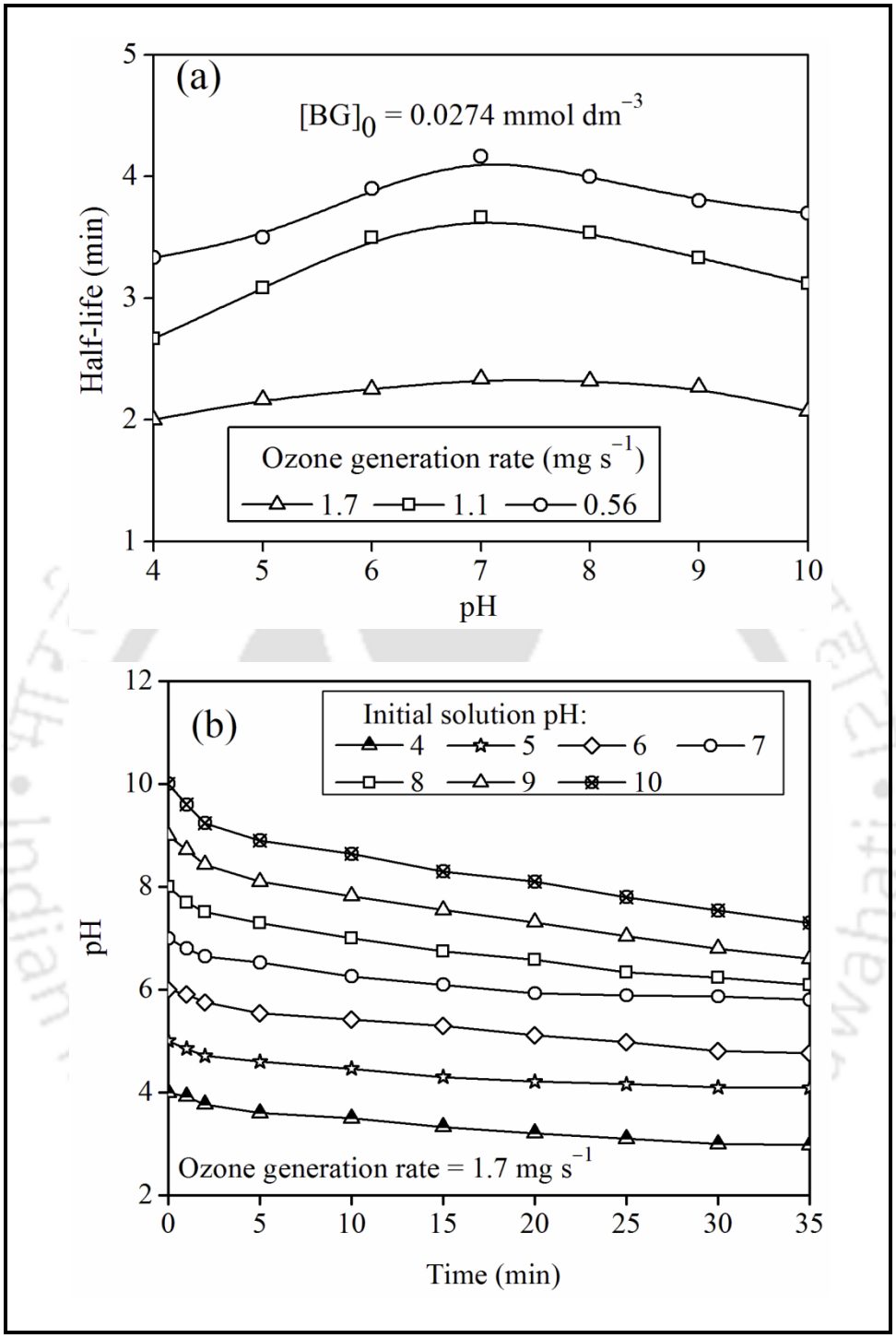

Figure 6.3 (a) Variation of the half life of BG with pH, and (b) variation of pH during ozonation of BG.

The oxidation of BG was effective in acidic as well as in alkaline conditions with ozone microbubbles. However, the decolorization efficiency was slightly less at the neutral

pH. The use of microbubbles helped in two ways for rapid decolorization. Firstly, the microbubbles were very efficient in transferring ozone from the gas phase to the aqueous phase. Secondly, at acidic pH, the microbubbles generated small amounts of hydroxyl radicals (Li et al., 2009), which is a very strong oxidizing agent. At pH 4−6, the cationic form of BG is more stable. A combination of hydroxyl radicals and molecular ozone reacted with this form of BG. The rapid decolorization of BG at pH 8−10 was due to the fact that the BG gets deprotonated to generate the less stable leuco-form. Although the generation of ·OH was less at alkaline pH, the decolorization was fast because the stability of BG decreased. At alkaline pH, molecular ozone is likely to be the main oxidizing species. At pH 7, the generation of ·OH was less than that at acidic pH. This implies that BG is more reactive in presence of hydroxyl radical, and the latter is a very effective oxidant for this dye.

6.3 TOC ANALYSIS

The degradation of BG produces various intermediate compounds which mineralize to CO_2 and H_2O. The measurement of TOC before and after oxidation gives an extent of the conversion of the organic compounds to CO_2. Figure 6.4 shows that more than 50% of TOC decreased within 30 min at all ozone generation rates at pH 7. Although 99% decolorization was achieved in 30 min, the TOC removal was about 50%. The removal of color is due to the cleavage of the central carbon atom in the dye molecule. However, the degradation of the dye forms many intermediates with aromatic rings. The cleavage of these aromatic rings takes a longer time (Rajkumar et al., 2007). Similar results on TOC reduction were observed at other pH. The reduction of TOC was almost invariant with pH. A very small increase in the TOC removal was observed at pH 4 and 10.

The kinetics of the reactions of the intermediates with either ·OH or molecular ozone may vary depending on the pH. However, these reactions did not have any overall effect on

the TOC reduction. Higher temperature and alkaline pH (> 9) can increase the generation of ·OH, which may increase the TOC removal (Konsowa, 2003; Rajeswari, 2000). The formation of ketones, carboxyl acids and phenols increased the demand of ozone, and some of these compounds further oxidized to form CO_2. Although the complete conversion of all organic compounds was not achieved in this work, but it is apparent that the ozone microbubbles most effectively decreased the TOC.

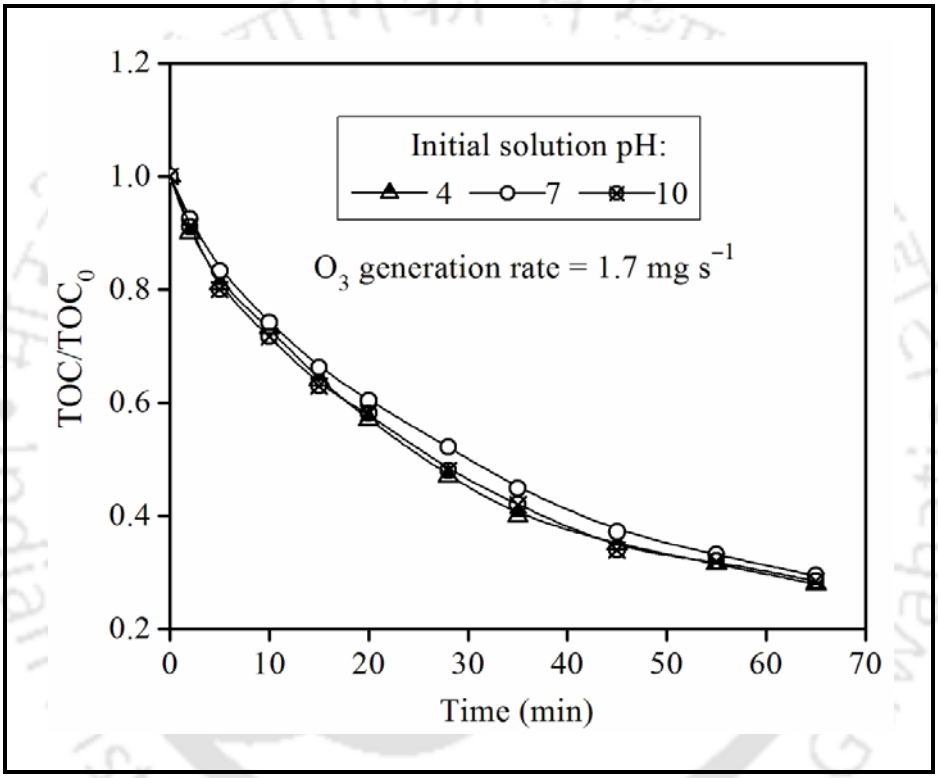

Figure 6.4 TOC profiles of oxidation of BG with ozone.

6.4 ANALYSIS OF INTERMEDIATES USING GC–MS

Total 13 different compounds were identified by GC–MS after 5, 15 and 30 min from the commencement of ozonation (Table 6.1). (3-dimethylamino-phenyl)-phenyl-methanone (a), 4-dimethylamino-phenol (b), (3-dimethylamino-phenyl)-(4-dimethylamino-phenyl)-methanone (c), and phenol (d) were detected in the sample collected after 5 min. Out of these four compounds, only phenol remained at 30 min, which reflects its stability against ozone.

Some of the intermediates such as 4-dimethylamino-benzoic acid (e) and Dimethyl-phenyl-amine (f) were not present at 5 min, but they were detected at 15 min. At 30 min, compounds such as (f), (3-amino-phenyl)-phenyl-methanone (g), 4-amino-phenol (h), 4-amino-benzoic acid (i), aniline (j), oxalic acid (k), acetic acid (l), and acetamide (m) were detected, which were not present at 5 and 15 min.

The GC–MS chromatograms of the intermediates at different time are given in Figure 6A.2. The mass spectra of the identified compounds obtained from the NIST library are shown in Figure 6A.3. On the basis of these intermediates identified from GC–MS, the degradation of BG is likely to occur by three steps. The first step is the cleavage of the conjugated structure of the dye, which happens at the central carbon atom present in the dye molecule (Figure 6.5). Subsequently, four primary intermediates may form, by two pathways. It is reported (Chen et al., 2002; Oturan et al., 2008) that the oxidation of BG initiates by the hydroxylation of the central carbon atom which quickly forms the compound (p1) as shown in Figure 6.5 (Table 6.2). This compound (i.e. p1) is the colorless carbinol base of BG, which was not identified in the current study. The formation of this compound has been reported in the photo-Fenton oxidation of BG (Chen et al., 2002) and photo-catalytic oxidation of crystal violet (Saquib and Muneer, 2003). This intermediate is shown in Figure 6.5 to give more insight into the degradation mechanism. After the formation of (p1), the central carbon atom further reacts with ozone, which leads to the formation of (a), (b'), (c) and (d) through two possible pathways (Figure 6.5). The ion (b') (i.e. dimethyl-phenyl amine ion), is an unstable intermediate. It was not detected as given in Table 6.2. However, in the next step, it forms a stable compound (b), which was detected. Pathway 1 depicts the formation of (a) and (b'), whereas the formation of (c) and (d) occurs by Pathway 2.

Table 6.1 Compounds identified from GC–MS analysis.

Compound No.	Name of the Intermediate	MW (g mol^{-1})	MF	Time (min)		
				5	15	30
a	(3-dimethylamino-phenyl)-phenyl-methanone	225	$C_{15}H_{15}NO$	✓	✓	×
b	4-dimethylamino-phenol	137	$C_8H_{11}NO$	✓	×	×
c	(3-dimethylamino-phenyl)-(4-dimethylamino-phenyl)-methanone	268	$C_{17}H_{20}N_2$	✓	✓	×
d	Phenol	94	C_6H_6O	✓	✓	✓
e	4-dimethylamino-benzoic acid	165	$C_9H_{11}NO_2$	×	✓	×
f	Dimethyl-phenyl-amine	121	$C_8H_{11}N$	×	✓	✓
g	(3-amino-phenyl)-phenyl-methanone	197	$C_{13}H_{11}NO$	×	×	✓
h	4-amino-phenol	109	C_6H_7NO	×	×	✓
i	3-amino-benzoic acid/4-amino-benzoic acid	137	$C_7H_7NO_2$	×	×	✓
j	Aniline	93	C_6H_7N	×	×	✓
k	Oxalic acid	90	$C_2H_2O_4$	×	×	✓
l	Acetic acid	60	$C_2H_4O_2$	×	×	✓
m	Acetamide	59	C_2H_5NO	×	×	✓

Table 6.2 Unidentified compounds included in the BG degradation mechanism.

Compound No.	Name of Compound	MW (g mol^{-1})	MF
a1	{3-(hydroxymethyl-methyl-amino)-phenyl}-phenyl-methanone	241	$C_{15}H_{15}NO_2$
a2	(3-methylamino-phenyl)-phenyl-methanone	211	$C_{14}H_{13}NO$
a3	3-{(hydroxymethyl-amino)-phenyl}-phenyl-methanone	227	$C_{14}H_{13}NO_2$
b'	Dimethyl-phenyl amine ion	120	$C_8H_{10}N^+$
b1	4-(hydroxymethyl-methyl-amino)-phenol	153	$C_8H_{11}NO_2$
b2	4-methyl-aminophenol	123	C_7H_9NO
b3	4-(hydroxymethyl-amino)-phenol	139	$C_7H_9NO_2$
e1	4-(hydroxymethyl-methyl-amino)-benzoic acid	181	$C_9H_{11}NO_3$
e2	4-methyl-aminobenzoic acid	151	$C_8H_9NO_2$
e3	4-(hydroxymethyl-amino)-benzoic acid	167	$C_8H_9NO_3$
f1	(Methyl-phenyl-amino)-methanol	137	$C_8H_{11}NO$
f2	Methyl-phenyl-amine	107	C_7H_9N
f3	Phenylamino-methanol	123	C_7H_9NO
p1	(3-dimethylamino-phenyl)-(4-dimethylamino-phenyl)-phenyl-methanol	346	$C_{23}H_{26}N_2O$

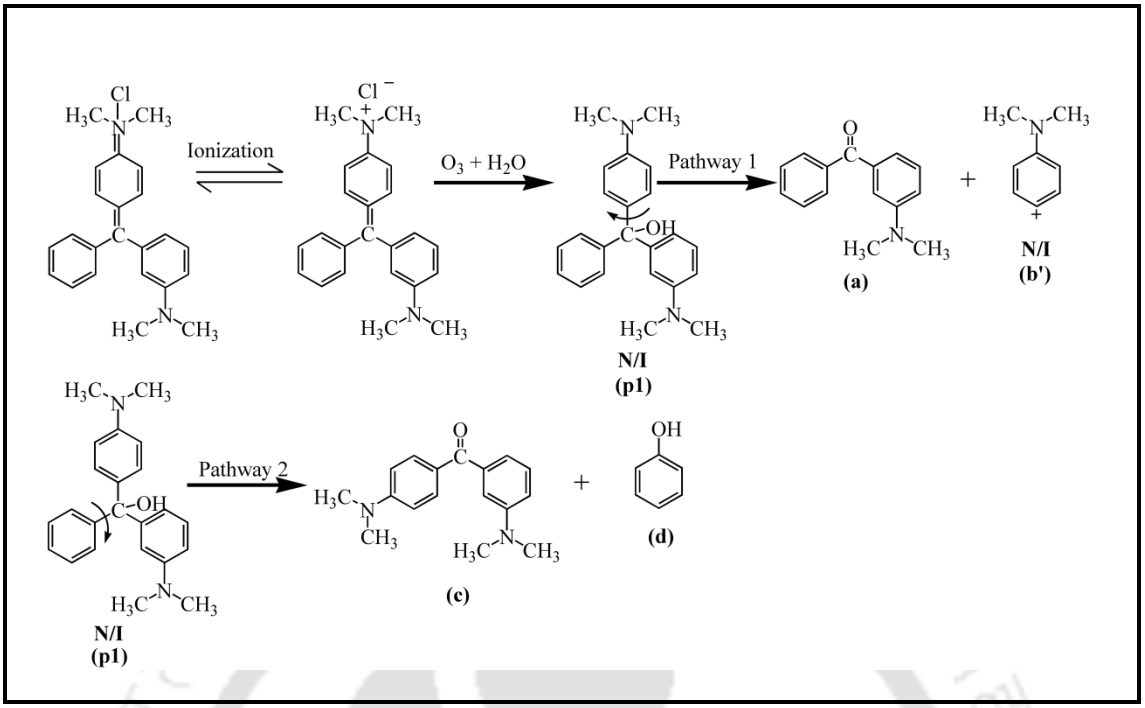

Figure 6.5 Formation of intermediates during ozonation of BG (N/I: not identified).

The formation of (a) from the degradation of BG was also reported by Oturan et al. (2008), Chen et al. (2002), Matsui et al. (1984) and Singh et al. (2013), which means that this is a major primary intermediate in most of the degradation processes. However, in these works, some more intermediates were formed before the formation of (a). For example, Singh et al. (2013) have reported that BG undergoes N-demethylation before the cleavage of the double bond at the central carbon atom. In the present work, however the intermediates found at 5 min are compounds with methyl groups. Therefore, demethylation of the BG molecule was not involved in this reaction pathway. Except (d), the compounds (a) and (c) further react with O_3 due to the presence of the amino functional groups to form some stable and unstable intermediates.

In the second step, the primary intermediates go through multiple N-demethylation steps (Figure 6.6). The compound (a) forms (g) thorough three N-demethylation steps by forming (a1), (a2), and (a3) successively (given in Table 6.2). The intermediates (a1), (a2),

and (a3) were not detected because these compounds are very unstable and readily react with ozone in water to form the more stable compound (g). The compound (b') forms (b), which is a more stable product. The N-demethylation of (b) leads to the formation of (h) via (b1), (b2), and (b3).

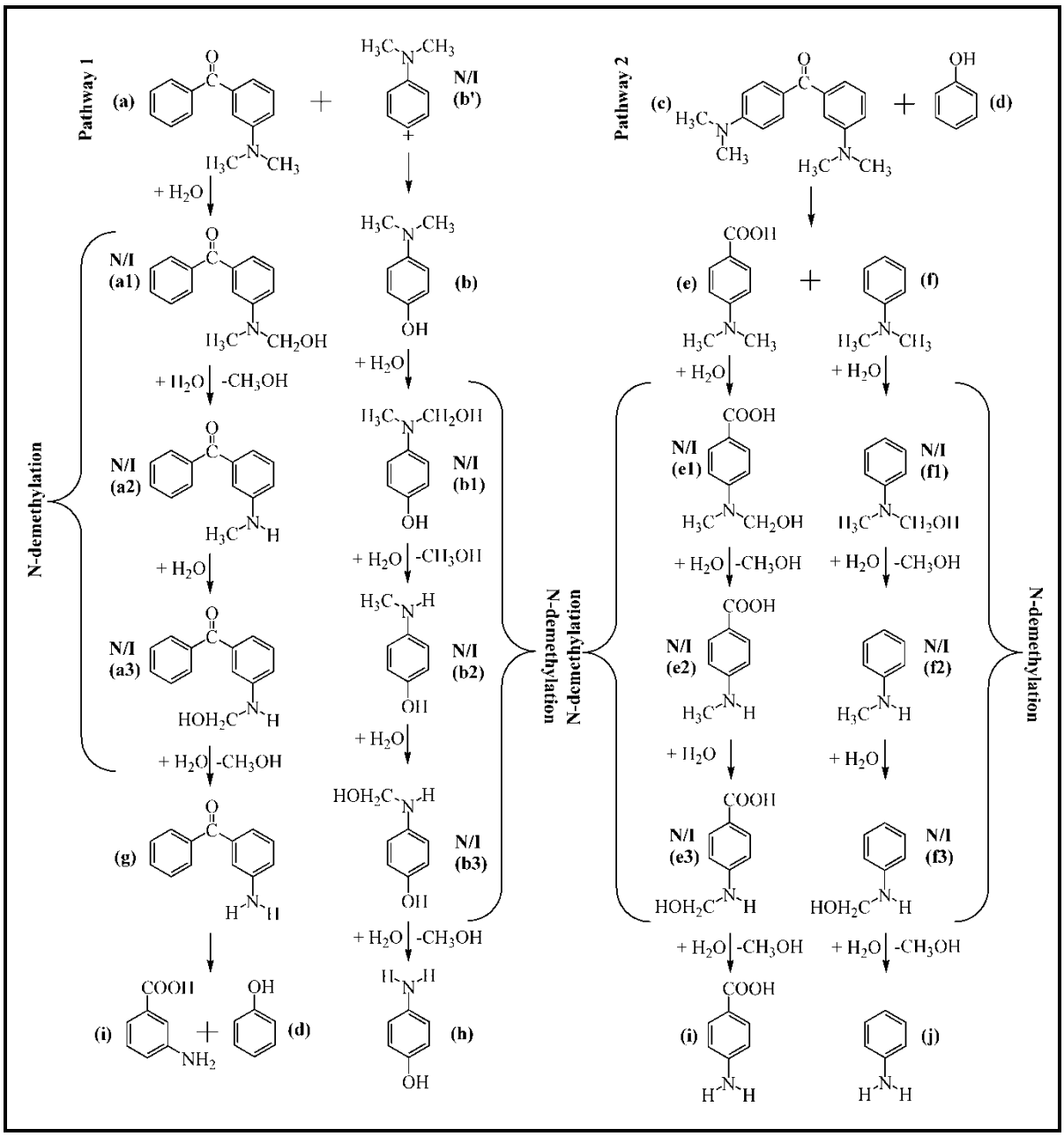

Figure 6.6 N-demethylation of unstable intermediates.

The primary intermediates found in Pathway 2 also go through various N-demethylation steps. But unlike Pathway 1, at 15 min, compound (e) was identified, which disappeared at 30 min. Therefore, these two compounds might have formed from the decomposition of (c). Subsequently, (e) and (f) form (i) and (j), respectively, each through three successive N-demethylation steps. The demethylation products of (e) are (e1), (e2), and (e3). The demethylation products of (f) are (f1), (f2) and (f3). The N-demethylation process continues until the formation of the complete demethylated products.

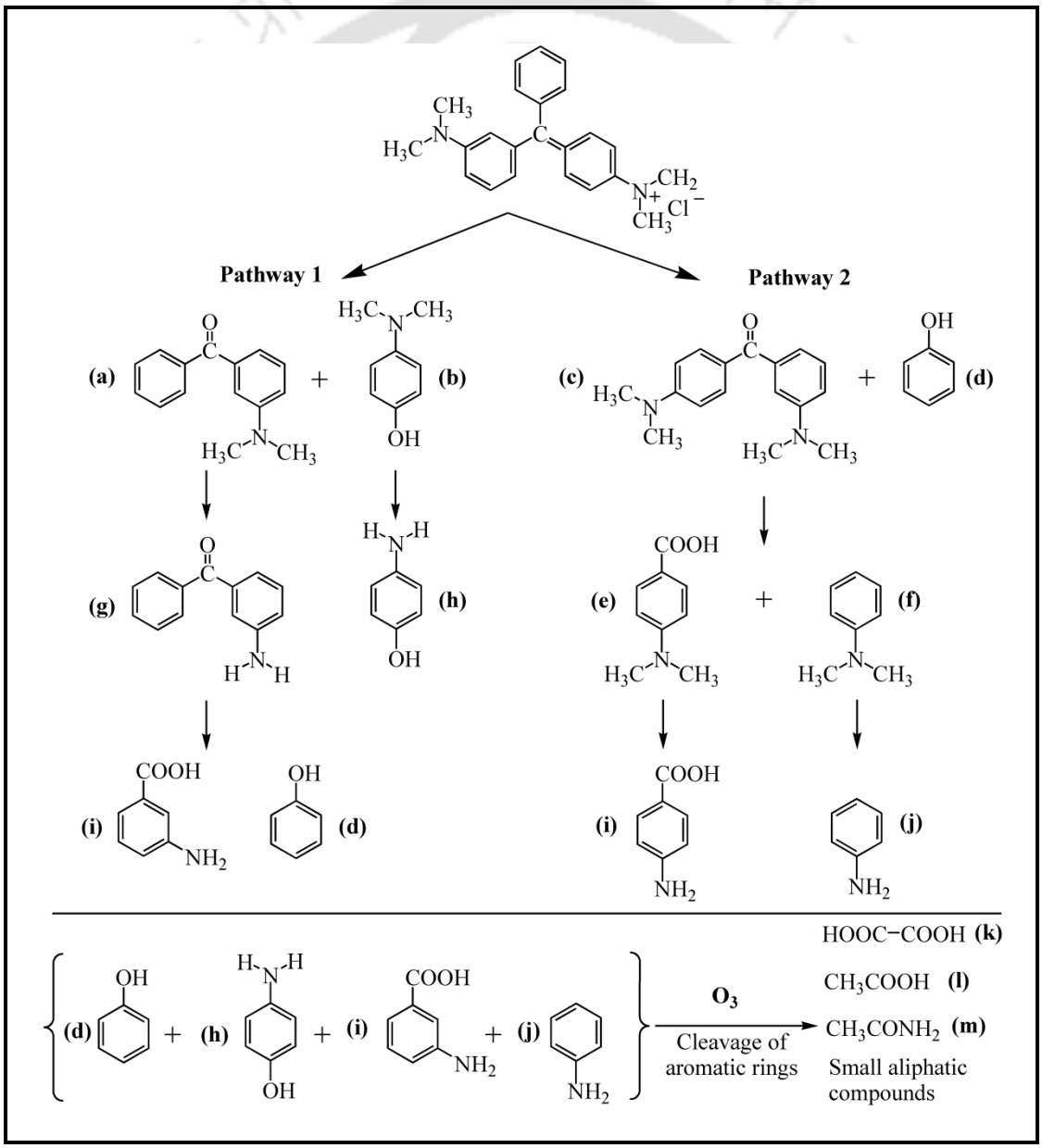

Figure 6.7 Overall degradation pathway of BG.

At 30 min, the compounds (g) and (h) were detected, which are the demethylated forms of (a) and (b), respectively. It demonstrates that the compounds having methyl groups go through demethylation in presence of ozone and water. The intermediate compounds generated during the N-demethylation processes were not identified. However, the possible demethylation reactions are shown to give a complete degradation mechanism. The compounds (d) and (g)–(j) are further oxidized by O_3 to form (k), (l) and (m) (Figure 6.7). In the final step, all or some of the intermediates oxidized to form CO_2 and H_2O. The complete pathway is described in Figure 6.7 with the identified intermediates.

6.5 FTIR ANALYSIS

Figure 6.8 shows the FTIR spectra of BG before and after oxidation. The spectra at t = 0 and t = 5 min are similar because the amount of the intermediates was too small at t = 5 min [Figure 6.8 (a)]. At t = 5 min, the peak at 3551 cm^{-1} became larger as well as sharper than that at t = 0 min. This is due to the C−H stretching of ketones [i.e. intermediates (a) and (c)], and O−H stretching of phenols [i.e. intermediates (b) and (d)]. A small and wide peak appears at 2360 cm^{-1} at both t = 0 and t = 5 min, which represents the C−H stretching of the tertiary amines. Besides the C−H stretching above 3000 cm^{-1}, two other regions of the spectra at 2000−1665 and 900−675 cm^{-1} confirm the presence of the aromatic ring in the compound (Patnaik, 2004). The peaks at 1730 and 1645 cm^{-1} are due to the weak aromatic bands, which are termed “overtones”. This could also appear due to the C = O stretching of ketones. The peak at 751 cm^{-1} is termed “out-of-plane” or “OOP” band. The peak at 1270 cm^{-1} is due to C−N stretching of the tertiary amines, which strongly appears at 1280–1180 cm^{-1}.

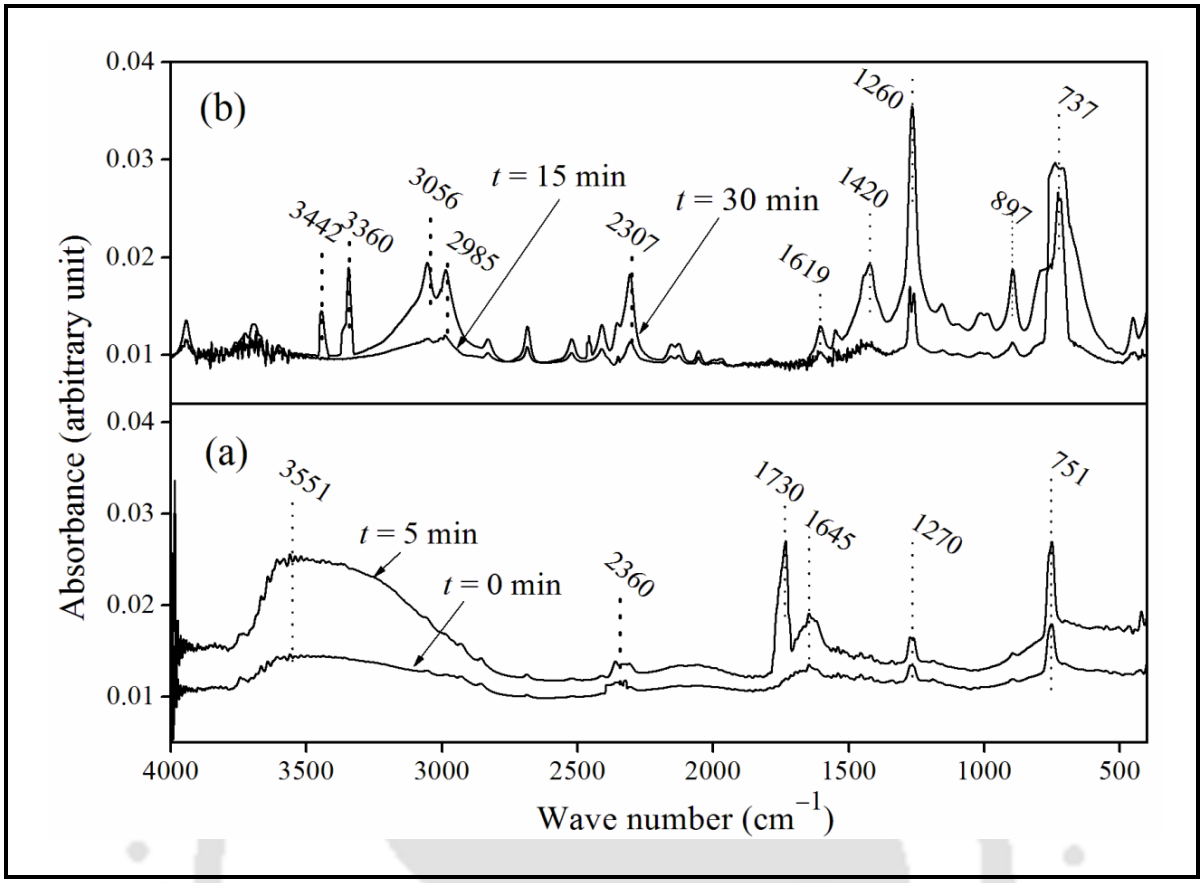

Figure 6.8 FTIR spectra of BG (a) at t = 0 and 5 min, and (b) t = 15 and 30 min.

Figure 6.8 (b) shows the spectra of BG after 15 and 30 minutes of reaction. At t = 15 min, although the spectra appear different from Figure 6.8 (a), but the peaks are small. At t = 30 min, many strong and large peaks appeared. The peak that appeared at 1420 cm^{-1} may be due to the C−N bond in intermediate (m), the carboxylic groups present in (k) and (l), or the CH_3 group of the aliphatic compounds formed due to the degradation of the dye. The strong peaks at 3056 and 2985 cm^{-1} are due to the O−H stretching of carboxyl acids [e.g. intermediates (i), (k) and (l)], ketone [i.e. intermediate (g)] and alcohol [i.e. intermediate (h)]. This peak also appeared in small intensity at t = 15 min due to the presence of O−H stretch of (e). Primary amines present in the reaction medium show two peaks for N−H stretching at 3442 and 3360 cm^{-1}. The peak for C−N stretching appears at 1260 cm^{-1} [i.e. intermediate (f)], N−H bending at 1611 cm^{-1} and N−H wag at 737 cm^{-1} [i.e. intermediate (j)]. All these

three peaks show the presence of primary amines in the sample (Pavia et al., 2008). The peak at 897 cm^{-1} is due to the presence of aliphatic compounds. Many small but clear peaks appear at 2000−2800 cm^{-1}. These peaks appeared due to the CO_2 released during the degradation of BG and the intermediates.

The functional groups identified from the FTIR analysis were matched with the compounds identified from GC–MS. The characteristic peaks of the samples collected at t = 0 and t = 5 min were clearly evident. Some of them were not present in the samples collected at t = 15 and t = 30 min. In the sample collected at t = 30 min, many additional strong peaks (such as the peaks at 897, 1420, 1730, 2985, 3360 and 3442 cm^{-1}) appeared, which reflect the presence of small aliphatic compounds and demethylation products that are generated from the oxidation of the dye.

6.6 KINETICS OF OZONATION OF BG

In aqueous medium pre-saturated with ozone, degradation of dye is considered as a pseudo first-order reaction (Saunders et al., 1983; Wu and Wang, 2001). Wu et al. (2008) have reported that the apparent rate constant (which is the product of the intrinsic rate constant and the dissolved ozone concentration) decreases with increasing dye concentration. When the initial dye concentration increases, generation of more intermediates consumes more dissolved ozone. As a result, the apparent rate constant decreases. However, in a semi-batch reactor, ozone gradually dissolves in water and simultaneously undergoes self-decomposition and reaction with the dye. Therefore, the reaction of dye with ozone may not follow the pseudo first-order kinetics (Chu and Ma, 2000; Demirev and Nenev, 2005; Langlais et al., 1990; Turhan and Turgut, 2007, 2009). Figure 6.9 represents the variation of concentration of BG with time at different initial BG concentrations. Temperature was maintained at 298 K

and the ozone generation rate was fixed at 1.7 mg s^{-1}. With increasing concentration of BG, ozonation had to be carried out for longer durations to achieve 99.5% oxidation.

When ozone dissolves in water, it undergoes a self-decomposition process, which is first-order in nature. The self-decomposition of ozone depends on pH, temperature and ionic strength (Beltrán, 2004). Ozone decomposition is initiated either thermally (in acidic media) (Sehested et al., 1984) or by the hydroxyl ion, OH^- (in alkaline media). The mass balance equation of ozone self-decomposition without any contamination is given by Eq. (5.16) (Chapter 5, Section 5.1.5) (Sotelo et al., 1987). The diffusivity of ozone in the gas phase is much higher than that in water. Therefore, the resistance to mass transfer in the gas phase is negligible as compared to the aqueous phase. In presence of BG, a part of ozone present in the aqueous phase will be consumed by the dye. The rate equation for the oxidation of BG with ozone is given by

$$\frac{\mathrm{d[BG]}}{\mathrm{d}t} = -k[\mathrm{BG}]^m[\mathrm{O_3}]^n \tag{6.1}$$

Incorporating the ozone decomposition and the rate of mass transfer of ozone, the mass balance equation of ozone becomes

$$\frac{\mathrm{d}\left[\mathrm{O_3}\right]}{\mathrm{d}t} = k_l a\left(\left[\mathrm{O_3}\right]^* - \left[\mathrm{O_3}\right]\right) - k_d\left[\mathrm{O_3}\right] - k\left[\mathrm{BG}\right]^m\left[\mathrm{O_3}\right]^n \tag{6.2}$$

Equations (6.1) and (6.2) were simultaneously solved by the Runge–Kutta method and the best-fit values of $k_l a$, k, m, and n were obtained with respect to the concentration profiles of BG and ozone in the reactor. The values of these parameters are presented in Table 6.3. The fits of the kinetic model to the concentration profiles of BG and ozone are shown in Figures 6.9 (a) and (b), respectively.

The oxidation of BG produces many intermediates, as discussed earlier, which react further with ozone. The individual rate constants for the reactions of these intermediates with ozone are not considered in Eqs. (6.1) and (6.2). From the values of *m* and *n*, it is apparent

that the reaction was first-order with respect to both BG and ozone, and therefore, the overall order of reaction was two. The rate constant was almost same for all the initial concentrations of BG. Therefore, this rate constant was the true rate constant.

Table 6.3 Kinetic and mass transfer parameters of oxidation of BG with ozone (O_3 generation rate = 1.7 mg s^{-1}).

$[BG]_0$ (mmol dm^{-3})	$k_l a$ (s^{-1})	$[O_3]^* \times 10^4$ (mol dm^{-3})	k [mol $dm^{-3})^{1-m-n}$ s^{-1}]	m	n	E
0.0274	0.0028	2.92	48.2	0.99	0.99	1.00
0.0411	0.0033	2.85	48.1	1.02	1.02	1.17
0.0548	0.0040	2.60	48.1	1.03	1.03	1.42
0.1100	0.0051	2.50	48.1	1.03	1.02	1.82
0.1640	0.0058	2.40	48.0	1.05	1.04	2.07

It is likely that this rate constant corresponds to the first step of the reaction (i.e. the formation of (p1), when the dye loses its color). The generation of the intermediates from (p1) is faster than its formation. This could be the reason behind the fact that the rate constant does not depend on the initial concentration of BG. The volumetric mass transfer coefficient, $k_l a$, increased with the initial dye concentration. When ozone is absorbed in water and it simultaneously reacts with the dye, its consumption depends on the concentration of the intermediates present in the medium because these intermediates also react with ozone and decrease the dissolved ozone concentration. This increases the driving force of mass transfer of ozone from the gas phase to the liquid phase (Wu et al., 2008). Therefore, $k_l a$ increased with increasing dye concentration.

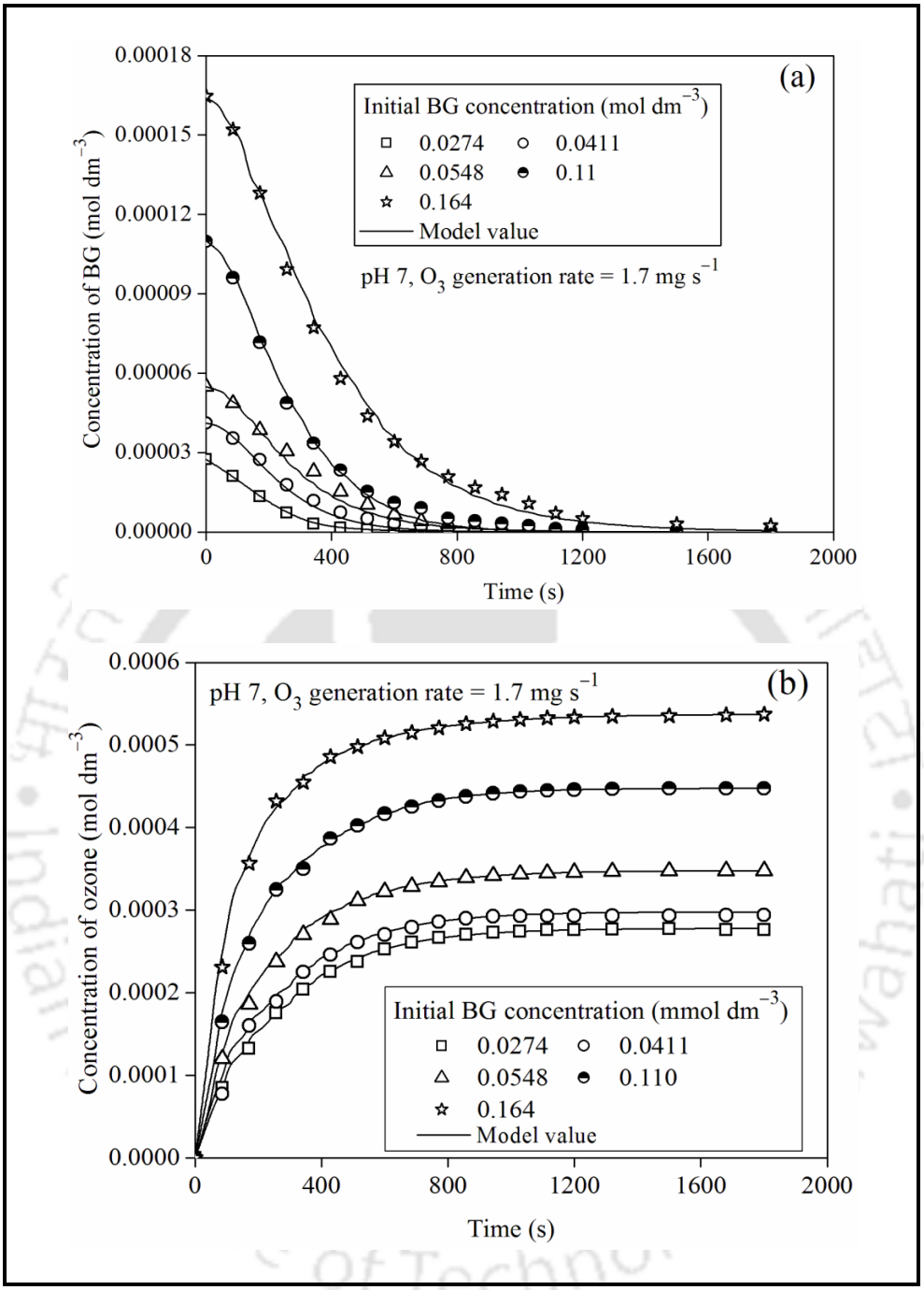

Figure 6.9 Concentration profiles of (a) BG and (b) ozone.

It is observed from Figure 6.9 that the saturation ozone concentration decreased with increasing concentration of BG. It is reported that some organic compounds present in water can inhibit the dissolution of ozone (Rhim, 2004; Staehelin and Hoigné, 1985). The intermediate products such as oxalic acid and acetic acid may trigger a salting-out effect,

thereby decreasing the saturation ozone concentration. The measure of increase in the rate of mass transfer of ozone due to the chemical reactions is expressed in terms of the enhancement factor (E), which is defined as the ratio of the volumetric mass transfer coefficient in the reacting and non-reacting systems, i.e.

$$E = \frac{(k_l a)_{\text{reacting}}}{(k_l a)_{\text{non-reacting}}} \tag{6.3}$$

The volumetric mass transfer coefficient were reported in Chapter 4 (Section 4.6). At pH 7 and ozone generation rate 1.7 mg s^{-1}, the enhancement factor increased linearly with increasing dye concentration, as shown in Figure 6.10.

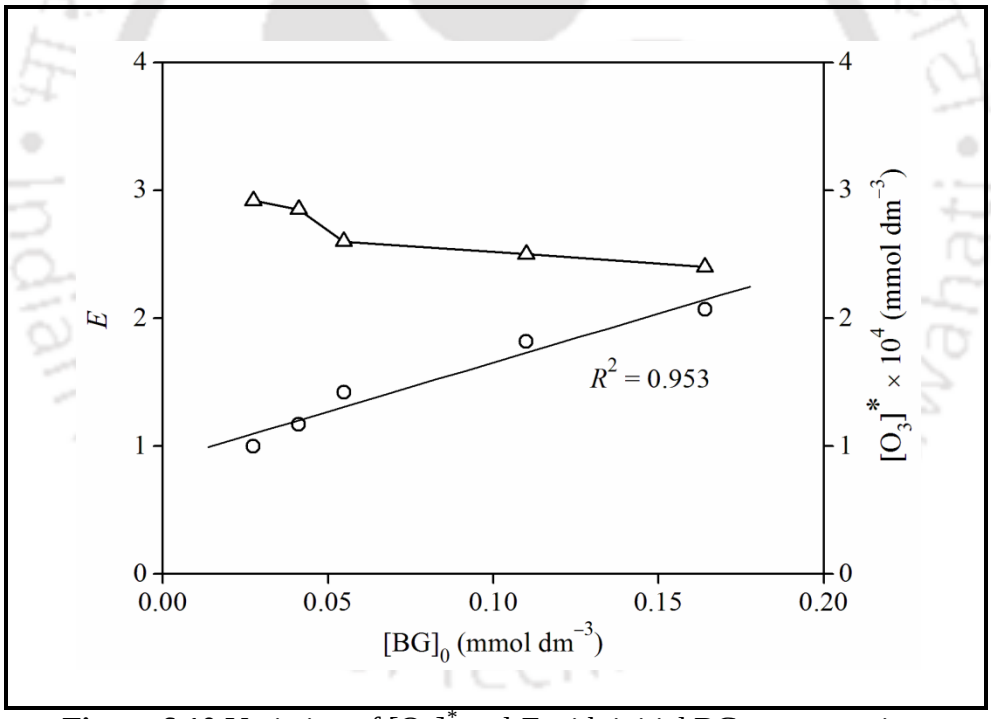

Figure 6.10 Variation of $[O_3]^*$ and E with initial BG concentration.

NOTATIONS

a	specific gas–liquid interfacial area, $m^2\ m^{-3}$
[BG]	concentration of Brilliant Green at time t, mol dm^{-3}
$[BG]_0$	concentration of Brilliant Green at t = 0, mol dm^{-3}
E	enhancement factor, dimensionless
k	rate constant for reaction of ozone with Brilliant Green, $(mol\ dm^{-3})^{1-m-n}\ s^{-1}$
k_d	decomposition rate constant of ozone, s^{-1}
$k_l a$	volumetric mass transfer coefficient, s^{-1}
$(k_l a)_{non\text{-}reacting}$	volumetric mass transfer coefficient of ozone in non-reacting system, s^{-1}
$(k_l a)_{reacting}$	volumetric mass transfer coefficient of ozone in reacting system, s^{-1}
m	order of reaction with respect to Brilliant Green, dimensionless
n	order of reaction with respect to ozone, dimensionless
$[O_3]$	ozone concentration at time t, mol dm^{-3}
$[O_3]^*$	saturated ozone concentration, mol dm^{-3}
R^2	coefficient of determination, dimensionless
t	time, s

Abbreviations

BG	Brilliant Green
FTIR	Fourier transformed infrared
GC–MS	Gas chromatography–mass spectrometry
MF	Molecular formula
MW	Molecular weight, g mol^{-1}
N/I	not identified

NIST	National Institute of Standards and Technology
TOC	Total organic carbon

REFERENCES

Behnajady, M.A., Modirshahla, N., Shokri, M., Vahid, B., 2008. Effect of operational parameters on degradation of Malachite Green by ultrasonic irradiation. Ultrason. Sonochem. 15, 1009−1014.

Beltrán, F.J., 2004. Ozone Reaction Kinetics for Water and Wastewater System. CRC Press, Boca Raton, Florida, USA.

Chen, F., He, J., Zhao, J., Yu, J.C., 2002. Photo-Fenton degradation of Malachite Green catalyzed by aromatic compounds under visible light irradiation. New J. Chem. 26, 336−341.

Chu, W., Ma, C.W., 2000. Quantitative prediction of direct and indirect dye ozonation kinetics. Water Res. 34, 3153−3160.

Demirev, A., Nenev, V., 2005. Ozonation of two acidic azo dyes with different substituents. Ozone Sci. Eng. 27, 475−485.

Konsowa, A.H., 2003. Decolorization of wastewater containing direct dye by ozonation in a batch bubble column reactor. Desalination 158, 233−240.

Langlais, B., Reckhow, D.A., Brink, D.R., 1990. Ozone in Water Treatment: Application and Engineering. Lewis Publishers, Boca Raton, Florida, USA.

Li, P., Takahashi, M., Chiba, K., 2009. Enhanced free-radical generation by shrinking microbubbles using a copper catalyst. Chemosphere 77, 1157−1160.

Matsui, M., Nakabayashi, H., Shibata, K., Takase, Y., 1984. Ozonization of triphenylmethane dyes. Bull. Chem. Soc. Jpn. 57, 3312−3316.

Mitrowska, K., Posyniak, A., Zmudzki, J., 2008. Determination of malachite green and leucomalachite green residues in water using liquid chromatography with visible and fluorescence detection and confirmation by tandem mass spectrometry. J. Chromatogr. A 1207, 94−100.

Oturan, M.A., Guivarch, E., Oturan, N., Sirés, I., 2008. Oxidation pathways of malachite green by Fe_3^+-catalyzed electro-Fenton process. Appl. Catal. B 82, 244−254.

Patnaik, P., 2004. Dean's Analytical Chemistry Handbook. McGraw-Hill, New York, USA.

Pavia, D.L., Lampman, G.M., Kriz, G.S., Vyvyan, J.R., 2008. Introduction to Spectroscopy. Thomson Brooks/Cole, Belmont, USA.

Rajeswari, K.R., 2000. Ozonation treatment of textile dyes wastewater using plasma ozonizer. Ph.D. Thesis, University of Malaysia, Malaysia.

Rajkumar, D., Song, B.J., Kim, J.G., 2007. Electrochemical degradation of Reactive Blue 19 in chloride medium for the treatment of textile dyeing wastewater with identification of intermediate compounds. Dyes Pigments 72, 1−7.

Rhim, J.A., 2004. Equilibrium concentration and overall Henry's law constant of the dissolved ozone. Environ. Eng. Res. 9, 88−95.

Saquib, M., Muneer, M., 2003. TiO_2-mediated photocatalytic degradation of a triphenylmethane dye (Gentian Violet) in aqueous suspensions. Dyes Pigments 56, 37−49.

Saunders, F.M., Gould, J.P., Southerl, C.R., 1983. The effect of solute competition on ozonolysis of industrial dyes. Water Res. 17, 1407−1419.

Sehested, K., Holcman, J., Bjergbakke, E., Hart, E.J., 1984. A pulse radiolytic study of the reaction OH + O_3 in aqueous medium. J. Phys. Chem. 88, 4144−4147.

Shu, H.Y., Chang, M.C., 2005. Decolorization effects of six azo dyes by O_3, UV/O_3 and UV/H_2O_2 processes. Dyes Pigments 65, 25−31.

Singh, S., Srivastava, V.C., Mall, I.D., 2013. Mechanism of dye degradation during electrochemical treatment. J. Phys. Chem. C 117, 15229−15240.

Sotelo, J.L., Beltrán, F.J., Benitez, F.J., Beltrán-Heredia, J., 1987. Ozone decomposition in water: kinetic study. Ind. Eng. Chem. Res. 26, 39−43.

Staehelin, J., Hoigné, J., 1985. Decomposition of ozone in water in the presence of organic solutes acting as promoters and inhibitors of radical chain reactions. Environ. Sci. Technol. 19, 1206−1213.

Turhan, K., Turgut, Z., 2007. Reducing chemical oxygen demand and decolorization of direct dye from synthetic wastewater by ozonation in a batch bubble column. Fresenius Environ. Bull. 16, 821−825.

Turhan, K., Turgut, Z., 2009. Decolorization of direct dye in textile wastewater by ozonization in a semi-batch bubble column reactor. Desalination 242, 256−263.

Wu, J., Doan, H., Upreti, S., 2008. Decolorization of aqueous textile reactive dye by ozone. Chem. Eng. J. 142, 156−160.

Wu, J., Wang, T., 2001. Ozonation of aqueous azo dye in a semi-batch reactor. Water Res. 35, 1093−1099.

APPENDIX 6A

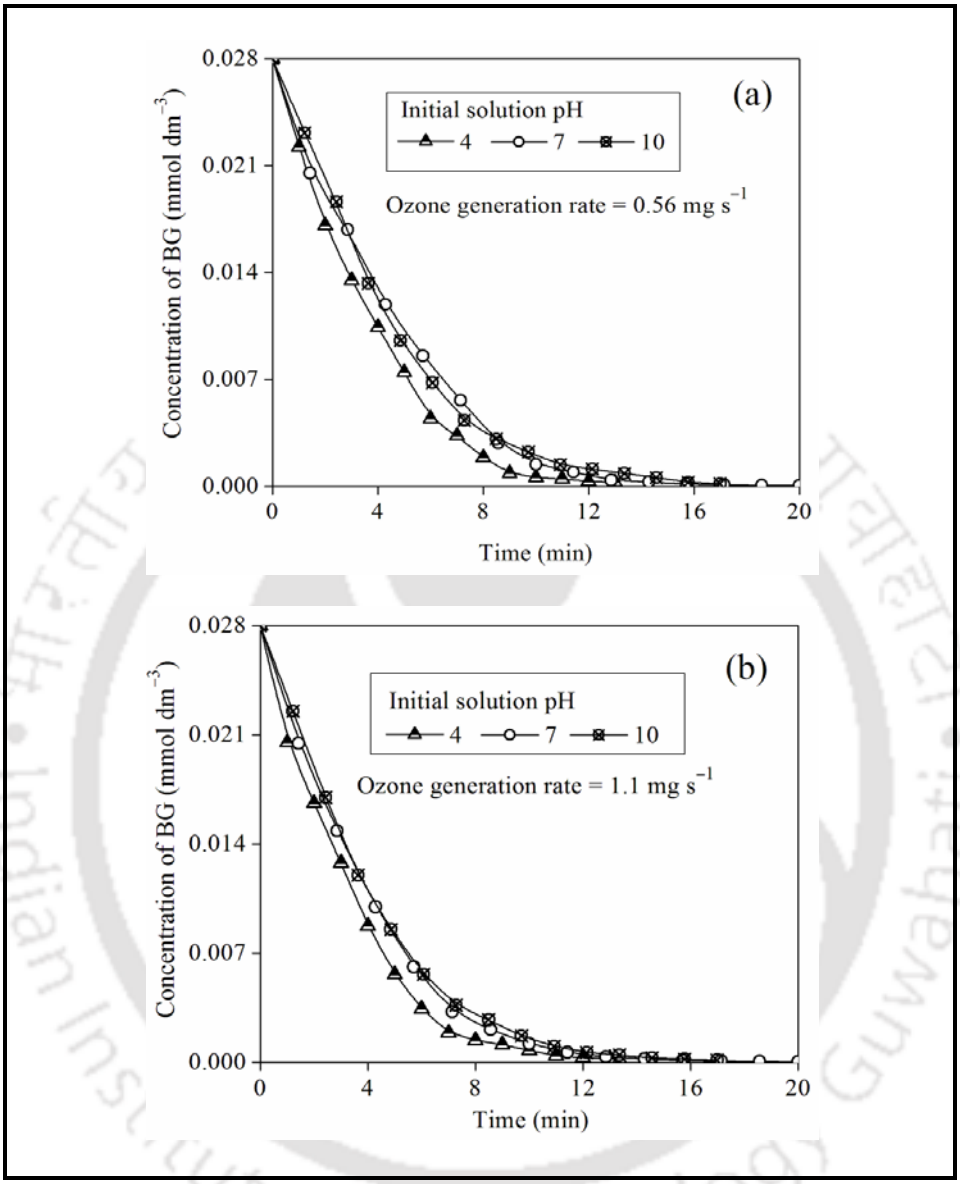

Figure 6A.1 Effect of pH on oxidation of BG at ozone generation rate (a) 0.56 mg s^{-1} and (b) 1.1 mg s^{-1}.

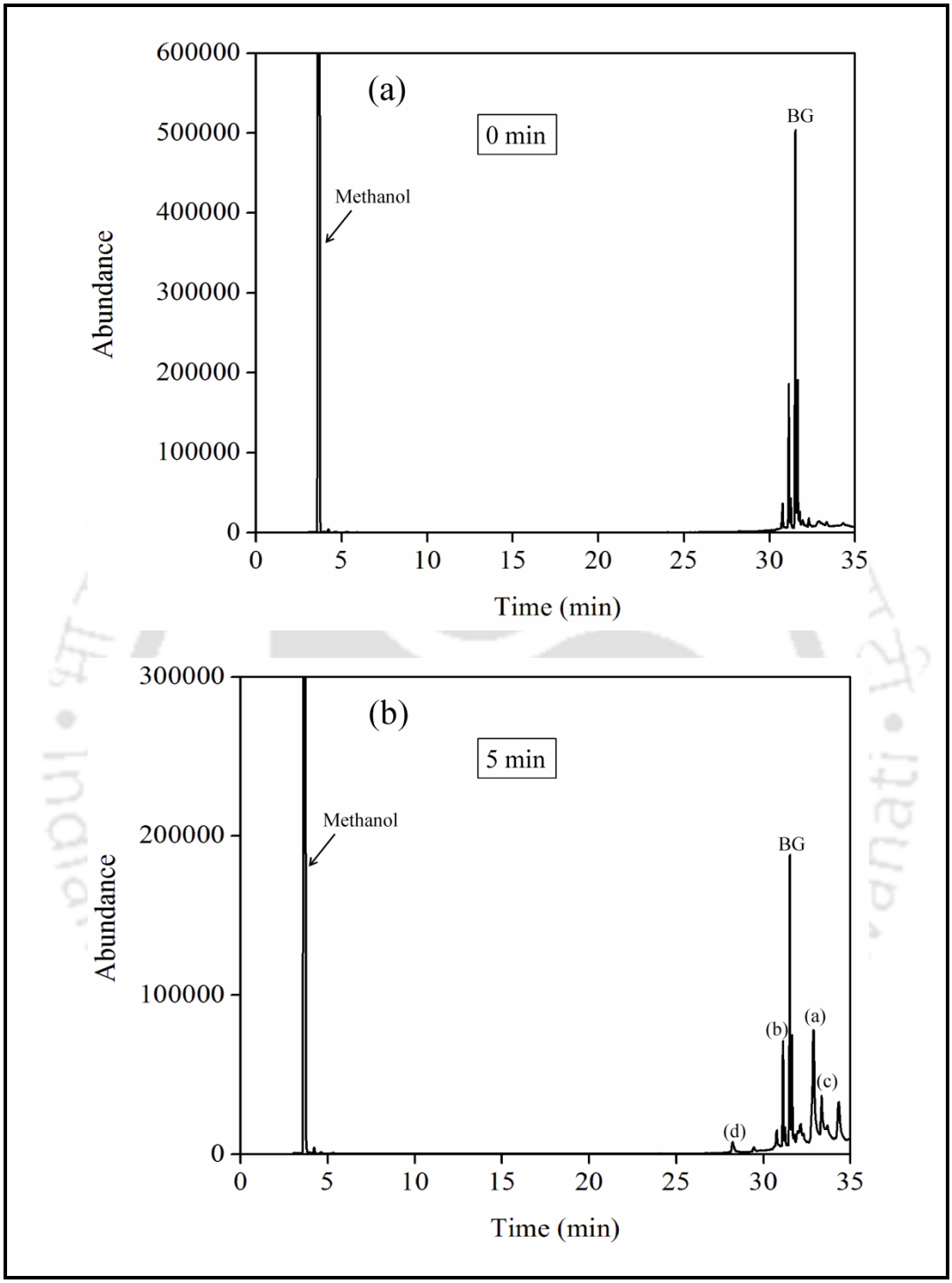

Figure 6A.2 GC–MS chromatograms of the intermediates at (a) 0 min, (b) 5 min, (c) 15 min, and (d) 30 min reaction time (Continued…).

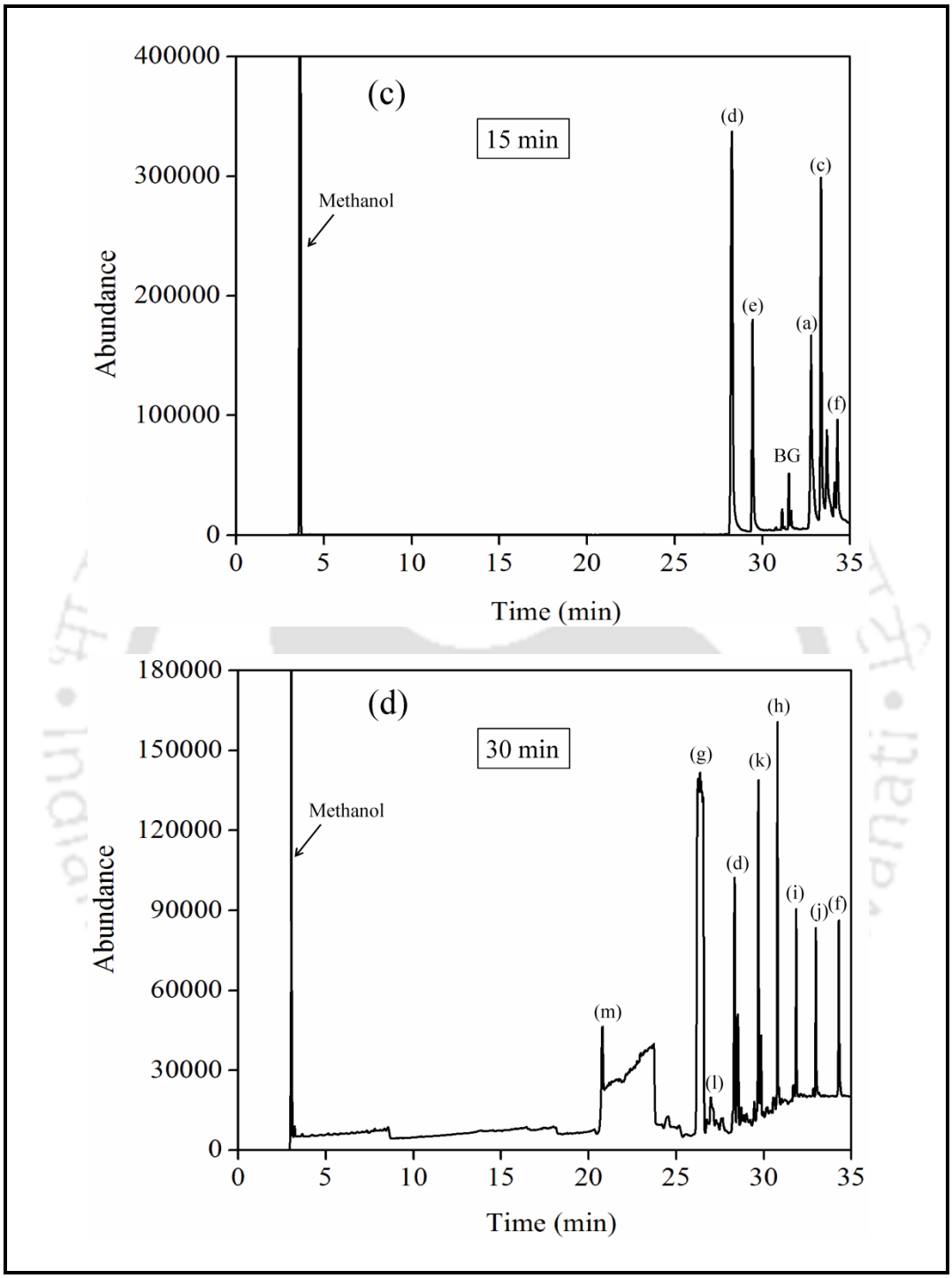

Figure 6A.2 GC–MS chromatograms of the intermediates at (a) 0 min, (b) 5 min, (c) 15 min, and (d) 30 min reaction time.

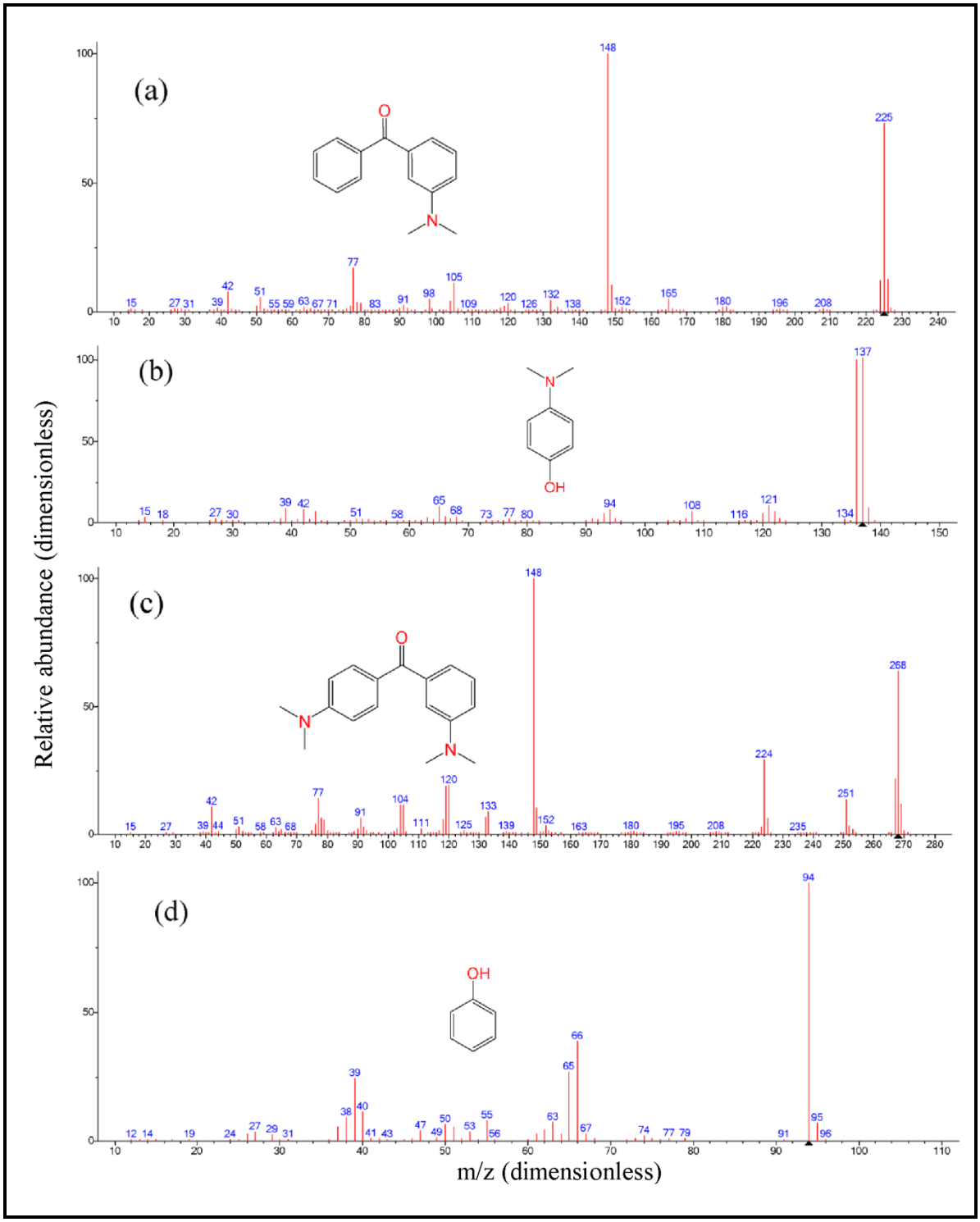

Figure 6A.3 The mass spectra of the identified compounds obtained from the NIST library (the figure number is same as the compound number) (Continued…).

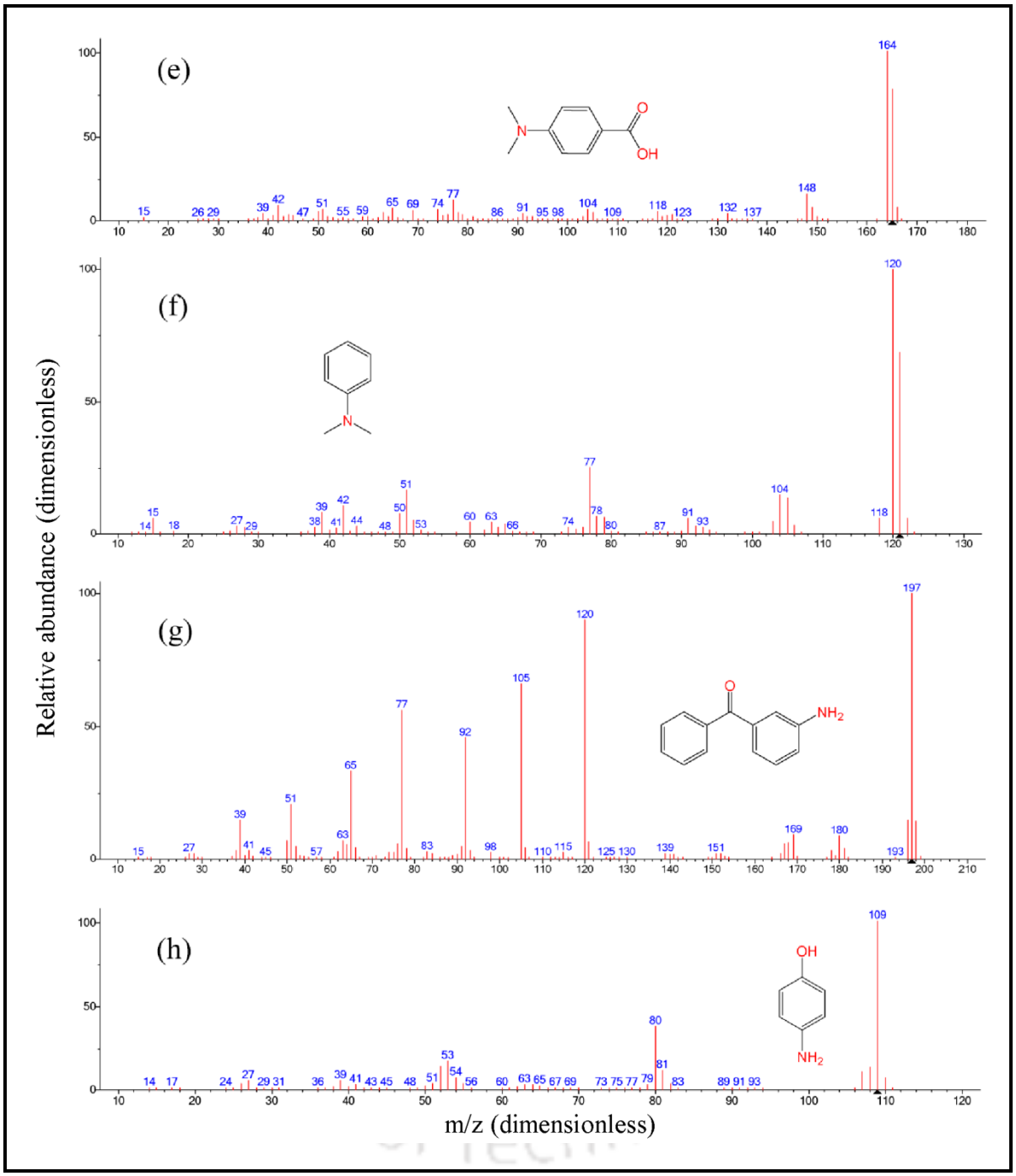

Figure 6A.3 The mass spectra of the identified compounds obtained from the NIST library (the figure number is same as the compound number) (Continued…).

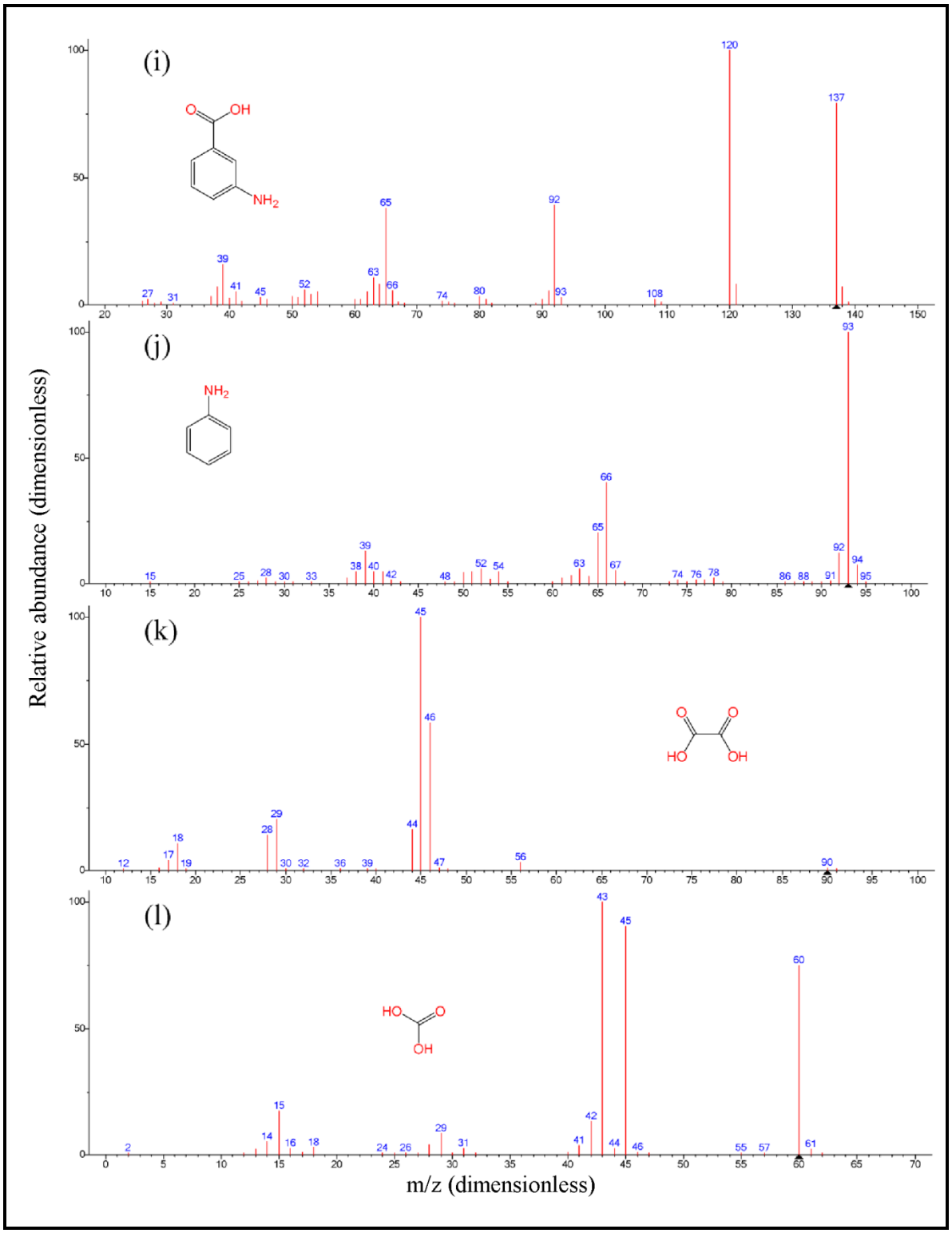

Figure 6A.3 The mass spectra of the identified compounds obtained from the NIST library (the figure number is same as the compound number) (Continued…).

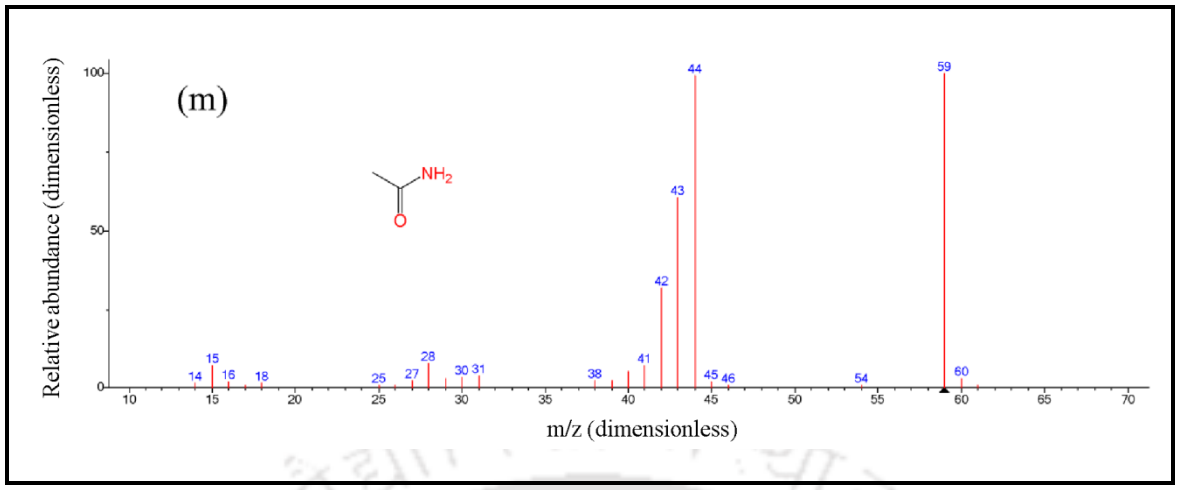

Figure 6A.3 The mass spectra of the identified compounds obtained from the NIST library (the figure number is same as the compound number).

CHAPTER 7

MEASUREMENT OF HYDROXYL RADICAL CONCENTRATION

CHAPTER 7
MEASUREMENT OF HYDROXYL RADICAL CONCENTRATION

This chapter presents the measurement of concentration of hydroxyl radicals generated from ozone microbubbles in the pH range 3−10. The effects of pH and carbonate ions on the generation of hydroxyl radicals have been studied. Degradation of phenol using molecular ozone and hydroxyl radicals was investigated at pH 3−10. The contribution of hydroxyl radicals on the degradation of phenol has been determined. The possible mechanism of the generation of hydroxyl radicals from ozone microbubbles under acidic and alkaline conditions has been explained.

7.1 THEORY

7.1.1 Decomposition of O_3 in Alkaline and Acidic Media

Several studies have described the mechanism of ozone decomposition in water (Gardoni et al., 2012). The mechanism depends on the pH of the medium. According to the model proposed by Tomiyasu et al. (1985) the decomposition reaction of ozone in alkaline medium proceeds as follows.

$$O_3 + OH^- \rightarrow HO_2^- + O_2 \qquad k_2 = 40\ dm^3\ mol^{-1}\ s^{-1} \qquad (7.1)$$

$$O_3 + HO_2^- \rightarrow \cdot O_3^- + HO_2\cdot \qquad k_2 = 2.2 \times 10^6\ dm^3\ mol^{-1}\ s^{-1} \qquad (7.2)$$

$$HO_2\cdot + OH^- \rightleftarrows \cdot O_2^- + H_2O \qquad pK = 4.8 \qquad (7.3)$$

$$\cdot O_2^- + O_3 \rightarrow \cdot O_3^- + O_2 \qquad k_2 = 1.6 \times 10^9\ dm^3\ mol^{-1}\ s^{-1} \qquad (7.4)$$

$$\cdot O_3^- + H_2O \rightarrow \cdot OH + O_2 + OH^- \qquad k_1 = 20{-}30\ s^{-1} \qquad (7.5)$$

$$\cdot O_3^- + \cdot OH \rightarrow \cdot O_2^- + HO_2 \cdot \qquad k_2 = 6 \times 10^9 \text{ dm}^3 \text{ mol}^{-1} \text{ s}^{-1} \qquad (7.6)$$

$$\cdot O_3^- + \cdot OH \rightarrow O_3 + OH^- \qquad k_2 = 2.5 \times 10^9 \text{ dm}^3 \text{ mol}^{-1} \text{ s}^{-1} \qquad (7.7)$$

$$\cdot OH + O_3 \rightarrow HO_2 \cdot + O_2 \qquad k_2 = 3 \times 10^9 \text{ dm}^3 \text{ mol}^{-1} \text{ s}^{-1} \qquad (7.8)$$

At alkaline pH, $\cdot OH$ is generated at only one step, given by Eq. (7.5). Higher concentration of OH^- augments the generation of HO_2^-, $\cdot O_2^-$, $\cdot O_3^-$ and $\cdot OH$ (Tomiyasu et al., 1985). At pH between 7 and 9, the generation of $\cdot OH$ is slow inasmuch as the rate constant of the reaction given by Eq. (7.5) is 20−30 s^{-1}. But the propagation and termination reactions [i.e. those given by Eqs. (7.6)−(7.8)] are very fast. This leads to a lower concentration of ·OH. Staehelin et al. (1984) have proposed a different set of chain reactions. They found the first-order rate constant for the generation of $\cdot OH$ to be 1.1×10^5 s^{-1}.

In acidic medium, however, a different mechanism is involved. Sehested et al. (1984, 1991) proposed the following mechanism of generation of hydroxyl radical from ozone in acidic medium. It involves thermal dissociation of ozone to form an oxygen atom, followed by the reaction of this atom with water to form hydroxyl radical.

$$O_3 \Leftrightarrow O + O_2 \qquad (7.9)$$

$$O + H_2O \rightarrow 2HO \cdot \qquad (7.10)$$

In acidic solution, the hydroxyl radical reacts with ozone to form the perhydroxyl radical, $HO_2\cdot$. A sequence of reactions follows as shown below.

$$\cdot OH + O_3 \rightarrow HO_2 \cdot + O_2 \qquad k_2 = 1.1 \times 10^8 \text{ dm}^3 \text{ mol}^{-1} \text{ s}^{-1} \qquad (7.11)$$

$$HO_2 \cdot + O_3 \rightarrow \cdot OH + 2O_2 \qquad k_2 < 10^4 \text{ dm}^3 \text{ mol}^{-1} \text{ s}^{-1} \qquad (7.12)$$

$$HO_2 \cdot \rightleftarrows \cdot O_2^- + H^+ \qquad pK = 4.8 \qquad (7.13)$$

At pH ≥ 1, the perhydroxyl radical reacts with ozone preferentially in its dissociated form (i.e. $\cdot O_2^-$) to form the ozonide radical ion, $\cdot O_3^-$, as shown by the reaction given in Eq. (7.4)

(Sehested et al., 1984). $\cdot O_3^-$ further reacts with H^+ to form $\cdot OH$, which can combine with $HO_2\cdot$

$$\cdot O_3^- + H^+ \rightarrow \cdot OH + O_2 \qquad k_2 = 9 \times 10^{10}\ dm^3\ mol^{-1}\ s^{-1} \qquad (7.14)$$

$$\cdot OH + HO_2\cdot \rightarrow H_2O + O_2 \qquad k_2 = 0.7 \times 10^{10}\ dm^3\ mol^{-1}\ s^{-1} \qquad (7.15)$$

In acidic conditions, $\cdot OH$ is generated by Eq. (7.10). In addition, $\cdot OH$ may be generated by the propagation reactions given by Eqs. (7.12) and (7.14). The reactivity of O_3 with $HO_2\cdot$ [i.e. Eq. (7.12)] is less than that with $\cdot O_2^-$ [i.e. Eq. (7.4)]. The reaction given by Eq. (7.4) is common to both alkaline and acidic conditions. $\cdot O_2^-$ reacts with O_3 and generates $\cdot O_3^-$ as per Eq. (7.4), which subsequently generates $\cdot OH$ by Eq. (7.14). It is evident from Eqs. (7.9)−(7.15) that the number of hydroxyl radicals produced from ozone is more in the acidic medium. In addition, a less number of hydroxyl radicals is consumed in the propagation and termination reactions in the acidic medium. Therefore, at acidic condition, the generation of $\cdot OH$ is more. However, the slowness of the reaction of $HO_2\cdot$ with ozone leads to a higher stability of ozone in the acidic medium.

7.1.2 Determination of ·OH Concentration

Direct determination of the concentration of hydroxyl radicals is rather difficult because they have a short life time (of the order of nanoseconds), and they react at the site of their formation (Dreosti, 1991; Roots and Okada, 2014). Therefore, an indirect method was proposed by Elovitz and von Gunten (1999) to measure the concentration of hydroxyl radicals. In this method, a probe compound (e.g. PCBA) is used, which readily reacts with $\cdot OH$, but remains almost indifferent towards O_3. To illustrate, the rate constants of the reaction of PCBA with $\cdot OH$ and O_3 are 5×10^9 and 0.15 $dm^3\ mol^{-1}\ s^{-1}$, respectively. When

the probe compound and the scavenger are both present in water, the consumption of ·OH will be due to both of them, as shown in Figure 7.1.

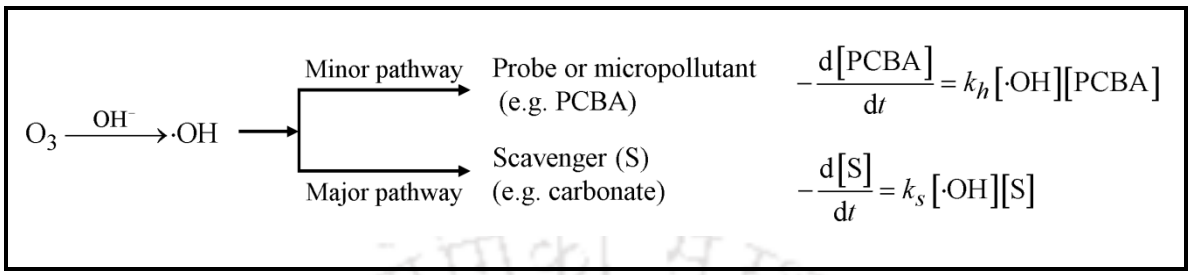

Figure 7.1 Mechanism of reaction of probe and scavenger with ·OH.

When PCBA is present at very low concentrations, the contribution of the probe on ·OH scavenging is negligible, and therefore, $k_h[\text{PCBA}] << k_s[S]$. As PCBA has much lower reactivity with O_3 as compared to ·OH, the rate equation for PCBA can be written as (Elovitz and von Gunten, 1999)

$$-\frac{d[\text{PCBA}]}{dt} = k_h[\cdot\text{OH}][\text{PCBA}] \tag{7.16}$$

Rearranging and integrating Eq. (7.16), we get

$$\ln\left(\frac{[\text{PCBA}]}{[\text{PCBA}]_0}\right) = -k_h\int[\cdot\text{OH}]dt \tag{7.17}$$

where the term $\int[\cdot\text{OH}]dt$ represents the time-integrated concentration of ·OH, which is termed *·OH exposure*. Equation (7.17) shows that, the decrease in the concentration of PCBA at any time, *t*, is an indirect measurement of the ·OH exposure for the reaction time period. Therefore, a term, R_{ct}, is defined as the ratio of ·OH exposure and O_3 exposure as

$$R_{ct} = \frac{\int[\cdot\text{OH}]dt}{\int[O_3]dt} \tag{7.18}$$

The O_3 exposure, $\int[O_3]dt$, can be calculated from the integral of the ozone concentration profile, as shown in Figure 7.2.

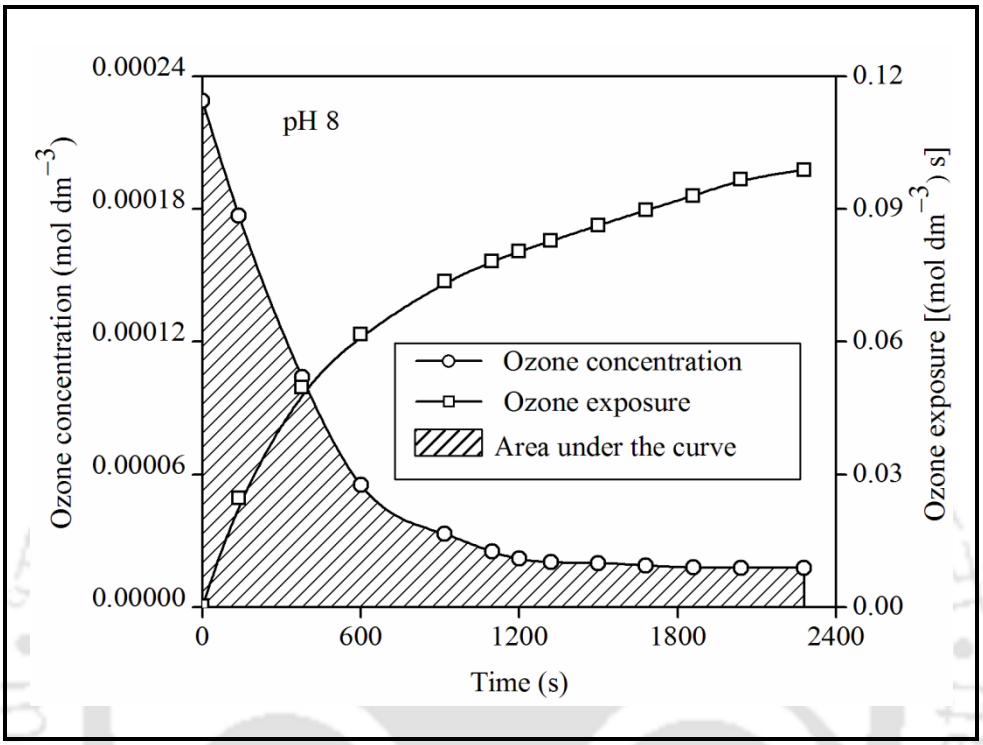

Figure 7.2 Variation of O_3 concentration and O_3 exposure with time.

From Eq. (7.17) and Eq. (7.18) we get

$$\ln\left(\frac{[\text{PCBA}]}{[\text{PCBA}]_0}\right) = -k_h R_{ct} \int[O_3]dt \tag{7.19}$$

Equation (7.19) shows that R_{ct} can be experimentally determined by measuring the decrease in the concentration of PCBA and O_3. The concentration profile of PCBA with time is shown in Figure 7.3. The ·OH generated from ozone is consumed by PCBA, and therefore, the concentration of PCBA decreases. However, the ozone dissolution in water increases with time, which results in the increase in the ozone exposure. By plotting the left-hand side of Eq. (7.19) versus the O_3 exposure, R_{ct} can be calculated from the slope of the plot (Figure 7.4).

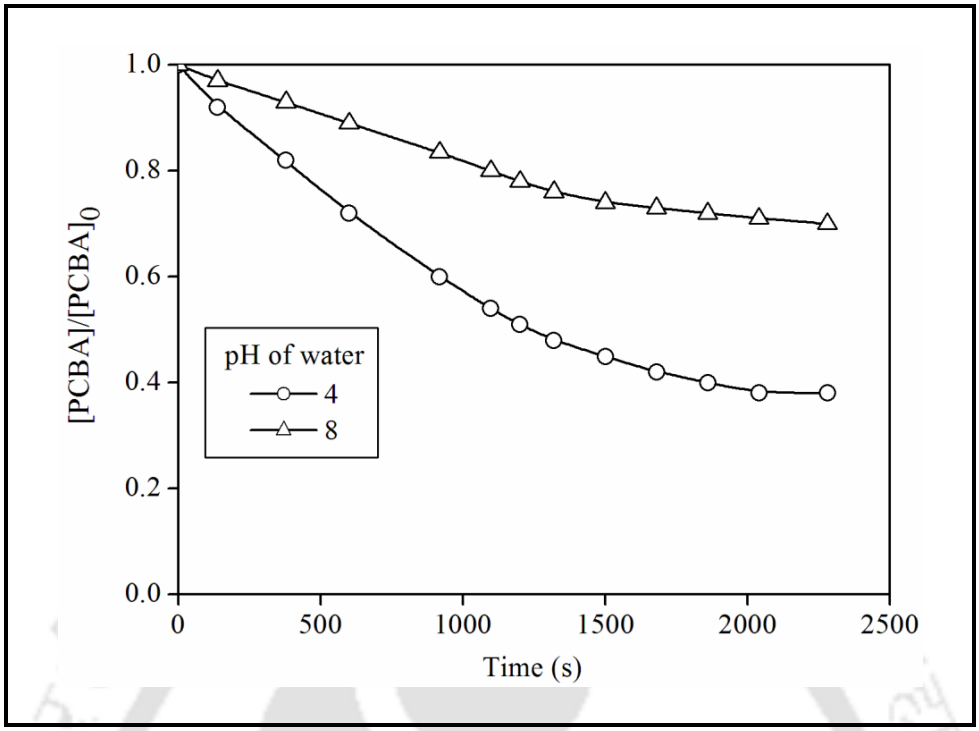

Figure 7.3 Variation of PCBA concentration with time.

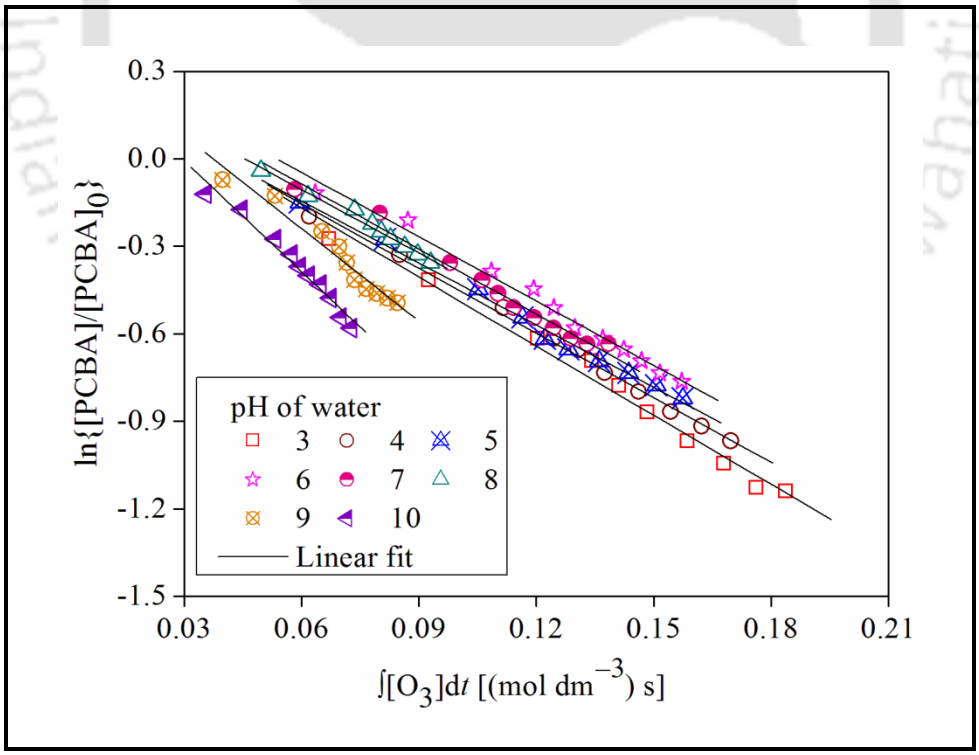

Figure 7.4 Linear fit of O_3 exposure with concentration of PCBA.

Figure 7.5 depicts the O_3 exposure profiles at various pH. The value of O_3 exposure was higher at the acidic pH than that at the alkaline pH. The decomposition of ozone increases with increasing pH. Therefore, at acidic pH, the molecular ozone is more stable.

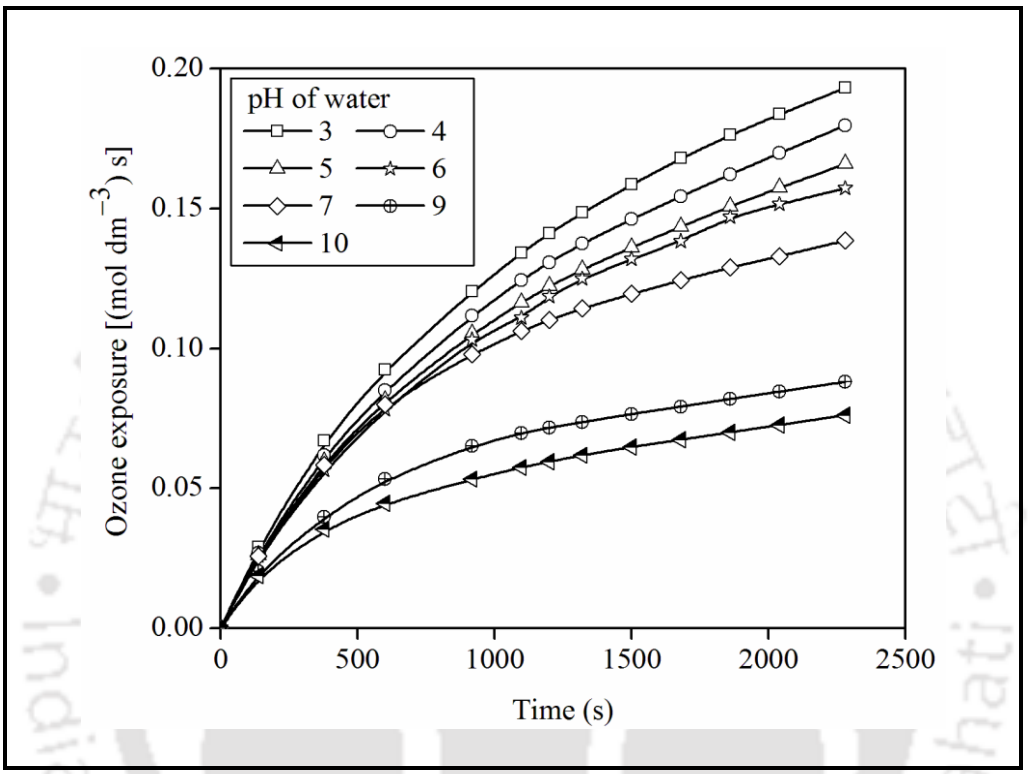

Figure 7.5 O_3 exposure profiles at various pH.

The relationship between $\ln\left([\text{PCBA}]/[\text{PCBA}]_0\right)$ and the O_3 exposure shows that R_{ct} is a constant and independent of the reaction time. Therefore, R_{ct} can be expressed as the ratio of $[\cdot\text{OH}]$ and $[O_3]$ at any time, *t*, during the reaction (Elovitz and von Gunten, 1999)

$$R_{ct} = [\cdot\text{OH}]/[O_3] \tag{7.20}$$

The value of $[\cdot\text{OH}]$ can be calculated from Eq. (7.20).

7.2 EFFECT OF pH ON GENERATION OF ·OH

The generation of hydroxyl radicals from the ozone microbubbles was investigated at different pH. The variation of [·OH], [O_3] and R_{ct} with pH is shown in Figure 7.6. The variation of ozone exposure with time at different pH is shown in Figure 7.7 (a). The variation of concentration of hydroxyl radicals with time is depicted in Figure 7.7 (b). At acidic pH, the value of ·OH exposure was more than that at the alkaline pH. This was the result of the higher generation of ·OH from the ozone microbubbles. However, the ozone decomposition was less at pH < 7, which increased the O_3 exposure. Therefore the value of R_{ct} was less at acidic pH.

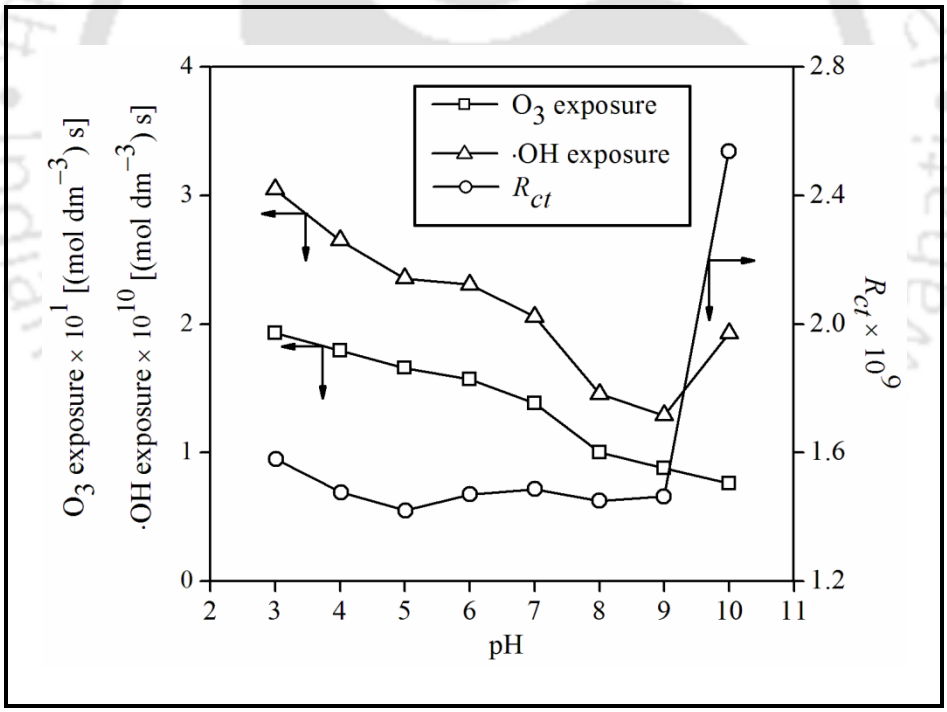

Figure 7.6 Comparison of ·OH exposure, O_3 exposure and R_{ct} at different pH.

At alkaline pH, the decomposition of ozone was more, and therefore, the O_3 exposure was decreased. The generation of ·OH was due to the chain reactions triggered by the OH^-.

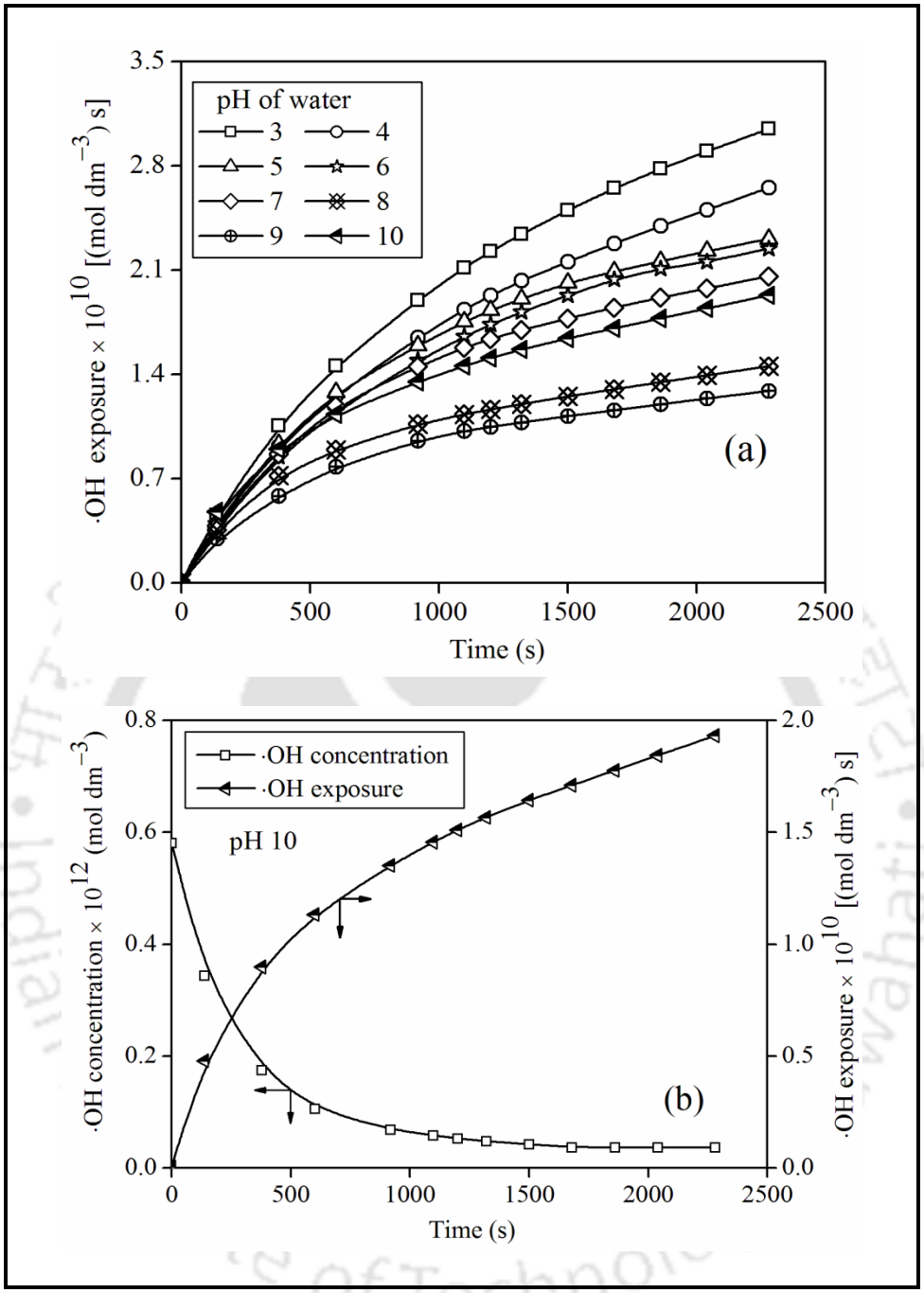

Figure 7.7 (a) Variation of ·OH exposure at different pH, and (b) variation of ·OH concentration and ·OH exposure at pH 10.

However, a significant amount of hydroxyl radicals was generated in the acidic conditions. Although the ·OH exposure was less at pH < 9, but R_{ct} was similar to that of the acidic conditions. At pH 10, the ·OH exposure and the ozone decomposition increased rapidly due

to the presence of OH^- ions. Thus, the O_3 exposure noticeably decreased and R_{ct} increased. Elovitz and von Gunten (1999) have reported that R_{ct} increased with pH, whereas the value of ·OH exposure did not vary much for pH 6–9 (viz. 5×10^{-14} mol dm^{-3} s). This happens due to the higher ozone decomposition and lower ·OH generation in the alkaline pH. However, they have not reported the values of [·OH], $[O_3]$ and R_{ct} at pH < 6. Haag and Yao (1993) have reported that the value of R_{ct} was almost constant at pH 7–8.2 for a variety of water samples ranging from clean surface water to wastewater. In our study, a higher depletion of PCBA at acidic pH clearly shows that the generation of ·OH from the ozone microbubbles in the acidic medium was more than that in the alkaline medium. Studies at pH < 3 or pH > 10 were not performed in our pilot plant due to the operational limitations of the microbubble generator (as mentioned in Section 4.1). The range of the pH could not be increased, as it would damage the internal materials of the microbubble generator.

7.3 EFFECT OF CARBONATE ON GENERATION OF ·OH

Carbonate and bicarbonate are the two main inhibitors of ·OH, and their inhibition mechanism is shown below.

$$HCO_3^- + \cdot OH \rightarrow H_2O + CO_3^- \cdot \quad (7.21)$$

$$CO_3^{2-} + \cdot OH \rightarrow OH^- + CO_3^- \cdot \quad (7.22)$$

Carbonate is a major ·OH scavenger, which inhibits the chain reaction of ozone decomposition (Beltrán, 2004). At alkaline pH, carbonate not only consumes ·OH but also inhibits the generation of HO_2^-, $\cdot O_2^-$, $\cdot O_3^-$, or any other intermediate that would accelerate the decomposition of O_3. Therefore, the presence of carbonate slows down the total ozone decomposition process and increases the stability of ozone. Increase in the carbonate

concentration in water increases the ozone exposure, but decreases the concentration of ·OH . The effect of carbonate on the generation of ·OH from the ozone microbubbles was studied at pH 4 and 8 at the carbonate concentrations of 1 and 2 mmol dm^{-3} (Figure 7.8). The values of ·OH exposure, O_3 exposure and R_{ct} vary differently at pH 4 and 8 in the presence of carbonate.

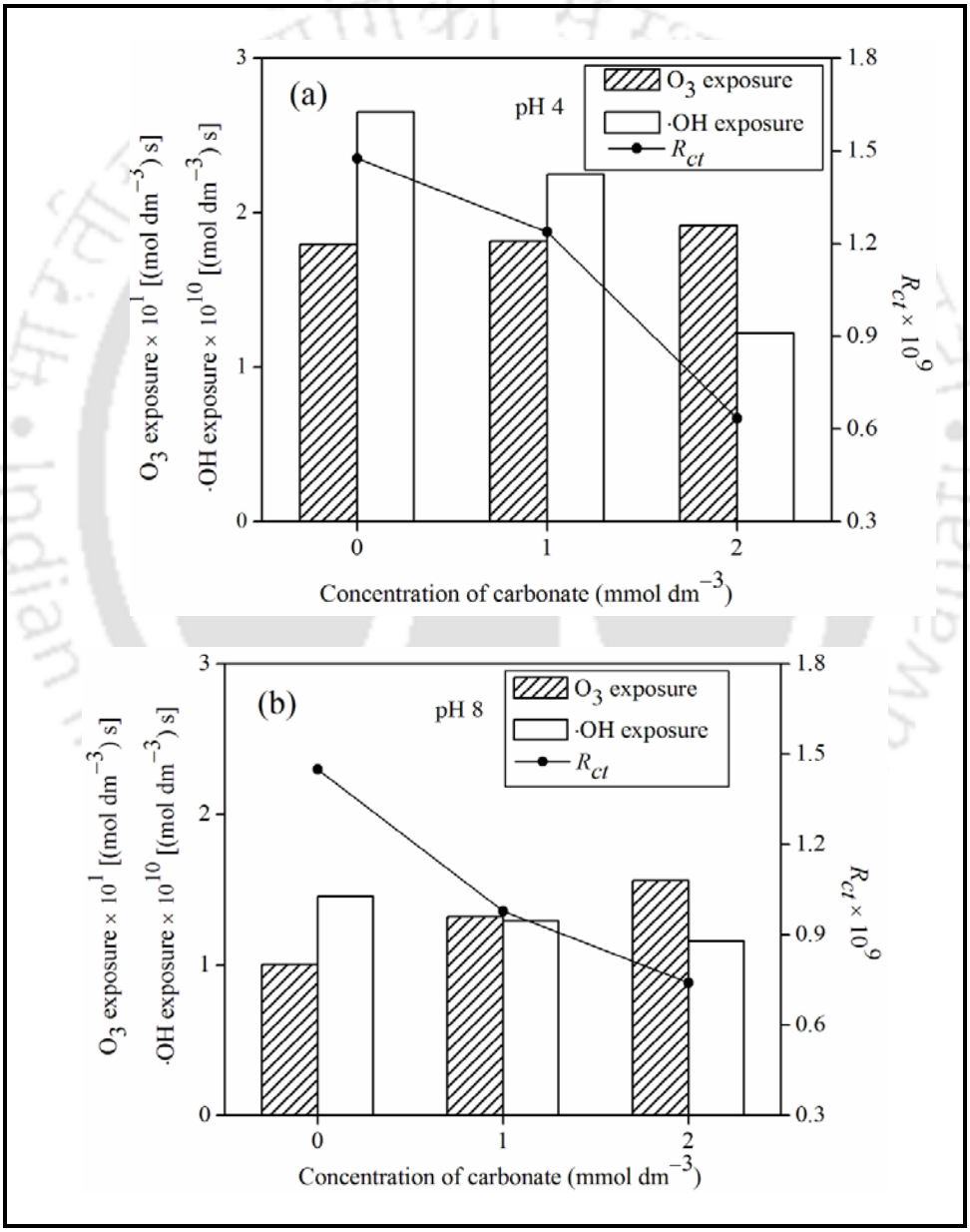

Figure 7.8 Effect of CO_3^{2-} on ·OH exposure, O_3 exposure and R_{ct} at (a) pH 4, and (b) pH 8.

At pH 4, the O_3 exposure remained same whereas at pH 8, it increased with increasing CO_3^{2-} concentration. At acidic pH and in presence of carbonate in water, ·OH is consumed and the chain reactions given by Eqs. (11)–(15) are inhibited. This increases the O_3 exposure and decreases the ·OH exposure. However, the decomposition of ozone was itself slower at acidic pH. So CO_3^{2-} shows almost no effect of O_3 exposure and only acts as the ·OH scavenger. Thus, the value of ·OH exposure decreased at acidic as well as alkaline pH, due to the competition between PCBA and CO_3^{2-} for ·OH, and therefore, the value of R_{ct} decreased.

7.4 MECHANISM OF HYDROXYL RADICAL GENERATION FROM MICROBUBBLES

The surface charge of the microbubbles depends on the pH of the medium. Above pH ~4, the microbubbles are negatively charged due to the preferential adsorption of OH^- at the air–water interface. However, below pH 4, the microbubbles are positively charged due to the adsorption of H^+ ions (Takahashi, 2005). The reactions involved in the generation of hydroxyl radicals in acidic and alkaline pH are given in Section 7.2. The microbubbles have high internal pressure due to their high surface curvature. The pressure difference across the bubble surface (Δp) is given by the Young–Laplace equation [Eq. (1.7)]. As pressurized gas efficiently dissolves in the aqueous phase, ozone rapidly dissolves in water due to the high internal pressure of the microbubbles. As a result, the microbubbles quickly reduce in size. The pressure inside a microbubble goes on increasing with its decreasing size. This ultimately leads to the collapse of the microbubble. The high concentration of dissolved ozone in the

aqueous phase (either in acidic or in alkaline medium) leads to the formation of hydroxyl radicals.

7.5 DEGRADATION OF PHENOL BY ·OH

Phenol and chlorinated phenols are commonly found as micropollutants in water. Experimental results reported in the literature reveal that ozonation at high pH favors the degradation of phenol and COD removal (Hoigné and Bader, 1983; Poznyak and Vivero, 2005; Xiang-feng and Xin-hua, 2004; Yamamoto et al., 1979). Hydroxyl radicals simultaneously react with the pollutants along with molecular O_3. Therefore, the depletion rate of the pollutant (D) with ozone may be written as

$$-\frac{\mathrm{d}[\mathrm{D}]}{\mathrm{d}t} = k_h[\cdot\mathrm{OH}][\mathrm{D}] + k_{\mathrm{O_3}}[\mathrm{O_3}][\mathrm{D}] \tag{7.23}$$

From Eqs. (7.18) and (7.23)

$$-\frac{\mathrm{d}[\mathrm{D}]}{\mathrm{d}t} = k_h R_{ct}[\mathrm{O_3}][\mathrm{D}] + k_{\mathrm{O_3}}[\mathrm{O_3}][\mathrm{D}] \tag{7.24}$$

$$-\frac{\mathrm{d}[\mathrm{D}]}{\mathrm{d}t} = \left(k_h R_{ct} + k_{\mathrm{O_3}}\right)[\mathrm{O_3}][\mathrm{D}] \tag{7.25}$$

where k_h and $k_{\mathrm{O_3}}$ are the second-order rate constants for reaction of micropollutant (D) with ·OH and O_3, respectively. The values of k_h and $k_{\mathrm{O_3}}$ can be determined from Eq. (7.25) if the value of R_{ct} is known. The rate constants of the reaction of phenol with ozone and ·OH vary with pH, as shown in Table 7.1. The degradation of phenol using ozone microbubbles at different pH is shown is Figure 7.9 (a). The O_3 exposure was slightly less in presence of phenol due to the consumption of ozone [Figure 7.9 (b)]. The degradation of phenol was more at acidic and alkaline pH than at pH 7. By using the PCBA probe, the values of R_{ct} were calculated. The rate constants of the reaction of phenol with ·OH and O_3

were determined by using Eq. (7.25), after calculating the values of R_{ct} at different pH (Table 7.2). The values of k_{O_3} and k_h were similar to that reported by Hoigne and Bader (1983), and Land and Ebert (1967), respectively. Furthermore, the values of k_{O_3} were of the same order at all pH. The R_{ct} parameter may be used for comparing the contributions of $\cdot OH$ and O_3 for the degradation of a micropollutant in water.

Table7.1 Rate constant of reaction of phenol with ozone and hydroxyl radical.

	pH	Order	Rate constant ($dm^3\ mol^{-1}\ s^{-1}$)	Reference
Molecular ozone	1.5	2	8.9×10^2	Li et al. (2004)
	2.7		2.1×10^3	
	3.7		4.4×10^3	
	5.2		2.9×10^4	
	2−6		1.3×10^3	Hoigné and Bader (1983)
	6		90	Joshi and Shambaugh (1982)
	7		1.4×10^2	
	8		1.8×10^2	
	9		2.5×10^2	
Hydroxyl radical	6−7	2	1.8×10^{10}	Adams et al. (1965)
	7		6.6×10^9	Fleld et al. (1982)
	7.6		1.4×10^{10}	Land and Ebert (1967)

The fraction of D degraded by $\cdot OH$ and O_3 can be expressed as

$$f_{\cdot OH} = \frac{\text{Amount of D reacted with } \cdot OH}{\text{Amount of D reacted with } \cdot OH + \text{Amount of D reacted with } O_3} \quad (7.26)$$

$$f_{\cdot OH} = \frac{k_h[\cdot OH][D]}{k_h[\cdot OH][D] + k_{O_3}[O_3][D]} \quad (7.27)$$

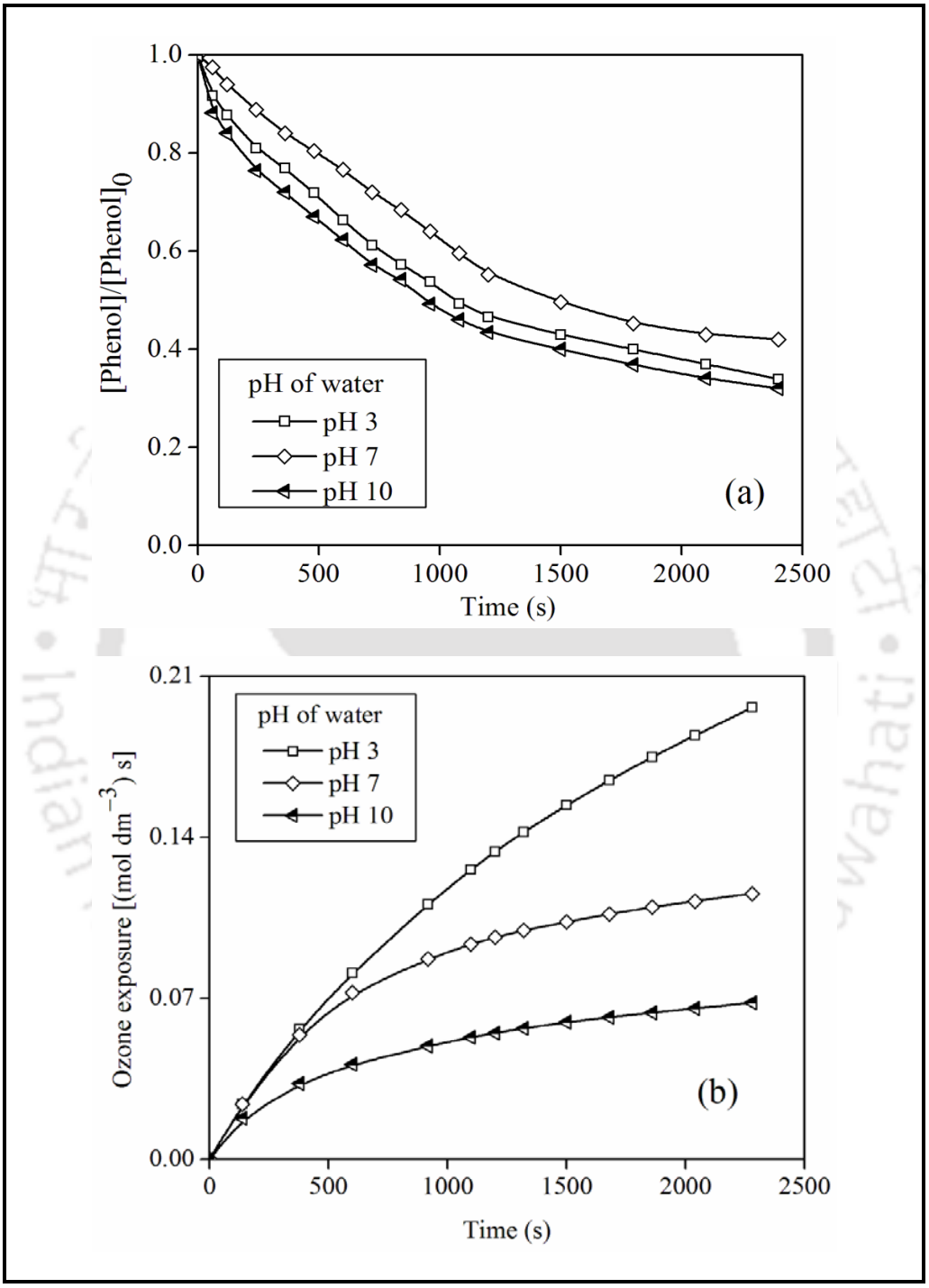

Figure 7.9 (a) Concentration profiles of phenol with time, and (b) O_3 exposure during the phenol oxidation.

Substituting Eq. (7.18) in Eq. (7.27) and rearranging

$$f_{\cdot OH} = \frac{k_h R_{ct}}{k_h R_{ct} + k_{O_3}} \tag{7.28}$$

Using Eq. (7.28), the fraction of phenol reacted with ·OH was calculated. These values are given in Table 7.2.

Table 7.2 Contribution of O_3 and ·OH on phenol oxidation.

pH	$R_{ct} \times 10^{10}$	k_{O_3} ($dm^3\ mol^{-1}\ s^{-1}$)			$k_h \times 10^{-10}$ ($dm^3\ mol^{-1}\ s^{-1}$)			R^2	$f_{\cdot OH} \times 10^3$
		Value	*95% UL	*95% LL	Value	*95% UL	*95% LL		
3	11.4	1203	1202.2	1203.8	1.49	1.47	1.51	0.97	14.00
4	10.2	1202	1201.6	1202.4	1.48	1.46	1.50	0.99	12.50
5	6.9	1262	1260.3	1263.7	1.50	1.49	1.51	0.96	8.08
6	5.5	1260	1259.1	1260.9	1.50	1.49	1.51	0.97	6.46
7	5.3	1359	1357.9	1360.1	1.51	1.50	1.52	0.98	5.78
8	5.2	1420	1418.0	1421.0	1.51	1.50	1.52	0.96	5.43
9	5.2	1420	1419.6	1420.5	1.49	1.48	1.50	0.97	5.43
10	7.9	1420	1419.0	1421.0	1.51	1.50	1.52	0.97	8.22

*95% confidence interval, upper limit (UL), lower limit (LL)

The R_{ct} values in phenol–PCBA system were lower than the same for the PCBA system. This is due to the competitive effect of phenol and its degraded products with PCBA for the consumption of ·OH. The presence of ·OH increased phenol degradation at acidic and alkaline pH, whereas at pH 6–9, the contribution of ·OH on phenol degradation was similar. The contribution of ·OH on phenol degradation may be higher in presence of catalysts (e.g. H_2O_2, Fe catalyst or the Fenton processes) due to higher generation of ·OH (Xiang-feng and Xin-hua, 2004).

NOTATIONS

$[D]$	concentration of the micropollutant, mol dm^{-3}
$f_{\cdot OH}$	fraction of micropollutant reacted with $\cdot OH$, dimensionless
k_1	first-order reaction rate constant, s^{-1}
k_2	second-order reaction rate constant, $dm^3\ mol^{-1}\ s^{-1}$
k_h	rate constant of reaction of micropollutant with $\cdot OH$, $dm^3\ mol^{-1}\ s^{-1}$
k_{O_3}	rate constant of reaction of micropollutant with ozone, $dm^3\ mol^{-1}\ s^{-1}$
$[O_3]$	concentration of ozone at time t, mol dm^{-3}
$\int O_3 dt$	O_3 exposure, mol dm^{-3} s
$[\cdot OH]$	concentration of hydroxyl radical at time t, mol dm^{-3}
$[OH^-]$	concentration of hydroxyl ion, mol dm^{-3}
$\int \cdot OH dt$	$\cdot OH$ exposure, mol dm^{-3} s
$[PCBA]_0$	concentration of PCBA at time $t = 0$, mol dm^{-3}
[PCBA]	concentration of PCBA at time t, mol dm^{-3}
R_{ct}	ratio of $\cdot OH$ exposure to O_3 exposure, dimensionless
t	time, s

Abbreviations

COD	chemical oxygen demand
HPLC	high-performance liquid chromatography
PCBA	*p*-Chlorobenzoic acid

REFERENCES

Adams, G.E., Boag, J.W., Currant, J., Michael, B.D., 1965. Absolute rate constants for the reaction of the hydroxyl radical with organic compounds, in: Pulse Radiolysis. Academic Press, NewYork, USA, pp. 131−143.

Beltrán, F.J., 2004. Ozone Reaction Kinetics for Water and Wastewater System. CRC Press, Boca Raton, Florida, USA.

Dreosti, I.E., 1991. Trace Elements, Micronutrients, and Free Radicals. Humana Press, Clifton, New Jersey, USA.

Elovitz, M.S., von Gunten, U., 1999. Hydroxyl radical/ozone ratios during ozonation processes. I. The R_{ct} concept. Ozone Sci. Eng. 21, 239−260.

Fleld, R.J., Raghavan, N.V., Brummer, J.G., 1982. A pulse radiolysis investigation of the reactions of $BrO_2\cdot$ with $Fe(CN)_6^{4-}$, Mn(II), phenoxide ion, and phenol. J. Phys. Chem. 86, 2443−2449.

Gardoni, D., Vailati, A., Canziani, R., 2012. Decay of ozone in water: a review. Ozone Sci. Eng. 34, 233−242.

Haag, W.R., Yao, C.C.D., 1993. Ozonation of U.S. drinking water sources: HO concentration and oxidation-competition values, in: Eleventh Ozone World Congress. San Francisco, California, USA, pp. 119−126.

Hoigné, J., Bader, H., 1983. Rate constants of reactions of ozone with organic and inorganic compounds in water–I. Water Res. 17, 173−183.

Joshi, M.G., Shambaugh, R., 1982. The kinetics of ozone-phenol reaction in aqueous solutions. Water Res. 16, 933−938.

Land, E.J., Ebert, M., 1967. Pulse radiolysis studies of aqueous phenol. Water elimination from dihydroxycyclohexadienyl radicals to form Phenoxyl. Trans. Faraday Soc. 63, 1181–1190.

Li, K.Y., Kuo, C.H., Weeks, J.J.L., 1979. A kinetic study of ozone-phenol reaction in aqueous solutions. AIChE J. 25, 583−591.

Poznyak, T., Vivero, J., 2005. Degradation of aqueous phenol and chlorinated phenols by ozone. Ozone Sci. Eng. 27, 447−458.

Roots, R., Okada, S., 2014. Estimation of life times and diffusion distances of radicals involved in X-ray-induced DNA strand breaks or killing of mammalian cells. Radiat. Res. 64, 306−320.

Sehested, K., Corfitzen, H., Holcman, J., Fischer, C.H., Hart, E.J., 1991. The primary reaction in the decomposition of ozone in acidic aqueous solutions. Environ. Sci. Technol. 25, 1589–1596.

Sehested, K., Holcman, J., Bjergbakke, E., Hart, E.J., 1984. A pulse radiolytic study of the reaction OH + O_3 in aqueous medium. J. Phys. Chem. 88, 4144−4147.

Staehelin, J., Buhler, R.E., Hoigné, J., 1984. Ozone decomposition in water studied by pulse radiolysis. 2. OH and HO_4 as chain intermediates. J. Phys. Chem. 88, 5999−6004.

Takahashi, M., 2005. Zeta potential of microbubbles in aqueous solutions: electrical properties of the gas–water interface. J. Phys. Chem. B 109, 21858−21864.

Tomiyasu, H., Fukutomi, H., Gordon, G., 1985. Kinetics and mechanism of ozone decomposition in basic aqueous solution. Inorg. Chem. 24, 2962−2966.

Xiang-feng, Z., Xin-hua, X., 2004. The mechanism of Fe(III)-catalyzed ozonation of phenol. J. Zhejiang Univ. Sci. 5, 1543−1547.

Yamamoto, Y., Niki, E., Shiokawa, H., Kamiya, Y., 1979. Ozonation of organic compounds. 2. Ozonation of phenol in water. J. Org. Chem. 44, 2137−2142.

CHAPTER 8

CONCLUSIONS AND SCOPE OF FUTURE WORK

CHAPTER 8

CONCLUSIONS AND SCOPE OF FUTURE WORK

This chapter summarized the conclusions drawn from this work and provides recommendation for future work.

8.1 CONCLUSIONS OF THE WORK

In this work, the oxidation of ammonia, As(III), and dyestuff (BG) has been studied by using ozone microbubbles. Along with that, the adsorption of As(V) and the detection of hydroxyl radicals generated from the ozone microbubbles have been illustrated. The effects of several important parameters on the oxidation of the above pollutants have been presented. Some important kinetic and mass transfer aspects of the ozonation in the semi-batch and batch reactors have also been studied. Adsorption of arsenic on two adsorbents has been studied. The salient accomplishments and the major conclusions are briefly presented in the following sections.

8.1.1 Removal of Ammonia from Water

- Ammonia present in water was effectively oxidized by ozone microbubbles. The oxidation was effective under alkaline conditions (i.e. at pH > 7). The effectiveness of ozonation of ammonia increased with increasing pH. Even for low-ammonia feed concentrations (e.g. 1 mg dm^{-3}), ozonation was quite effective.
- At pH ≥ 8, ozonation of ammonia seems to occur by the direct reaction with molecular ozone. On the other hand, at pH 6 and 7, hydroxyl radicals also contribute in the oxidation process.
- The rate of ozone generation had a significant effect on the ammonia oxidation. The concentration of ozone in the gas coming out of the ozonator (and fed to the microbubble

generator) increased with increasing ozone generation rate. As a result, the concentration of ozone in the aqueous phase increased, and the rate of ozonation was increased.

- During the ammonia ozonation process, the pH of the reaction medium decreased with time due to the formation of H^+ ions.
- The anions of the ammonium salts do not have any effect on the ozonation of ammonia. No difference was found between ammonium chloride and ammonium sulfate in this regard.
- Oxygen microbubbles are not effective in oxidizing ammonia.
- The rate of oxidation of ammonia by ozone was faster in presence of bromide ions. The advantage of the use of bromide was that the nitrate formed by the oxidation of ammonia was ultimately converted to nitrogen. Water containing bromide salts may take advantage of this phenomenon.
- As the concentration of ozone in the gas phase increased, the equilibrium ozone concentration in the aqueous phase increased. This resulted in a higher solubility of ozone in water. The volumetric mass transfer coefficient increased with increasing ozone generation rate.
- The volumetric mass transfer coefficient increased with increasing pH as a result of the faster rate of self-decomposition of ozone at the high pH, which enhanced the rate of mass transfer.

8.1.2 Removal of Arsenic from Water

- Oxidation of As(III) by using ozone microbubbles was fast. The rate of oxidation increased with increasing ozone application rate.
- The pH of the medium was a controlling factor for oxidation of As(III). At slightly acidic pH (e.g. pH 6), the conversion of As(III) to As(V) was fast as compared to pH 7. There

was a slight increase in the rate of the oxidation of As(III) with increasing pH in the alkaline range. The variation in the speciation of As(III) with pH is the likely reason for this behavior.

- Both the molecular ozone and the hydroxyl radicals were involved in the oxidation process. The use of 2-propanol as the hydroxyl radical scavenger confirmed the participation of this radical in the oxidation of As(III).
- The carbonate ion radicals were also found to be effective for the oxidation of As(III). The reaction of As(III) with ozone followed a modified pseudo first-order kinetics. The value of the dimensionless rate constant was ~0.75, and it slightly varied with the pH of the medium.
- As(V) strongly adsorbed on Zr–AC and Am-Zr.
- Electric charge of the surface of these adsorbents changed from positive to negative as the pH of the aqueous medium was increased. The adsorption of As(V) was effective at slightly acidic conditions at which the value of the zeta potential was positive.
- The adsorbents were mesoporous with a large specific surface area. Both the adsorbents were amorphous in nature.
- The adsorption of As(V) followed a pseudo second-order kinetics. It also followed an intra-particle diffusion model.
- The adsorption isotherms were best fitted with the Freundlich and Redlich–Peterson models.
- The maximum adsorption capacity of Am-Zr was greater than that of Zr–AC.
- The adsorption of As(V) on these adsorbents was spontaneous and endothermic in nature. It led to an increase in the entropy.

8.1.3 Removal of Dyestuff from Water

- Oxidation of BG using ozone microbubbles was very effective. The dissolution of ozone into water was rapid due to the microbubbles. This enhanced the decolorization efficiency and decreased the loss of ozone.
- BG decolorization was effective in the acidic as well as in the alkaline pH. The hydroxyl radicals were the dominating oxidizing species in the acidic pH, whereas molecular ozone was dominant at alkaline pH.
- The TOC removal was ~80% in 1 h, which implies that the use of ozone microbubbles is a promising method for the degradation of BG.
- Thirteen intermediate compounds were identified using GC–MS and FTIR. The intermediates were formed by two reaction pathways. The changes in the FTIR spectra of BG before and after oxidation supported the degradation mechanism.
- The reaction of BG with ozone was overall second-order in nature and first-order with respect to dye as well as ozone. The volumetric mass transfer coefficient and the enhancement factor increased with increasing initial BG concentration.

8.1.4 Measurement of Hydroxyl Radical Concentration

- The indirect method of determination of the concentration of hydroxyl radicals is promising.
- The depletion rate of PCBA was high in the acidic condition, and it decreased with increasing pH. But at pH 10, the PCBA depletion rate increased. From the rate of depletion of PCBA and ozone, the values of O_3 exposure, ·OH exposure and R_{ct} were calculated.
- At acidic pH, the generation of ·OH was due to the thermal dissociation of ozone. However, ozone was more stable in the acidic condition than in the alkaline condition.

Therefore, both O_3 and ·OH exposures were higher in the acidic media than the alkaline conditions. At alkaline pH, ozone decomposition increased due to the presence of OH^-. However, the generation of ·OH was less than that at the acidic pH. At pH 10, ·OH exposure strongly increased due to the high concentration of OH^-.

- CO_3^{2-} was used as the radical scavenger at both acidic and alkaline pH. At acidic pH, CO_3^{2-} acted only as the radical scavenger. At alkaline pH, CO_3^{2-} inhibited ·OH and slowed down the ozone decomposition reactions. As a result, the O_3 exposure increased.
- The degradation of phenol by ·OH was higher at acidic pH than that at the alkaline pH. The rate constant of reaction of phenol with ·OH was much higher than that of O_3, and it was constant at all pH.

8.2 SCOPE OF FUTURE WORK

In this work, the ozonation of ammonia, arsenic and dyestuff were performed by using microbubbles. However, some more works are required for practical use of the process.

- The presence of various cations and anions in water can alter the rate of oxidation of these above compounds. The effect of such ions on ozone microbubbles may be studied.
- Other important studies such as variation of temperature, and a more detailed mass transfer study can be performed in other reactors.
- The use of catalysts such as metal ions and H_2O_2 along with the ozone microbubbles will be very efficient in oxidizing the pollutants. This will enhance the generation of ·OH. Therefore, further works can be done by using these catalysts to enhance the oxidation of various organic and inorganic pollutants.

ANNEXURE 1

CALCULATION OF CONCENTRATION OF OZONE IN THE FEED GAS (%)

The concentration of ozone in the ozone–oxygen gas mixture was calculated as follows.

Molar mass of ozone = 48 g mol^{-1}

As per the ideal gas law: $PV = nRT$

P = atmospheric pressure (1 atm)

T = temperature (298 K)

R = gas constant (0.082 L atm mol^{-1} K^{-1})

For ozone generation rate = 2 g h^{-1}, volume of ozone in the gas = $\left(\frac{2}{60}\right)\times\left(\frac{0.082\times 298}{1\times 48}\right)$ L min^{-1} = 0.017 L min^{-1} = 17 ml min^{-1}

Total gas flow rate (ml min^{-1}) (as displayed by the rotameter)	Ozone flow rate (g h^{-1}) (as displayed by the ozone generator)	Volumetric ozone flow rate (ml min^{-1})	Concentration of ozone in the feed gas (%)
2500	2.0	17.0	0.68
	4.0	34.0	1.36
	6.0	51.0	2.04

ANNEXURE 2

COST ANALYSIS OF THE MICROBUBBLE-AIDED OZONATION PLANT

The cost analysis of the pilot plant set-up for the microbubble ozonation system (working volume 25 L) is given below.

(I) Capital cost

Item	cost (INR)
Microbubble generator	4,51,500
Ozone generation system (oxygen concentrator, ozone generator, ozone destructor, step-down transformer, and voltage stabilizer)	2,51,990
Total cost	7,03,490

(II) Running cost

Item	Power consumption (W)	Hours/month*	Electricity consumption (kW h)
Microbubble generator	450	35†	15.75
Ozone generator	205	30	6.15
Oxygen concentrator	350	30	10.50
Step-down transformer	300	30	9.00
Voltage stabilizer	350	30	10.50
Total Units (kW h)			51.90

*Average hours/month; †Includes 5 hr for cleaning

Cost of electricity for one unit in Assam = 4.5 INR

Total running cost of the microbubble ozonation system per month = 233 INR for purifying 25 L water per day.

CURRICULUM VITAE

Snigdha Khuntia

PhD, Department of Chemical Engineering

IIT Guwahati, Assam, India

Email: snigdha@iitg.ernet.in; lipi.sarang@gmail.com

Mobile No: 08761875254

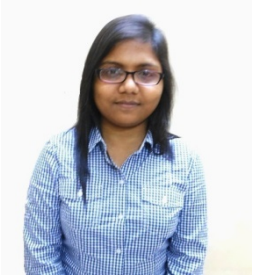

EDUCATION

Ph.D, IIT Guwahati, Assam (2011−2015)

Department: Chemical Engineering

Adviser/s: Prof. Pallab Ghosh and Dr. Subrata K. Majumder

Thesis Title: Removal of ammonia, arsenic and dyestuff from water by ozone microbubbles

M.Tech, IIT Guwahati, Assam (CPI: 8.4, 2009−2011)

Department: Chemical Engineering, Specialization in Petroleum Refinery Engineering

Adviser: Dr. A. K. Golder

Thesis Title: Reduction of hexavalent chromium using *Spirilina* sp. biomass.

B.Tech, IGIT Sarang, BPUT, Orissa (CGPA: 7.78, 2009)

Department: Chemical Engineering

12th, TTPS.HS. School, CHSE, Orissa (73%, 2004)

Subjects: PCMB, Oriya, English

10th, IGIT Campus High School, HSC, Orissa (72%, 2002)

Research Interests

The major areas of research includes advanced oxidation processes, ozone based water/wastewater treatment, biosorption, adsorption, heavy metal removal from wastewater. Additional research includes mass transfer study of ozone, oxygen using millibubbles and microbubbles, kinetics and decomposition of ozone in water, synthesis of adsorbents for metal removal.

Subject Interests

Interest in subjects of chemical engineering includes mass transfer, reaction engineering, colloid interface science, heat transfer, separation science, petroleum refinery engineering.

Research Experiences

Ph.D Researcher (IIT Guwahati)

- Performing the ozonation of water/wastewater.
- Mass transfer study of ozonation process.
- Performance calculation of pilot plants for bubble columns and microbubble systems.
- Investigation of oxidation mechanism of inorganic pollutants such as ammonia, and arsenic using ozone microbubbles.
- Investigation of oxidation mechanism of organic pollutants such as azo-dyes using ozone microbubbles.
- Qualitative and quantitative detection of hydroxyl radicals.
- Modification of activated carbon based adsorbents, synthesis of zirconium based adsorbents.
- Characterization of adsorbents to use in As(III) and As(V) adsorption.
- Modeling of experimental data obtained.
- Use of various instruments such as, Atomic absorption spectrophotometer (AAS), GC−MS, HPLC, XRD, BET, FTIR, UV-Vis, Zeta potentiometer for sample analysis, BOD and TOC analyzer.

Teaching Assistantship (TA)

- Colloid interface science (Course for M.Tech)
- Fundamentals of Material science (Course for M.Tech)
- Characterization of materials (Laboratory TA for M. Tech)
- Mechanical Operation (Laboratory TA for B.Tech)

List of Publications

Published Online

1. **Khuntia, S.**, Majumder, S. K., and Ghosh, P., Microbubble-aided water and wastewater purification: a review, *Rev. Chem. Eng.*, 28, 191−221 (**2012**).

2. **Khuntia, S.**, Majumder, S. K., and Ghosh, P., Removal of ammonia from water by ozone microbubbles, *Ind. Eng. Chem. Res.*, 52, 318−326 (**2013**).

3. **Khuntia, S.**, Majumder, S. K., and Ghosh, P., Oxidation of As(III) to As(V) using ozone microbubbles, *Chemosphere*, 97, 120−124 (**2014**).

4. **Khuntia, S.**, Majumder, S. K., and Ghosh, P., A pilot plant study of the degradation of Brilliant Green dye using ozone microbubbles: mechanism and kinetics of reaction, *Environ. Technol.*, 36, 336−347 (**2015**).

5. **Khuntia, S.**, Majumder, S. K., and Ghosh, P., Adsorption of As(V) on zirconium based adsorbents, *Desalin. Water Treat.*, DOI. 10.1080/19443994.2014.978389 (**2014**).

6. **Khuntia, S.,** Majumder, S.K., Ghosh, P., Quantitative prediction of generation of hydroxyl radicals from ozone microbubbles. Chem. Eng. Res. Des, 98, 231−239 (**2015**).

Conference/Presentations

1. **Snigdha Khuntia**, Subrata Kumar Majumder and Pallab Ghosh, Enhanced Oxidation of Ammonia Using Ozone Microbubbles, International Conference on Frontiers in Chemical Engineering (ICFCE-2013), NIT Rourkela, Odisha, India, pp 351−356, ISBN 978-93-80813-24-0, **09−11 December, 2013**.

M. Tech (IIT Guwahati)

- Performance of biosorption of Chromium using *Spirulina* sp. Biomass using batch and column study.
- Synthesis of algenate + biomass spherical beads and sorption study of Cr(V).
- Kinetic and thermodynamic study of biosoprtion.
- Use of Atomic absorption spectrophotometer (AAS), UV-Vis, FTIR for sample analysis and characterization.

Teaching Assistantship (TA)

- Process control (Laboratory TA for B.Tech)
- Engineering Mechanics (Course for B.Tech)
- Process Equipment Design III (Course for B.Tech)
- Chemical Reaction Engineering I (Course for B.Tech)

Conferences/Presentations

1. **Khuntia, S.**, Gagrai, M. K., Das C. and Golder, A. K., Effect of background ions on reduction of Cr (VI) to Cr (III) using saline water algae, Res. J. Chem. Environ., 15, 450−453 (**2011**).

2. **Khuntia, S.** and Golder, A. K., Hexavalent chromium reduction by immobilized green microalgae in continuous treatment, 2nd International Conference on Algal Biorefinery (ICAB-2014): A potential source of food, feed, biochemicals, biofuels and biofertilizers, Technical University of Denmark, Lybgby, Denmark, **August 27−29**, **2014**.

Skills

Equipments Operated: Atomic absorption spectrophotometer (AAS), GC−MS, HPLC, BET, FTIR, UV-Vis Spectrometer, Zeta potentiometer.

Software Skills: MATLAB, Polymath, C++.

Selected Awards and Recognitions

- **Khuntia, S.**, Majumder, S. K., and Ghosh, P., Microbubble-aided water and wastewater purification: a review, *Rev. Chem. Eng.*, 28, 191−221 (**2012**), has been included in one of the most downloaded article.
- MHRD Govt. of India scholarship for Ph.D work from July 2011 to June 2015.
- MHRD Govt. of India scholarship for M. Tech course from August 2009 to May 2011.
- Qualified GATE-2009 and secured all India rank of 438 in Chemical engineering.
- National Rural Talent Scholarship Examination (NRTS) qualified and district 2nd rank holder in Higher Secondary School (1999).

Personal Information

Date of Birth	29-05-1987	**Permanent Address**	D/O: Mr. Hrushikes Khuntia
Gender	Female		AT/PO: Sarang
Marital status	Single		Dist: Dhenkanal
Nationality	Indian		Odisha, India
Religion	Hindu		PIN: 759146
Category	OBC		
Hobbies	Reading novels, listening music		

References

Prof. Pallab Ghosh

Department of Chemical Engineering, IIT Guwahati, Assam, India–781039

E-mail: pallabg@iitg.ernet.in; Phone: +913612582253; Fax: +913612582291

Dr. Subrata K Majumder

Department of Chemical Engineering, IIT Guwahati, Assam, India–781039

E-mail: skmaju@iitg.ernet.in; Phone: + 913612582265; Fax: + 913612582291

Dr. Animes Kumar Golder

Department of Chemical Engineering, IIT Guwahati, Assam, India−781039

E-mail: animes@iitg.ac.in; Phone: +913612582269; Fax: +913612582291

Declaration

I hereby declare that I have carefully read and understood the instructions and particulars supplied to me, and that all entries in this curriculum vitae are true to the best of my knowledge and belief.

Date: 08/June/2015

Place: IIT Guwahati, Assam

Signature of Applicant